A Spectrophotometric Study of Polymethyl Methacrylate

Construction of a Recording Raman Spectrograph

by

PER-OLOF KINELL

Almqvist & Wiksells Boktryckeri AB

UPPSALA 1953

A Spectrophotometric Study of Polymethyl Methacrylate

Construction of a
Recording Raman Spectrograph

by

PER-OLOF KINELL

Almqvist & Wiksells Boktryckeri AB

UPPSALA 1953

R. UNIV.
BIBLIOTHEEK
LEIDEN

Contents

Preface 6
Introduction 7
Chapter 1. Construction of a Recording Raman Spectrograph 9
Introduction 9
A. Previous Work 9
B. Present Work 10
The Light Source Unit 12
A. The Mercury Vapour Discharge Lamps 12
a. The Visible Mercury Spectrum 12
b. Spectral Characteristics of Some Lamps 14
c. The Properties of Mercury Vapour Discharge Lamps 16
d. The Lamp Circuit 22
B. The Lamp House 23
a. General 23
b. Construction 26
C. The Condensing Lens System 28
a. Maximum Illumination Condition 28
b. Influence of Refractive Index 32
c. Influence of Absorption 33
d. Construction 34
The Spectrograph 34
The Recording Unit 34
A. Mechanical System 35
a. General 35
b. Performance 36
B. Optical System 39
a. General 39
b. Performance 39
C. Driving Mechanism 40
D. Check of Performance 41
E. Electrical System 43
a. General 43
1. Properties of Multiplier Photo Tubes 43
2. Noise in Input Circuit of Amplifier 52
b. Design and Performance 57
1. The Photo Tube System 57
2. The Amplifier System 64
3. The Homodyne Rectifier, Cathode Follower and Recorder 67
General Performance 73
A. Interpretation of Recorded Spectra 73
B. Linearity of Response 75

C. Signal-to-Noise Ratio 77
D. Influence of Amount of Liquid in Raman Tube 77
E. Stability of Electrical System 78
F. Purity of Mercury Spectrum 78
G. Reproducibility of Wave Number and Intensity Measurements 80
a. Determination of Wave Numbers 80
b. Intensity Measurements 82
H. Some Applications 85

Chapter 2. Preparative Work 88
Materials for Polymerization Experiments 88
A. Monomer 88
B. Initiator 88
C. Determination of Degree of Conversion 89
a. Gravimetric Method 89
b. Photometric Method 89
Materials for Ultra Violet and Infra Red Measurements. 92
A. Purification and Pre-Treatment 92
B. Fractional Precipitation 93
C. Viscosity Measurements 97
Other Materials 100

Chapter 3. Raman Spectra of Polymerizing Mixtures 101
Previous Work 101
A. Vinyl Compounds 101
B. Diene Compounds 103
Present Work 103
A. Polymerization Technique 104
B. Raman Spectrum of Monomeric Methyl Methacrylate 105
C. Raman Spectrum of Polymeric Methyl Methacrylate 109
D. Bond Frequencies in Monomeric and Polymeric Methyl Methacrylates . . . 114
E. Raman Spectra of Partially Polymerized Methyl Methacrylates 115

Chapter 4. Ultra Violet Studies of End Groups 123
Previous Work 123
Present Work 125
A. General Considerations 125
B. Experimental Work 126
a. Experimental Technique 126
b. Sources of Error 127
1. Losses due to Scattering. 127
2. Presence of Stray Light 127
3. Influence of Finite Wave Band 130
4. Other Influences 130
c. Results 130
1. Benzoyl Peroxide and Methyl Methacrylate 130
2. Unfractionated Samples 131
3. Fractionated Samples 131
C. Discussion 132

Chapter 5. Some Infra Red Measurements 138
Previous Work 138
Present Work 140
A. General Considerations 140
B. Experimental Work 141
a. Experimental Technique 141
b. Sources of Error 142
c. Results 142
1. Polymers of High Molecular Weight 142
2. Polymers of Low Molecular Weight 143
C. Discussion 145

Summary 149
Appendix I. List of Symbols 151
Appendix II. Details of Coupling Elements in Electronic Circuits 153
References 157

Preface

The present investigation was carried out at the Institute of Physical Chemistry of the University of Uppsala during the years 1948–1952.

I would like to take this opportunity of expressing my sincere gratitude to Professor The Svedberg, my teacher in physical chemistry. He has encouraged me in every way, not least by the lively personal interest which he has shown for my work.

To the present head of the Institute, Professor Stig Claesson, I am very grateful for the many ways in which he has facilitated the completion of this thesis.

My friend Dr. Philippe Traynard, Grenoble, did a great deal of the preliminary work connected with photo-electric recording of spectra during his stay at the Institute. I would like to thank him for his valuable contributions.

I am indebted to my colleagues at the Institute for interesting discussions and helpful advice. I also wish to thank the technical staff for their very valuable assistance.

The expenses incurred in connection with this work were in part defrayed by grants from Stiftelsen Svensk Gummiforskning (AB. Liljeholmens Kabelfabrik, Stockholm, Goodyear Gummifabriks AB., Stockholm, Svenska Gummifabriks AB., Gislaved, AB. Sieverts Kabelverk, Sundbyberg, Viskafors Gummifabriks AB., Viskafors), AB. Werner och Carlström, Göteborg, Knut och Alice Wallenbergs Stiftelse, and Statens Naturvetenskapliga Forskningsråd.

Uppsala, November 1952.

Per-Olof Kinell.

Introduction

The formation and properties of macromolecular compounds have, during the last twenty-five years, been extensively investigated by research workers all over the world. The reason for this is not only the very interesting properties of these compounds but also their great importance from a technical point of view. Our knowledge of the high molecular weight materials is to-day very large but nevertheless far from complete. Briefly it can be stated that research work follows two main routes: the study of the polymerization process, and the investigation of the properties of the large molecules.

The present investigation is mainly a contribution to our knowledge of the polymerization process, but it is also concerned with some questions of importance in the study of macromolecules. Interest has been directed towards those properties of high polymeric systems which can be revealed by spectrophotometric methods. Much of the investigation has been devoted to an elucidation of the possibilities offered by the use of raman spectroscopy. Investigations along similar lines have been made before; but due to the difficulties of measuring the intensity of raman lines, the results obtained are not very accurate. It was therefore found necessary to try a new arrangement for intensity measurements, namely, a direct determination by means of photo-electric tubes. This work implied many and various difficulties and consequently much of the time had to be devoted to the purely constructional side.

In addition to the raman work, experiments have been made in the use of ultraviolet and infrared spectroscopic methods for structural investigations.

The construction of the recording raman spectrograph is presented in Chapter 1. There are also given data about the precision by which wave-number and intensity determinations can be made. Both spectra with strong and weak raman lines have been studied. Some examples are also given of the selectivity of the photo-electric method compared with the photographic one.

Chapter 2 is devoted to a description of the preparative work done; purification of monomer, fractionation of polymers and so on. The methods used for the determination of degree of conversion in polymerization experiments and for the characterization of polymer samples by means of viscosity measurements are also discussed.

In Chapter 3 the application of raman spectroscopy to the study of polymerization mixtures is presented. Spectra are given for the pure monomer, different stages of polymerization and for the polymer. The information which can be obtained about the polymerization process from data of this kind is discussed.

Some ultraviolet measurements on end groups are given in Chapter 4. The possibilities of detecting different end groups are discussed. The value of a knowledge of the structure of the ends of the macromolecules in connection with the study of termination reactions and in the estimation of degree of branching of the molecules is elucidated.

Finally, in Chapter 5, an infrared analysis of the structure of the macromolecules is presented. Some differences in spectra obtained on films and solutions are discussed.

All investigations have been made on polymethyl methacrylate, the reason for this being that the author has previously studied the physico-chemical properties of the molecules of this substance (*cf.* (1, 2)), and found among other things, that the frequency curve of the molecular weights has several maxima. This necessitated an extension of the investigations into problems concerning the reaction mechanism.

Chapter 1

Construction of a Recording Raman Spectrograph

Introduction

As is well known most of the work in raman spectroscopy has been done photographically. This is a very reliable method especially in the determination of the position of the raman lines. However, when making intensity measurements the photographic plate has definite disadvantages, therefore several attempts have been made to use some methods of direct detection of raman lines. A short review of the main steps in this work is given below.

A. Previous Work

Kudrjawzewa (3) tried in 1935 to detect the raman lines from benzene by means of a photon counter with a potassium cathode. From the number of pulses he got the relative intensities of both Stokes and anti-Stokes lines. In 1936 Menzies (4) made some observations with a photo-tube and a Lindemann electrometer. These were point by point measurements and no automatic scanning. The first successful attempts to design recording instruments were made six years later by Rank *et al.* (5, 6), using an RCA-931 photo-multiplier tube and a plane-grating monochromator. The spectra were recorded by means of a galvanometer and a photographic galvanometer deflection recorder. The scanning was done by turning the grating. Later, Rank and his school developed this instrument further (7–9). Chien and Bender (10) in 1947 used a 1P21 photo-multiplier and a direct-current amplification system. The spectrograph had three glass prisms and the scanning was done by moving the photo-tube. Records were obtained by a galvanometer and a photographic plate. The same year the present author, in collaboration with Traynard (11), built an instrument using a spectrograph with one prism and an RCA-931 multiplier tube. The recorder used was originally a writing mA-meter and later a potentiometer recorder (Brown Electronik Potentiometer).

A considerable improvement in the performance of instruments of this type was made independently by Thompson[1] *et al.* (12) and by Sushchinskii (13, 14) as far

[1] The author is much indebted to Dr. H. W. Thompson, Oxford, England, for placing a manuscript at his disposal before publication.

as the electronic circuit is concerned. They used an alternating-current amplifier followed by a homodyne rectifier. In this way a remarkable reduction in disturbing noise could be obtained.

A very good instrument based on a three prism spectrograph has been constructed by Black *et al.* (15, 16).[1] The scanning is made by moving the two outer prisms. The multiplier tube used was an RCA-C-7073B (not available on the market).

Finally, it should be mentioned that instrument-firms also have contributed to the development. Thus Hilger and Watts Ltd., England (catalogue CH 334), has built an instrument with two glass prisms, where the scanning is made by turning a mirror placed just behind the dispersing prism, in this way the light passes both prisms twice. The photo-tube used is an English analogue to the RCA-tubes. Applied Research Laboratories, U.S.A., uses a three prism spectrograph with a reflective optics camera. The scanning is made by moving the photo-tube. Both of these instruments use the homodyne rectification principle to decrease the band width of the amplification system.

B. Present Work

The work described in this chapter is a report of the attempts made since 1948 to improve the original design made by the author and Traynard. Improvements have been made chiefly in the amplification and illuminating systems. The first has been changed from a direct-current to an alternating-current system, and in this work the results of Thompson *et al.* (12) have been followed to a great extent. The second system has been completely changed and the problem of obtaining a low-pressure mercury lamp has been solved in a simple way.

The general scheme of the arrangement is given in Figure 1. The light-source is operated through a relay from the mains supply, the light emerging from the lamps excites, in the raman tube, the spectrum to be investigated. In the spectrograph this is dispersed, and the various wave-lengths are detected by the photo-tube which can be moved by a synchronous motor. The voltage over the anode impedance of the photo-tube is amplified in a tuned amplifier (100 c./s.) and then rectified. Through a cathode-follower step the voltage obtained operates a potentiometer recorder. The various supplies of the electronic units are also shown in the block diagram. Necessary electrical connections are also indicated. In Figure 2, a total view of the spectrograph with attached units is shown. (*A*) is the spectrograph, (*B*) the lamp-house with connections to the tap water, (*C*) is the casing for the scanning arrangement, and (*D*) is the racks used for the different electric units (*E* amplifier,

[1] The author is very indebted to Dr. P. H. Holt, Esso Laboratories, U. S. A., for making a manuscript available before publication.

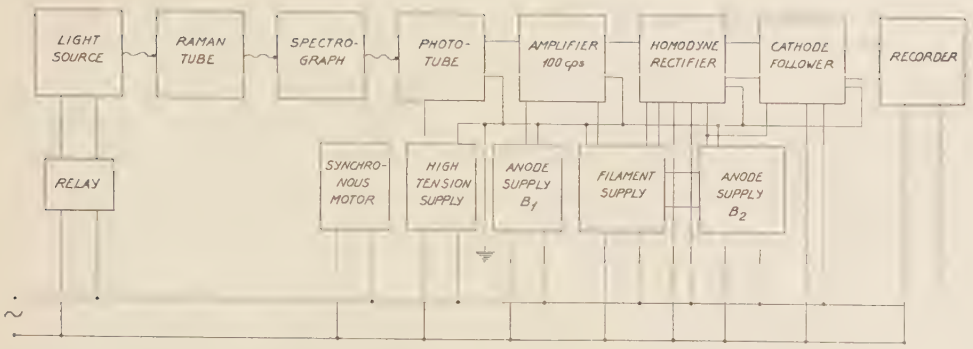

FIGURE 1. Block diagram of raman spectrograph arrangement.

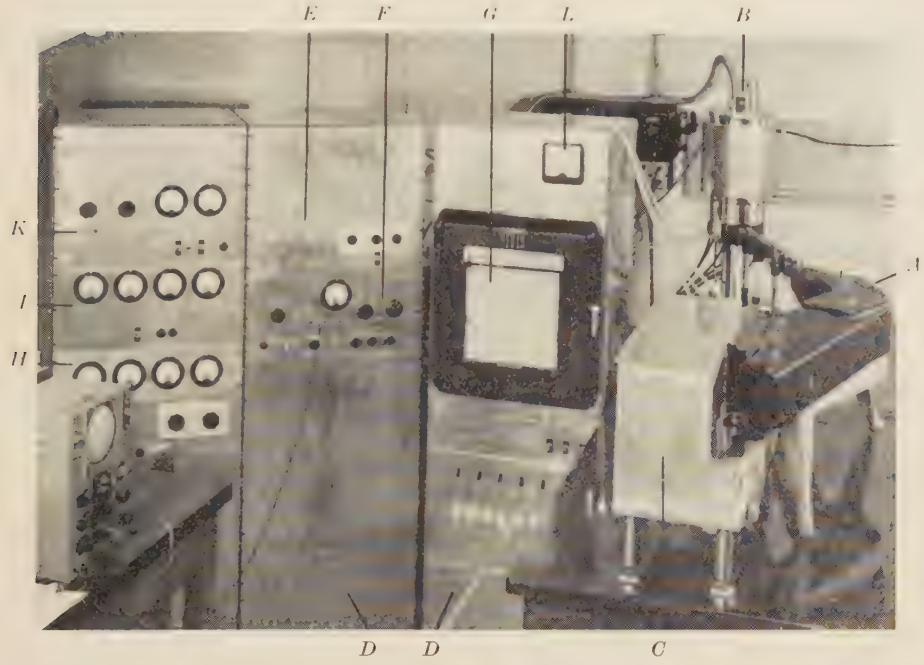

FIGURE 2. Total view of the raman spectrograph (*A* spectrograph, *B* lamp-house, *C* casing for scanning arrangement, *D* racks, *E* amplifier, *F* homodyne rectifier, *G* recorder, *H* high-tension supply, *I* anode-voltage supply, *K* filament-current supply, and *L* relay and flow meter).

F homodyne rectifier, *G* recorder, *H* high-tension supply, *I* anode-voltage supply, *K* filament-current supply, *L* relay and flow meter for the cooling water).

A detailed description of the raman spectrograph is given in the following sections. Those readers who are interested in the over-all properties of the instrument only, are referred to the section General Performance, p. 73.

The Light Source Unit

The light-source unit consists of mercury-vapour discharge lamps placed vertically in a lamp-house, in the centre of which is the raman tube surrounded by a filter jacket. An image of this tube is formed in the collimator aperture of the spectrograph by means of a condensing lens.

A. The Mercury Vapour Discharge Lamps

The excitation of raman spectra is mostly done by lines in the ultraviolet and visible part of the mercury spectrum. Here, strong, discrete lines are separated by almost line-free regions in which the raman spectrum can be studied without interference from foreign radiation. The weakness of the raman lines necessitates the use of excitation sources of very high intensity. This is especially important in the direct recording of raman spectra, because a light sensitive photo-cathode has not the accumulating properties of a photographic plate. Further, the spectrum of the source must not contain a continuous background which will disturbingly superimpose upon the raman spectrum to be observed.

Similar problems are met with, in another field of spectroscopy, namely, in the study of hyperfine structure by means of high resolution techniques, where light-sources producing very sharp lines of high intensity and of constant brilliancy are necessary. Owing to the great achievements in this field, sources are available giving lines of such a sharpness that it is difficult to find instruments capable of taking full advantage of them (*cf.* Tolansky (17)). In raman spectroscopy the requirements are not so exacting but many existing types of light-sources are far from ideal. With sensitive, photo-electric recording methods the availability of raman spectra is considerably enhanced. Consequently an increased interest in light-sources will follow.

a. The Visible Mercury Spectrum

The part of the mercury spectrum which is of interest in photo-electric recording of raman spectra extends from about 4000 Å to 6000 Å. In this region the spectral sensitivity of the antimony-cesium photo-cathode mostly used in modern photo-tubes is high. The spectrum above 6000 Å is of minor importance mainly because the intensity of the scattered light decreases rapidly with increasing wave-length. Furthermore the photo-tubes used in this region have a lower work-function of the photo-cathode material. This causes a decrease in sensitivity due to production of thermionic noise (*cf.* p. 47). The short wave-length part of the spectrum offers great advantages with regard to the intensity of the scattered radiation and to the

better resolution power of optical glasses in this region. Photo-tubes are also available which present a rather high sensitivity down to about 2000 Å. (Zworykin and Ramberg (18), Schwetzoff and Robin (19), Morrish, Williams and Darby (20)). However, ultraviolet radiation easily initiates chemical reactions. This causes trouble, especially, in work with unsaturated compounds. Also, fluorescence spectra can be excited. Even small amounts of foreign material can produce a fluorescence high enough to disturb the recording of the raman spectrum. The fluorescence radiation may also extend to the visible part of the spectrum, which necessitates filtering away of the ultraviolet light.

In the present case it was found most convenient to use the blue mercury line, λ 4358 Å, for excitation purposes.

In its normal state the mercury atom contains two electrons with a wave function in the P-shell. The atom can be excited by changing one, or both, of these valence electrons to a wave function of higher energy. The quantum state of the two electron systems is characterized by the quantum numbers L and S, corresponding to total angular momentum and resultant spin angular momentum respectively. The total resultant momentum is then characterized by the quantum number $J = L + S$ (LS-coupling). Since the contributions to the angular momenta from the closed shells are zero, the maximum value of S is one, *i.e.* the sum of the spin angular momenta of the two electrons, and the only other possible value is equal to zero, due to the integrally spacing of the S-values. Then we get two classes of LS-terms, singlet terms with $S = 0$ and triplet terms with $S = 1$ (multiplicity equal to $2S + 1$). Due to the inequality $|L - S| \leq J \leq |L + S|$, and the rule that J-values belonging to a LS-term are integrally spaced, the following singlet and triplet states are possible:

Singlets: $^1S_0$; $^1P_1$; $^1D_2$ . . .

Triplets: $^3S_1$; $^3P_0$; $^3P_1$; $^3P_2$; $^3D_1$; $^3D_2$; $^3D_3$ . . .

The ground state is a $^1S_0$ state. The three ^3P levels of the $6s6p$ configuration are metastable. Due to the weak LS-coupling in the mercury atom the transition $6s6p\ ^3P_1 \rightarrow 6s^2\ ^1S_0$ ($\Delta S = 0$) occurs and gives rise to λ 2537 Å, one of the most intense lines in the mercury spectrum. Inter-combination lines are very frequently obtained in mercury. It is also interesting to note that mercury atoms will accumulate in the states $6s6p\ ^3P_0$ and $6s6p\ ^3P_2$ because radiative jumps to $6s^2\ ^1S_0$ with $\Delta J = 0$ and $\Delta J = 2$ respectively are forbidden by the selection rules for J. As a consequence most of the radiative jumps producing lines in the ultraviolet and visible region will end in these metastable states. All of the most common transitions correspond to jumps of only one of the $6s$ electrons. Only a few levels ascribed to the $6p^2$ configuration have been discovered. Under certain conditions even lines from singly ionized mercury atoms can be obtained. In this case $S = {}^1/_2$, and consequently all terms are doublets except the ground term. The terms are:

$$^2S_{1/2};\ ^2P_{1/2};\ ^2P_{3/2};\ ^2D_{3/2};\ ^2D_{5/2}\ \ldots$$

The most important lines in the spectrum are: λ 4046.6 Å ($6p\ ^3P_0 \rightarrow 7s\ ^3S_1$); λ 4077.8 Å ($6p\ ^3P_1 \rightarrow 7s\ ^1S_0$); λ 4339.2 Å ($6p\ ^1P_1 \rightarrow 7d\ ^3D_2$); λ 4347.5 Å ($6p\ ^1P_1 \rightarrow 7d\ ^1D_2$); λ 4358.3 Å ($6p\ ^3P_1 \rightarrow 7s\ ^3S_1$); λ 4916.0 Å ($6p\ ^1P_1 \rightarrow 8s\ ^1S_0$); λ 5460.7 Å ($6p\ ^3P_2 \rightarrow 7s\ ^3S_1$); λ 5769.6 Å ($6p\ ^1P_1 \rightarrow 6d\ ^3D_2$); λ 5789.7 Å ($6p\ ^1P_1 \rightarrow 6d\ ^3D_1$) and λ 5790.7 Å ($6p\ ^1P_1 \rightarrow 6d\ ^1D_1$).

Many atomic spectra have a hyperfine structure of the spectral lines caused by the properties of the atomic nucleus. The influence of the nucleus is due to its mass and its spin. The mass (isotope) effect can, with heavy elements, be traced back to a change of nuclear radius with mass. The spin effect consists of an interaction between the angular momentum of the nucleus (quantum number I) and the resultant angular momentum of the electrons (quantum number J). This IJ-coupling is exactly analogous to the LS-coupling. The splitting of the lines is small and is of interest in this connection only because it contributes to the shape of the spectral lines. According to Görlich and Lau (21) the line λ 4358 Å consists of thirteen components, all of them falling in the region ± 1 cm.$^{-1}$ (0.2 Å) from the main line. A photo-electric record of the hyperfine structure of λ 4358 Å is reported by Glansholm and Kleman (22). This shows one central, main line of high intensity and four weaker lines, two on each side of the large one.

b. Spectral Characteristics of Some Lamps

As has been stated above it is very important to have a light-source giving an exciting line which is sharp, has a high intensity and a low background in the neighbourhood of the line. The suitability of available mercury lamps for spectrographic work varies considerably. This is to be expected since many of these lamps are mainly intended for illuminating purposes.

Information about the properties of various mercury lamps may be found in an investigation by Rank and McCartney (23). They have compared two commercial Westinghouse lamps type H-1 (at 400 and 530 W.) and type H-11 (at 75 W.) and two low-pressure mercury arcs (20 and 70 cm. in length respectively and 4 cm. in diameter) operated at different conditions. The background was measured at λ 4420 Å, λ 4392 Å and λ 4369 Å and was compared with the intensity of λ 4358 Å. At the same time the intensity of λ 4347 Å and λ 4339 Å was recorded. The results are summarized in Table 1. The background has been reduced to entrance and exit slits of 1 Å effective width and referred to unit intensity of λ 4358 Å.

The H-1 lamp had a very high background, also the lines were broad. The H-11 lamp had a low background but had other disadvantages: the lines had low intensity and the lamp contained a carrier gas. The low-pressure arcs showed very good properties even when a strong current was used. A pronounced change occurs in intensity of the weak mercury lines λ 4347 Å and λ 4339 Å with the operating conditions. Decrease of the current in the low-pressure arc influences the background slightly; the intensity of the weak lines, however, decreases with a factor of about three. This is of importance because the suppression of the intensity of these lines eliminates disturbing drabant raman lines.

Menzies and Skinner (24) report that underrunning of the lamps (General Electric Co., type MA/V 250 W.) gives a background in the wave-length region λ 4358–4916 Å considerably reduced relative to the line intensity. Later Menzies (4) has used lamps from the B.T.H. Company which contained a controlled amount of mercury. He does not specify the properties of these lamps, but judging from the

Table 1

Comparison of mercury lamps (from Rank and McCartney (23))

Lamps	Background × 10^5			Intensity		
	λ 4420 Å	λ 4392 Å	λ 4369 Å	λ 4358 Å	λ 4347 Å	λ 4339 Å
H-1 at 400 W.	53	94	640	1	0.046	0.016
H-1 at 530 W.	78	150	1000	1	0.059	0.020
H-11 at 75 W.	6.3	11.7	34	1	0.019	0.008
Low-pressure arc[1] 20 cm.						
at 110 W.	4.8	9.6	31	1	0.008	0.003
at 150 W.	5.8	10.0	30	1	0.011	0.004
at 260 W.	6.1	11.1	33	1	0.023	0.008
Low-pressure arc[2] 70 cm.				1	0.008	0.003

[1] Cathode water-cooled.

[2] Anode and cathode water-cooled.

reproduced spectra the background seems to be very low. The lamp gives a barium line, λ 4554 Å, emitted from the electrodes (Hilger and Watts Ltd., Catalogue CH 334).

Thompson *et al.* (12) remark that high-pressure mercury arcs such as the Osira lamps (General Electric Co., Ltd., England) are less satisfactory. They use a Hanovia lamp (Hanovia Chemical Manufacturing Co., U.S.A.) which has less continuous background and is free from foreign lines.

The Physics Department of the University of Toronto, Canada, has constructed a low-pressure mercury arc which is used by Heigl, Dudenbostel, Black and Wilson (16). They have compared it with a General Electric high-pressure arc, Model H-1, and found the Toronto type source superior both with respect to line intensity and continuous background radiation. No details of the comparison are given.

Kemp[1] (25) has discussed a lamp similar to the Toronto lamp with water-cooled condensers. At a condenser temperature of 20 °C. the intensity ratios λ 4358 Å/λ 4347 Å and λ 4358 Å/λ 4339 Å are 1 : 0.0062 and 1 : 0.0021 respectively; at 50 °C. temperature they increase to 1 : 0.0082 and 1 : 0.0024. The background at λ 4369 Å was less than $5 \cdot 10^{-4}$ of the λ 4358 Å intensity. These figures compare well with those given by Rank and McCartney (23).

As is obvious from the foregoing, the best light-sources are water-cooled *low*-pressure mercury arcs: extremely sharp lines can be obtained, the continuous background is low and the suppression of the singlet transitions is large. In some cases high-pressure mercury arcs have been used in connection with selective filters

[1] The author is very much indebted to Dr. Kemp, Applied Research Laboratories, U. S. A., for making a copy of his manuscript available before publication.

(Simon and Jentzsch (26)) mainly in order to get a higher intensity and thus a shorter exposure time.

In the present investigation the Philips HO-2000 high-pressure mercury lamps have been used. These lamps are similar to the Osram HgH lamp and the General Electric Osira lamp (*cf.* Uyterhoeven (27)) and have no ideal properties. A comparison with a low-pressure lamp has also confirmed this (p. 21). The working-pressure is about 1 atm. and the total luminous flux about 20 000 lm. In the following a short discussion will be given on the properties of this type of lamps.

c. The Properties of Mercury Vapour Discharge Lamps

The phenomena underlying the emission of light in a discharge lamp have been thoroughly studied and the knowledge of the nature of both low-pressure and high-pressure discharges is very good. The mechanisms are complicated and therefore only a very brief account of the general ideas can be given. For more complete information reference is made to the work of Uyterhoeven (27, 28). An exhaustive treatment of the high-pressure mercury vapour discharge is given by Elenbaas (29). A more elementary discussion of discharges in various gases is given by Heller (30). It should be noted that the work referred to here is mainly concerned with the construction of lamps for illuminating purposes; therefore the composition of the total luminous flux has been the main problem and not the structure of single spectral lines.

The Discharge. Elementary physics teaches that in the space between the cathode and the anode in a discharge, different regions can be distinguished. The most important of these are the positive column because, here, an excitation of the gas atoms occurs besides the transport of electricity. In the direction of the electrical field the electrons will gain an amount of energy from the field which, under steady state conditions, equals the loss in energy through elastic collisions, excitation and ionisation. The average energy per volume element will be the same throughout the column.

The distribution of electrons and positive ions in a cross-section of the discharge is of great importance. The potential in the cross-section is highest in the centre, and decreases towards the walls of the discharge tube as a consequence of a radial, ambipolar diffusion of charged particles to the wall. This will take a negative charge and hence attract the positive ions and repell the electrons. A steady state will be reached, and the space charge set up near the wall is responsible for the radial variation in potential. It can be shown that the concentration of both electrons and positive ions as well as the current density has a maximum in the centre of the discharge and then decreases towards the walls. This is of considerable importance, since most of the ionisation will take place in the centre. Then the ions formed on an average have a longer way in their move to the wall and can stay a longer time in the discharge. The number of positive ions necessary for space charge compensation is then reduced and, hence, also the energy used up in the ionisation. It is an empirical fact that the voltage over a discharge tube is low; this is possible only if the space-charge set up by the electrons in the direction of the tube is neutralized by the presence of positive ions.

With a high current density in the centre the importance of cumulative effects will be greater; with a high concentration of electrons the chance that an already excited atom will undergo ionisation through inelastic collisions with another electron will increase. Thus the energy of the electrons need not be at least equal to the ionisation energy but can have a lower value. Consequently the mean energy of the electrons can be chosen in such a way that the maximum of their Maxwellian velocity distribution better corresponds to the energy which is necessary for excitation of a certain energy level in the atoms. In this way the luminous flux per unit input energy will be the highest possible.

Especially in a gas of mercury atoms where the emission of visible light occurs as transitions between excited levels (*v. supra*), conditions favouring cumulative effects must be very desirable. Therefore the current distribution mentioned above is favourable in the case of mercury; but not in the case of, for instance, sodium, where the luminous flux mainly consists of resonance radiation. With a high current density, the chance of a transition to the ground state is reduced and consequently under these conditions a sodium lamp will have a lower efficiency. In mercury the cumulative effects will be still more favoured by the fact that the $6p\ ^3P_{0,2}$ levels are metastable and the $6p\ ^3P_1$ level is a resonance level. As was mentioned earlier, atoms will accumulate in the $6p\ ^3P_0$ and $6p\ ^3P_2$ levels, because radiative jumps to the ground state are forbidden. Return to this state will mostly occur by collisions of the second kind. A consequence of this will be that the half-lives of the metastable states will be great (about 10^{-4} sec.) and therefore the excited atoms will have every chance of undergoing further excitations. The resonance radiation will very soon be absorbed by neutral atoms, emitted again, absorbed, and so on, several thousand times before the light quanta leave the discharge.[1] A direct consequence will be that the resonance level will have a high apparent half-life (about 10^{-4} sec. compared to 10^{-8} sec. for a single event) and the chance of an excitation to a higher level is, therefore, enhanced. With a lower average energy of the electrons the excitation of the singlet levels will be more improbable.

One drawback in connection with discharges in low-pressure mercury gas is the high mean free path of the electrons, about 5 cm. The electrons will frequently strike the tube wall; the number of collisions with mercury atoms is low and excitation a rare event. In lamps used for illuminating purpose the luminous flux is increased by adding a rare gas (mostly argon), when the mercury atoms will undergo more inelastic collisions. There is no — or only an insignificant — excitation of the rare gas atoms because the necessary excitation energy is much higher than for mercury. In making lamps for raman spectroscopy this technique should be avoided. Instead, the number of collisions may be increased by using a larger tube diameter.

The luminous efficiency of mercury discharge lamps, *i.e.* the amount of input energy transformed into visible light (measured as lumens per watt), depends upon the mercury pressure. At low pressures ($< 10^{-3}$ cm. Hg) the efficiency is low because the conditions favour the production of the resonance lines (λ 2537 Å, $6p\ ^3P_1 \rightarrow 6s\ ^1S_0$, and λ 1850 Å, $6p\ ^1P_1 \rightarrow 6s\ ^1S_0$). With increasing pressure the imprisonment of the resonance radiation causes a larger population of the higher levels and in accordance with the discussion above, the luminous flux will be larger. At a pressure of about 10^{-2} cm. Hg the luminous efficiency passes through a maximum. A further increase of pressure makes elastic

[1] This phenomenon of imprisonment has been studied by Holstein (31–33). He introduces an escape factor which is defined as the reciprocal of the number of emissions and absorptions of an individual unit of atomic excitation prior to its escape from the enclosure. The escape factor depends upon vapour density, enclosure geometry and shape of the resonance line.

collisions more frequent, and consequently the dissipation of energy by thermal conduction becomes important. The temperature of the gas starts to rise and at a still higher pressure (10^{-1} – 1 cm. Hg), temperature radiation sets in. Now the discharge has completely changed character and the typical high-pressure discharge begun. Eventually this means a higher luminous efficiency and, as regards spectral characteristic, broader lines and a continuous background radiation. At the same time the luminous flux "moves" towards higher wave-lengths, *i.e.* the intensity of the yellow and red mercury lines increases considerably. The discrete spectrum disappears completely at a sufficiently high pressure (about 200 atm.). The set in of the high-pressure discharge is distinctly noticeable. At low pressures the discharge fills the total cross-section of the tube; at higher pressures it starts to contract towards the axis of the tube. Finally an annular dark space forms between the discharge and the tube wall. The contraction is a consequence of the radial temperature gradient set up in the tube. The population of the higher levels in the atoms will thus decrease with the decreasing temperature (*cf.* Elenbaas, (29)).

Finally, a few remarks will be made about the continuous spectrum associated with the discharge (Elenbaas, (29), and Borchert (34)). There are two explanations for this phenomenon. (The pressure broadening of the spectral lines and the continuous spectrum in the neighbourhood of resonance lines are not discussed.) Firstly, it may be due to recombination of electrons with positive ions and secondly, it can be caused by collisions of an excited atom with a normal atom. In the first case the continuum will increase proportionally to the pressure, in the second case proportionally to the square of the pressure. The intensity of the spectral lines is proportional to the pressure and thus in the first case the line-to-background intensity-ratio should be constant, in the second case decreasing with the pressure. Experimental data indicate that both processes are conceivable explanations.

Structure of Spectral Lines. The preceding discussion was mainly concerned with the production of spectral lines in a discharge lamp. Another important question is the influence of the conditions prevailing in the lamp upon the shape of the spectral lines. To begin with it should be stated that due to the Heisenberg uncertainty principle, the accuracy, ΔE, with which an energy level of an atomic system can be defined within a limited time of observation, Δt, is determined by the expression

$$\Delta E \, \Delta t = h/2\pi \tag{1}$$

Let $\Delta \nu$ be the change in frequency corresponding to the uncertainty in energy, then $\Delta E = h \, \Delta \nu$. Furthermore Δt corresponds to the life time of an excited state, which is related to the total transition probability per unit time, γ. Thus in the simplest case the natural line half-width, $\Delta \nu$, is proportional to γ (*cf.* Heitler (35)). This effect is due to the emission of radiation itself and is therefore fundamentally unavoidable. There are, however, several other effects which influence the structure of a spectral line. A detailed discussion of this is given by Tolansky (17) and therefore only the more important aspects will be elucidated here.

Due to the movement of the atoms relative to the observer of the emitted light a displacement (Doppler effect) in the observed frequencies will occur. As the effect from all possible velocities will contribute at the same time the emitted line will appear broadened and have the shape of a probability distribution curve. Due to this effect the half-width of the mercury line λ 4358 Å at a temperature of 6000 °K. would be 0.3 cm.$^{-1}$, compared to a natural half-width of about 0.001 cm.$^{-1}$. At large distance from the central frequency the Doppler width is negligible compared to the natural width because the latter decreases only as $1/(\Delta \nu)^2$.

Perturbations of the energy levels in an atom can arise from several causes. The type of forces in action depends upon the nature of the perturbing particle. A neutral particle of a kind differing from the emitter itself acts through van der Waals forces (collision broadening). When the particle is of the same kind as the emitter itself, resonance (exchange) forces operate (resonance broadening). Further ions, electrons or particles with permanent dipoles may interact through Coulomb forces (Stark broadening, inter-atomic Stark broadening). The broadening of spectral lines by these perturbations can be very large especially in the case of resonance broadening. Half-widths a hundred times larger than those obtained in collision broadening can often occur. The order of magnitude of the width is 0.5 cm.$^{-1}$ at a pressure of 1 cm. Hg. To reduce the resonance broadening it is very important to keep the pressure of the emitting gas low. In extreme cases it should be present only as an impurity in the discharge maintained by a foreign gas (helium or argon). The Stark broadenings occur when the emitter is suffering Stark displacements of continuously variable magnitudes, mainly as a result of a non-uniform electric field set up in the discharge or of varying electric fields from charged particles. The effect is not very great for mercury (second order Stark effect) but high current densities may even in this case produce a noticeable effect. Ishida and Hiyama (36) have measured the Stark effect of mercury and found, at an electric field strength of 560 kV./cm., a displacement of -1.6 cm.$^{-1}$ for the λ 4358 Å line. The other lines generally showed larger displacements.

Experimental data on the actual structure of spectral lines from mercury-vapour discharge lamps are very scarce. Rompe and Schultz (37, *cf.* 38) have given the following half-widths of lines from a high-pressure lamp at 5850 °K. and a density of $1.54 \cdot 10^{20}$ atoms per cm.^{3} (about 120 atm.): λ 4916 Å 34 cm.$^{-1}$ (8.2 Å); λ 5770 Å and λ 5791 Å both 63 cm.$^{-1}$ (21.0 Å). Blet (39) has found that the width of λ 5461 Å in a high-pressure lamp increases from 0.5 Å (1.7 cm.$^{-1}$) at 50 V. to 2 Å (6.8 cm.$^{-1}$) at 110 V. running voltages. He has also studied the profile of the lines and reports a reversal of most of them (λ 4358 Å included). This is due to the fact that the absorption in the colder parts of the discharge is a maximum at the centre wave-length (there may always be a sufficient amount of atoms present in different atomic states to ensure absorption not of the resonance lines alone; the effect is of course largest for the latter ones). The absorption produces an increase in the half-width of the lines which is proportional to the square root of the number of molecules in the line of sight. A spurious structure can be produced at high densities of the absorbing layer. The centre of the line will be relatively more absorbed than the line wings until complete self-reversal sets in, when a spurious doublet is produced. (This effect has occasioned reports of many false structures; for example it has been stated that the resonance line of mercury, λ 2537 Å, should consist of twenty-five components (*cf.* Tolansky (17)), and further, these spurious lines may interfere in the interpretation of Brillouin spectra (Kastha (40).)

In summing-up it can be stated that all the broadening effects discussed will more or less influence the shape of the spectral lines from a mercury-vapour discharge lamp. The amount of broadening which can be tolerated depends upon the resolving power of the optical instrument and, to a certain extent, on the lowest intensity which can be used. In raman spectroscopy it is impossible to use a sufficiently low intensity to reduce the broadening effects to a negligible amount and these effects must therefore be taken into due account.

Finally it should be added that the raman lines themselves may be broader than might be expected with regard to the width of the exciting line. This is due to unresolved rotation-vibration bands. A similar broadening of the recorded exciting-line itself occurs

Table 2

Influence of operation conditions on luminous flux

Supply voltage	Current	Intensity			Background
		λ 4358 Å	λ 4358 Å/λ 4347 Å	λ 4347 Å/λ 4339 Å	
86	71	77	83	100	73
100	100	100	100	100	100
110	120	120	106	100	122

in all cases where the molecules show a rotation raman spectrum. The presence of Brillouin spectra (*cf.* Brillouin (41), Gross (42), and Rank, McCartney and Szasz (43)) must also be taken into account at high-resolution work.

Luminous Flux and Operation Conditions of Lamps. The operating conditions of a discharge lamp can be varied to a certain extent. Such variations influence the total luminous flux. An increase in the supply voltage will increase the current and consequently also the luminous flux. Table 2 gives some data obtained for the Philips HO-2000 lamps. All values are given in per cent of the normal values (voltage 220 V., current 3.7 A.). The intensity of the lines is measured as the maximum height. The background is recorded where the decrease of the intensity of the λ 4358 Å line ceases. Evidently current, λ 4358 Å intensity and background follow each other closely. Thus the line-to-background intensity-ratio is substantially constant. These results are not in conformance with the findings of Menzies and Skinner (24). The intensity ratio λ 4358 Å/λ 4347 Å has at 220 V. a value of about 7.5 and λ 4347 Å/λ 4339 Å the value 2.6. The time required for the lamp to reach full intensity decreases with increasing supply voltage. — Uyterhoeven (27) has given similar data for a HO-1000 lamp. The change in current is approximately the same as found here. He gives a variation of the total luminous flux which is somewhat higher than the variation found here for single lines.

The sensitivity of the luminous flux to variations in supply voltage makes it necessary to use a stabilized supply. A variation of one per cent gives about one and a half per cent variation in intensity. In accurate measurements, therefore, variations of the input voltage not larger than a fraction of a per cent can be allowed. In the present case a voltage stable to about one per cent was used.

Some experiments were also made to run the lamps under heavy cooling. This was done mainly in order to study the change in background radiation. A lamp was placed upside down in a bottle containing circulating tap-water (temperature about 12 °C.) and ignited. No steady operation could be reached. From time to time concentrated parts of the discharge slowly moved from the upper to the lower electrode ("fire-balls"). Better results were obtained when the outer glass envelope was removed and the lamp cooled by blowing with a fan. In this way the intensity

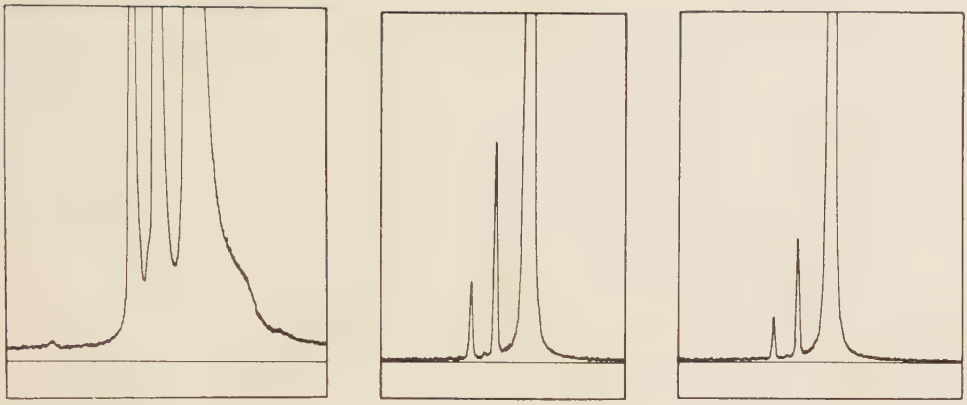

a b c

FIGURE 3. Comparison of the blue mercury lines of different lamps. The ratio of the λ 4358 Å intensities is 1 : 0.88 : 0.94. a) HO-2000, normal operation; b) HO-2000, cooled; c) 93123 E.

of the lamp (measured on the line λ 4358 Å) decreased about ten times but the line-to-background intensity ratio increased. At the same time a change from the contracted, typical high-pressure discharge to a more low-pressure-like phenomenon occurred. When the fan was stopped the discharge immediately started to contract and had, after some minutes, reached full intensity.

A comparison of the spectral characteristics of the HO-2000 lamp run under the conditions described and of a low-pressure mercury lamp (Philips 93123 E; *cf.* ELENBAAS and RIEMENS (44)) has been made. The results are given in Table 3 and in Figure 3. Evidently a considerable improvement can be obtained. Cooling of the HO-2000 lamp makes it a good light-source for raman spectroscopy.

Distribution of Luminous Flux at Alternating Current Operation. The description previously given about the phenomena occurring in a mercury discharge is valid when a direct current is applied. No theory about the positive column at alternating-current

TABLE 3

Comparison of mercury discharge lamps

Lamps	Voltage over the discharge. V.	Current through the discharge. A.	Intensity			Background at λ 4400 Å
			λ 4358 Å	λ 4347 Å	λ 4339 Å	
93123 E	—	—	1	0.0054	0.0020	$6.6 \cdot 10^{-5}$
HO-2000 (cooled with a fan)	22	5.7	1	0.0087	0.0033	$11.6 \cdot 10^{-5}$
HO-2000 (normal operation)	145	3.7	1	0.094	0.035	$83 \cdot 10^{-5}$

operation is worked out; *cf.* UYTERHOEVEN (27). Probably rather complicated conditions prevail and no contribution to this problem will be given here. However, it is of considerable importance with respect to the recording system used to know the distribution of luminous flux during each cycle. A treatment of the electrical behaviour of a discharge lamp is given by DORGELO (45) and by UYTERHOEVEN (27).

An estimation of the amount of harmonics contained in the luminous flux is found in an investigation on flickering by BOUMA (46). He has studied the distribution of light during one half-cycle for different, alternating-current operated lamps. For the HO-type lamp (HO-1000) he gives the following Fourier expansion

$$I = \bar{I}[1 + 0.750 \sin(2\omega t + \varphi_1) + 0.021 \sin(4\omega t + \varphi_2) + 0.017 \sin(6\omega t + \varphi_3) + \cdots] \qquad (2)$$

where I is the intensity, $\bar{I}$ the average intensity and φ phase angles. The main components are the two first. All the others are small. Due to the large "direct-current" component a considerable amount of the luminous energy is never utilized with the detection system used here. Only at a direct-current operation of the lamps, and with a direct-current amplifier in the detection system can full advantage be taken of the lamps. On the other hand this arrangement has definite other disadvantages.

d. The Lamp Circuit

Almost every gas discharge lamp shows a negative characteristic, *i.e.* when the current increases the voltage over the discharge tube will decrease. In order to stabilize such a discharge it is necessary to use a current-limiting device in series with the lamp. At alternating-current operation a choke is very convenient (UYTERHOEVEN (27)) and also very advantageous with regard to the re-ignition of the lamp each half-cycle. Due to the inductance of the choke the current will have a phase-lag with respect to the supply voltage. At the moment when the lamp is going to re-ignite, both the current, i, and the differential coefficient, $\mathrm{d}i/\mathrm{d}t$, are zero, and

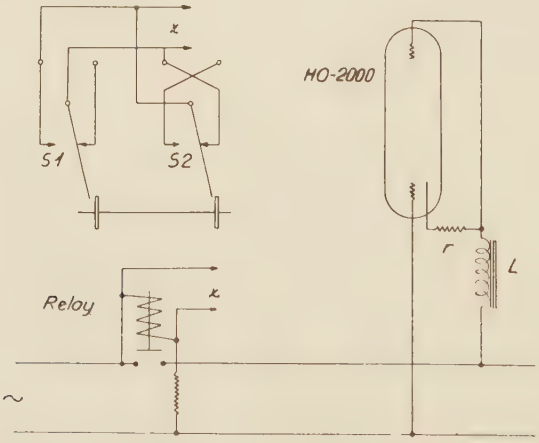

FIGURE 4. Wiring diagram of the lamp circuit.

hence the total momentary value of the supply voltage is available for the ignition of the discharge. Even at the extinction-moment the choke has a beneficial effect. The voltage of the tube rises and prevents the current from being zero before the end of the half-cycle. Thus the residual ionisation will be large and will make re-ignition easier.

The wiring diagram of the lamp-circuit is given in Figure 4. The third electrode in the lamp is an auxiliary electrode necessary for the ignition of the cold lamp. The resistance, r, on some ten thousand ohms is contained in the lamp envelope. The relay is connected to the switches S 1 and S 2 of a Flowtrol unit (Type FSM-1, W. Edwards and Co., London). The switches are operated by the cooling water for the lamp-house (*v. infra*) in such a way that switch S 1 shortens the coil in the relay at over-high flow-rates and the switch S 2 at over-low rates. Then the lamp passes current only when the water flows at a rate within a maximum and a minimum value.

B. The Lamp House

a. General

The requirements which the lamp-house has to fulfil are the following: firstly, the largest possible amount of light energy has to be sent from the lamps to the raman tube, secondly, it must provide possibilities for the use of different types of filters, including polarizers, and thirdly, the lamp-house and the attached condensing lens system must send a maximum of scattered radiation and a minimum of stray radiation into the spectrograph.

The original lamp-house used by the present author and Traynard (11) contained cylindrical lenses between the lamp and the raman tube (B, A, and C' respectively in Figure 5). These lenses concentrated the luminous flux in the tube. A calculation of the total luminous flux entering the tube in this case and in a case where the raman tube was placed at C'' (the light bundle from the lamp has the same angular aperture, α, in the horizontal plane but a larger aperture, $\beta'' > \beta'$, in the vertical plane) showed that in the last case about 80 per cent more luminous energy was sent into the tube. Further, the dimensions of the lamp-house could be smaller: the distance between the lamps and the raman tube decreased from 25 cm. to 7 cm.

As has already been pointed out, it is very important when working with photoelectric recording systems to reduce the loss of light energy as far as possible. In photographic work such losses can be compensated by increasing the exposure time. Further, low-pressure mercury lamps have not the same intrinsic brilliancy as high-pressure lamps and therefore the methods for sample illumination must depend upon the total flux-output of the source if the most effective use is to be made of the former. This necessitates the use of very efficient reflectors behind

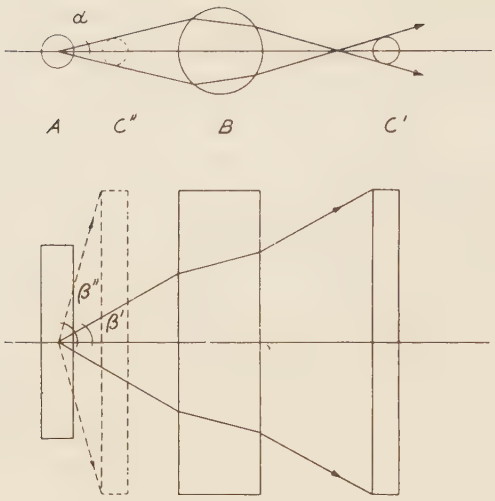

FIGURE 5. Different arrangements to illuminate the raman tube. (A lamp; B cylindrical lens; C', C'' raman tube.)

the lamps. MENZIES and SKINNER (24) have used reflectors coated with magnesium oxide. CARR and ZIMM (47) have shown that the diffuse reflection from such a surface follows Lambert's "cosine law" with only very small deviations. The reflectivity is high: about 0.97–0.98 at λ 4358 Å (*cf.* also HARRISON (48), and BENFORD, LLOYD, and SCHWARZ (49, 50)). This means that between 75 to 100 reflections can be made before the intensity drops below 10 per cent of the original value. After a large number of reflections the total amount of light energy in the lamp-house is approximately $1/(1-q)$ times that originally emitted from the lamps (q is the reflectivity). Evidently an increase of the reflectivity to values near to one gives quite considerable improvements. MENZIES and SKINNER (24) have shown that the use of a diffuse reflector of this kind is superior to any system using specular reflection. CARR and ZIMM (47) report a slight polarization of the diffuse light.

This method of sample illumination will, however, introduce a considerable convergence error when making depolarization measurements. The system can be used for precise measurements if a series of baffles are used to render the incident light strictly perpendicular to the direction of observation (EDSALL and WILSON (51)), and then using polaroid cylinders to polarize the light in any desired direction (*cf.* CRAWFORD and HORWITZ (52) and DOUGLAS and RANK (53)). However, the baffles imply a considerable reduction in the efficiency of the diffuse reflector. To overcome these difficulties RANK and KAGARISE (54) have suggested the use of an empirical correction for the convergence error. This method is, in principle, a determination of the average angle, θ, between the incident light on the scattering tube and planes perpendicular to the direction of observation. RANK and KAGARISE

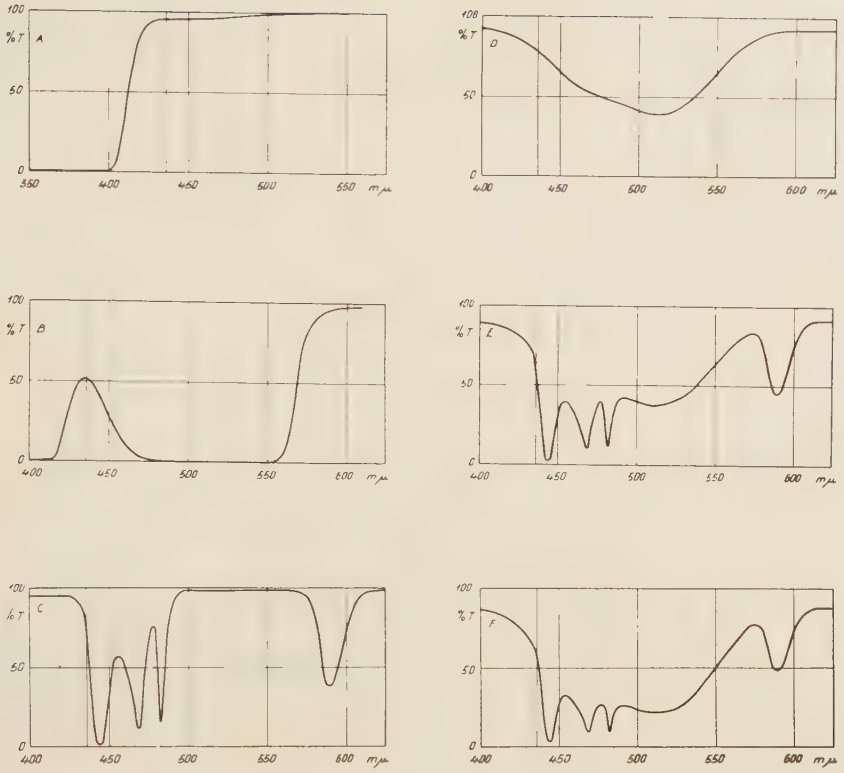

FIGURE 6. Transmission of liquid filters used in raman spectroscopy. A) 90 g. of sodiumnitrite in 250 ml. of distilled water. B) 13 g. of *p*-nitrotoluene, 0.01 g. of Rhodamine 5GDN Extra and ethanol to 100 ml. C) Equal volumes of concentrated praseodymium nitrate solution and distilled water. D) 2.5 g. of cobaltous nitrate and distilled water to 100 ml. E) 3 vols. of concentrated praseodymium nitrate solution and 5 vols. of a 4 per cent cobaltous nitrate solution. F) 3 vols. of concentrated praseodymium nitrate solution and 5 vols. of an 8 per cent cobaltous nitrate solution. The position of λ 4358 Å indicated. Slit width used 0.04 mm.

have shown that the following relation between the observed depolarization factor, ϱ_0, and the true one, ϱ_t, is approximately valid:

$$\varrho_0 = \varrho_t \cos \theta + \sin \theta \tag{3}$$

A plot of ϱ_0 against ϱ_t for a given experimental arrangement for raman lines with known values on ϱ_t enables determination of ϱ_t even for other lines. RANK and KAGARISE have experimentally verified Equation (3).

In most cases it is very advantageous to use filters of various types. The purpose may be the elimination of unwanted parts of the mercury spectrum, the isolation of single lines or the reduction of the continuous background. Liquid filters are mostly used. Several recipes may be found in the literature (for a review *cf.* OTTING

(55)). For the present investigation three types of filters were prepared: a sodium nitrite solution to prevent excitation from the lines λ 4047 Å and λ 4078 Å and to minimize the action of the ultraviolet light, a solution of *p*-nitrotoluene and Rhodamine 5 GDN Extra in ethanol to isolate λ 4358 Å and finally a praseodymium nitrate–cobaltous nitrate solution to diminish the background for wave-lengths longer than λ 4358 Å. The transmissions of these filters in 1 cm. layers are shown in Figure 6, where complete recipes are also given. The measurements were made with a Beckman Model DU Quartz Spectrophotometer. Generally the sodium nitrite filter was used, since the raman lines excited by the lines λ 4047 Å and λ 4078 Å very much disturbed the measurements.

b. Construction

The details of the lamp-house are given in Figure 7.

Six mercury lamps (1) are arranged symmetrically around a raman tube (2). This has the shape of a test tube with a plane bottom and is made of fused silica glass. The lamps are supported by sockets (3) placed on cylindrical pieces (4) of heat resistant bakelite. These pieces are placed in the bottom of cylindrical cups (5) attached to a plate (6) with double bottoms. This plate is mounted on a cylinder (7) and constitutes the support of a water jacket (8). In the upper part of the jacket are six tubes (9) which give the lamps their correct vertical position. A toroidal enclosure (10) placed on the tubes distributes over the lamps a stream of air from a compressor. The air then escapes through holes in the cups (5). In the centre of the upper part of the water jacket is a large hole which supports a holder (11) for a filter jacket (12). The holder has a collar (13) in the middle securing the raman tube in a vertical position. The lower end of the tube slides into a collar (14) in the cylinder (7). The water cooling system has an inlet (15) in the plate (6) and an outlet (16) from the holder (11). During its passage through the bottom plate and the water jacket, the tap-water becomes sufficiently warmed-up to prevent fogging of the filter jacket by condensation of water vapour from the air.

The inner walls of the lamp-house are coated with a white lacquer. A layer of smoked magnesium oxide could not be used because of the streaming air in the lamp-house.

In the lower end of the cylinder (7) is a conical hole which fits to a standard (17) placed on a box (18). A plug (19) adjusts the position of a diaphragm (20) in the cylinder in relation to diaphragms (21) in the standard (17). The box (18) is connected to a tube (22) which, through a ring (23), rests on the foot of the lamp-house. The foot consists of a bottom plate (24) with an optical bench (25) in the middle and two side-pieces (26). On these a plate (27) rests with a tube (28) supporting the tube (22). Underneath, the plate (27) has a carriage (not visible in the figure) placed on the optical bench and giving the lamp-house its correct lateral position. A small

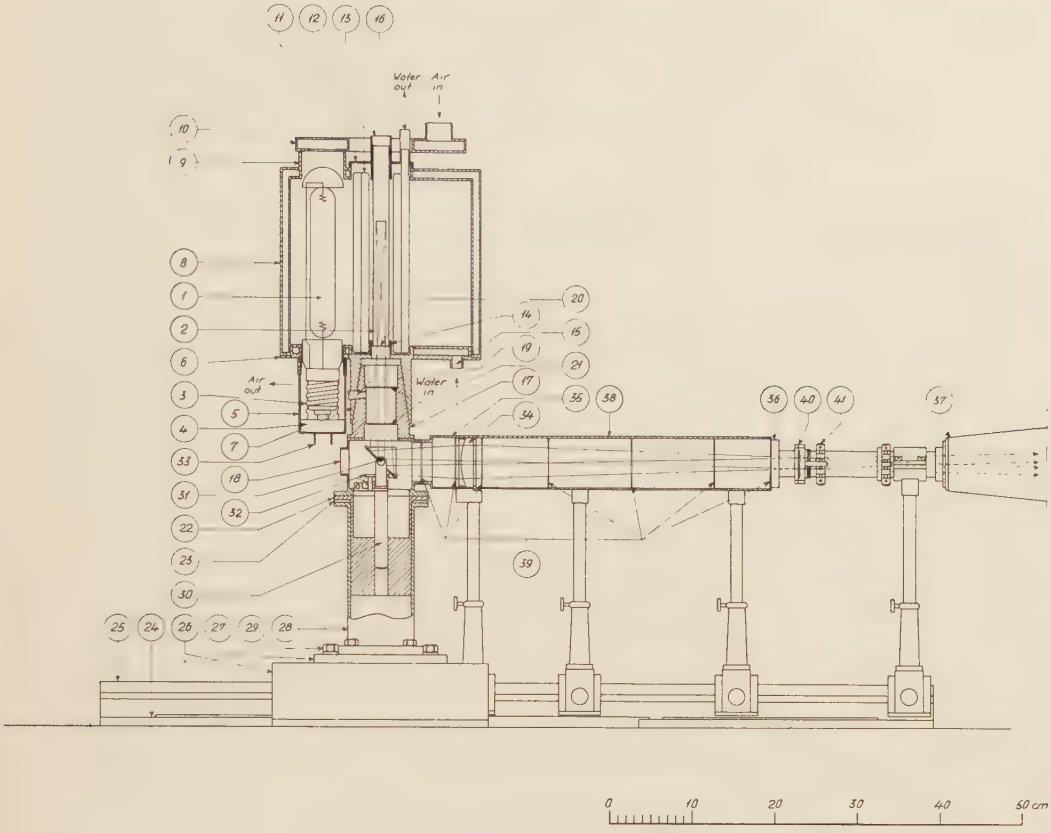

FIGURE 7. Construction of the lamp-house.

play (less than 0.1 mm.) between the side-pieces (26) and the plate (27) makes it possible to fix the carriage firmly to the optical bench by means of the screws (29).

The tube (22) has a hole in its lower end for the support (30) of a total reflecting prism (31). The position of the prism can be adjusted both in the horizontal and the vertical planes by means of the screws (32). Further, the prism with its support can be moved down into the tube (22) making possible the use of a light-source placed on the optical bench behind the lamp-house. To the box (18) is attached the condensing lens system (*v. infra*).

The filter jacket (12) is made of pyrex glass and contains two compartments, the outer one for cooling water and the inner one for filter liquids. With this arrangement both the liquid in the raman tube and the filter liquid are protected from the heat produced by the lamps.

There is sufficient space between the raman tube and the filter jacket to permit the introduction of polaroid cylinders.

Electrical connections to the lamps can be made from male plugs (33) in the bottom of the cups (5).

The adjustable orifice unit of the Flowtrol unit in the lamp circuit (p. 23) is placed on the inlet side of the water-cooling system (the unit is not shown in the figure).

C. The Condensing Lens System

In raman spectroscopy the light-source can have considerable extension along the optical axis of the collimating system of the spectrograph. Therefore certain problems arise as to the most efficient way of arranging the illumination of the entrance slit in the spectrograph. These problems have been discussed by NIELSEN (56) and by SLYUSAREV and CHULANOVSKY (57) for a non-absorbing light-source. DONZELOT and BARRIOL (58) have given a brief treatment to this problem, taking the absorption into account.

a. Maximum Illumination Condition

NIELSEN has calculated the amount of luminous energy which can be sent into a spectrograph from a light-source having a cross-section sufficiently large to cover the collimator aperture. He finds that the amount of luminous energy, F, in a case when a condensing lens is not used is proportional to the longitudinal extension of the light-source and independent of its position:

$$F = B \frac{8\,a\,b}{f^2} \delta s\,(z_2 - z_1) \tag{4}$$

Here B is the amount of radiation emitted equally in all directions in unit time by unit volume of the source and by unit solid angle, z_2 and z_1 are the distances of the ends of the light-source from the spectrograph slit, $2\,\delta$ is the width and $2\,s$ the height of the slit, $2\,a$ is the width and $2\,b$ the height of the parallel beam of light which enters the spectrograph prism, f is the focal distance of the collimator lens. When using a condensing lens the same amount of luminous energy will enter the spectrograph, presupposing that the condensing lens is large enough to cover the collimator aperture and the lateral extension of the light-source is sufficiently large. The merit of NIELSEN is to have shown that with a source of limited cross-section, the use of a condensing lens can considerably increase the length of the light-source which can be efficiently utilized. This length depends upon the focal distance, f_0, of the condensing lens. The most favourable value is $f_0 = h\,f/(b - s)$ ($2\,h$ is the height of the light-source cross-section), which corresponds to a length of the light-source of $h^2\,f/s\,b$. This is $h^2(b + s)/s\,(h - s)\,b$ times the length of the longest source which can be efficiently utilized when no condensing lens is used. The image of the

light-source is formed between the entrance slit and the collimator lens. These conditions will send the maximum amount of luminous energy into the spectrograph without any false light from the walls of the light-source.

NIELSEN's treatment applies to a light-source having a rectangular cross-section. In most cases, the light-sources have a circular cross-section, and then the formulae of NIELSEN do not immediately give the conditions to be desired. The calculations are also in the circular case a straightforward application of the simple lens formula. Only the results are given; principally these are the same as those of NIELSEN. The following new notations are used:

R the radius of the cross-section of the light-source.

z_0 the distance from the spectrograph slit to the condensing lens.

z' the distance from the spectrograph slit of the image of that cross-section of the light-source which is nearest to the condensing lens.

z'' the distance from the spectrograph slit of the image of that cross-section of the light-source which is farthest away from the condensing lens.

z the distance from the spectrograph slit of the image of any other cross-section of that part of the light source which can be efficiently utilized.

l_{max} maximum length of the light-source in a certain case.

$R_0 = \sqrt{a^2 + b^2}$ the effective radius of the collimator lens.

All the distances z are positive in the direction of the condensing lens.
Then the following data are valid (calculation of case III, *cf.* p. 31):

Case I.

$$f_0 \leq f_1 = \frac{R}{R+s} z_0; \tag{5}$$

$$z_0 = \frac{\sqrt{R^2(b+s)^2 + a^2(R^2 - s^2)} - s(b+s)}{(b+s)^2 + a^2} f; \tag{6}$$

$$l^I_{max} = \frac{R+s}{s} f_1; \tag{7}$$

$$z' = z_0;$$

$$z'' = 0.$$

Extension of image of light-source: $+\infty \geq z \geq z_0$;

$$0 \geq z \geq -\infty.$$

Case II.

$$f_1 \leq f_0 \leq f_2 = \frac{R}{\sqrt{(b+s)^2+a^2}}\, f; \tag{8}$$

Subcase II′:

$$R > R^* = \frac{R_0 s}{R_0^2 - s^2}\sqrt{(b+s)^2+a^2}; \tag{9}$$

$$z_0 = \frac{R+s}{R}\, f_2; \tag{10}$$

$$l_{\max}^{II'} = \frac{R}{s}\, f_2; \tag{11}$$

$$z' = -\infty;$$

$$z'' = 0.$$

Extension of image of light-source: $0 \geq z \geq -\infty$.

Subcase II″:

$$R^* \geq R > s; \tag{12}$$

$$z_0 = \frac{\sqrt{R^2(b+s)^2 + a^2(R^2-s^2)} - s(b+s)}{(b+s)^2+a^2}\, f; \tag{13}$$

$$l_{\max}^{II''} = \frac{R}{R_0}\,(z_0+f); \qquad f_0 = f_2; \tag{14}$$

$$z' = z_0;$$

$$z'' = -f.$$

Extension of image of light-source: $+\infty \geq z \geq z_0$;

$$-f \geq z > -\infty.$$

Case III.

$$f_2 \leq f_0 \leq f_3 = \frac{R}{R_0 - s}\, f; \tag{15}$$

$$z_0 = \frac{R+s}{R}\, f_3; \tag{16}$$

$$l_{\max}^{III} = \frac{R(R_0-s)}{R_0 s}\, f_3; \tag{17}$$

$$z' = -f;$$

$$z'' = 0.$$

Extension of image of light-source: $0 \geq z \geq -f$.

Case IV.

$$f_3 \leq f_0. \tag{18}$$

The maximum length corresponds to the length obtained in case III. The length decreases with increasing f_0 and eventually reaches a limiting value.

When $R > s$ it is found that

$$l_{\max}^{III} > l_{\max}^{II''} > l_{\max}^{II'} > l_{\max}^{I} > l_0, \tag{19}$$

where

$$l_0 = \frac{\sqrt{R^2(b+s)^2 + a^2(R^2 - s^2)} - s(b+s)}{(b+s)^2 + a^2} f \tag{20}$$

is the maximum length of the light-source which can be efficiently utilized when no condensing lens is used. Hence the most favourable conditions are obtained when the image of the light-source is placed between the slit and the collimator lens. This is completely in accordance with NIELSEN's result as it should be.

From a practical standpoint it may be advantageous to look at the problem from a somewhat different point of view. In most cases, both the length and the cross-section of the light-source are given. Then the question arises as to where the image of the light-source should be placed in order to make the height of the slit as large as possible (this treatment disregards the fact that the height of the slit may be limited for other reasons, for instance, the disadvantage of having curved spectral lines of large height in direct recording of spectra).

The real image of a cylindrical light-source obtained by means of a positive lens is a frustrum of a cone whose end-surface farthest away from the lens is the largest one. The radii of the end surfaces, R' and R'', are given by the expressions

$$R' = R\,\frac{z_0 - z'}{z_1 - z_0} = R\left(\frac{z_0 - z'}{f_0} - 1\right); \tag{21}$$

$$R'' = R\,\frac{z_0 - z''}{l + z_1 - z_0} = R\left(\frac{z_0 - z''}{f_0} - 1\right), \tag{22}$$

where z_1 is the distance between the slit and the end surface of the light-source facing on to the condensing lens, l is the length of the light-source. Let s and z_0 be chosen in such a way that the circle R'' will just embrace the collimator aperture between the slit and the condensing lens ($z_0 \geq z'' \geq 0$) and the circle R' embrace the aperture behind the collimator lens ($z' \leq -f$) then the following conditions for s have to be fulfilled:

$$\left(s + z''\frac{b+s}{f}\right)^2 + \left(z''\frac{a}{f}\right)^2 = R''^2; \tag{23}$$

$$\left(s + z'\frac{b+s}{f}\right)^2 + \left(z'\frac{a}{f}\right)^2 = R'^2. \tag{24}$$

Equations (21)–(24) constitute the same set of equations which must be used to calculate the values of the length when the height of the slit is kept constant. From these equations we get

$$F(s,\ l;\ z',\ z'') = -\frac{R'(z';\ s)\,R''(z'';\ s)}{z''-z'} - \frac{R^2}{l} = 0. \tag{25}$$

To determine the largest values of s and l we need the following differential coefficients

$$\frac{\partial s}{\partial z'} = -\frac{\partial F/\partial z'}{\partial F/\partial s};\qquad \frac{\partial s}{\partial z''} = -\frac{\partial F/\partial z''}{\partial F/\partial s};$$

$$\frac{\partial l}{\partial z'} = -\frac{\partial F/\partial z'}{\partial F/\partial l};\qquad \frac{\partial l}{\partial z''} = -\frac{\partial F/\partial z''}{\partial F/\partial l}.$$

Now we have

$$\frac{\partial F}{\partial l} = \left(\frac{R}{l}\right)^2 \quad \text{and} \quad \frac{\partial F}{\partial s} = \frac{R''\dfrac{\partial R'}{\partial s} + R'\dfrac{\partial R''}{\partial s}}{z''-z'}. \tag{26}$$

Both of these quantities are positive in the intervals for z' and z'' considered. Consequently the conditions which determine the maximum value of l will also determine that of s.

In continuing the calculation we get

$$\frac{\partial F}{\partial z'} = \frac{R''}{(z''-z')^2}\left[(z''-z')\frac{\partial R'}{\partial z'} + R'\right] = \frac{R''}{R'(z''-z')^2}\left[\left(s + z'\frac{b+s}{f}\right)\left(s + z''\frac{b-s}{f}\right) + \right.$$

$$\left. + \left(z'\frac{a}{f}\right)\left(z''\frac{a}{f}\right)\right]; \tag{27}$$

$$\frac{\partial F}{\partial z''} = \frac{R'}{(z''-z')^2}\left[(z''-z')\frac{\partial R''}{\partial z'} - R''\right] = \frac{R'}{R''(z''-z')^2}\left[\left(s + z'\frac{b+s}{f}\right)\left(s - z''\frac{b+s}{f}\right) - \right.$$

$$\left. + \left(z'\frac{a}{f}\right)\left(z''\frac{a}{f}\right)\right]. \tag{28}$$

When $z''>0$ and $z'<-f$ then $\partial F/\partial z'<0$ and $\partial F/\partial z''>0$; hence $\partial s/\partial z'$ and $\partial l/\partial z'>0$ and $\partial s/\partial z''$ and $\partial l/\partial z''<0$. Consequently the largest value of both s and l is obtained for $z''=0$ and $z'=-f$. Solving the equation $F(s,\ l;\ -f,\ 0)=0$ for l we get $l^{III}_{\max}$.

b. Influence of Refractive Index

In raman spectroscopy, the light-source contains a liquid with a certain refractive index, n'. Let l denote the geometrical length of the light-source and n'' the refractive

index of the surrounding medium, then the total flux of luminous energy through the entrance slit is given by

$$F = B\left(\frac{n''}{n'}\right)^2 \frac{8ab}{f^2}\,\delta s\, l, \tag{29}$$

where s for maximum conditions is obtained from

$$s = \frac{R^2 f}{R_0 l}\,\frac{n'}{n''}, \tag{30}$$

because, optically, the light-source now has the length $l(n''/n')$. Evidently it is not possible to arrange maximum conditions for more than one refractive index, *i.e.* for one liquid. Let us suppose that the cross-section of the light-source which corresponds to the length $l(n''/n_1')$ has been focused on the slit of the spectrograph. Then any cross-section corresponding to a length $l(n''/n_2')$ will be focused in a plane between the slit and the *collimator* lens if $n_2' > n_1'$, and in a plane between the slit and the *condensing* lens if $n_2' < n_1'$. The last case should be avoided because then false light will be sent into the spectrograph. Thus the light-source should be focused in the collimator aperture for the lowest refractive index, n_1', to be used. Then for any other refractive index, $n_2' > n_1'$, the distance $z'' < 0$ and the amount of luminous energy sent into the spectrograph

$$F = B\left(\frac{n''}{n_2'}\right)^2 \frac{8ab}{f^2}\,\delta s\, l. \tag{31}$$

This amount is dependent on the refractive index in two ways, firstly, through the quantity B and secondly, through the factor $1/n_2'^2$. When comparing intensities of scattered radiation it seems necessary to eliminate the influence of the second dependence by referring the data to the same refractive index basis.[1]

c. Influence of Absorption

A certain amount of the luminous energy scattered from the different volume elements of the liquid in the light-source will be dissipated as heat before it leaves the raman tube. This, of course, decreases the amount of luminous energy which can be utilized for observation. Absorption does not, in any other way, influence the maximum illuminating conditions. When the absorption is taken into account Equation (31) will be

$$F = B\left(\frac{n''}{n_2'}\right)^2 \frac{8ab}{f^2}\,\delta s\,\frac{1}{\varkappa}\,(1 - e^{-\varkappa l}), \tag{32}$$

where $\varkappa$ is the absorption coefficient. Mostly, however, the absorption is very low and can therefore be neglected.

[1] When the manuscript was ready for publication, it was noticed that Woodward and George (58 a) have arrived at the same conclusion.

d. Construction

The raman tube had a geometrical length of 200 mm. For a refractive index of $^4/_3$ this gives the optical length of 150 mm. The condensing lens was an achromatic doublet with a focal length of 194 mm. The following values are obtained:

distance between slit and condensing lens: 392 mm.
distance between light-source and condensing lens: 245 mm.
height of spectrograph slit, $2s$: 12.0 mm.
effective radius of light-source: 6.0 mm.

These data then constitute the best arrangement.

The construction of the condensing lens system is given in Figure 7 (p. 27). The condensing lens (34) is placed in a holder connected to the box (18) through a tube (35) and connected to a shutter (36) on the spectrograph (37) through tubes (38). A series of diaphragms (39) are placed between the lens, the box and the spectrograph respectively. These diaphragms correspond to the light bundle defined by the slit (40) and a square-shaped diaphragm (of the same size as the image of the diaphragm (20) formed by the condensing lens) in the collimator lens. The purpose of all the diaphragms is to prevent stray radiation from the lamp-house to reach the spectrograph.

The Spectrograph

The spectrograph used was a Hilger E 390 All-metal Glass Spectrograph. This contains one prism of rather small dimensions: the base is about 5 cm. The collimator lens has a diameter of about 4.9 cm. and a focal distance of about 60.5 cm. This gives a focal ratio of 12.4. The camera lens has a focal distance of about 54 cm. giving a focal ratio of 11.0. The instrument is therefore not so good for raman spectroscopy.

The entrance slit is unilateral and can be tilted (the screw (41) in Figure 7) in a plane perpendicular to the optical axis of the collimator lens. The height of the slit can be changed by means of a wedge-shaped diaphragm.

The inverse linear dispersion of the spectrograph has been measured to about 15 Å per mm. at λ 4358 Å.

For the photo-electric recording of spectra it was necessary to remove some parts from the camera-side of the spectrograph. However, the instrument could easily be changed over from photo-electric to photographic recording and *vice versa*.

The Recording Unit

The recording unit consists of three parts: one *mechanical*, which by means of a slit in the focal plane of the spectrograph selects the spectral lines to be recorded, one *optical*, which gives an image of the slit on the light sensitive cathode of the

photo-tube, *i.e.* passes to the cathode, with a minimum of losses, the luminous energy entering the slit, and one *electrical*, which amplifies the photo-current and transforms it into a deflection on a recording instrument.

A. Mechanical System

a. General

The requirements which the mechanical system has to fulfil are the following: firstly, the slit must be kept in the focal plane of the spectrograph for the whole wave-length range to be investigated (λ 4000–5500 Å), secondly, for each wave-length, the optical axis of the optical system of the recording unit must coincide with the central ray in the light bundle emerging from the camera lens of the spectrograph. The solution to this problem is made clear in Figure 8. The notations have the following meaning:

S_1 the entrance slit of the spectrograph;
S_2 the slit of the recording unit;
L_1 the collimator lens (only principal planes indicated);
L_2 the camera lens (only principal planes indicated);
L_3 and L_4 the lenses in the optical system of the recording unit (principal planes only indicated);
P the dispersing prism of the spectrograph;
PH the photo-tube;
$O_4 S_2 O_6$ the focal plane of the spectrograph;
$O_1 O_2$, $O_1 O_4$ and $O_1 O_6$ indicate three light bundles of different wave-lengths (the dispersion of these bundles in the prism and to the left of the lens L_2 is not shown in the figure).

The fundamentals of optics teach that a ray passing through the optical centre of a lens is not deviated by it. This ray, if projected, will intersect the optical axis of the lens in the nodal points. The position of these points depends on the wave-length. In an ideal construction the axis of the optical system has to coincide with the undeviated ray. This means that a simultaneous rotation and translation would have to be performed. The translation, however, will be very small, as is evident from the following. The distance, e, from the surface of the lens to the corresponding nodal point is given by

$$e(n) = \frac{R_1 d}{n(R_1 + R_2) - (n-1)d} \tag{33}$$

where R_1 and R_2 are the radii of the lens surfaces, d the thickness of the lens and n the refractive index of the lens material. The translation, Δx, at a change of the refractive index from n to $n + \Delta n$ is then given by the approximative expression

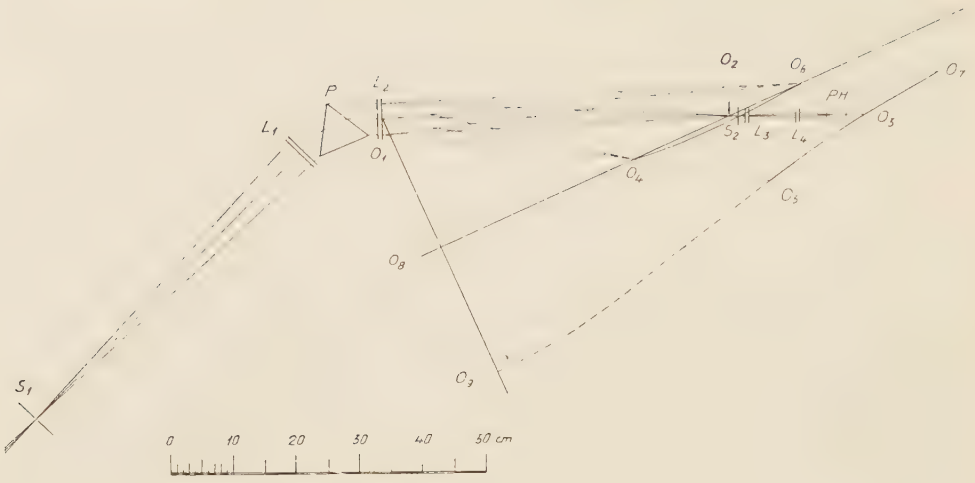

FIGURE 8. Principle of the mechanical system.

$$\Delta x = \Delta e \sin \theta = e'(n) \sin \theta \Delta n, \tag{34}$$

where θ is the angle which the ray forms with the optical axis of the lens. Using $d = 1$ cm., $R_1 = R_2 = 30$ cm. and the values given by SAWYER (59) for dense flint, namely $\lambda_1 = 4358.3$ Å; $n_1 = 1.68030$ and $\lambda_2 = 4861.3$ Å; $n_2 = 1.66911$ we get

$$\Delta x = 0.00194 \sin \theta \text{ cm.}$$

Now $\theta < 10°$ and hence

$$\Delta x < 3.4 \cdot 10^{-4} \text{ cm.}$$

This displacement is of no importance, it means that the image of the slit moves a little on the surface of the photo-cathode. This has a constant sensitivity over a rather large area (*v. infra*) and therefore the change in photo-current will be negligible.

Consequently, in Figure 8 the point O_1, the principal point in the right principal plane, can be regarded as a common point of the rays O_1O_2, O_1O_4 and O_1O_6. The optical axis of the system S_2PH can always be directed towards the point O_1 in the following way. O_2O_3 is a constant distance, O_2 is movable on the line $O_8O_4O_6$ and O_3 forced to follow the curve $O_9O_5O_7$, the conchoid to the line $O_8O_4O_6$ with respect to the point O_1. The slit S_2 can be adjusted in the focal plane $O_4S_2O_6$ by a movement along O_2O_3.

b. Performance

The details of the mechanical system follow from Figures 9 and 10.

At the camera end of the spectrograph is placed a table (1) with three adjustable feet (2). This table supports a bridge (3) having a frame (4). The frame can be attached to the spectrograph by lowering the cassette holder (5) by means of the knob (6).

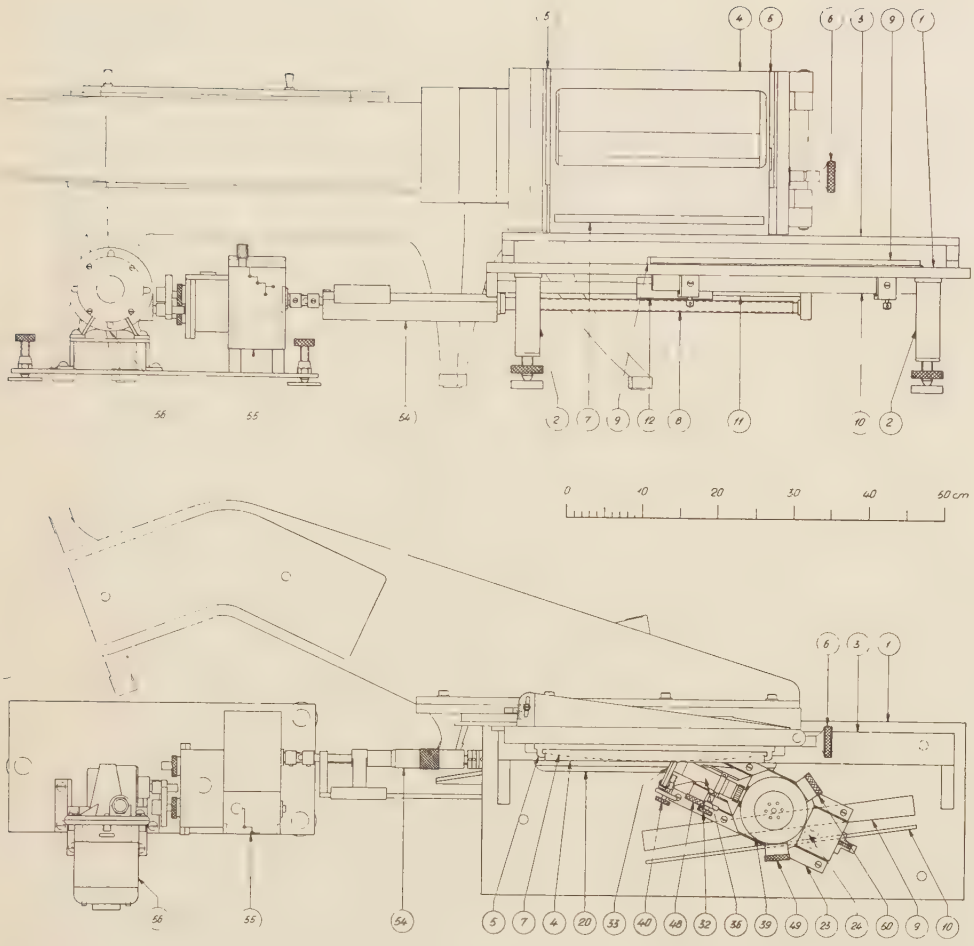

FIGURE 9. Mechanical system (in the upper figure some of the parts have been omitted).

The opening in the frame is sufficiently large to allow a convenient scanning of the spectrum. In a recess in the frame a cylindrical surface (7) has been arranged. The curvature of this surface in the horizontal plane has a point to point correspondence to the curvature of the focal plane. The under-side of the table has two plates which support the bearings of a screw (8) (diameter 15 mm.; thread 1 mm.). The axis of this screw is parallel with the frame (4) and follows as closely as possible the projection of the surface (7). This position of the screw makes the movement along the line O_2O_3 small (*cf.* p. 41).

On the table there are two rules. One of them (9) has one side formed as the arc of the conchoid generated by the point O_3 when the point O_2 is moved between O_4 and O_6 along the axis of the screw (Figure 8). The other one (10) is simply a

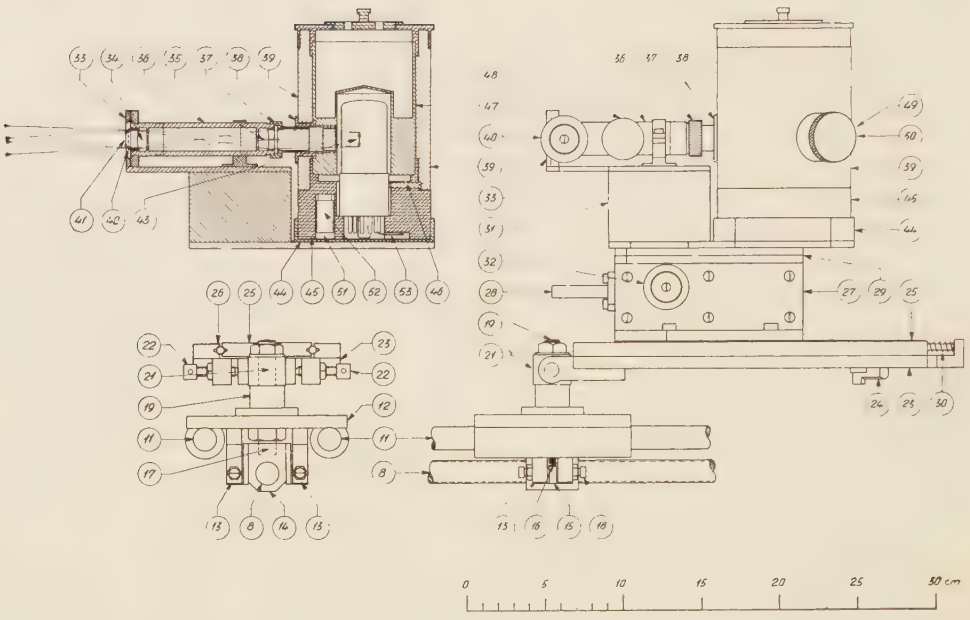

FIGURE 10. Mechanical and optical system. Details.

parallel-rule. The position of these rules can be adjusted: (9) in the plane of the table and (10) in a plane at right angles to the table.

Two cylindrical rods (11) placed in a position parallel to the screw guide the movement of a plate (12). On the under-side of this there are two forks (13) grasping the two wings (15) of a nut (14). A coil-spring (16) and a pin (17) keep the nut in its right position when the screw is turned. By means of the screws (18) the play between the wings and the forks can be properly adjusted. On the upper side of the plate (12) there is a standard (19) going up through an opening (20) in the table (1). The upper part of the standard forms the support for a piece (21) which, by means of the screws (22), holds one end of a table (23). The other end of this table rests on the rule (10) through a support (24). This support is pressed against the rule (9) by means of a coil-spring mounted between the plate (12) and the table (23) (not shown in the figures). When the rule (9) is correctly adjusted the line O_2O_3 will be directed towards a point situated vertically below the point O_1. The rule (10) is adjusted so that the table (23) moves in the horizontal plane.

The slit S_2 (Figure 8) is kept in the focal plane by the following arrangement: on a plate (25), movable on a straight ball-bearing (26), a holder (27) is attached (both the plate, the balls and the rules of the bearing are made of specially annealed steel because the strain on this bearing is rather great). This carries a support (28) and a slide (29). The support (28) is forced against the cylindrical surface (7) by means of the coil-spring (30). In this way the position of the holder (27) is deter-

mined by the focal plane. The slide (29) carries a holder (31) supporting the optical system of the recording unit. By means of a screw (32) this holder can be moved to and fro so that the slit (33; S_2) can be adjusted exactly in the focal plane.

B. Optical System

a. General

The requirements which the optical system has to fulfil are the following: firstly, the position and the openings of lenses and lens holders must be chosen in such a way that no aperture stops for the light bundle defined by the camera lens and the image of the entrance slit in the focal plane will be obtained; secondly, stray light from the spectrograph must be excluded.

The distance between the slit and the photo-tube must, due to limitations of space, be kept rather short. As lenses with a short focal length and a large diameter are expensive, the use of two lenses of a small diameter has been preferred. The first lens is placed near to the slit and makes the light bundle less divergent (the image of the slit is virtual). This bundle can then pass the second lens without being stopped down and form a real image of the slit on the photo-cathode. It may be mentioned that in some cases (for instance in measuring light scattering, *cf.* Zimm (60)) the first lens is arranged to form an image of the slit (or light-source) in the second lens; this lens gives an image of the first one on the photo-cathode. In this way compensation for variable or unsymmetrical radiation of the light-source can be achieved. Furthermore, the differences in sensitivity of the photo-cathode are less important. In the present case the "light-source" consists of an image of the entrance slit. Each point of this image does not radiate in all directions. Thus an application of this method would be inappropriate.

b. Performance

The details of the optical system follow from Figures 8 and 10.

The optical system is placed on the holder (31). It consists of a slit (33; S_2) and two lenses, (34; L_3) and (35; L_4), in a lens holder (36). By means of two tubes, (37) and (38), the lens holder is attached to the photo-tube compartment (39). The width of the slit can be adjusted with the screw (40). The height of the slit is not variable. The image (41) of the entrance slit is, by means of the lens (34) (diameter 14 mm.; focal length 48 mm.), transformed to a virtual image (42). The lens (35) (diameter 14 mm.; focal length 35.5 mm.) then gives the real image (43) on the photo-cathode. The maximum height of the entrance slit which can be used in the arrangement is 12 mm. Both of the lenses (34) and (35) are achromatic doublets. No special arrangements have been made to eliminate stray light from the spectrograph.

The image of the entrance slit of the spectrograph is made parallel to the slit of the optical system by tilting the entrance slit ((41) in Figure 7).

The photo-tube is installed in the compartment (39) in the following way. In a holder (44) a cylindrical piece (45) is placed. This has a hole in the centre which fits to the base of the photo-tube. By means of three screws (46) the photo-tube can be fixed vertically in such a position that the light bundle hits the most sensitive part of the cathode surface. The pieces (44) and (45) are made of polymethyl methacrylate. The photo-tube is covered by a house (47) made of aluminum. This is attached to the lens holder (36) by the tubes (37) and (38) made of ebonite. Three pots, (48), (49) and (50), contain drying agent to prevent condensation of water vapour on the photo-tube envelope and the lens surfaces when the photo-tube is cooled. This can be done by placing solid carbon dioxide in the house (47) which is insulated from the surroundings by a porous material. The cylindrical holder (45) can be turned in the holder (44) and in this way the image of the slit can be placed on the most sensitive part of the cathode-surface. In the holder (45) there are also eleven holes (51) for the bleeder resistances (52). These are connected to the pins of the photo-tube by means of wires (53).

C. Driving Mechanism

The screw (8) (Figure 9) is *via* a micrometer screw (54) connected to a gear box (55) and a synchronous motor (56) (Bodine Electric Company, U. S. A., Type NSY-13RG) the shaft of which makes 2.5 rev./min. The gear reduces the speed to $2\,^1/_2$, $1, {}^1/_2$, and ${}^1/_4$ rev./min. respectively. The motor is reversible which makes recording in two directions possible.

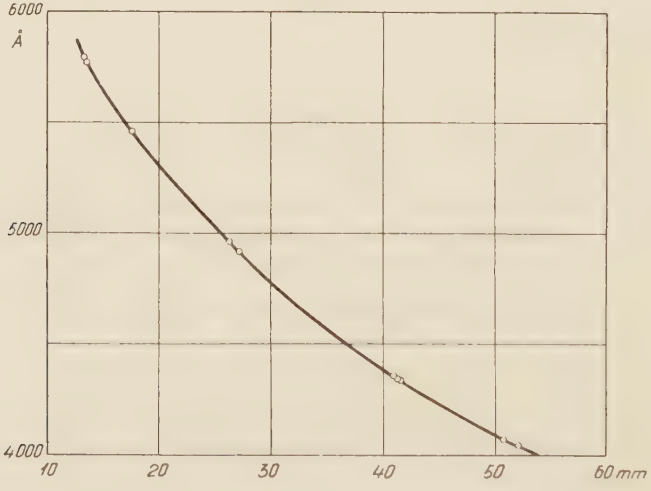

FIGURE 11. Calibration of micrometer screw in Å-units.

The calibration of the micrometer screw in Å-units is given in Figure 11. From this it follows that an inverse linear dispersion of 15 Å/mm. can be obtained at λ 4358 Å. Then the following recording speeds are possible: 40, 15, 8, and 4 Å/min. or about 200, 80, 40, and 20 cm.$^{-1}$/min.

D. Check of Performance

Due to errors in the adjustment of the conchoid rule (9), irregularities in its form *etc.*, the optical system $S_2L_3L_4PH$ (Figure 8) will not have the correct position $AF'B$ but the position $AF''C$ (Figure 12). This means that a reading on the micrometer screw does not correspond to the true wave-length λ' but to λ''. The difference $\lambda' - \lambda''$ is a measure of the precision of the recording arrangement. In Figure 12 EFG is the focal plane of the spectrograph, $OF' = \varrho \quad f(v)$, OH one of the principal planes of the camera lens, O the corresponding principal point, OE the optical axis of the camera lens, BD a true conchoid, EAG the screw (8) (*cf.* Figure 9) and OAB the central ray in a light bundle. Let $OI = a$, $\wedge OAH = \Delta\theta$ and $\wedge AOI = v$, then

$$F'F'' = \left(\varrho - \frac{a}{\cos v}\right)\left[1 + \left(\frac{1}{\varrho}\frac{\mathrm{d}\varrho}{\mathrm{d}v}\right)^2\right]^{\frac{1}{2}} \tag{35}$$

The first factor in this expression is the distance along the ray OAB between the focal plane and the centre-line of the screw EAG. Thus $F'F''$ can be made small if this distance is small in the spectral region where the recording is going to be done. In the present case this distance is less than 10 mm. The magnitude of the

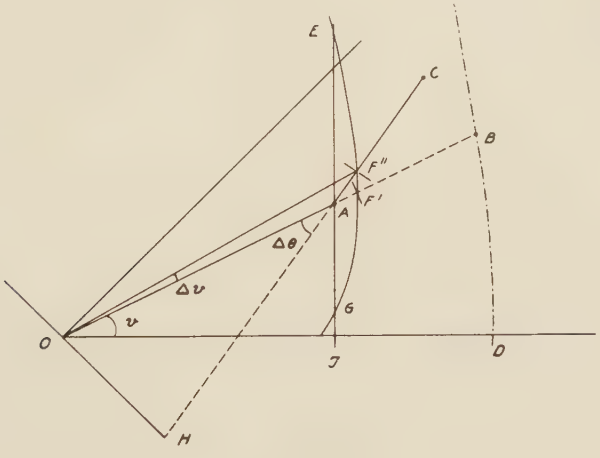

Figure 12.

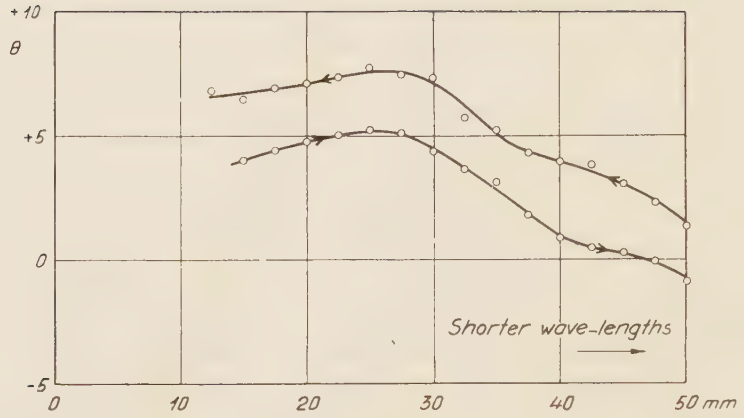

FIGURE 13. Angle between axis of optical system and central ray of light bundle from spectrograph as a function of readings on the micrometer screw (θ in minutes).

second factor depends upon the value of $\mathrm{d}\varrho/\mathrm{d}v$. For the spectrograph used we have $\mathrm{d}\varrho/\mathrm{d}v \approx 800$ mm./radian at $\varrho \approx 500$ mm. This makes the square root < 2. Consequently

$$F'F'' < 20\,\Delta\,\theta \text{ mm.}$$

In order to determine $\Delta\,\theta$ the optical system was removed and a telescope placed on the holder (31). A scale placed just in front of the camera lens was observed. The rule (9) was adjusted until the deviation corresponding to the whole length of the micrometer screw (50 mm.) was a minimum. The deviations for intermediate positions were then determined. The result is given in Figure 13. The upper and lower curves correspond to movement towards longer and shorter wave-lengths respectively. The discrepancies between the two curves are due to play in the mechanical system. The maximum deviation is less than $8' = 0.00233$ radians. Thus

$$F'F'' < 0.047 \text{ mm.}$$

The maximum uncertainty, $\lambda' - \lambda''$, in position of the recorded spectral lines is thus less than 0.7 Å. It should be pointed out that this uncertainty is a systematic deviation which will be corrected in a calibration.

After these adjustments were made, the direction of the axis of the optical system was checked. The centre of the light bundle through the system was displaced 0.3 mm. at λ 4358 Å and 0.7 mm. at λ 5461 Å in the direction of shorter wave-lengths. This means that the optical axis does not intersect the camera lens exactly in the point O_1 (Figure 8) but in a point situated 1.8 and 4.3 mm. respectively to the left of O_1, when looking at the lens from the camera side of the spectrograph.

E. Electrical System

a. General

The purpose of the electrical system is to transform the pulsating light signal into an alternating voltage which after amplification and rectification can operate the recording instrument. It is necessary to build the electrical system in such a way that the noise originating from various sources is eliminated as much as possible. The following discussion is concerned with some of the problems met with in this work.

1. Properties of Multiplier Photo Tubes

The multiplier photo-tube has been described several times in connection with its increased use in a variety of applications. A description of the construction and general properties of mainly American tubes is given by Zworykin and Ramberg (61). Its characteristics, especially when applied to the measuring of low light levels, are discussed by Engstrom (62). A short, but good, discussion is given by Rodda (63). A valuable complement to the above-mentioned articles is the paper by Winans and Pierce (64) about the operation of photo-multipliers. English multipliers are discussed by Sommer and Turk (65), and some French tubes by Lallemand (66). Dieke (67, 68), gives a report on the general properties of the multiplier tubes in connection with their use for intensity measurements in spectroscopy. During the latter years the principles applied in the multiplier photo-tubes have been utilized in scintillation counters. This has given rise to studies of certain properties of the photo-tubes especially with regard to pulse distribution. Reference can be made to papers by Morton and Mitchell (69), Morton (70), Westöö and Wiedling (71), Drigo (72), and Ageno, Chiozzotto and Querzoli (73). Multiplier tubes of a construction similar to that of the photo-tubes have been used as counters for high energy particles. A general discussion of different counters is given by Corson and Wilson (74) and a review of work done up to 1949 by Stone (75).

It is by no means the intention of the present author to give a review of this very large field. The different applications of the multiplier principle have produced a considerable amount of information about the properties of secondary emission tubes and therefore some of the general lines will be discussed.

Noise. When discussing noise, the following terminology introduced by Schremp (76) will be used: let $V(t)$ be a noise variable quadratically integrable, then

$$\int_{-\infty}^{+\infty} V^2(t)\,\mathrm{d}\,t = \overline{V^2} \tag{36}$$

is finite and equal to the mean square value of $V(t)$. Consequently $V(t)$ has a Fourier transform

$$v(j\omega) = \int_{\infty}^{\infty} V(t)\, e^{-j\omega t}\, \mathrm{d}t, \tag{37}$$

where the variable $\omega = 2\pi f$ is the angular frequency, and a spectrum

$$S(\omega) = v^2(j\omega) = \int_{\infty}^{\infty}\int_{\infty}^{\infty} V(t)\, V(t')\, e^{j\omega(t'-t)}\, \mathrm{d}t\, \mathrm{d}t'. \tag{38}$$

The measured spectrum, $\bar{S}(\omega)$, is interpreted as the statistical spectrum of $V(t)$ and is experimentally the frequency average of $S(\omega)$

$$\bar{S}(\omega_0) = \int_{\infty}^{\infty} \delta(\omega - \omega_0)\, S(\omega)\, \mathrm{d}\omega, \tag{39}$$

where

$$\delta(\omega - \omega_0) = \begin{cases} 0 & \omega \neq \omega_0; \\ \infty & \omega = \omega_0; \end{cases} \tag{40}$$

and

$$\int_{\infty}^{\infty} \delta(\omega - \omega_0)\, \mathrm{d}\omega = 1. \tag{41}$$

$\bar{S}(\omega)$ can also be regarded as the mean square of the noise variable $V(t)$ per unit frequency interval. Hence

$$\bar{S}(\omega) = \frac{\mathrm{d}\,\overline{V^2}}{\mathrm{d}f} = \overline{|v(j\omega)|^2}. \tag{42}$$

According to the theory of noise for electron multipliers developed by Shockley and Pierce (77), the noise in the multiplier is correlated with the secondary-emission properties of the dynodes, consequently the output noise will consist of one part caused by noise in the input, and another part originating from the way in which secondary electrons are produced. Let $\mathrm{d}\,\overline{I_0^2}/\mathrm{d}f$ and $\mathrm{d}\,I_n^2/\mathrm{d}f$ denote the statistical spectra of the primary and secondary noise currents respectively. Then

$$\frac{\mathrm{d}\,\overline{I_n^2}}{\mathrm{d}f} = m_n^2 \frac{\mathrm{d}\,\overline{I_0^2}}{\mathrm{d}f} + 2\,e\,I_0\,m_n^2\,B, \tag{43}$$

where m_n is the over-all multiplication at n dynodes, e is the charge of the electron and B is the mean square deviation in m_n. The derivation of this equation presupposes that the multiplication is linear in the sense that there is no interference between the effects of different input electrons, that each electron entering one electrode has a probability $p(g)$ of producing g electrons at the next one, and that the output

electrons appear simultaneously at a time t_0 after the input electron enters the multiplier. The over-all multiplication, m_n, is

$$m_n = \prod_{\nu=1}^{n} m_{\nu\ 1,\nu}, \tag{44}$$

where $m_{\nu\ 1,\nu}$ is the average number of secondary electrons produced by one primary at the electrode ν. The factor B is given by

$$B = b_1 + \frac{b_2}{m_{0,1}} + \frac{b_3}{m_{0,1}\, m_{1,2}} + \cdots + \frac{b_n}{m_{0,1}\, m_{1,2} \cdots m_{n-2,\,n-1}}, \tag{45}$$

where

$$b_\nu = (\overline{g^2} - \bar{m}^2_{\nu\ -1,\nu}) / \bar{m}^2_{\nu\ 1,\nu} \tag{46}$$

is the relative mean square deviation of $m_{\nu-1,\nu}$.

Assuming that the number of electrons produced at one electrode follows a Poisson distribution the probability that g electrons will be emitted is

$$p(g) = \frac{m^g\, e^{-m}}{g!} \tag{47}$$

and from this it is easily found that $b = 1/m$. Consequently

$$B = \frac{1}{m_{0,1}} + \frac{1}{m_{0,1}\, m_{1,2}} + \cdots + \frac{1}{m_{0,1}\, m_{1,2} \cdots m_{n-1,\,n}} \tag{48}$$

and if $m_{0,1} = m_{1,2} = m_{2,3} = \cdots = m_{n-1,\,n} = m$

$$B = \frac{m_n - 1}{m_n\,(m-1)}. \tag{49}$$

Furthermore, if the noise in the input is considered to be that of shot effect, the statistical spectrum of $\overline{I_0}$ will be equal to $2\,e\,\overline{I_0}$. Then we get from Equation (43)

$$\frac{\mathrm{d}\,\overline{I_n^2}}{\mathrm{d}\,f} = 2\,e\,\overline{I_0}\,\frac{m_n\,(m_n\,m-1)}{m-1}. \tag{50}$$

This expression is also given by Zworykin, Morton and Malter (78) and by Lallemand (66). As is shown by Shockley and Pierce (77) the condition $b\,m - 1$ is not always fulfilled. From data measured by Zworykin, Morton and Malter, they calculate deviations as large as 20 per cent. Further, in their study of photo-pulse distribution Morton and Mitchell (69) have found that the second moment of the measured distribution was about twice the value calculated from an assumed Poisson distribution. However, they leave the question open as to what extent

this discrepancy may be because the secondary electrons do not follow a Poisson distribution or it may be because of a loss of electrons between one stage and the next. The assumption of a Poisson distribution seems to have a weak experimental justification and consequently Equation (50) is to be regarded as an approximate expression; but one of the most important properties of the multiplier photo-tube is more easily demonstrated from it than from the complete Equation (43). Rewriting Equation (50) in terms of m and neglecting 1 in comparison with m^{n+1} we get

$$\frac{\mathrm{d}\,\overline{I_n^2}}{\mathrm{d}f} = 2e\,\overline{I_0}\,\frac{m^{2n+1}}{m-1}. \tag{51}$$

If the measurements are made over a frequency interval, Δf, the mean square noise current will be

$$\Delta\,\overline{I_n^2} = 2e\,\overline{I_0}\,\frac{m^{2n}}{m-1}\,\Delta f. \tag{52}$$

The signal-to-noise ratio is then given by

$$S^2_{n,\Delta f} = \frac{\overline{I_0}}{2e\,\Delta f}\,\frac{m-1}{m}. \tag{53}$$

Therefore the signal-to-noise ratio from the multiplier differs from the fundamental limit imposed by the photo-electric emission by the factor $[(m-1)/m]^{1/2}$. As the total amplification is m^n, a considerable increase in the original current can be obtained without any serious reduction in signal-to-noise ratio.

Dark Currents. Even an unilluminated multiplier photo-tube passes a certain amount of current. This dark current originates mainly from three sources (*cf.* Rajchman (79), Zworykin and Ramberg (61) and Engstrom (62)): 1) ohmic leakage between the electrodes both inside and outside the glass envelope; 2) thermionic emission from the photo-cathode and the dynodes; 3) positive ion impact on the photo-cathode and the dynodes and field emission from projecting points of the electrodes. It is evident that the magnitude of the currents arising from sources 1) and 3) is very much dependent upon the construction of the tubes and may thus vary considerably from tube to tube. The thermionic emission, however, depends solely on the work-function of the emitting surfaces and their temperatures. Engstrom (62) has studied how the dark current depends on the voltage per stage. At low voltages the ohmic leakage is dominant up to about 50 or 60 V./stage. One can distinguish between leakage inside the tube caused by traces of cesium and other conductive materials on the stem and insulator spacers, and base leakage, which is particularly evident when operating the tube in a humid atmosphere. The current caused by thermionic emission becomes important above 60 V./stage

and increases rapidly with increasing voltage. The regenerative ionization effect begins above about 100 V./stage and will, at higher voltages, cause a complete breakdown.

The thermionic emission dark current is, at ordinary operating voltages, the most serious source of disturbances and constitutes the ultimate limitation to signal detection. The specific emission of a surface is given by RICHARDSON's equation

$$j = A T^2 \exp(-w/k T), \tag{54}$$

where j is the current density, A a constant, T the absolute temperature, k the Boltzmann constant and w the work-function of the surface (*cf.* for instance ZWORYKIN and RAMBERG (61) or RICHTMYER and KENNARD (80)). From this equation it is evident that specific thermionic emission can be minimized in two ways, either by decreasing the temperature of the surface or by increasing the work-function. The increase of the work-function seriously limits the photo-emissivity of the surface in the infrared and the visible region of the spectrum, and can therefore only be applied successfully in cases where the incident light quantum is large or for high energy particles. A photo-sensitive surface of smaller size will reduce the total dark current but will also reduce the photo-current. At a high photo-sensitivity, *i.e.* a high yield of electrons per incident quantum of light, the surface of the photo-cathode can be kept small and nevertheless the photo-current will be high. However, SOMMER and TURK (65) have pointed out that the yield of electrons cannot be made better than for a Sb-Cs-surface. Therefore the only practical way to decrease the thermionic emission is to cool the emitting surfaces. This can be done without a serious drop in the signal output as shown by ENGSTROM (62). One disadvantage with the cooling of the photo-tube is that the fatigue effect (*v. infra*) will be more pronounced, as found by DE BOER and TEVES (81). This has to be kept in mind, especially, when the working range of the tube covers both high and low intensities (DIEKE, (68)). In cases where only weak light signals are to be measured the fatigue effect is generally small and therefore cooling of the tube is free from objections. At high light signals cooling is not necessary. — An arrangement for such cooling of the photo-tube has been described by ENGSTROM (82).

In connection with the application of multiplier tubes as counters of discrete particles, studies of the dark-pulse distribution have been made by MORTON and MITCHELL (69), by MORTON (70) and by WESTÖÖ and WIEDLING (71) (*cf.* also ENGSTROM (62)). These investigators find a decrease in the number of dark pulses with temperature. MORTON and MITCHELL have observed a decrease with a factor of 4–10 at a temperature change from 50 to 30 °C. The large pulses decreased more slowly in number than the small ones. MORTON and MITCHELL, and DRIGO (83) have studied the influence of an electrostatic shield on the number of dark pulses. As a function of the shield potential the number of pulses shows a rather flat minimum

with a width of about 200 V., the centre of which corresponds to a potential of about 100 V. less than the cathode potential. On both sides of this minimum the number of pulses increases very rapidly. DRIGO has also made a study of how the shield potential acts in the case where only pulses of a height greater than a certain value is registered. He finds that the minimum at large pulses is more flat and at the same time displaced towards higher shield potentials. A similar behaviour of the dark current has been reported by TAYLOR (84) and DRIGO (83). The dependence of noise on the potential of the glass envelope is also mentioned by MARSHALL, COLTMAN and BENNETT (85). TAYLOR makes a thorough investigation of the phenomenon. The high dark current at shield potentials much higher than the potential of the cathode is due to scintillations from the glass envelope, caused by electrons which are attracted by the glass which is positive with respect to most of the dynodes. The minimum noise is the ordinary thermionic emission. The increase in dark current at shield potentials lower than the cathode potential is due to thermionic emission from traces of photo-emissive substance on the inside of the glass envelope. The electrons set free are attracted to the cathode, where they produce secondary electrons which are then multiplied in the ordinary way. Without special arrangements the potential of the glass envelope will reach an equilibrium value of about half the voltage difference between the anode and the cathode. This voltage corresponds roughly to one end of the flat minimum. DRIGO has found that the effect of the shield potential is the more pronounced the lower the cathode potential. As pointed out, for instance, by MORTON and MITCHELL, the behaviour of the tubes in this respect varies very much. Generally the dark current of a tube which shows a small number of dark pulses per second is very little influenced by the potential of the envelope. A considerable improvement can be obtained, however, in the case of a particularly noisy multiplier. They also express the opinion that the effect of the shield potential greatly depends on the conductivity of the glass, because the potential of the inner surface of the glass is altered by the leakage through the glass to the external shield. Thus the noise in a 1P28 tube which has an envelope of high-resistance glass is very insensitive to the potential of an external shield. DRIGO has noticed that the effect of the shield potential is less at low temperatures and explains this as a consequence of the increased resistance of the glass.

In the present case the behaviour of the 1P21 tubes used have not shown any pronounced dependence on the potential of an external shield.

As the thermionic emission may occur from any of the electrodes in the multiplier, the statistical spectrum of the total dark current is a function of all the separate emission currents from the electrodes, I'_ν, the corresponding multiplication factors, $m_{\nu,n}$, and the relative mean square deviations $B_{\nu,n}$, *i.e.* (*cf.* Equation (43))

$$\frac{\mathrm{d}\,\overline{I'^2_n}}{\mathrm{d}\,f} = \frac{\mathrm{d}}{\mathrm{d}\,f}\left(\sum_{\nu=0}^{n} \overline{I'^2_{\nu,n}}\right) = 2\,e \sum_{\nu=0}^{n} m_{\nu,n}\,(1 + B_{\nu,n})\,\overline{I'_{\nu,n}}\,. \tag{55}$$

where $\overline{I'_{\nu,n}} = m_{\nu,n}\,\overline{I'_\nu}$ is the anode dark current corresponding to emission current $\overline{I'_\nu}$ at dynode ν; (*cf.* WINANS and PIERCE (64)). Making the assumption that $\overline{I'_\nu}$ is equal to $\overline{I'_0}$ and that the multiplication for each stage, m, is the same and that the product $b\,m = 1$ (*v. supra*) we get

$$m_{\nu,n} = m^{n-\nu}; \tag{56}$$

$$1 + B_{\nu,n} = \frac{m^{n-\nu+1} - 1}{m^{n-\nu}(m-1)}; \tag{57}$$

$$\overline{I'_{\nu,n}} = m^{n-\nu}\,\overline{I'_0}. \tag{58}$$

Thus

$$\sum_{\nu=0}^{n} m_{\nu,n}(1 + B_{\nu,n})\,\overline{I'_{\nu,n}} = \overline{I'_0}\,\frac{(m_n m - 1)(m_n m^2 - 1)}{(m-1)(m^2-1)} \tag{59}$$

and

$$\frac{\mathrm{d}\,\overline{I'^2_n}}{\mathrm{d}f} = 2e\,\overline{I'_0}\,\frac{(m_n m - 1)(m_n m^2 - 1)}{(m-1)(m^2-1)}. \tag{60}$$

m_n is a large number and thus

$$\frac{\mathrm{d}\,\overline{I'^2_n}}{\mathrm{d}f} = 2e\,I'_0\,\frac{m_n^2 m}{m-1}\,\frac{m^2}{m^2-1}. \tag{61}$$

Hence the contribution from all electrodes except the cathode is small only if the multiplication factor per stage is large. For a nine stage multiplier m has to be >5 until the contribution is less than 5 per cent. This corresponds to $m_n > 10^6$.

The total noise in the output current will be the sum of the contributions from Equations (50) and (60), *i.e.*

$$\frac{\mathrm{d}\,\overline{I_t^2}}{\mathrm{d}f} = 2e\,\overline{I_0}\,\frac{m_n(m_n m - 1)}{m-1} + 2e\,\overline{I'_0}\,\frac{(m_n m - 1)(m_n m^2 - 1)}{(m-1)(m^2-1)} \approx$$

$$\approx 2e\,m_n^2\,\frac{m}{m-1}\left(\overline{I_0} + \overline{I'_0}\,\frac{m^2}{m^2-1}\right). \tag{62}$$

The signal-to-noise ratio for the frequency range Δf will be

$$S^2_{t,\Delta f} = \frac{m-1}{m}\,\frac{1}{2e\,\Delta f}\,\frac{\bar{I}_0^2}{\overline{I_0} + \dfrac{m^2}{m^2-1}\,\overline{I'_0}}. \tag{63}$$

This is independent of m_n and hence of the number of dynodes in the photo-tube. It is not to be expected that this holds good in all cases: the assumptions made may not be allowed, and the properties of various tubes may not be the same.

Dieke (67) has found a constant signal-to-noise ratio of a 1P28 tube operated up to 100 V./stage. Engstrom (62) reports a decrease in signal-to-noise ratio in 931-A tubes of about 10 db. for a voltage interval of 50 V. Similar results have been found by Marshall, Coltman and Bennett (85). The signal-to-noise ratio, as well as the decrease with dynode voltage, changes from tube to tube. Among 53 tubes (931-A) investigated, only 6 had a signal-to-noise ratio higher than 6 (arbitrary units), and only one higher than 10. From Equation (63) it is evident that the signal-to-noise ratio can be increased by increasing the photo-electric sensitivity of the cathode, decreasing the band-width of the measuring device and by decreasing the thermionic emission by cooling the tube.

Fatigue. When the photo-tube is illuminated a decrease in sensitivity will occur. This is a fatigue effect which rapidly increases with the amount of current taken from the tube. As shown by Dieke (67), the effect also increases when the plate voltage is increased at a constant dynode voltage. The fatigue effect varies considerably from tube to tube. After some time in the dark the tube will recover and regain its original sensitivity. This recovery is a very much slower process than the fatigue. As the current from the photo-cathode in a multiplier photo-tube is always very small compared to the output current, there is reason to believe that the fatigue at the cathode will not play any important part. Chiefly, the fatigue will be contributed by the last dynode, as pointed out by Dieke, who also gives evidence for this view. The same conclusions have been arrived at by Marshall, Coltman and Hunter (86), who explain the fatigue phenomenon as a deficiency of cesium in the cesium-antimony layer on the dynodes caused by the bombardement from the electrons. Dieke (67) stresses the fact that the fatigue phenomenon on the dynodes is similar to that found on cesium-containing photo-cathodes, where it is explained as a difficulty to neutralize cesium ions when electrons remain fixed upon internal surfaces. The ionized atoms can no longer contribute to the photo-current (*cf.* also Rodda (63)).

In practical work it is essential to bear this effect in mind and, if necessary, make corrections for it. If the recovery was not a slow process the fatigue could be avoided by using intermittent light. The only way out of the difficulty is to use either very small currents or to keep the tube illuminated for such a long time that the sensitivity will take a constant value. The last possibility, of course, applies especially in the case of strong currents. According to Dieke one has to avoid currents higher than one μA. if the fatigue effect is not to interfere with the measurements.

Flicker Effect. Due to the properties of the cathode surface in a photo-tube a flicker effect (*cf.* Moullin (87)) similar to that occurring in tubes with oxide-coated cathodes may be expected. An accidental change in work-function over the surface will produce a fluctuation in the photo-current. However, as pointed out by Rodda (63), the photo-current is less sensitive to changes in work-function than is the thermionic emission.

The flicker effect can therefore be disregarded as far as photo-emission is concerned. The dark current, however, is definitely subjected to flicker effect. The only remedy in this case is a reduction of the thermionic emission by cooling as discussed above.

Satellite Pulses. Godfrey, Harrison and Keuffel (88) have observed satellite pulses occurring about 1 μsec. after the main pulse (signal or dark current). The number of such pulses is about one per main pulse. The time delays of the satellites are consistent with their being due to single positive ions, produced by the electrons of the main pulse, drifting back and striking an electrode.

Sensitivity Structure of Photo Cathode. In the practical use of photo-tubes it is of great importance to know the variations of sensitivity in different parts of the photo-cathode surface. This is especially important when the light is focused on a small area of the cathode. A calibration is true only when the light spot has a position within an area of the same sensitivity on the cathode surface. Another slit-width or a movement of the tube in the socket will almost certainly necessitate a recalibration. Even from other points of view the sensitivity structure is of importance. Thus the stability in the output current may be influenced by unsuitable mounting of the tube, and a change in distribution of a given amount of light energy in the entrance slit of a spectrograph may cause instability.

The structure of the photo-sensitive cathode surface has been investigated by Dieke (67), who found some variations from tube to tube. A diffusing screen placed in front of the tube smoothes out the effect of the irregularities of the photo-surface. On the other hand this screen will scatter the radiant energy in all directions and in this way cause a loss in overall sensitivity. Marshall, Coltman and Bennett (85) found small variations from tube to tube. At a hundred volts per stage they got a light-sensitive surface (RCA 931-A tubes) of about 5 mm. in width and 12 mm. in height. It was quite well-demarcated laterally but more diffuse in the upper and lower edges. They point out that the photo-sensitivity of a tube is not due to positional effects only: it also depends upon the focusing of the photo-electrons from a certain point against the dynodes. Normand and Kay (89) have measured the sensitivity contours of 1P28 photo-tubes. Both position on the photo-cathode and size of the most sensitive area varies from tube to tube. Peterson and Holland (90) have given evidences that the sensitivity increases with increased dynode voltage. This indicates that the electrons at low voltages may pass directly to the second dynode. Morton and Mitchell (69) have measured the fraction of photo-electrons reaching dynode number one and found that electrons emitted from the inner edge and the centre of the photo-cathode are totally collected already at fairly low voltages. Electrons coming from the outher edge require very high voltages for efficient collection (200 V. or more). Finally it may be mentioned that Rodda (63) has measured the multiplication factor as a function of the position of a light spot on the photo-cathode. He found that the multiplication has a maximum in a centre position and decreases at the inner and outer edges of the photo-cathode respectively. This non-uniformity of multiplication is disadvantageous with respect to noise generation when a large area of the cathode is illuminated, because the r.m.s.-value of the multiplication factor determines the noise but the mean value the output current.

Polarization Selectivity of Photo Cathode. A plane-polarized beam of light with an oblique incidence against a photo-sensitive surface gives a current response dependent on the direction of the electric vector in relation to the surface. The effect is considered to depend on photo-ionization of adsorbed atoms by the component of the electric vector in the plane of incidence. Clancy (91) and Brice, Halwer, and Speiser (92) have measured the response as a function of the angle between the electric vector of the in-

cident light and the longitudinal axis of the tube for different photo-tubes. For 1P21 photo-tubes the response at 90° is about 2 per cent higher than at 0°. The corresponding figure for 931-A tubes is about 20 per cent. Brice, Halwer, and Speiser use a solid opal glass plate near the photo-tube to depolarize the radiation before it strikes the cathode.

Multiplier Efficiency. The efficiency of a multiplier photo-tube as a source of obtaining electrons is given by the output current, I, per watts, W, supplied by the primary current. When the target is bombarded with a primary current, I_0, at a voltage V_0, we have

$$\frac{I}{W} = \frac{m}{V_0}\frac{I_0}{I_0} = \frac{m}{V_0}. \tag{64}$$

Thus the known properties of the secondary emission surface (m as a function of V_0) makes it possible to calculate I/W as a function of V_0.

Another way to consider efficiency is to study the gain as a function of the number of stages and voltage per stage at a given over-all voltage (Zworykin, Morton and Malter (78) and Rodda (63)). Let V_t be equal to the over-all voltage, n the number of stages, $V_n = V_t/n$ the bombarding voltage, $m = (V_n/V_1)^\beta$ where β is a constant for a given surface and V_1 is the voltage per stage, which gives unit gain. Then the total magnification is given by

$$m_n = (V_n/V_1)^{n\beta} = (V_t/n\,V_1)^{n\beta} \tag{65}$$

Keeping V_t constant, we easily get the following condition that m_n is a maximum

$$\log\,(V_t/n\,V_1) - 1 = 0\,; \qquad n = V_t/e\,V_1 \tag{66}$$

and thus

$$(m_n)_{\max} = \exp\,(\beta\,V_t/e\,V_1). \tag{67}$$

Maximum conditions are obtained when the voltage per stage is e times the voltage which gives unit gain. Rodda gives for a Sb-Cs-dynode $V_1 = 20$ V.; thus the optimum voltage per stage is about 55 V. This gives eighteen stages as the optimum number at 1000 V. over-all voltage. When the number of stages is given, for example nine, the only way to realize optimum conditions at over-all voltages lower than about 500 V. is to reduce the number of stages by inter-connecting some of the dynodes.

Zworykin, Morton and Malter have shown that in a multiplier where cesiated silver dynodes are used and which is built to give maximum gain the efficiency with regard to power consumption is nearly maximum.

2. Noise in Input Circuit of Amplifier

Generally the grid circuit of a high gain amplifier has to be designed with special precautions against various noise sources, otherwise it is not possible to use the circuit for measuring small signals. Using multiplier photo-tubes to detect weak light signals it is possible to have an amplifier of lower gain and therefore the construction of the grid circuit simplifies. This subject will be briefly discussed in the

following: references can be made to the papers by RODDA (63), by SOMMER and TURK (65) and by LUBSZYNSKI (93).

Thermal Noise in Resistors. According to JOHNSON (94) the fluctuations in the motion of electrons in a resistance will cause a voltage between the end points of the resistance. The statistical spectrum of this voltage, V_R, is given by

$$\frac{\mathrm{d}\,\overline{V_R^2}}{\mathrm{d}f} = \overline{|v_R(j\omega)|^2} = 2kTR. \tag{68}$$

If the circuit is open, *i.e.* $E_R(t) = V_R(t)$, the statistical spectrum of the thermal-noise electromotive force is given by the same expression. This equation is valid at thermal equilibrium. For more complicated networks the statistical spectrum of the thermal-noise electromotive force is obtained from NYQUIST's (95) thermal-noise theorem:

$$\overline{|e(j\omega)|^2} = 2kTR(j\omega), \tag{69}$$

where $R(j\omega)$ is the real part of the impedance of the network:

$$R(j\omega) = \sum_n R_n |Y_{nm}(j\omega)|^2 |Z(j\omega)|^2. \tag{70}$$

R_n is a component resistance in the network, Y_{nm} the transfer admittance between the generator, $e_n(j\omega)$, and the output, (m, m), $Z(j\omega)$ the driving point impedance at the output.

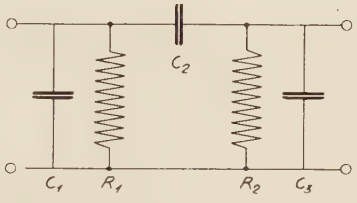

FIGURE 14. Coupling impedance between photo-tube and amplifier.

In the present case the coupling impedance is composed according to Figure 14. The statistical spectrum of the thermal noise occurring at the grid of the first amplifier tube and originating from the resistances R_1 and R_2 is then given by

$$\frac{\mathrm{d}\,\overline{V_R^2}}{\mathrm{d}f} = 2kTR_{\mathrm{eff}}, \tag{71}$$

where

$$R_{\mathrm{eff}} = \frac{R_2\{1+\omega^2 R_1[R_1(C_1+C_2)^2 + R_2 C_2^2]\}}{[1-\omega^2 R_1 R_2(C_1C_2+C_1C_3+C_2C_3)]^2 + \omega^2[(R_1+R_2)C_2 + R_1C_1 + R_2C_3]^2}. \tag{72}$$

At low frequencies the capacitances C_1 and C_3, constituting the output capacitance of the photo-tube and the input capacitance of the amplifier tube respectively, correspond to very high impedances and can consequently be neglected in comparison with R_1 and R_2. Furthermore, the impedance of C_2 must be small in comparison with R_2 in order to avoid attenuation of the input signal. Thus

$$R_{\text{eff}} \approx \frac{R_1 R_2}{R_1 + R_2} . \tag{73}$$

The order of magnitude of R_{eff} will be $10^6\,\Omega$.

Grid Current Noise. In most amplifier tubes there will flow a grid current even if the grid is at a negative potential with regard to the cathode. This grid current has several sources (*cf.* ZWORYKIN and RAMBERG (61, p. 254)), one being the positive ions formed by the gas still present in the tube or emitted from the cathode. The presence of this grid current also contributes to the noise in the input circuit of the amplifier. Denoting the Fourier transform of the instantaneous value of the grid current by $i_g(j\omega)$, the statistical spectrum of the noise voltage, V_g, over the input impedance is easily found to be

$$\frac{\mathrm{d}\,\overline{V_g^2}}{\mathrm{d}\,f} = \overline{|i_g(j\omega)|^2}\, R_2 R_{\text{eff}} \frac{1}{1+\alpha}, \tag{74}$$

where

$$\alpha = \frac{\omega^2 R_1 R_2 C_2^2}{1 + \omega^2 R_1^2 (C_1 + C_2)^2} \approx \frac{R_2}{R_1} . \tag{75}$$

Assuming that the statistical spectrum of the grid current is proportional to the mean grid current, $\overline{I_g}$, *i.e.*

$$\overline{|i_g(j\omega)|^2} = 2e\,\overline{I_g} \tag{76}$$

we get

$$\frac{\mathrm{d}\,\overline{V_g^2}}{\mathrm{d}\,f} = 2e\,\overline{I_g}\, R_2 R_{\text{eff}} \frac{1}{1+\alpha} \approx 2e\,\overline{I_g} \left(\frac{R_1 R_2}{R_1 + R_2}\right)^2 . \tag{77}$$

Often the grid current noise is expressed in terms of an equivalent grid resistance $R_g = 4kT/2e\overline{I_g}$ (*cf.* ELMORE (96)).

Shot Effect Noise. The emission of electrons from the cathode of the amplifier tube is subjected to random fluctuations. This phenomenon known as shot effect (*cf.* MOULLIN (87, p. 40)) will cause a fluctuation in the anode current. The statistical spectrum of the variation in the anode current for a negative grid triode at low frequencies is given by (*cf.* VALLEY and WALLMAN (97, p. 561))

$$\frac{\mathrm{d}\,\overline{I_p^2}}{\mathrm{d}\,f} = \overline{|i_p(j\omega)|^2} = \left(\frac{\theta}{\sigma}\right) 2kT_c g_m \tag{78}$$

where g_m is the transconductance of the tube, T_c the cathode temperature,

$$\theta \approx 3\,(1 - \pi/4)$$

a space-charge factor and σ a geometrical factor, $^1/_2 < \sigma < 1$. This current can be replaced by an equivalent shot-noise electromotive force in the grid-cathode input circuit having the Fourier transform $e_{cg}(j\omega)$. Then the following relation holds

$$i_p(j\omega) = g_m e_{cg}(j\omega), \tag{79}$$

where $e_{cg}(j\omega)$ is regarded to be in series with the impedance in the grid circuit. Then the statistical spectrum of $e_{cg}(j\omega)$ is given by

$$\frac{\mathrm{d}\,\overline{E_{cg}^2}}{\mathrm{d}\,f} = \overline{|e_{cg}(j\omega)|^2} = \frac{\theta}{\sigma}\,\frac{2\,k\,T_c}{g_m} = 2\,k\,T\,R_{cg}, \tag{80}$$

where

$$R_{cg} = \frac{\theta}{\sigma}\,\frac{T_c}{T}\,\frac{1}{g_m}. \tag{81}$$

The true source of shot noise is thus replaced by a fictitious one, namely the resistance R_{cg}, in series with the grid circuit impedance, emitting thermal noise but for all other purposes regarded to be absent. (It should be emphasized that the last transformations are only formal and Equation (80) does not tell anything about the true state of affairs as does the representation in Equation (78)).

Flicker Effect and Microphonics. The flicker effect (*cf.* MOULLIN (87, p. 155)) which is caused by random variations in the surface conditions of the thermionic cathode of the tube is not an inherent property of the tube in the same way as the shot effect. It can be minimized or eliminated by selecting a good tube. Further, at a temperature-limited anode current a reduction can be obtained by decreasing the temperature of the cathode, *i.e.* the filament current (*v. infra*). — Microphonics are low frequency disturbancies which arise from instabilities in the tube components and can therefore be avoided by careful selection or/and mounting of the tubes.

Noise from Multiplier Photo Tube. The current from the multiplier photo-tube will pass the input impedance of the grid circuit and on the grid produce a voltage which is then amplified. Due to the noise in the photo-current and the noise produced by the photo-tube itself this voltage will be subjected to random fluctuations. The statistical spectrum of the total output current, I_t, from the photo-tube is

$$\frac{\mathrm{d}\,\overline{I_t^2}}{\mathrm{d}\,f} = \overline{|i_t(j\omega)|^2}. \tag{82}$$

Using the Fourier transform representation, it is easy to show that the statistical spectrum of the voltage, V, on the grid follows the equation:

$$\frac{\mathrm{d}\overline{V^2}}{\mathrm{d}f} = \overline{|i_t(j\omega)|^2}\, R_1 R_{\mathrm{eff}}\, \frac{\alpha}{1+\alpha} \approx \overline{|i_t(j\omega)|^2} \left(\frac{R_1 R_2}{R_1 + R_2}\right)^2 \tag{83}$$

where $\overline{|i_t(j\omega)|^2}$ is given by Equation (62).

Adding up all the contributions we will get for the total noise voltage, V_{tot}, on the grid of the first amplifier tube:

$$\frac{\mathrm{d}\overline{V^2_{\mathrm{tot}}}}{\mathrm{d}f} = \frac{\mathrm{d}\overline{V^2_R}}{\mathrm{d}f} + \frac{\mathrm{d}\overline{V^2_g}}{\mathrm{d}f} + \frac{\mathrm{d}\overline{E^2_{cg}}}{\mathrm{d}f} + \frac{\mathrm{d}\overline{V^2}}{\mathrm{d}f}. \tag{84}$$

Using Equations (71), (77), (80) and (83) we get

$$\frac{\mathrm{d}\overline{V^2_{\mathrm{tot}}}}{\mathrm{d}f} = 2kT R_{\mathrm{eff}} + 2e\overline{I_g} R_2 R_{\mathrm{eff}} \frac{1}{1+\alpha} + 2kT R_{cg} +$$

$$+ \left[2e\overline{I_0}\, \frac{m_n(m_n m - 1)}{n-1} + 2e\overline{I_0'}\, \frac{(m_n m - 1)(m_n m^2 - 1)}{(m-1)(m^2-1)}\right] R_1 R_{\mathrm{eff}}\, \frac{\alpha}{1+\alpha}. \tag{85}$$

If we regard a small frequency interval, Δf, R_{eff} and α can be assumed to be approximatively independent on frequency, then the noise voltage in this interval is given from

$$\Delta\overline{V^2_{\mathrm{tot}}} = \frac{\mathrm{d}\overline{V^2_{\mathrm{tot}}}}{\mathrm{d}f}\, \Delta f. \tag{86}$$

The voltage, V_{signal}, at the grid as a result of the signal current through R_1 (Figure 14) is given by

$$V_{\mathrm{signal}} = m_n \overline{I_0} \left(\frac{\alpha}{1+\alpha} R_1 R_{\mathrm{eff}}\right)^{\frac{1}{2}}. \tag{87}$$

Then we finally get for the signal-to-noise ratio, S, at the grid of the first tube of the amplifier when the band-width of the system, Δf, is regarded as small

$$\frac{1}{S^2_{\Delta f}} = \frac{\Delta\overline{V^2_{\mathrm{tot}}}}{V^2_{\mathrm{signal}}} = \frac{\Delta f}{m_n^2 \bar{I}_0^2}\left[2e\overline{I_0}\, \frac{m_n(m_n m - 1)}{m-1} + 2e\overline{I_0'}\, \frac{(m_n m - 1)(m_n m^2 - 1)}{(m-1)(m^2-1)}\right] +$$

$$+ \frac{1+\alpha}{\alpha}\, \frac{2kT\Delta f}{m_n^2 \bar{I}_0^2 R_1}\left(1 + \frac{R_{cg}}{R_{\mathrm{eff}}}\right) + \frac{\Delta f}{\alpha}\, \frac{2e\bar{I}_g}{m_n^2 \bar{I}_0^2}\, \frac{R_2}{R_1}. \tag{88}$$

Evidently for high values of m_n the only noise sources which will contribute to the signal-to-noise ratio are those localized within the photo-tube. In this limiting case we get

$$\lim_{m_n \to \infty} \frac{1}{S^2_{\Delta f}} = \frac{2e\Delta f}{\bar{I}_0^2}\, \frac{m}{m-1}\left(\overline{I_0} + \overline{I_0'}\, \frac{m^2}{m^2-1}\right). \tag{89}$$

This shows one of the great advantages of a multiplier photo-tube over an ordinary tube, namely, that the photo-current can already before reaching the amplifier be brought up to such a level that the noise contribution from the first step in the amplifier is negligible. This is possible without any appreciable reduction in the signal-to-noise ratio within the photo-tube as shown above (p. 46). Equation (88) also shows that high values of the resistances R_1 and R_2 improve the signal-to-noise ratio.

b. Design and Performance

As is shown in the block diagram, Figure 1, the electrical system consists of the photo-tube, an amplifier, a homodyne rectifier, a cathode follower and a recorder. It also contains necessary supplies for these units.

1. The Photo Tube System

Voltage Divider. The electrical arrangements for operating the photo-tube consist of a simple bleeder, R in Figure 17 (p. 64), which divides the voltage from a high-tension supply to the voltages for all the dynodes and the cathode. The anode is grounded through the resistance R_1. The voltage between the last dynode and the anode is kept somewhat lower than the voltages between other dynodes by choosing R' less than R. At the low light-levels occurring in raman spectroscopy this lower voltage is sufficient for collecting all the electrons emitted. The values of the resistances R and R' are not critical. WINANS and PIERCE (64) have found that a variation of ± 5 per cent of the dynode voltage is tolerable. The constancy of the resistances during operation with regard to various influences is, however, rather important.

Let V_ν ($\nu = 1, 2, \ldots, n+1$) be the voltage drop over the resistance R_ν and $m_\nu(V_1, V_2, \ldots, V_\nu)$ the multiplication factor between the photo-cathode and dynode ν, then the following relations hold

$$V_\nu = R_\nu(i_0 - I_0 m_{\nu-1}) \quad \nu = 1, 2, 3, \ldots n+1, \tag{90}$$

where i_0 is the current taken from the high-tension supply and I_0 is the primary photo-current ($m_0 \equiv 1$). Further, the total voltage, V_t, is determined from the mode of operation of the high-tension supply. This can be written as:

$$V_t = \sum_{\mu=1}^{n+1} V_\mu = E - R_i i_0, \tag{91}$$

where E is an equivalent electromotive force and R_i is an internal resistance. (In a more complete discussion an impedance Z_i had to be introduced, since the current drawn from the high-tension supply alternates with the pulsating stream of photons on the photo-cathode). Eliminating i_0 we get

$$\frac{V_\nu}{R_\nu}+\frac{1}{R_i}\sum_{\mu=0}^{n+1} V_\mu=\frac{E}{R_i}-I_0 m_{\nu-1}. \tag{92}$$

These $n+1$ equations define the voltages $V_1, V_2, \ldots, V_{n+1}$ as functions of the resistances $R_1, R_2, \ldots, R_{n+1}$ and the current I_0.

The output current from the photo-tube, I_n, is given by

$$I_n = I_0 m_n(V_1, V_2, \ldots, V_n). \tag{93}$$

The change of I_n with changes $\mathrm{d}R_\nu$ and $\mathrm{d}I_0$ in the resistances and the primary current is then obtained from

$$\mathrm{d}I_n=\left(m_n+I_0\sum_{\mu=1}^{n}\frac{\partial m_n}{\partial V_\mu}\frac{\partial V_\mu}{\partial I_0}\right)\mathrm{d}I_0+I_0\sum_{\nu=1}^{n+1}\left(\sum_{\mu=1}^{n}\frac{\partial m_n}{\partial V_\mu}\frac{\partial V_\mu}{\partial R_\nu}\right)\mathrm{d}R_\nu. \tag{94}$$

Here $\partial V_\mu/\partial I_0$ and $\partial V_\mu/\partial R_\nu$ are obtained from the Equations (92). The complete solution is rather involved and will not be presented. It is just necessary to draw attention to the fact that at sufficiently large primary photo-currents the sensitivity of the system will change and an increased dependence on the stability of the resistances in the bleeder will occur. WINANS and PIERCE recommend for the current through the bleeder a value about five times as large as the output current from the photo-tube. In the present case the total bleeder resistance $2.35 \cdot 10^6\,\Omega$ and the lowest over-all voltage 400 V. give a minimum current of about 175 μA. The highest current which can be taken from the tube is, with regard to fatigue effect, 1 μA. The present design, therefore, seems to give a safe arrangement.

In cases where the secondary photo-current, I_n, can be neglected in comparison with the current, i_0, Equations (90) simplify to

$$V_\nu = R_\nu i_0. \tag{95}$$

Then with respect to Equation (91)

$$V_\nu = \frac{E R_\nu}{R_i+\sum_{\mu=1}^{n+1} R_\mu} \tag{96}$$

and consequently

$$\mathrm{d}I_n = m_n \mathrm{d}I_0 + I_0\sum_{\nu=1}^{n+1}\left(\sum_{\mu=1}^{n}\frac{\partial m_n}{\partial V_\mu}\frac{\partial V_\mu}{\partial R_\nu}\right)\mathrm{d}R_\nu, \tag{97}$$

where $\partial I_n/\partial I_0$ is independent on I_0 but $\partial I_n/\partial R_\nu$ still dependent on changes in the voltages with R_ν. To estimate this dependence let

$$m_n = \prod_{\mu=1}^{n}\left(\frac{V_\mu}{V}\right)^\beta, \tag{98}$$

where V is the voltage giving unit gain. Then

$$\frac{\partial m_n}{\partial V_\mu} = \frac{\beta m_n}{V_\mu} \tag{99}$$

and

$$\frac{\partial I_n}{\partial R_\nu} = I_0 \beta m_n \sum_{\mu=1}^{n} \frac{1}{V_\mu} \frac{\partial V_\mu}{\partial R_\nu}. \tag{100}$$

From Equations (96) we get

$$\frac{1}{V_\mu} \frac{\partial V_\mu}{\partial R_\nu} = \begin{cases} -\dfrac{1}{R_i + \sum\limits_{\mu=1}^{n+1} R_\mu}; & \mu \neq \nu \\ \dfrac{1}{R_\nu} - \dfrac{1}{R_i + \sum\limits_{\mu=1}^{n+1} R_\mu}; & \mu = \nu \end{cases} \tag{101}$$

and finally for the relative change of I_n

$$\left(\frac{\mathrm{d}\, I_n}{I_n}\right)_{I_0} = \beta \sum_{\nu=1}^{n+1} \left(1 - \frac{n R_\nu}{R_i + \sum\limits_{\mu=1}^{n+1} R_\mu}\right) \frac{\mathrm{d}\, R_\nu}{R_\nu}. \tag{102}$$

Let us assume $\mathrm{d}\, R_\nu / R_\nu$ to be the same for all the resistances R_ν. Then

$$\left(\frac{\mathrm{d}\, I_n}{I_n}\right)_{I_0} = \beta \left(1 + \frac{n R_i}{R_i + \sum\limits_{\mu=1}^{n+1} R_\mu}\right) \frac{\mathrm{d}\, R_{\mathrm{tot}}}{R_{\mathrm{tot}}}. \tag{103}$$

The term $n R_i / \left(R_i + \sum\limits_{\mu=1}^{n+1} R_\mu\right)$ is always small compared to unity as $R_i \ll R_{\mathrm{tot}}$. Then the stability of the output current is directly proportional to changes in the bleeder resistances. For a temperature change, $\mathrm{d}\, t$, we have $\mathrm{d}\, R_{\mathrm{tot}} / R_{\mathrm{tot}} = \alpha\, \mathrm{d}\, t$. With regard to the low temperature coefficient of resistivity, α (at 25 °C. $\alpha = 2 \cdot 10^{-6}$ for constantan and zero for manganin), there is no difficulty in reaching a sufficient temperature stability. Other causes, however, may be more serious.

The output impedance in the anode circuit of the phototube must be chosen with some care. The voltage drop over this impedance will decrease the effective voltage between the anode and the last dynode. This can cause deviations from the linear operation of the photo-tube. Now the anode current has to be kept below 1 μA. Therefore the voltage drop over the output impedance ($|Z| < 10^6\,\Omega$) will not exceed one volt and this has no importance at the low light levels used here.

High Tension Supply. In a multiplier photo-tube the change in over-all amplification with the dynode voltage $\mathrm{d}\, m_n / \mathrm{d}\, V$ takes very large values. In Figure 15 this

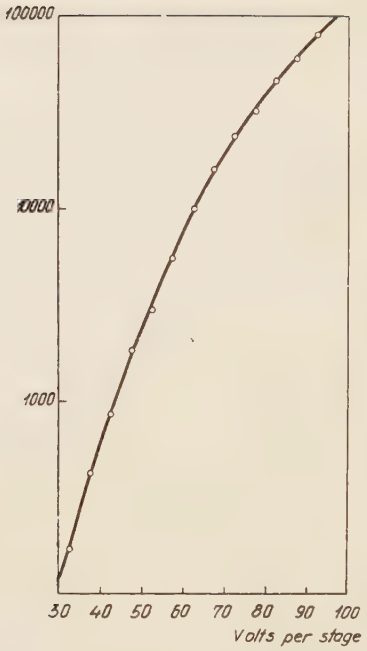

FIGURE 15. Change in amplification factor with dynode voltage, $\mathrm{d}\,m_n/\mathrm{d}\,V$, as a function of dynode voltage (calculated from data in RCA Tube Handbook).

dependence is given as a function of the voltage per stage for an RCA 1P21 photo-tube. A usual working range is 50–70 V./stage which means that $\mathrm{d}\,m_n/\mathrm{d}\,V$ takes values between 2000–20000. Small changes in the voltage from the high-tension supply, especially ripple, can, therefore, easily give rise to undesirable hum in the output current. The change in output current with changes in the over-all voltage. V_t, can be found in the following way. From Equation (93) we have

$$\mathrm{d}\,I_n = I_0 \sum_{\mu=1}^{n} \frac{\partial m_n}{\partial V_\mu}\,\mathrm{d}\,V_\mu = I_0 \beta m_n \sum_{\mu=1}^{n} \frac{\mathrm{d}\,V_\mu}{V_\mu}. \tag{104}$$

But $\mathrm{d}\,V_\mu/V_\mu = \mathrm{d}\,V_t/V_t$, thus

$$\frac{\mathrm{d}\,I_n}{I_n} = \beta n \frac{\mathrm{d}\,V_t}{V_t} \approx n \frac{\mathrm{d}\,V_t}{V_t}. \tag{105}$$

$|\mathrm{d}\,I_n/I_n| \leq 10^{-3}$ gives for a 9-stage multiplier $|\mathrm{d}\,V_t| \leq 55$ mV. at $V_t = 500$ V. As long as the photo-tube is operated in a range where β does not change with the applied voltage, the stabilizer must be designed for the best absolute stability at the lowest voltage used. When β increases with the applied voltage the requirements on the stability of the stabilizer voltage also increases.

At current levels where I_n is of the same order of magnitude as the dark currents, I'_n, the total relative variation (hum/signal ratio) is given by

$$\frac{\mathrm{d}\,(I_n + I'_n)}{I_n} = \frac{I_n + I'_n}{I_n} \left(\frac{\mathrm{d}\,I_n}{I_n}\right)_{I'_0=0} \tag{106}$$

Evidently the detection of very weak signals is only possible when the stability of V_t is very good.

The circuit diagram of the rectifier and stabilizer for high voltage to the photo-tube is shown in Figure 16.[1] The rectifier is of conventional type. The alternating voltage from the high-tension transformer, T_4, is subjected to one-way rectification in the tube V_1. The resulting pulsating voltage is smoothed by an LC-circuit before it is applied to the input of the stabilizer. In this, the control element consists of the tube V_2, the control grid of which is excited by a fraction of the output-voltage variation, collected in the voltage divider $R_{13}-R_{17}$ and then compared with a reference voltage in tube V_4 and finally amplified in tubes V_4 and V_3. The condensers C_4-C_6 are necessary to prevent the circuit from oscillating. The condenser C_7 constitutes a low-impedance channel for the ripple voltage. The networks C_7, R_{14} and C_3, R_1 also contribute to the stability of the circuit by phase-correcting action. The meter M_1 measures the total current taken from the rectifier. M_2 is used to measure the voltage over tube V_2 for checking purposes; finally M_3 indicates the actual output voltage. This can, by means of the switch S_1, be changed from 400 V. to 1400 V. in steps of 200 V. S_1 also changes the input on the primary side of the transformer T_4 in order to prevent overloading of the control tube V_2. A fine adjustment can be made with the switch S_2, which divides the 200 V. intervals in 20 V. intervals; this means that the voltage per stage in the photo-tube can be adjusted to about 2 V. On the primary side, the high-tension transformer is connected to the voltage source through the relay tube V_9 which closes the circuit after about 45 sec.; this is to give the cathodes in the tubes time to warm up before the high-tension is applied.

The comparising circuit in the stabilizer corresponds principally to an arrangement used by Miller (98) (*cf.* also Greenwood, Holdam and Macrae (99)) and the motive with this circuit — except the comparison action — is to compensate for effects caused by changes in the filament voltage and aging processes in the tube. Let v denote an equivalent electromotive force in the cathode circuit representing the combined action of the two effects. Further let e be the corresponding response in the voltage output for the tube. Then the ratio e/v is a measure of the compensating action of the circuit. If both triode units of the tube are assumed to have the same tube constants the following expression is easily obtained

---

[1] I am much indebted to Fil. kand. A. Bengtsson for placing this diagram at my disposal and his permission to publish it.

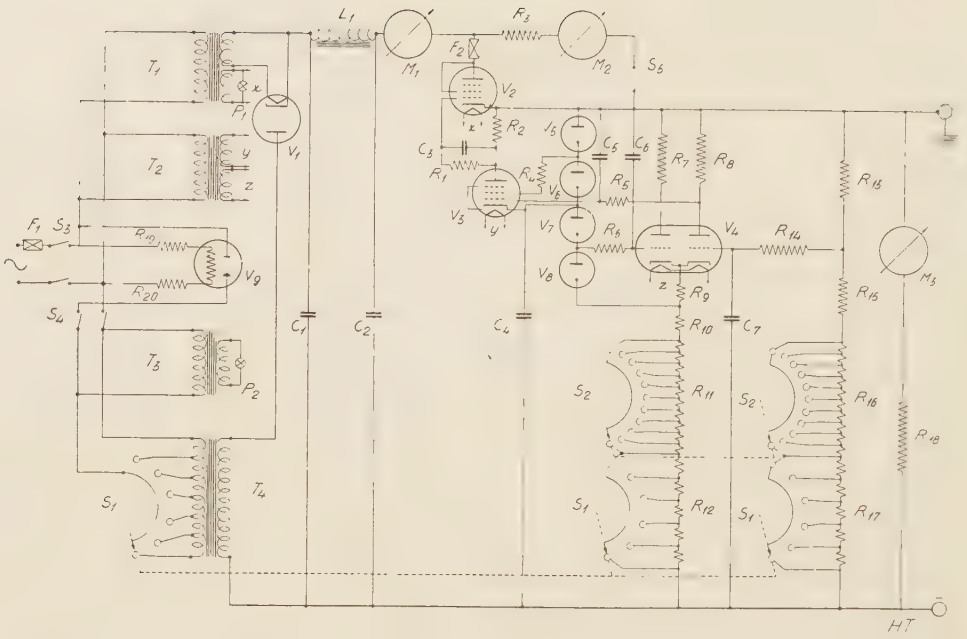

FIGURE 16. Circuit diagram of the high-tension supply. Details about coupling elements are given in Appendix II.

$$\frac{e}{v} = \left[1 + R_9\left(\frac{1+\mu}{r_p + R_7} + \frac{1+\mu}{r_p + R_8}\right)\right]^{-1}. \tag{107}$$

Using the values $R_7 = R_8 = 10^6\,\Omega$, $R_9 = 2 \cdot 10^5\,\Omega$, $r_p = 10^5\,\Omega$ and $\mu = 70$ we obtain $e/v = 0.04$.

As reference elements, tubes V_5–V_8, the Philips voltage-regulator tube 85A1 has been used. The excellent performance of these tubes — especially their high stability — is ascribed by JURRIAANSE (100) firstly, to a carefully prepared molybdenum cathode and secondly, a thick layer of molybdenum deposited on the walls of the tube. This layer acts both as a screen between the discharge and the glass envelope and as a getter by adsorbing any residual impurities. Performance tests made by BLOMGREN have been reported by BOERS (101). When the current, through tubes taken at random from stock, was rigorously kept constant the voltage did not change more than a few hundredths of a per cent during a period of up to 14 h. BENSON (102–105) has, in a series of papers, studied the properties of the 85A1 tubes compared with other types. The extinction voltage of 85A1 tubes does not show any change after as much as 10000 h. running. With other tubes this voltage has a tendency to increase after some time so that they are of no further use as reference elements. Furthermore he has found that the drift in the running voltages is small already one minute after firing. For a series of tubes the average drift was about a tenth of a per cent of the running voltage (the current was kept constant within a tenth of a per cent). The temperature coefficient was found to be -0.03 mV./V./°C. TITTERTON (106) reports that the voltage-current characteristics

of glow-discharge tubes show negative-resistance discontinuities. The characteristics vary from tube to tube but show a smaller variation for 85A1 tubes than for any other voltage regulator tubes tested. Overloading of the tube changes the characteristic, but after ten minutes it usually assumes a steady-state value. He recommends that the 85A1 tube should be operated at a current of 5 mA.: it is then an excellent reference element. With regard to elimination of ripple the dynamic characteristics of the tubes are of importance. TITTERTON has found appreciable hysteresis effects in some types of tubes. The 85A1 tube showed good reproducibility in this respect, and no sharp discontinuities in the voltage were observed. A capacitor shunting the tube decreases the hysteresis and smoothes the irregularities. Oscillations may sometimes occur, especially when the capacity is too high (> 0.1 μF). Thus the tubes are not as effective as a filter for ripple voltages as the static characteristic would indicate.

The performance of the stabilizer will be expressed in the parameters introduced by GILVARRY and RUTLAND (107) (*cf.* also HUNT and HICKMAN (108)). Let e_i denote the variational input voltage to the stabilizer, i_i the variational input current, e_o the variational output voltage and i_o the variational output current. Then the following four performance parameters are necessary and sufficient to specify the behaviour of the stabilizer under no load and zero supply resistance conditions:

stabilization ratio $s = (e_i/e_o)_{i_o=0}$

internal resistance $r = -(e_o/i_o)_{e_o=0}$

open-circuit input resistance $q = (e_i/i_i)_{i_o=0}$

reciprocal difference of the short-

circuit input and transfer conductances $p = (e_i/(i_i - i_o))_{e_o=0}$.

The quantities $1/q$ and $1/p$ are equivalent shunt conductances for open and short-circuited output respectively, since these conductances correspond to shunt currents diverted from the load by the stabilizer itself. (HUNT and HICKMAN treat stabilizers where p is equal to q, a condition which is fulfilled in many cases.) The corresponding parameters under load condition and a non zero supply resistance are denoted by S, R, Q, and P.

At an output voltage of 450 V. and a load current of 0.7 mA. the following values have been found:

$$S > 6000$$

$$R < 4.5\,\Omega$$

$$Q > 85 \cdot 10^5\,\Omega$$

$$P = \infty\,\Omega.$$

This indicates a performance of the stabilizer which is quite satisfactory for the present purposes.

The ripple voltage did not exceed 2 mV. for output voltages up to 1100 kV.

2. The Amplifier System

Amplifier. The pulsating current coming from the photo-tube gives rise to a pulsating voltage over the output impedance in the photo-tube anode circuit. This impedance constitutes the input impedance of the main amplifier in the electrical system. The circuit diagram of the amplifier is shown in Figure 17. It is a five stage resistance-capacitance-coupled amplifier, which is tuned to have its maximum band-pass at 100 c./s. (twice the frequency of the mains supply). The tubes used are RCA 5693.

The input circuit of the first stage consists of the resistor, R_1, connected to the grid through a capacitor, C_1, chosen with regard to grid resistor, R_2, to give a moderate attenuation of the signal. The tube V_1 is used as a triode and is self-biased through the cathode resistor R_3. This resistance is by-passed with a condenser C_2 to give higher amplification to the stage. In the second stage a feed-back loop is introduced through the C_4R_5-network. An attenuator, R_{10}, is placed between the second and third stages which reduces the signal in powers of ten. A second attenuator, R_{25}, between the fourth and fifth stages gives attenuation in the steps 0.1, 0.2, ..., 0.9, 1. A continuous change in the signal is obtained through the resistor R_{26}. The tuning system of the amplifier is the same as that used by THOMPSON *et al.* (12). A combination of a low-pass and a high-pass feed-back network on the third and fourth stages gives the amplifier a band-pass with the centre at 100 c./s. and an almost constant amplification between 95 c./s. and 105 c./s. The actual relative amplification around the centre frequency is given by the following figures:

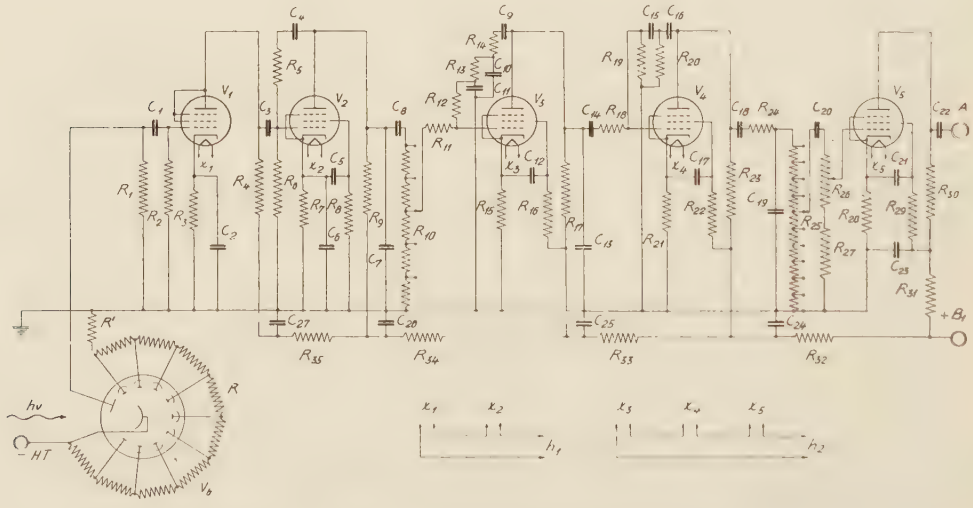

FIGURE 17. Circuit diagram of amplifier. Details about coupling elements are given in Appendix II.

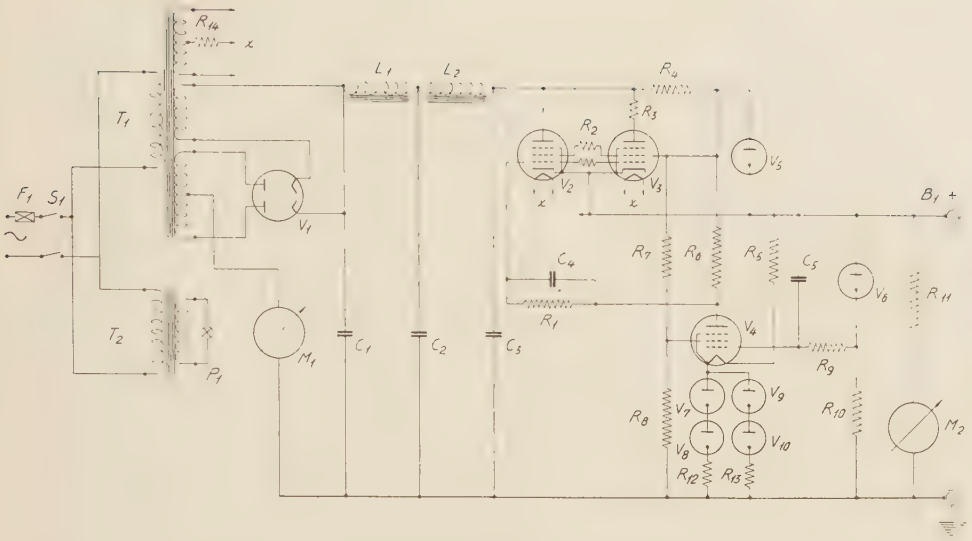

FIGURE 18. Circuit diagram of anode-voltage supply of amplifier. Details about coupling elements are given in Appendix II.

95 c./s.	0.987	100 c./s.	1
96 ,,	0.989	101 ,,	1.000
97 ,,	0.994	102 ,,	1.000
98 ,,	0.996	103 ,,	0.996
99 ,,	1.000	104 ,,	0.994
		105 ,,	0.989

The maximum amplification is about 70000 times. The band-width at 50 per cent transmission is 80 c./s. which is a rather high value. On the other hand the tuning of this amplifier is not critical since the main noise reduction is obtained later, by means of the homodyne rectification. However, a certain amount of noise reduction is necessary to prevent overloading of the later stages of the amplifier. The cathode resistors of the three last stages are not by-passed. This gives additional feed-back and increased stability.

The first two stages of the amplifier have been carefully screened to prevent pick-up in the coupling elements. Following the principles outlined by GUSTAFSON (109), LYONS (110) and ELLWOOD (111) a combination of a conductive and a high permeability material has been used. The most sensitive parts have been shielded with copper cases; these are then placed in iron cases, in a large case of copper. Iron has not the necessary magnetic properties to screen off weak magnetic fields. The use of very high-permeability materials such as Permalloy, Mumetal *etc.* was not, however, convenient. It was also found that with the present arrangement the

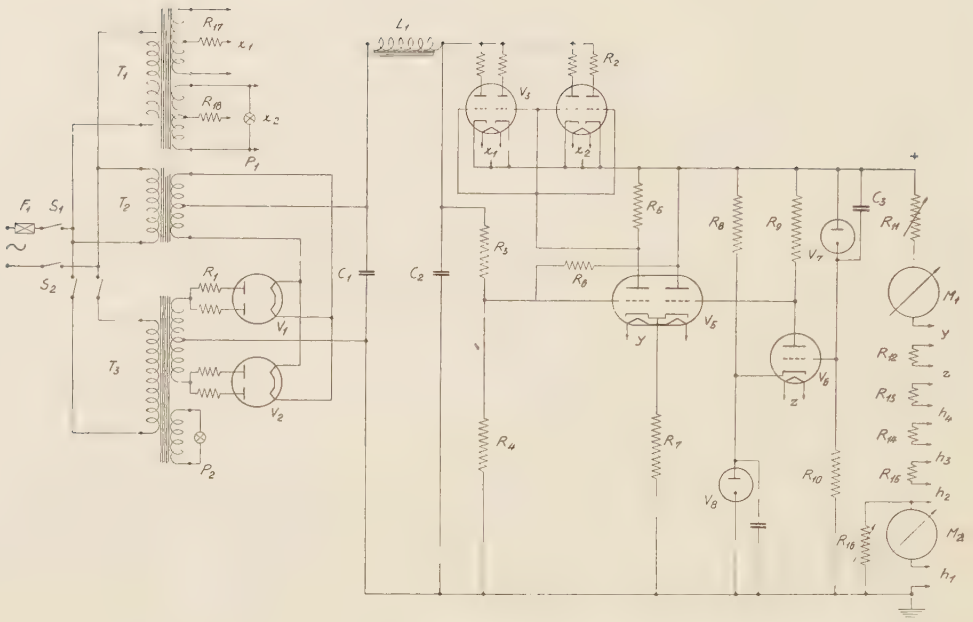

FIGURE 19. Circuit diagram of filament-current supply. Details about coupling elements are given in Appendix II.

pick-up gave an input signal on the first grid having a sufficiently low value in comparison to the noise from the photo-tube system.

Extreme precautions were also taken with respect to the grounding connections. All the amplifier stages, the supply circuits, the high-tension supply, the rectification circuits and the photo-tube system were separately grounded to the first amplifier stage. The chassis for all the units, as well as the racks, were also grounded to this stage. Connections between different parts were always made with screened wires which on critical points were also coaxial.

Anode Voltage Supply. The anode voltage (B_1) is applied to the anode resistors through *RC*-networks which filter away any residual ripple in the output voltage from the anode supply (Figure 18). This supply consists of a rectifier and a stabilizer. Both are of conventional design. Through the twin-diode V_1 a full-wave rectification is obtained. The pulsating voltage is smoothed in an *LC*-network and fed into the stabilizer. The sampling circuit consists of the tube V_6 and the resistor R_{10}. The voltage variation is compared with a reference voltage from the cathode circuit of the tube V_4. After amplification it controls the grids of the tubes V_2 and V_3 constituting the control element of the stabilizer. A compensation network, consisting of the tube V_5 and the resistors R_7 and R_8, introduces a fraction of the unstabilized voltage on the screen grid of V_4 and produces an additional control-signal on the

grids of V_2 and V_3. The filament current of tube V_4 is taken from the stabilizer. The meter M_1 measures the total current and the meter M_2 indicates the output voltage.

Filament Current Supply. The filament current for the amplifier is a carefully stabilized direct current. The circuit diagram of the supply is shown in Figure 19. The design is very similar to that given by ROESS (112). Full-wave rectification is obtained in a double twin-diode arrangement. The pulsating voltage is smoothed in an *LC*-filter before it enters the stabilizer. The control element of this consists of two twin-triodes V_3, V_4. The sampling circuit is the resistor R_{10} connected to the output through the tube V_7. The voltage variation is compared with the reference voltage from the tube V_8 in the triode V_6 and then after amplification fed to the grid of one of the triode halves of a twin-triode tube V_5. The other grid is excited by a fraction of the unstabilized voltage collected in the compensating network $R_3 R_4$. The resultant output signal from the twin-triode controls the grids of the tubes V_3 and V_4. The filament current of the tubes V_5 and V_6 is taken from the stabilizer. h_1 and h_2 constitute the outputs of the filament current to the amplifier: h_1 supplies the two first stages and h_2 the three last stages. h_1 is shunted with a variable resistor R_{16} by means of which the magnitude of the filament current of the first steps can be decreased in order to minimize the noise arising from flicker effect (*cf.* ROESS (112)). This current is measured by the meter M_2; the ordinary current by the meter M_1.

3. The Homodyne Rectifier, Cathode Follower and Recorder

Homodyne Rectifier. The amplitude modulated alternating current signal coming from the amplifier is rectified before it is fed into the recording instrument. The rectification is done in a homodyne rectifier. The signal is mixed with a voltage of the same frequency. The output signal will then contain a direct current component and a number of alternating current components of various frequencies. After filtering, the direct current component will remain and the magnitude of this is proportional to the amount of luminous energy entering the slit of the spectrograph. The homodyne principle was first discussed in a series of papers by TUCKER *et al.* (113–117) in connection with its application to radio receivers. It has been used by THOMPSON *et al.* (12) and by CHUSHCHINSKII (13, 14) for the purpose under discussion. The circuit used here is almost identical with THOMPSON's.

The signal from the amplifier, V_{g_1}, is fed to the first grid of a mixer tube and there mixed with a signal, V_{g_3}, fed to the third grid. The transconductance first grid to plate of the mixer tube will vary with the voltage of the third grid (*cf.* HEROLD (118)) and can be expressed by the following Fourier expansion

$$g_m = a_0 + a_1 \cos \omega_0 t + a_2 \cos 2\,\omega_0 t + \cdots, \tag{108}$$

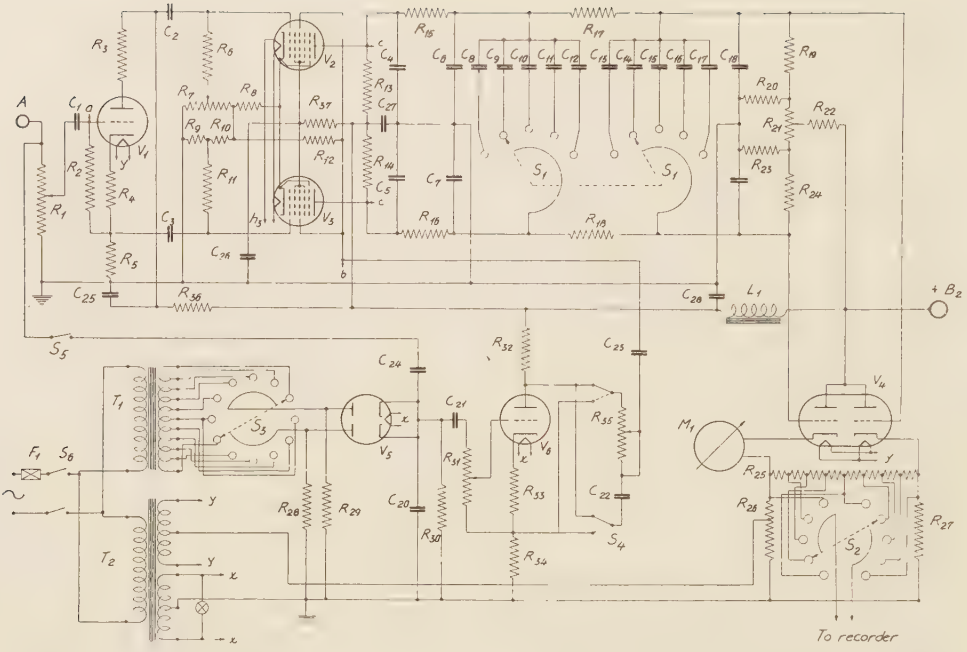

FIGURE 20. Circuit diagram of homodyne rectifier and cathode follower. Details about coupling elements are given in Appendix II.

where ω_0 is the frequency of V_{g_3}. Let $V_{g_1} = E \sin(\omega_s t + \varphi)$, then the corresponding current is given by

$$i_p = g_m E \sin(\omega_s t + \varphi). \tag{109}$$

Introducing the value of g_m and applying simple trigonometric formulae we get

$$i_p = a_0 E \sin(\omega_s t + \varphi) + \tfrac{1}{2} E \sum_{n=1}^{\infty} a_n \{\sin[(\omega_s - n\omega_0)t + \varphi] + \sin[(\omega_s + n\omega_0)t + \varphi]\}. \tag{110}$$

Consequently the voltage at the anode will be

$$V = R i_p, \tag{111}$$

which in the case of synchronous signals, $\omega_s = \omega_0$, simplifies to

$$V = \tfrac{1}{2} R E a_1 \sin\varphi + \text{alternating current components}. \tag{112}$$

The rectified signal is thus sensitive to the phase difference between the voltages V_{g_1} and V_{g_3}.

In the actual design (Figure 20), the signal passes a phase-inverter stage (tube V_1) where it is split into two components differing 180° in phase. These components

are then fed to the first grids of the tubes V_2 and V_3 respectively. The demodulating voltage is obtained from the mains supply after full-wave rectification in the tube V_5. The transformer T_1 and the switch S_3 give a choice of various amplitudes. The phase adjustment of this voltage is made possible by the stage V_6. This circuit gives a voltage of variable phase but of constant amplitude (*cf.* VILLARD (119)). A continuous variation of the amplitude is possible by means of the potentiometer R_{31}. For the voltage difference between the anodes we get

$$\Delta V = Z E a_1 \sin \varphi + \text{alternating current components.} \tag{113}$$

It has been assumed that the two tubes V_2 and V_3 work identically and that their load impedances, Z, are the same. The tubes can be balanced by the potentiometer R_7.

The filter after the mixer stage is an RC-network which passes low frequency signals only. The transmission can be altered by changing the capacitors C_8–C_{12} and C_{13}–C_{17} respectively by means of the switches S_1. This also changes the time constant of the system. Let us denote by $T(j\omega)$ the complex transmission between the two anodes of the mixer tubes and the grids of the cathode follower stage, then the complex voltage difference, $\Delta V'$, between the grids is given by

$$\Delta V' = \Delta V \, T(j\omega)^1 \tag{114}$$

The transmission T is determined from

$$T(j\omega) = \frac{r'}{2r + r' - \omega^2 r^2 r' (2C + C')^2 + j\omega r (r + 3r') (2C + C'')}, \tag{115}$$

where

$$r = R_{15} = R_{16} = R_{17} = R_{18};$$

$$r' = R_{19} + \frac{R_{20} R_{21}}{2R_{20} + R_{21}}; \quad R_{19} = R_{24}; \quad R_{20} = R_{23};$$

C is one of the capacitors C_8–C_{12} (or C_{13}–C_{17});

$$C' = C_6 = C_7 = C_{18} = C_{19}.$$

[1] To prove this relation let us regard the filter as a six-terminal network with transmissions as indicated in Figure 21. Then

$$V_{01'} = T_{11} V_{01} + T_{21} V_{02}$$

$$V_{02'} = T_{12} V_{01} + T_{22} V_{02}$$

and

$$\Delta V' = V_{01'} - V_{02'} = (T_{11} - T_{12}) V_{01} + (T_{21} - T_{22}) V_{02}.$$

For a symmetrical network $T_{11} = T_{22}$ and $T_{12} = T_{21}$, thus

$$\Delta V' = (T_{11} - T_{12}) (V_{01} - V_{02}) = T \Delta V.$$

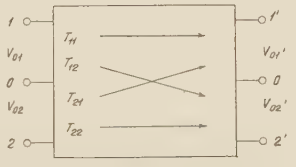

FIGURE 21.

Table 4

Transmission of filter

f	Capacitor C (μF)				
	0.1	0.25	1	4	8
0.1	$4.91 \cdot 10^{-1}$	$4.75 \cdot 10^{-1}$	$3.17 \cdot 10^{-1}$	$9.82 \cdot 10^{-2}$	$3.34 \cdot 10^{-2}$
1	$2.26 \cdot 10^{-1}$	$1.46 \cdot 10^{-1}$	$1.87 \cdot 10^{-2}$	$1.50 \cdot 10^{-3}$	$3.85 \cdot 10^{-4}$
10	$6.15 \cdot 10^{-3}$	$2.05 \cdot 10^{-3}$	$2.10 \cdot 10^{-4}$	$1.51 \cdot 10^{-5}$	$3.86 \cdot 10^{-6}$
100	$6.33 \cdot 10^{-5}$	$2.07 \cdot 10^{-5}$	$2.10 \cdot 10^{-6}$	$1.51 \cdot 10^{-7}$	$3.86 \cdot 10^{-8}$

Using $r = 500\ \text{k}\Omega$, $r' = 1015\ \text{k}\Omega$, $C' = 0.2\ \mu\text{F}$ we get the values given in Table 4 for T at different frequencies and different values of C. Evidently the filter effectively eliminates the alternating current components in the output current even at low frequencies. The homodyne mixer, in combination with the filter, makes the whole amplification system very sharply tuned and this is very advantageous with respect to the noise output of the system. Taking also a noise voltage, $E' \sin(\omega' t + \varphi')$ into acount, we get for the total voltage difference between the grids of the cathode follower

$$|\Delta V_{\text{tot}}| = |T(0)|\,|Z(0)|\,a_1 E \sin\varphi + |T(j\Delta\omega)|\,|Z(j\Delta\omega)|\,a_1 E' \sin(\Delta\omega t + \varphi'), \qquad (116)$$

where $\Delta\omega = \omega_s - \omega'$. From this expression it is seen how the noise voltage is superimposed upon the direct current voltage. The amplitude is decreased as the bandwidth of the system is lowered.

For control purposes the voltage from tube V_5 can, by means of the switch S_5, be fed to the input of the homodyne rectifier. Through outputs from the anodes and the third grids of the mixer tubes, external connections to voltmeters or oscillographs can be made.

Cathode Follower. The output voltage from the homodyne rectifier is fed to the grids of a twin-triode tube V_4 (Figure 20). When the signal increases one of the grids will become more positive and the other more negative. This gives a voltage difference, ΔV_R, between the cathodes determined from

$$\Delta V_R = \frac{g_m}{\frac{2}{R_{25}} + \frac{1}{R_{26}} + \frac{1+\mu}{r_p}}\,\Delta V' \qquad (117)$$

(it has been assumed that both triode halves have identical characteristics and that $R_{26} = R_{27}$). This equation shows that the resistance between the two cathodes, R_{25}, should have a high value in order to make the gain of the stage near to one.

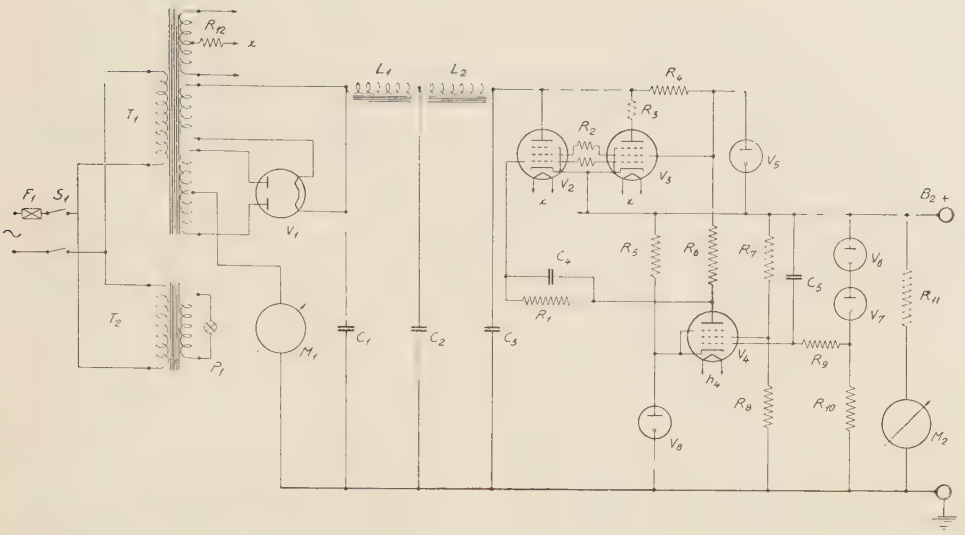

FIGURE 22. Circuit diagram of anode-voltage supply of homodyne rectifier. Details about coupling elements are given in Appendix II.

Due to the input capacitance of the recorder, however, the value of R_{25} should not be so high that the response time of the recorder is considerably increased. The value $2 \cdot 10^3\ \Omega$ gives a gain about 0.9 and has no noticeable influence on the response time. By means of the switch S_2 the voltage $\Delta V_R\, 10^{-n}$ ($n = 0,\ 1,\ 2,\ 3,\ \infty$) can be measured by the recorder. The grids of the tube V_4 is balanced by the potentiometer R_{21} which also functions as a zero control. The meter M_1 measures the current through one of the triodes and is used to control the circuit when the recorder is not in operation.

Anode Voltage and Filament Current Supplies. The anode-voltage supply (Figure 22) is built in the same way as the anode supply of the main amplifier (p. 65). A few alterations were made to get a higher output voltage (300 V.) and a higher output current (about 50 mA.). The tube V_4 does not take its filament current from the stabilizer but from the filament supply previously described (h_4 in Figure 19). A compensation network from the tube V_5 to the screen grid of tube V_4 is not used here because it was judged that the action of such a compensation would be of little importance, due to the low internal resistance of the VR-75 tube used as tube V_5, compared with the resistance of an 85A1 tube used before.

The filaments of the tubes V_1, V_4, V_5 and V_6 are heated directly from the mains supply through a step-down transformer T_2. The current to the tubes V_2 and V_3 is taken from the filament supply (h_3 in Figure 19). A special test showed that the latter tubes were the most sensitive to changes in the heater voltage.

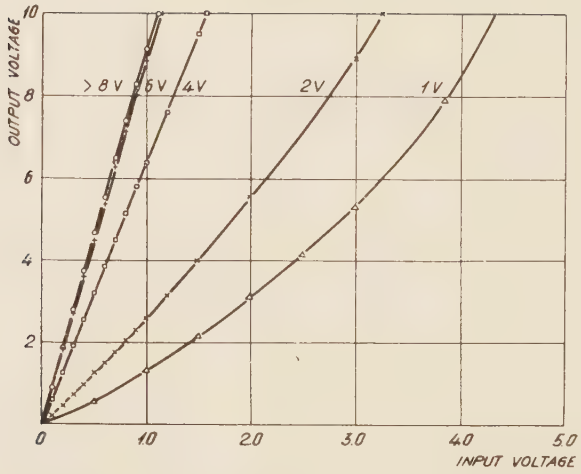

FIGURE 23. Output voltage from cathode follower as a function of input voltage. Measurements have been done at different voltages on third grids of mixer tubes.

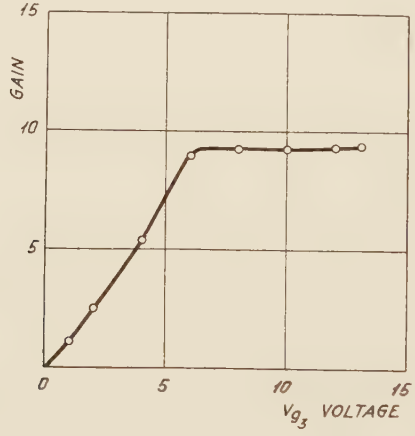

FIGURE 24. Gain of homodyne rectifier and cathode follower at different voltages on third grids of mixer tubes.

Recorder. The recording instrument was a Leeds and Northrup Speedomax Type G Recorder with a response-time of $2\,^1/_2$ seconds for full scale deflection. The instrument has a rather high sensitivity. The full scale corresponds to 10 mV. The output voltage of the cathode follower has a maximum value of 10 V. Therefore a high attenuation before the recorder is necessary. The full sensitivity of the recorder cannot, however, be utilized because of the noise produced in the system; *i.e.* some attenuation is always necessary. This flaw was caused by the fact that the recorder had to be ordered some time before the details of the circuits had been worked out.

Performance. To check the performance of the rectification and recording units the output voltage, as a function of input voltage, was determined at different voltages on the third grids of the mixer tubes. The results follow from Figures 23 and 24. These curves show that a maximum gain of about 9.3 is possible as soon as the voltage of the third grids exceeds 8 V. The circuit is then linear for input signals up to 1 V. These figures are valid when the phase is adjusted to give a maximum output voltage. The constant gain at third grid voltages higher than 8 V. is of considerable importance because it eliminates the influence of variations in the mains supply. Usually a voltage of about 10 V. is used.

General Performance

Before the spectrograph arrangement was used for the study of polymerizing mixtures it was checked in various ways with respect to its general performance. A survey of this work is given below.

A. Interpretation of Recorded Spectra

The curve drawn by the pen of the recorder will not represent a true picture of the energy distribution of the light emerging from the raman tube. The reason for this is the change in distribution caused by the total optical system and by the recording system.

Let $E(\lambda)$ be the original energy distribution. Then $\int_{\lambda_1}^{\lambda_2} E(\lambda)\,\mathrm{d}\,\lambda$ will be the total amount of light energy in the wave-length interval $\lambda_1 \leq \lambda \leq \lambda_2$. The optical system: condensing lens-collimator-dispersing prism-camera can be characterized by a spectral transmittance function $T(\lambda, x)$ describing the change (diffraction, absorption, scattering *etc.*) that a beam of monochromatic light of wave-length λ entering the system will undergo. When leaving the system the beam has its energy spread out over a certain interval around the wave-length λ. The ideal sharp spectrum is blurred out. Any detector system will now make the spectrum still more diffuse. Let the detector have a spectral sensitivity function $S(y)$ and the optical system of the detector unit a spectral transmittance function $T_D(x, y)$. Then the signal from the detector is proportional to

$$E_1(x) = \int_{\lambda_1}^{\lambda_2} \int_{y_1}^{y_2} \int_{x-\delta}^{x} E(\lambda)\, T(\lambda, x)\, T_D(x, y)\, S(y)\,\mathrm{d}\,\lambda\,\mathrm{d}\,y\,\mathrm{d}\,x \qquad (118)$$

where $2\,\delta$ is the width of the exit slit of the spectrograph. x should be interpreted as the nominal wave-length in the focal plane. y_1 and y_2 are the wave-length limits

of the spectral sensitivity of the detector. The solution of Equation (118) for $E(\lambda)$ requires knowledge of the three functions $T(\lambda, x)$, $T_D(x, y)$ and $S(y)$.

Obviously $E_1(x)$ is the spectrum obtained if the recording of the spectrum is done infinitely slowly or with an electrical system having a momentary response. In practical cases the properties of the electrical system is such that a driving function $E_2(t)$ will be changed into a response function $E_3(t)$. The relation between these two functions is determined from the electrical network. Using the Laplace transform representation (*cf.* Doetsch (120) or Valley and Wallman (97)) the solution of the network equations will give

$$F_3(p) = G(p) \cdot F_2(p) \tag{119}$$

where

$$F(p) = \mathfrak{L}[E(t)] = \int_0^\infty e^{-pt} E(t)\,\mathrm{d}t \tag{120}$$

$G(p)$ is the system transform including all the network parameters. Applying the convolution theorem $E_3(t) = E_2(t) * g(t)$ where

$$g(t) = \mathfrak{L}^{-1}[G(p)] = \frac{1}{2\pi j} \int_{c\,j\infty}^{c+j\infty} e^{pt} G(p)\,\mathrm{d}p \tag{121}$$

we get

$$E_3(t) = \int_0^t E_2(t-T)\, g(T)\,\mathrm{d}T \tag{122}$$

The relation between $E_2(t)$ and $E_1(x)$ is obtained from the speed of scanning, $\mathrm{d}x/\mathrm{d}t = v(t)$. Due to the fact that the recorder has an upper limit for the speed of the pen the spectral lines will acquire a false shape as soon as $\mathrm{d}E_3/\mathrm{d}t$ is larger than this limiting value.

Evidently it is a rather difficult problem to obtain a true energy distribution.

In a case where the electrical network can be described by one time constant, τ, the function $g(T)$ is simply $\frac{1}{\tau} e^{-T/\tau}$ and Equation (122) gives after integration

$$E_2(t) = E_2(0)\, e^{-t/\tau} + E_3(t) + \tau \frac{\mathrm{d}E_3}{\mathrm{d}t}. \tag{123}$$

This gives $E_2(t)$ from the measureable quantities E_3 and $\mathrm{d}E_3/\mathrm{d}t$. When $g(T)$ is not known, the best way out of the difficulty is to investigate which combination of scanning speed and time constant gives a true shape of the spectral lines.

Due to the phenomena mentioned here, the meaning of intensity of a recorded spectral line is rather dubious. When intensity is mentioned in connection with my own measurements in the following pages, it always means the maximum height of the line above a background line or the ratio of such a height to a reference height.

B. Linearity of Response

The accuracy and reproducibility of intensity measurements depend upon the linearity of the detecting system; *i.e.* to what extent the anode current from the photo-tube is proportional to the light intensity falling on the photo-cathode. The response of the system to different amounts of light has been tested in a way indicated by Dieke (67). In this method the anode current is measured for a given intensity level. The light is then weakened by a screen and the anode current measured again. It will be smaller in proportion to the absorption of the screen if the response is linear. The weakening will be the same independent of the intensity level used in the measurement.

The following arrangement was used: the water and filter-jackets were removed from the lamp-house and a mercury lamp (Philips 93123 E) was placed horizontally above the ordinary lamps. The light was made diffuse by means of ground-glass plates. The intensity level was adjusted by means of circular apertures placed

Table 5

Linearity of response

Anode current from photo-tube $\times 10^{13}$ A.	Transmission of screen					
	Series 1		Series 2		Series 3	
4.3	—	—	—	—	0.5024	1.015
18.0	—	—	0.4764	1.011	—	—
19.3	—	—	—	—	0.4922	0.994
30.0	0.4679	1.011	—	—	—	—
50.0	—	—	0.4684	0.994	—	—
53.0	—	—	—	—	0.4908	0.991
135	0.4470	0.990	—	—	—	—
178	—	—	0.4743	1.006	—	—
296	—	—	0.4687	0.994	—	—
322	0.4480	0.992	—	—	—	—
475	—	—	0.4679	0.993	—	—
498	0.4503	0.997	—	—	—	—
679	—	—	0.4727	1.003	—	—
938	0.4504	0.998	—	—	—	—
1032	—	—	0.4710	0.999	—	—
1259	0.4502	0.997	—	—	—	—
1324	—	—	0.4715	1.000	—	—
1646	—	—	0.4717	1.001	—	—
2190	0.4535	1.004	—	—	—	—
2200	—	—	0.4715	1.000	—	—
3670	0.4564	1.011	—	—	—	—
Mean value	0.4515	1	0.4714	1	0.4951	1

above the entrance aperture of the lamp-house ((20) in Figure 7). The screen consisted of a photographic plate exposed for a sufficient length of time to produce an absorption of about 50 per cent. It was placed above the apertures on a small tube. It was necessary to place the screen at some distance from the apertures to eliminate the influence of grains in the photographic plate, especially at very small apertures. The apertures were from 0.5 to 5 mm. in diameter.

The results of the measurements are given in Table 5. The first column gives the anode current. This was calculated from the deflection of the recorder and the known gain of the electrical system. It should be noted that the values given correspond to that part of the total anode current which is measured by the system. The following

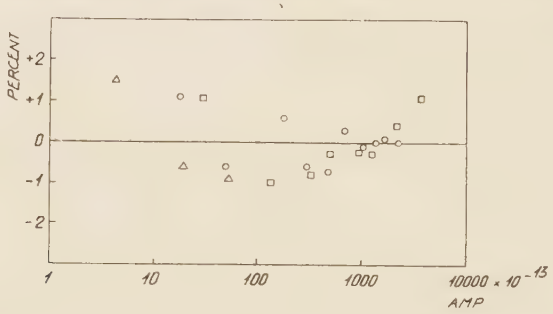

FIGURE 25. Per cent deviation from linearity of response at different light intensities.

columns give the transmission values and the ratio between the actual values and the calculated mean value for three series covering a large range of light intensities. In Figure 25 the per cent deviations from the mean values are plotted against the anode current. Evidently the transmission values in each series are constant within about ± 1 per cent. The change in the values between the series depends upon the arrangement with the ground-glass plates. In series 2 and 3 the plates were placed between the aperture and the screen and thus a small amount of light (due to stray light from the parts of the lamp-house and different things in its surroundings) could enter the aperture through the ground-glass without being weakened by the screen. In series 1 the ground-glass was placed above the screen. The explanation given is consistent with the fact that two ground-glass plates were used in series 3. This will increase the amount of stray light which is not weakened by the screen.

The lowest light level used corresponds to the intensities of fairly strong raman lines, while the highest level represents strong lines in the exciting spectrum. The measurements were made at λ 4358 Å.

In this connection it may be pointed out that the zero point of the recorder sometimes has to be displaced rather much (the potentiometer R_{21} in Figure 20). This can influence the linearity of the cathode-follower unit because of a change in position of the operating point on the tube characteristic. But these deviations can be corrected by a calibration.

C. Signal-to-Noise Ratio

The signal-to-noise ratio of the whole system was measured at three different dynode voltages. The following results were obtained:

	Voltage over the photo-tube		
	500	660	860 V.
Noise without signal, mV.	0.047	0.072	0.093
Signal, mV.	3.17	3.82	4.72
Noise with signal, mV.	0.128	0.136	0.180
Signal-to-noise ratio	24.8	28.1	26.3

The noise was measured as the r.m.s.-value of the variations on the record. The signal was taken as the difference between the arithmetic means at the zero level and the signal level respectively. The measurements are not very accurate but they show that the signal-to-noise ratio does not vary very much with the dynode voltage; probably it has an optimum value at 600–700 V.

D. Influence of Amount of Liquid in Raman Tube

Undesirable effects may be obtained if the proper amount of liquid in the raman tube is not used. Firstly, the amount of continuous background radiation becomes unnecessarily high and secondly, the collimator aperture is not utilized to its full capacity. These questions were studied in a series of measurements of raman and rayleigh line intensities at different fillings of the tube. The liquid used was carbon tetrachloride. From Figure 26 it follows that the intensity of the raman lines increases

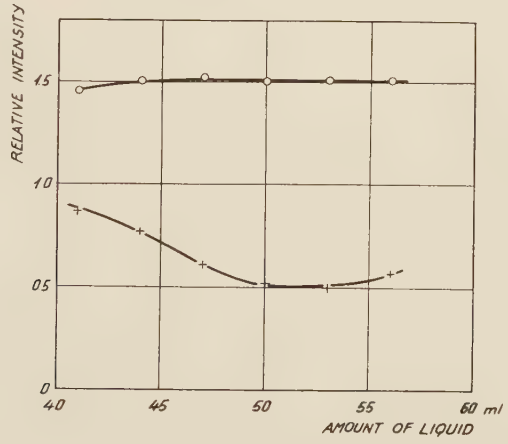

FIGURE 26. Intensity of raman (○) and rayleigh (+) scattering as a function of amount of liquid (carbon tetrachloride) in raman tube.

only slightly when the amount of liquid increases. The intensity of the rayleigh line (λ 4358 Å) however, decreases considerably with an increase in the volume of liquid up to 47 ml., when it is almost constant. In all probability this is a meniscus effect. At volumes less than 47 ml. the meniscus is directly illuminated from the lamps and reflects a large amount of this light into the spectrograph. The small changes in raman line intensity show that the illumination of the raman tube above a level corresponding to 45 ml. is very weak.

E. Stability of Electrical System

A precise determination of line intensities can only be made if the stability of the electrical system is very good both with regard to fortuitous phenomena and to long-time drift. The rectifier and the cathode follower showed excellent behaviour in this respect. The drift was zero for several hours after warming up for less than half an hour. The small variations detected could be correlated with simultaneous changes in the signal voltage taken from the mains supply. The amplifier did not show a similar stability. A very careful investigation of all the stages gave no hint as to the main reason. Replacement of critical coupling elements gave some improvements but still the amplifier drifted with time. After a warming-up period of about three to four hours the drift is still one or two per cent an hour. As the decrease in amplification is quite regular a correction can be applied to the measured line intensities assuming the drift to be linear with time.

F. Purity of Mercury Spectrum

When searching for weak raman lines it is very necessary to know exactly where the weak lines of the mercury spectrum are situated. These lines may be true mercury lines or originate from a carrier gas or from the coating of the electrodes. An investigation of the weak parts of the exciting spectrum was made. The spectrum of the lamps is given in the Figures 27 and 28. Only those parts which are of interest in raman work were recorded: the region 0–1800 cm. $^{-1}$ (Figure 27) and the region about 3000 cm.$^{-1}$ (Figure 28). The wave numbers are given from λ 4358 Å. The first part contains only the lines at 980 cm.$^{-1}$ and 1230 cm.$^{-1}$. The line $\Delta\nu$ 980 cm.$^{-1}$ is probably a barium line from the electrodes (*cf.* p. 15). In the second part there are several lines. A comparison with a low-pressure lamp (Philips 93123 E) showed that the lines at 2490, 2600, 2865, 2980, 3040, 3125 and 3400 cm. $^{-1}$ were common to both spectra. Of these the two lines at 2600 cm.$^{-1}$ and 2980 cm. $^{-1}$ are mercury lines. The remaining lines were not identified but in order to find out if any of them might originate from the electrodes, the light from this region was examined. It was found that the line at 3040 cm.$^{-1}$ increased in intensity.

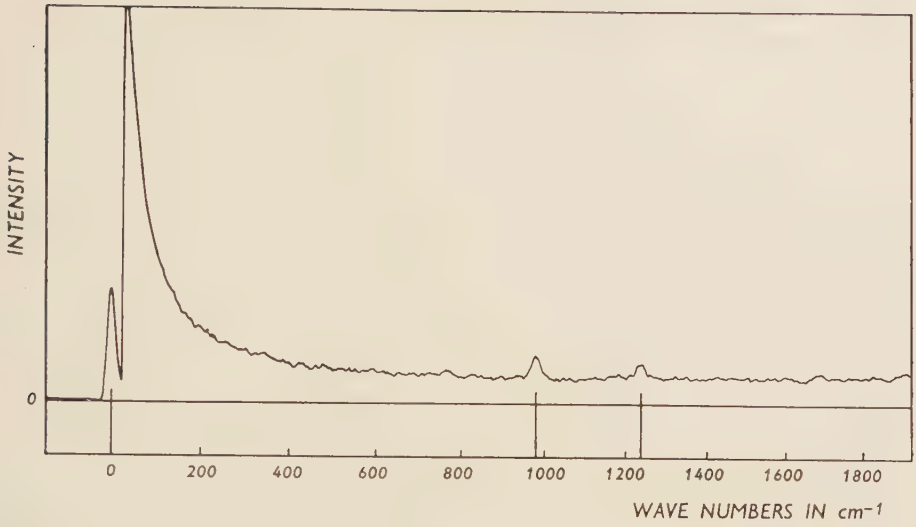

FIGURE 27. Spectrum of mercury lamps in the region 0–1800 cm.$^{-1}$ from λ 4358 Å.

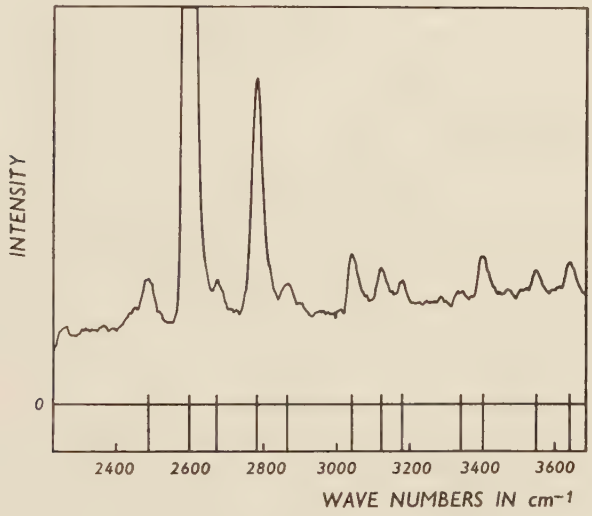

FIGURE 28. Spectrum of mercury lamps in the region about 3000 cm.$^{-1}$ from λ 4358 Å.

A further difference between the two parts of the spectrum is the higher background of the 3000 cm.$^{-1}$ region. The lines falling in this region, however, are mainly due to vibration of hydrogen atoms in the direction of the bond. They are mostly more intense than the other raman lines and therefore the recording can be done at a lower gain, thus to some extent avoiding the difficulties of the background and foreign lines.

G. Reproducibility of Wave Number and Intensity Measurements

a. Determination of Wave Numbers

The spectrograph used is equipped with a single, rather small prism (p. 34). This gives a low resolving power and consequently the instrument is not very useful for determination of wave-lengths. In many cases, however, it is absolutely necessary to be able to identify the lines in a spectrum. Attempts were therefore made to measure raman displacements. Three different liquids were used, namely, carbon tetrachloride, benzene and methyl isobutyrate. The two first liquids contain strong and very strong lines, the third, mainly rather weak lines.

The measurements on carbon tetrachloride and benzene are given in Table 6 and Figure 29. The positions of the lines, Δl, are given in mm. and are obtained as mean values from three separately recorded spectra. The standard deviation of the mean is about 3–4 pro mille. The wave numbers, $\Delta \nu$, have been taken from KOHLRAUSCH (121) (carbon tetrachloride, benzene) and RANK *et al.* (8) (benzene). The value $\Delta \nu$ 1591 cm.$^{-1}$ for benzene is a mean of the values $\Delta \nu$ 1596 cm.$^{-1}$ and $\Delta \nu$ 1581 cm.$^{-1}$ (RANK) respectively $\Delta \nu$ 1605 cm.$^{-1}$ and $\Delta \nu$ 1584 cm.$^{-1}$ (KOHLRAUSCH). The line $\Delta \nu$ 775 cm.$^{-1}$ is a mean of $\Delta \nu$ 760 cm.$^{-1}$ and $\Delta \nu$ 790 cm.$^{-1}$. These lines could not be resolved. From the Δl and $\Delta \nu$-values we get by the method of least squares the following relation

$$\Delta \nu = 4.0190\ \Delta l(1 + 0.19644 \cdot 10^{-3}\ \Delta l) \qquad (124)$$

(the slightly curved line in Figure 29). The $\Delta \nu_{cal}$-values in Table 6 have been obtained from this equation using the measured Δl-values. The relative deviations from the true values show that a fairly good precision is possible.

TABLE 6

Determination of wave numbers

Substance	Δl, mm.	$\Delta \nu$, cm.$^{-1}$	$\Delta \nu_{cal}$, cm.$^{-1}$	Difference per cent
CCl_4	54.1	217	220	+1.38
,,	77.0	313	314	+0.32
,,	111.2	459	457	−0.44
C_6H_6	145.6	604	602	−0.33
CCl_4	187.1	775	780	+0.65
C_6H_6	202.2	847	845	−0.24
,,	235.1	990	989	−0.10
,,	277.0	1173	1174	+0.09
,,	369.1	1591	1591	±0.00

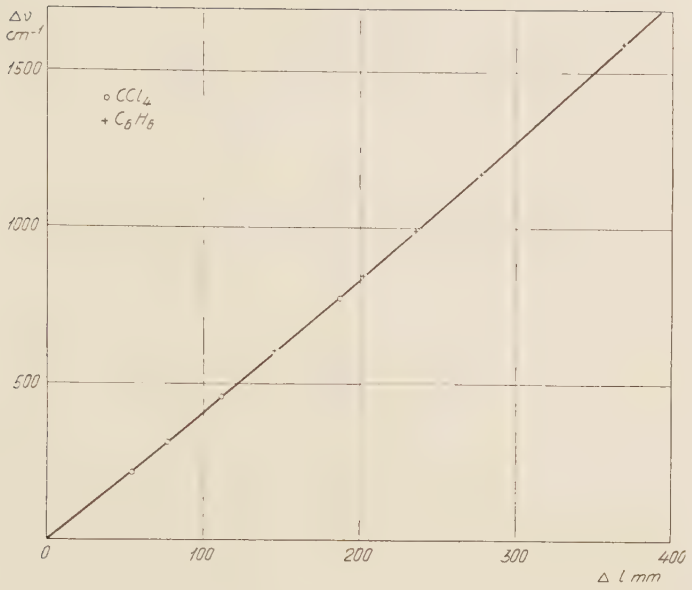

FIGURE 29. Relation between wave number difference, $\Delta\nu$, and line position on chart, Δl.

TABLE 7

Position of raman lines in methyl isobutyrate

Δl, mm.	M, mm.	M, per cent	$\Delta\nu_{cal}$	$\Delta\nu$ Ref. (122)
—	—	—	—	313
79.4	± 0.7	± 0.9	324 ± 3	—
—	—	—	—	361
114.65	± 0.25	± 0.2	471 ± 1	478
145.15	± 0.4	± 0.3	600 ± 2	608
—	—	—	—	755
194.3	± 0.7	± 0.3	811 ± 3	—
—	—	—	—	822
210.5	± 0.9	± 0.5	881 ± 4	892
—	—	—	—	948
232.2	± 1.0	± 0.4	976 ± 4.5	—
—	—	—	—	991
260.25	± 1.2	± 0.5	1099 ± 5.5	1104
273.95	± 1.2	± 0.45	1160 ± 5	1154
306.2	± 1.4	± 0.45	1305 ± 6	1303
337.35	± 1.4	± 0.4	1446 ± 6.5	1453
398.05	± 1.3	± 0.3	1725 ± 6	1733 ± 6

In a spectrum where the lines are weak, they will change their shape between different records owing to the unavoidable noise. In order to investigate to what extent this may influence the accuracy in the determination of the corresponding wave numbers the raman spectrum of methyl isobutyrate was studied. The spectrum is reproduced in Figure 30 on p. 84. Four spectra were measured. The result is collected in Table 7. The first column gives the mean value of Δl, the second and third the mean deviation of the mean. The last columns give the wave numbers calculated from Equation (124) and those obtained from KOHLRAUSCH, KÖPPL and PONGRATZ (122). The lines $\Delta\nu$ 324 cm.$^{-1}$, $\Delta\nu$ 811 cm.$^{-1}$ and $\Delta\nu$ 976 cm.$^{-1}$ are not resolved. Even in this case rather good results can evidently be obtained.

b. Intensity Measurements

The possibilities of making accurate intensity measurements were tested on carbon tetrachloride and methyl isobutyrate. On the former, two series of measurements were made: one after a warming-up period of the electrical system of about five hours and one at an earlier stage. The intensities were measured as the vertical distance from the peak of the line to a base line drawn for $\Delta\nu$ 459 cm.$^{-1}$ between the flat part just to the right and the minimum to the left of the line and for $\Delta\nu$ 313 cm.$^{-1}$ and $\Delta\nu$ 217 cm.$^{-1}$ from this minimum and the minimum to the right of the exciting-line (*cf.* Figure 31 p. 85). Further, an attempt to measure the area of the lines was made. The procedure used by HEIGL, BLACK and DUDENBOSTEL (15) was applied. The results are given in Table 8. In the first series there may be a slight drift of the values. The reproducibility, however, is satisfactory. REITZ (123) has given a standard deviation of the mean of $\pm$ 14 per cent for the carbon tetrachloride lines. The deviation for the area measurements will naturally be somewhat larger due to uncertainties of two dimensions. In the second series the values are larger than in the first one and a drift is noticeable. This series clearly illustrates the necessity of allowing the electrical circuits to warm up for a sufficient length of time.

The ratios of the raman line intensities are (height measurements):

$$\Delta\nu\,459 : \Delta\nu\,313 : \Delta\nu\,217 = 1 : 0.869 : 0.728 \text{ (first series)}$$
$$= 1 : 0.852 : 0.724 \text{ (second series)}$$
$$= 1 : 0.872 : 0.726 \text{ (}v.\ infra\text{)}$$

CHIEN and BENDER (10) have given the ratios 1 : 0.93 : 0.82. From a spectrum obtained with a spectrograph built by Applied Research Laboratories the ratios 1 : 0.85 : 0.69 have been calculated.

The measurements on methyl isobutyrate were made on four spectra. Before and after the recording of each of these spectra the three strong carbon tetrachloride lines were recorded. This reference procedure was first employed by RANK *et al.* (8). The intensity measurements were made as height determinations. All the carbon

TABLE 8

Intensities of carbon tetrachloride lines (L mean value, m standard deviation, M standard deviation of the mean)

Spectrum No.	Intensity from					
	Height measurements, mm.			Area measurements, mm.^{2}		
	217 cm.$^{-1}$	313 cm.$^{-1}$	459 cm.$^{-1}$	217 cm.$^{-1}$	313 cm.$^{-1}$	459 cm.$^{-1}$
54 b 1	89.2	106.5	122.7	583	649	783
2	87.0	105.0	119.0	557	630	790
3	87.7	104.6	121.5	556	637	765
4	89.5	105.7	122.0	557	655	822
5	87.5	104.5	120.2	538	621	774
6	84.6	99.7	116.2	532	579	759
7	85.2	102.6	120.6	511	619	782
8	87.1	104.0	118.5	522	618	769
9	84.0	100.2	115.3	512	590	737
10	84.9	101.6	114.5	522	583	715
L	86.67	103.44	119.05	539.0	618.0	768.6
m	$\pm$ 1.92	$\pm$ 2.32	$\pm$ 2.89	$\pm$ 23.6	$\pm$ 26.8	$\pm$ 31.4
M	$\pm$ 0.61	$\pm$ 0.73	$\pm$ 0.91	$\pm$ 7.5	$\pm$ 8.5	$\pm$ 9.9
	$\pm$ 0.7 %	$\pm$ 0.7 %	$\pm$ 0.8 %	$\pm$ 1.4 %	$\pm$ 1.4 %	$\pm$ 1.3 %
55 b 1	97.6	113.2	132.0	575	634	890
2	94.3	114.5	129.1	561	675	825
3	94.5	107.1	129.0	581	616	850
4	89.5	107.7	127.1	519	613	857
5	87.9	103.0	123.0	518	582	767
L	92.76	109.10	128.04	550.8	624.0	837.8
m	$\pm$ 3.87	$\pm$ 4.72	$\pm$ 3.32	$\pm$ 30.4	$\pm$ 34.2	$\pm$ 45.8
M	$\pm$ 1.73	$\pm$ 2.11	$\pm$ 1.49	$\pm$ 13.6	$\pm$ 15.3	$\pm$ 20.5
	$\pm$ 1.9 %	$\pm$ 1.9 %	$\pm$ 1.2 %	$\pm$ 2.5 %	$\pm$ 2.5 %	$\pm$ 2.5 %

tetrachloride lines were measured and the corresponding ratios calculated. The mean of these values was taken (*v. supra*) and the intensities of the two lines $\Delta\nu$ 217 cm.$^{-1}$ and $\Delta\nu$ 313 cm.$^{-1}$ were corrected to the same level as the line $\Delta\nu$ 459 cm.$^{-1}$. Then the mean value of these three intensities was determined for the spectra taken immediately before and after a spectrum of methyl isobutyrate. In this way the influence of an accidental change in the intensity of the $\Delta\nu$ 459 cm.$^{-1}$ lines is partly eliminated. The scattering coefficients given in Table 9 have been calculated as the ratio between the measured heights of the methyl isobutyrate lines and the carbon tetrachloride reference line. A correction was made for the different gains of the amplifier in recording the spectra of the two liquids. No correction was applied for the difference

TABLE 9

Scattering coefficients of raman lines of methyl isobutyrate

Wave numbers $cm.^{-1}$	Scattering coefficients						
	Spectrum No. 56	Spectrum No. 56 a	Spectrum No. 56 b	Spectrum No. 56 c	Mean value	M	M per cent
324	0.0355	0.0355	0.030	0.039	0.035	$\pm$ 0.002	$\pm$ 5.2
471	0.079	0.071	0.072	0.073	0.073	$\pm$ 0.002	$\pm$ 2.5
600	0.038	0.028	0.030	0.028	0.031	$\pm$ 0.002	$\pm$ 7.3
811	0.1875	0.164	0.185	0.1885	0.181	$\pm$ 0.006	$\pm$ 3.2
881	0.083	0.077	0.066	0.079	0.076	$\pm$ 0.004	$\pm$ 4.8
976	0.107	0.092	0.092	0.103	0.098	$\pm$ 0.004	$\pm$ 3.9
1099	0.083	0.075	0.074	0.060	0.073	$\pm$ 0.005	$\pm$ 6.6
1160	0.071	0.0695	0.061	0.062	0.066	$\pm$ 0.0025	$\pm$ 3.7
1305	0.024	0.028	0.026	0.0345	0.028	$\pm$ 0.002	$\pm$ 8.4
1446	0.213	0.201	0.2215	0.2245	0.215	$\pm$ 0.005	$\pm$ 2.4
1725	0.093	0.098	0.098	0.103	0.098	$\pm$ 0.002	$\pm$ 2.2
					Average	$\pm$ 0.0033	$\pm$ 4.6

in refractive index. The way in which the base line has been drawn is illustrated in Figure 30. According to these measurements an average accuracy of about 5 per cent in the mean values can easily be obtained. Improvements in the present construction, mainly as regards the stability of the amplifier and of the lamp voltage, will be necessary before a higher precision can be reached.

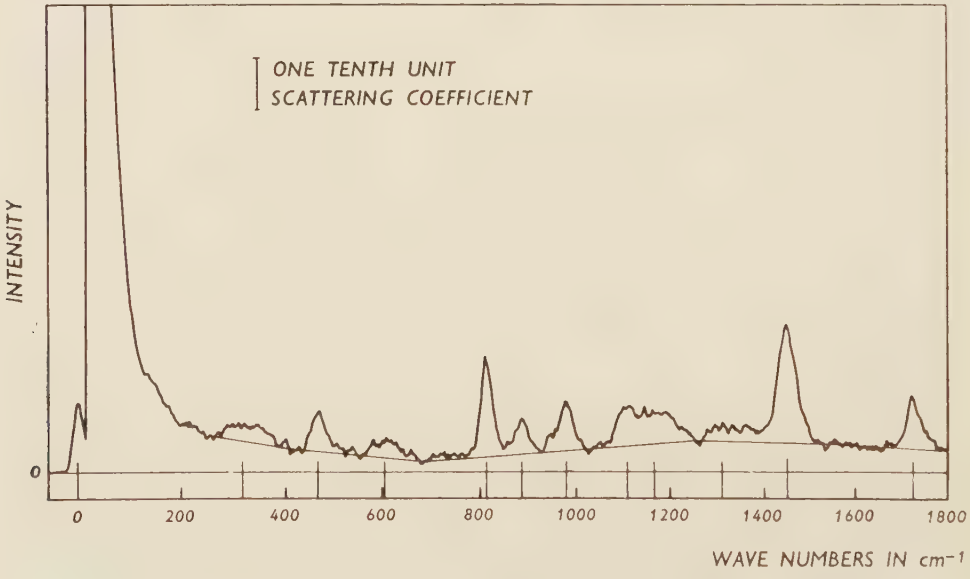

FIGURE 30. Raman spectrum of methyl isobutyrate. (Spectrum No. 56 b.)

H. Some Applications

Mainly to illustrate some of the applications of a photo-electric recording method a few qualitative results will be given.

Figure 31 is the raman spectrum of carbon tetrachloride taken with an entrance slit width of 10 cm.$^{-1}$ and an exit slit width of 5 cm.$^{-1}$. The lines $\Delta\nu$ 760 cm.$^{-1}$ and

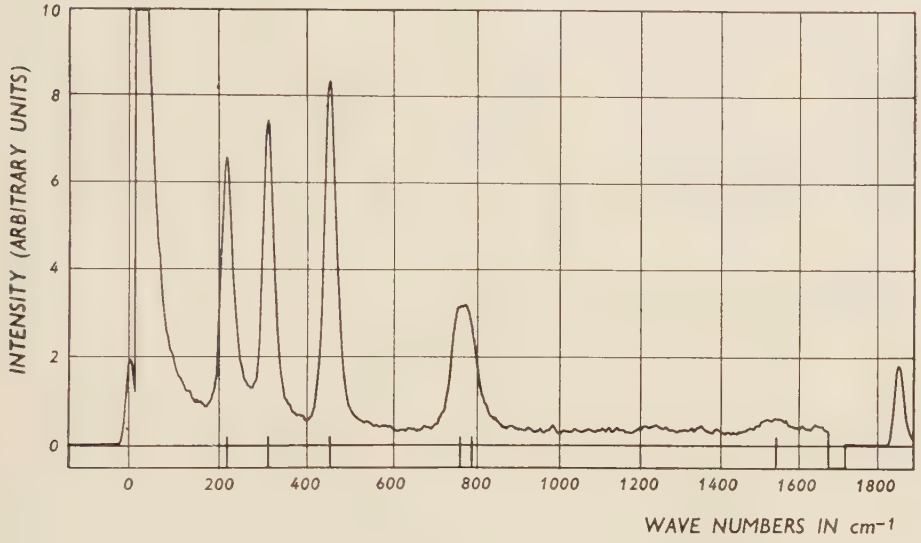

FIGURE 31. Raman spectrum of carbon tetrachloride.

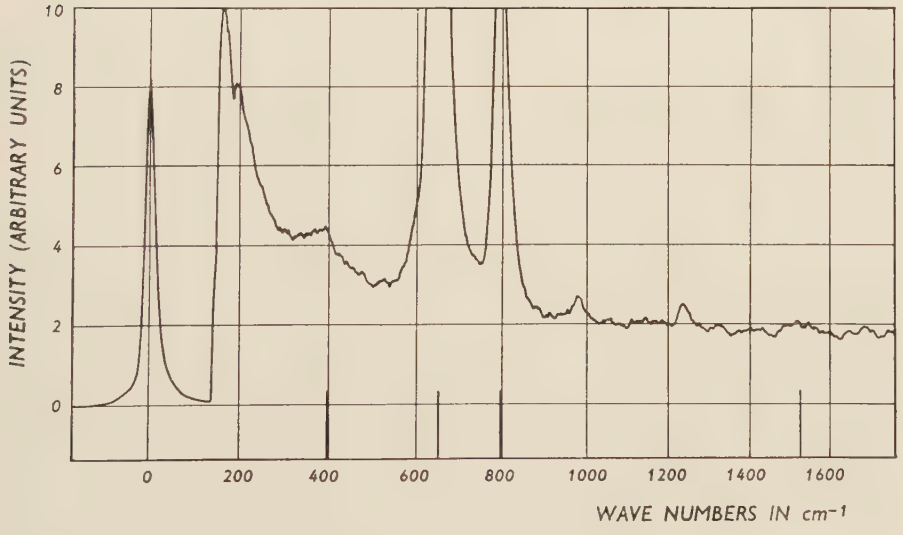

FIGURE 32. Raman spectrum of carbon disulfide.

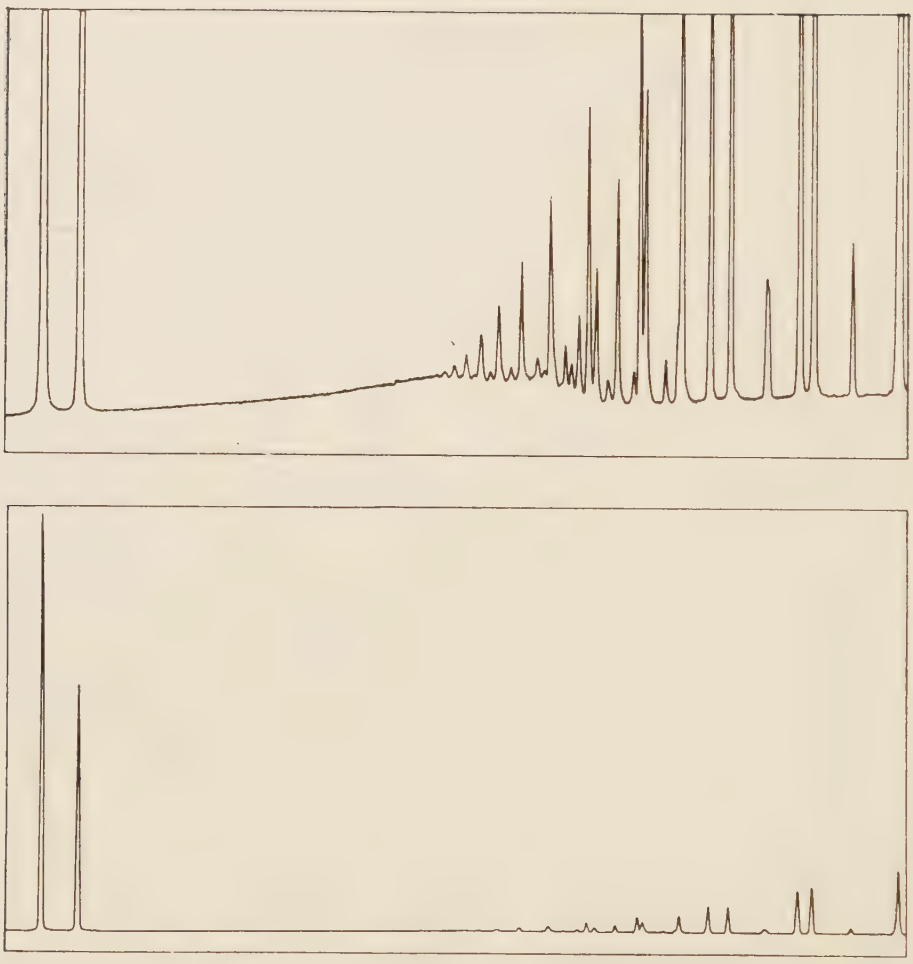

FIGURE 33. Emission spectrum of cesium.

$\Delta\nu$ 790 cm.$^{-1}$ have not been resolved. The weak line at $\Delta\nu$ 1536 cm.$^{-1}$ is clearly visible. There is no doubt about its existence. The weak lines from the mercury lamps $\Delta\nu$ 980 cm.$^{-1}$ and $\Delta\nu$ 1230 cm.$^{-1}$ are hardly visible at the gain used.

In Figure 32 the raman spectrum of freshly-distilled carbon disulphide is given. This spectrum contains one very strong line at $\Delta\nu$ 655 cm.$^{-1}$ and a strong line at $\Delta\nu$ 796 cm.$^{-1}$. The last one is the first harmonic of a very weak fundamental frequency at $\Delta\nu$ 397 cm.$^{-1}$. The third fundamental frequency is situated at $\Delta\nu$ 1523 cm. ^{1} and is also very weak. The $\Delta\nu$ 397 cm.$^{-1}$ line is clearly visible, the possibility of detecting a line $\Delta\nu$ 1523 cm.$^{-1}$ is more doubtful. A slight increase in the background can be seen but a positive statement of the existence of this line would require some

more runs. However, both the recorded spectrum of carbon tetrachloride and the last one, illustrate a considerable advantage of the photo-electric method over the photographic one. In the latter case, a plate exposed to visualize the weak lines would be completely overexposed in the other regions and weak lines near the strong ones would not be visible (*cf.* RANK and MCCARTNEY (23) for a reproduction of photographically obtained spectra of carbon tetrachloride and carbon disulphide).

An ordinary emission spectrum is shown in Figure 33. It is part of the visible cesium spectrum from a Philips discharge lamp 93105 E (*cf.* ELENBAAS and RIEMENS (44)) and shows the two strong lines λ 4555 Å and λ 4593 Å respectively from the fundamental series. The right part of the spectrum is the series limit for the sharp and diffuse series and shows very clearly the convergence both with respect to wavelength and intensity. The lower spectrum is recorded at about 35 times lower gain. The entrance and exit slit widths were 7.5 cm.$^{-1}$ and 3 cm.$^{-1}$ respectively.

Chapter 2

Preparative Work

The preparative work done for the present investigation mainly consisted of the purification of starting materials and samples for investigation. In some cases analytical methods have been necessary. The determination of limiting viscosity numbers for the characterization of fractions of high polymers were also made.

Materials for Polymerization Experiments

A. Monomer

The monomer used was methyl methacrylate (delivered by AB. Bofors Nobelkrut). It was purified by means of distillation in a bead-packed column of about eight theoretical plates. To prevent the formation of peroxides the distillation was made at a low temperature at reduced pressure (28 °C. at 40 mm. Hg) and in a stream of oxygen-free nitrogen. (The author is indebted to Fil. mag. Fredrik Eriksson for placing this nitrogen at his disposal). On each lot distilled the refractive index at 20 °C. was determined. The purified liquid was stored in a refrigerator at about — 5 °C. An earlier work by Kinell *et al.* (124) has shown that the presence of small amounts of peroxides formed from the monomer and atmospheric oxygen influences the course of the polymerization. These peroxides were removed with aluminum oxide just before the monomer was filled into the reaction tubes. This precaution was not taken in the present case since the course of the polymerization reaction was not of primary interest but only the degree of conversion.

B. Initiator

The initiator used to start the polymerization reaction was benzoyl peroxide ("R. o. H", Rudolph Grave AB, Stockholm). The crude product was dissolved in acetone and then precipitated with distilled water. The precipitate was collected on a fritted-glass filter and then dried at about 30 °C. Another method tried was to recrystallize the peroxide from a concentrated solution in acetone. This gave large,

almost colourless, crystals. A determination of the amount of peroxide oxygen gave the following values[1]:

Precipitate from acetone: 100.0 per cent.
Crystals „ „ 97.9 per cent.

C. Determination of Degree of Conversion

The degree of conversion was determined in two ways; the amount of polymer formed was obtained gravimetrically and the remaining amount of monomer photometrically.

a. Gravimetric Method

A sample from the polymerizing mixture (about 1 g.) was dissolved in chloroform (about 30 g.). This solution was poured into methanol (about 100 ml.) while stirring with a glass rod. After rinsing the original bottle with chloroform and methanol the precipitate was allowed to sediment. The supernatant solution was checked for complete precipitation and decanted off after about two hours. The precipitate was thoroughly washed with excess of methanol for two or three hours and then collected on a filter paper and dried at room temperature. The supernatant was evaporated in vacuum to a smaller volume and again checked with methanol for complete precipitation. Any precipitate formed was added to the main lot. Drying to constant weight was then made at a temperature of 75–80 °C.

b. Photometric Method

Methyl methacrylate has an absorption band at $\Delta\nu$ 1631 cm. $^{-1}$ (6.13 μ). This band is connected to the presence of a carbon–carbon double bond in the molecule. There-

Table 10

Determination of methyl methacrylate (concentration in g./100 g.)

c_{mon}	D_{mon}	D_{mon}^{cal}	ΔD_{mon}
6.616	0.489	0.488	−0.001
4.009	0.327	0.326	−0.001
3.172	0.260	0.265	+0.005
2.406	0.205	0.206	+0.001
1.596	0.145	0.141	−0.004
0.758	0.073	0.069	−0.004

[1] I am indebted to Fil. kand. A. Bengtsson for carrying out these determinations.

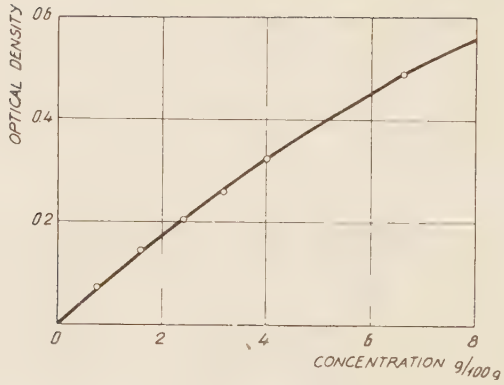

FIGURE 34. Optical density of methyl methacrylate at 6.13 μ as a function of concentration.

fore the absorption will change during the polymerization. For the analysis, an investigation of the absorption properties of monomer and polymer in this region was necessary.

The optical density of a series of solutions of methyl methacrylate in chloroform was determined in a Beckman Infra Red Spectrophotometer IR-2 (*v. infra*). The thickness of the absorbing layer was 0.1 mm. The slit-width used was 0.25 mm. The results are given in Table 10 and Figure 34. The following relation between the optical density of the monomer, D_{mon}, and the corresponding concentration, c_{mon}, was obtained from the data by means of the method of least squares (concentration in g./100 g.):

$$D_{\text{mon}} = 0.09258\, c_{\text{mon}}\,(1 - 0.03061\, c_{\text{mon}}). \tag{125}$$

The fitting of this curve to the experimental points follows from the values, $D_{\text{mon}}^{\text{cal}}$, of Table 10. Their differences from the measured values, ΔD_{mon}, show a fairly good precision.

Further, the optical density was determined for a series of solutions containing a mixture of monomer and polymer corresponding to different degrees of conversion.

TABLE 11

Determination of methyl methacrylate in the presence of the polymer (concentration in g./100 g.)

c_{mon}	$D_{\text{mon}}^{\text{cal}}$	c_{pol}	D_{tot}	D_{pol}	$D_{\text{pol}}^{\text{cal}}$	ΔD_{pol}
3.957	0.322	1.319	0.334	0.012	0.009	−0.003
4.007	0.325	4.003	0.351	0.026	0.027	+0.001
4.081	0.331	12.013	0.413	0.082	0.082	±0.000

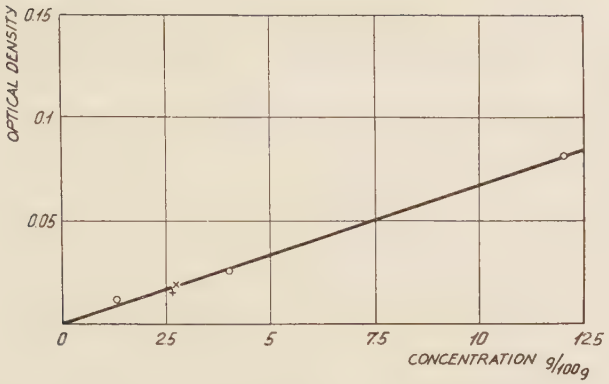

FIGURE 35. Optical density of polymethyl methacrylate at 6.13 μ as a function of concentration: P2b6 ○; P2a1 ×; P2c1 +.

The polymer used was preparation P2b6 (*cf.* next section). The results are given in Table 11. The values $D_{\text{mon}}^{\text{cal}}$ have been calculated from Equation (125) and then substracted from D_{tot}. The differences, D_{pol}, have been plotted *versus* the concentration of polymer (Figure 35). The straight line has been determined by the method of least squares and has the form (concentration in g./100 g.):

$$D_{\text{pol}} = 0.00682\, c_{\text{pol}}\,. \tag{126}$$

The values of $D_{\text{pol}}^{\text{cal}}$ in Table 11 have been obtained from Equation (126) using the experimental values of c_{pol}. The differences, ΔD_{pol}, are of the same order of magnitude as in Table 10. Adding the two equations gives

$$D_{\text{tot}} = 0.08576\, c_{\text{mon}} - 0.002834\, c_{\text{mon}}^2 + 0.00682\, c_{\text{tot}} \tag{127}$$

where $c_{\text{tot}} = c_{\text{mon}} + c_{\text{pol}}$. From this equation the photometrically determined degrees of conversion have been calculated.

It may be objected that the optical density of the polymer depends upon the degree of polymerization and hence this way of analysing the reaction mixture is of little value unless the average degree of polymerization is also determined. To illustrate the magnitude of this dependence the optical density of two preparations P2a1 ($[\eta] = 0.689$) and P2c1 ($[\eta] = 0.593$) was measured. The results correspond to the point × and + respectively in Figure 35. Within the experimental errors no significant deviations from the optical density of P2b6 ($[\eta] = 1.180$) can be stated.

Materials for Ultra Violet and Infra Red Measurements

The materials for the structure analysis in the ultraviolet and infrared were the following polymers:

P2a[1]: a photopolymerized polymethyl methacrylate having a number average molecular weight in acetone of 74000,

P2b[2]: a benzoyl peroxide polymerized polymethyl methacrylate made in suspension.

P2c[1]: a benzoyl peroxide polymerized polymethyl methacrylate having a number average molecular weight in acetone of 57000.

P2d: a polymethyl methacrylate of German origin having a molecular weight of about 9000000 (from sedimentation and diffusion in acetone).

These polymers were purified, partially or completely fractionated and characterized by viscosity measurements as described below.

A. Purification and Pre-Treatment

Preparation P2a1. The crude polymer was left for about a week in benzene. During this time some of the polymer had dissolved. The solution was cleansed from solid impurities by filtering through a fritted-glass filter (porosity G 3). It was then poured into twice its volume of cyclohexane under intensive stirring. The precipitate was allowed to settle for about two hours, the supernatant was filtered off, the precipitate washed for about three hours with a large amount of cyclohexane and then dried in a vacuum desiccator.

The remaining part of the crude polymer had dissolved after about a month. It was not used for the present investigation.

Preparation P2b6. The crude polymer was left for a month in methanol in order to remove the impurities from the polymer preparation. The methanol was filtered away, the polymer dried and then extracted once again with methanol for two days. After drying, the polymer was left in benzene (about 100 g. polymer in 500 ml. benzene) for two days. Part of the polymer had then dissolved. The solution was decanted off and filtered through a fritted-glass filter (porosity G 3) and poured into twice the volume of cyclohexane. The continuation of the preparation was then the same as for P2a1.

[1] These polymers were kindly supplied by Dr. I. Harris of Imperial Chemical Industries, Ltd., England (his notations BCD 31 resp. A 903). The molecular weights have been determined by Dr. Harris.

[2] The author is indebted to Fil. mag. G. Jacobson for this sample.

The remaining part of the polymer was not used for the present investigation.

Preparation P2c1. The crude polymer was dissolved in benzene and then treated in the same way as P2a1.

Preparation P2d1. This was an old benzene solution of the polymer which had been standing for several years. The solution was directly used for fractional precipitation.

Drying of the Samples. It was very soon found that a pressure of about 8–10 mm. Hg was insufficient for drying the samples at room temperature. Therefore an oil-sealed, rotary-piston pump was substituted for the air ejector. The pressure could then be decreased to about 0.01–0.005 mm. Hg giving a more efficient drying. A cooling trap was placed between the desiccator with the samples and the pump. By means of dry ice in alcohol the temperature in the trap was kept at about − 70 °C. GRASSIE (125) has pointed out that complete removal of volatile materials from a polymer is only possible at a temperature above the softening point. In the present case the volatile materials are mainly benzene and cyclohexane of which benzene as the solvent is more strongly bound to the polymer molecules. By measurements in the ultraviolet it has been shown that no traces of the characteristic benzene peaks are detectable if the drying at low pressure is extended for a sufficient length of time. Mostly the precipitate formed in the benzene/cyclohexane system gives a finely grained polymer powder which dries in about a month. In this investigation it has been of great importance to avoid structural changes in the samples and therefore they were not heated. GRASSIE states that decomposition of polymethyl methacrylate begins at 200 °C. The softening point is about 170 °C. He does not give any evidence that structural changes do not occur at this temperature.

B. Fractional Precipitation

The fractional precipitation of the polymer samples was done in benzene solution with cyclohexane as the precipitant. This combination of solvent–non solvent has been used earlier by the present author (KINELL (2)) and is very convenient to work with. The general procedure was as follows: the polymer was treated for two days with a mixture of benzene and cyclohexane at room temperature. Then the sol phase of the system was decanted off. The gel phase was completely dissolved in benzene. Both these solutions were then treated with suitable amounts of cyclohexane. The supernatants were decanted off after one day at room temperature and the gels separately dissolved in about 50 ml. of benzene. After some hours the solutions were separately poured into 100 ml. of cyclohexane. The gels were allowed to settle, the liquid decanted off, the precipitate treated with about 100 ml. of hexane and finally collected and pre-dried on a fritted-glass filter. The drying was then made as described above. In this way a series of fractions was obtained, always two at

a time. Sometimes the solutions had to be evaporated to a smaller and more convenient volume. This was always done in vacuum at about 30–40 °C. The evaporation was never made to the point of dryness. The solutions were always checked for complete precipitation. Nevertheless some losses were obtained, mainly due to the fact that the polymer powder easily became electrically charged and was attracted by the glass. The repulsion between the particles often made it difficult to transfer the polymer from the fritted-glass filter to the weighing glasses. In fractionating P2a1 and P2c1, the polymer left in the beacher where it was reprecipitated was dissolved in a small amount of benzene (about 10 ml.) and then transferred to the weighing glass and the benzene evaporated before the main lot of the fraction was added from the glass filter. In some cases the precipitate became rather hard and had a tendency to adhere to the beacher walls after a time if the supernatant liquid was not removed at once and the washing with hexane started. This was particularly noticeable at the lower fractions.

The fractionation schemes are given below:

Preparation P2a1.

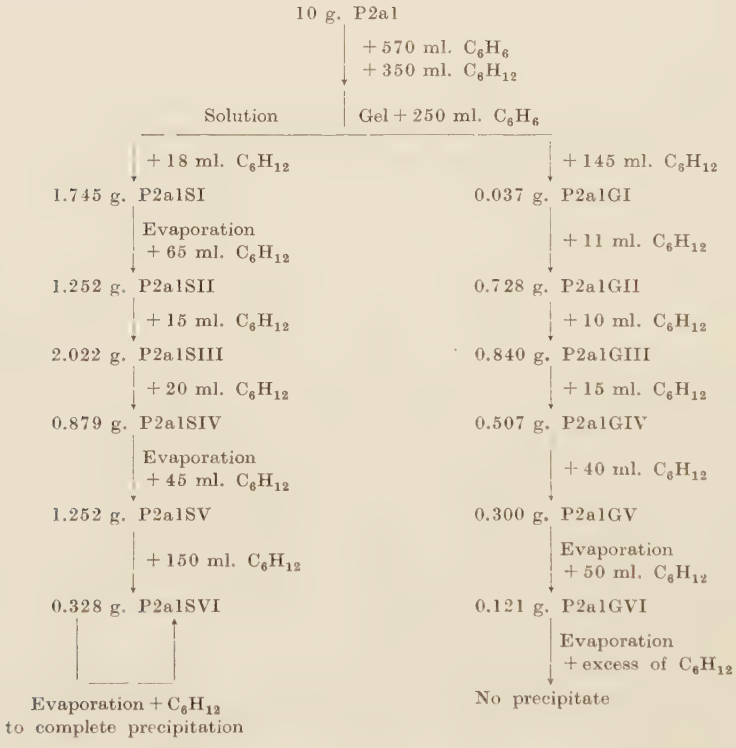

Total weight of fractions: 10.011 g.

Preparation P2b6.

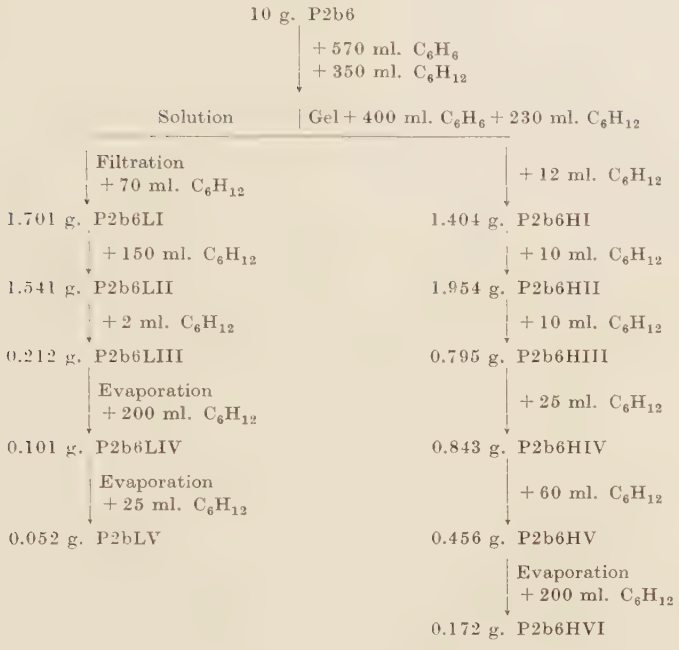

Total weight of fractions: 9.231 g.

Preparation P2d1.

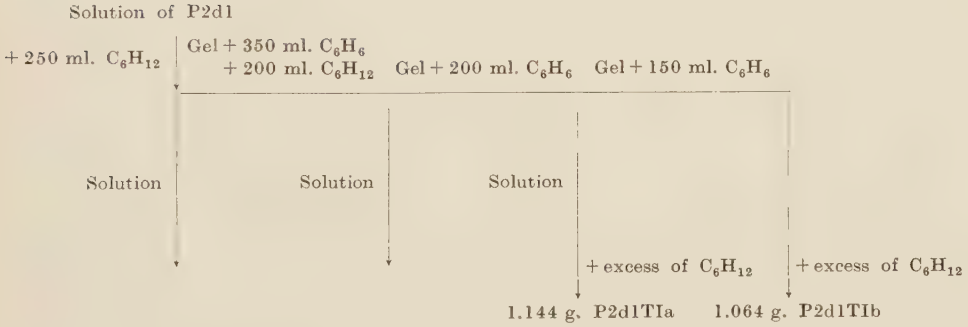

The fractionation was not continued because the aim was only to obtain two high molecular-weight fractions.

Preparation P2c1.

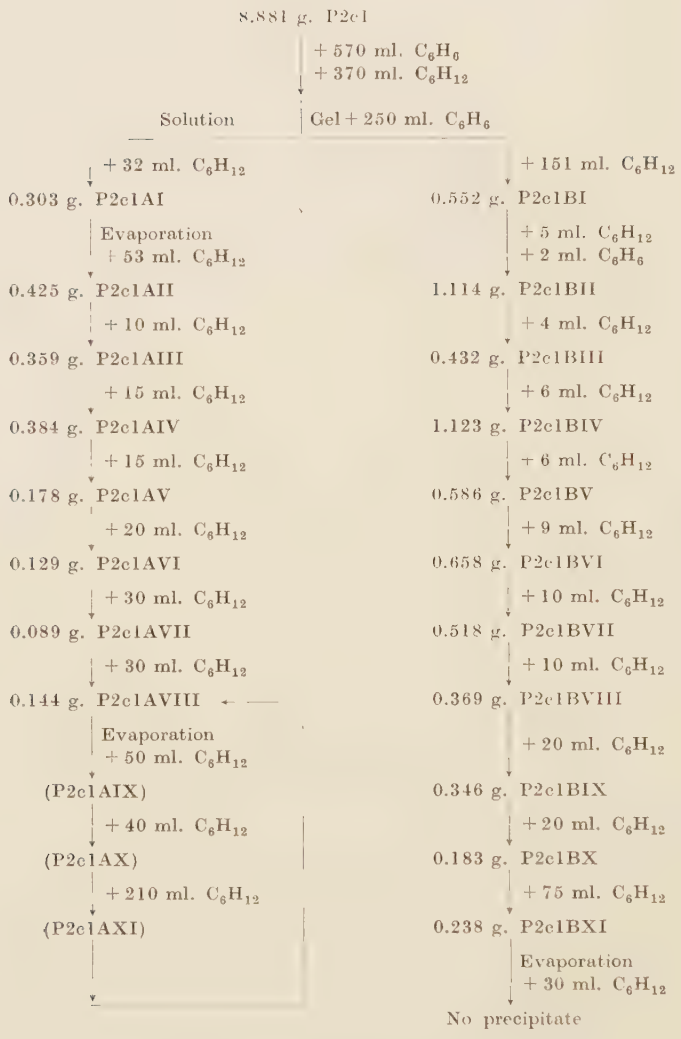

Total weight of fractions: 8.130 g.

C. Viscosity Measurements

The molecular properties of the polymer samples were characterized by their viscosity numbers determined in chloroform solution. An Ostwald capillary viscometer was used. The diameter of the capillary was 0.34 mm., its length 130 mm., the outflow volume about 2 ml. and the pressure head about 150 mm. water. The precision that could be reached in a series of measurements was tested by determining the efflux time of distilled water. Between each series the viscometer was dried in a stream of air filtered through a fritted-glass filter (porosity G 3). The distilled water was filtered five times through a filter of porosity G 4. Three minutes were always allowed for the filling pipette to empty. The surface of the liquid in the lower bulb of the viscometer reached about 2–3 mm. above the nib of the pipette. The thermostat was kept at 25 °C. The temperature variations were read on a Beckmann thermometer. In Table 12 the results of four series are given. The following notations are used: mean value $L = \frac{1}{n} \sum l_i$; standard deviation

$$m = \pm \sqrt{\frac{\sum \delta_i^2}{n-1}} \left(1 \pm \sqrt{\frac{1}{2(n-1)}}\right);$$

standard deviation of the mean $M = \frac{m}{\sqrt{n}}$ and the mean deviation

$$\vartheta = \pm \frac{\sum |\delta_i|}{\sqrt{n(n-1)}} \left(1 \pm \sqrt{\frac{\pi - 2}{2(n-1)}}\right); \qquad \delta_i = l_i - L.$$

Evidently the mean values do not coincide within the calculated errors of the mean values. These errors are in agreement with the variation of the reaction time of the observer given by Washburn and Williams (126). (A series of twenty measurements gave an M-value of $\pm 0.020 \pm 0.005$ sec.) Possible sources of error, with the exception of temperature variations in the viscometer, are changes in the pressure head due to errors in filling and inclination. A relative variation in the pressure head of 0.1 pro mille requires that the volume filled into the viscometer can be reproduced within 0.04 ml. This can easily be done. A determination of the volume of the pipette under normal operating conditions gave 5.3172 ml. with a maximum deviation of ± 0.0008 ml. An error of only 1′.5 in the inclination is sufficient to give the same change in pressure head when the viscometer is mounted with the capillary vertical. (In the more favourable position where the bulbs are placed above each other the angle will be about 35′.) Certainly the observed deviations may, to a large extent, be ascribed to changes in the position of the viscometer. Taking all variations to be of random nature we get as the mean value of all measurements $L = 494.978$ sec. The probability of a deviation larger than ± 0.05 pro mille is less than 0.06.

Table 12

Reproducibility test of an Ostwald capillary viscometer

Series 12		Series 13		Series 14		Series 15	
Temp., °C.	Time, sec.	Temp., °C.	Time, sec.	Temp., °C.	Time, sec.	Temp., °C.	Time, sec.
0.102	494.84	0.102	495.00	0.102	495.02	0.102	494.87
	494.90		494.99		495.00		494.94
0.102	495.06		494.97		495.12		494.94
Pause 2 hours		0.102	494.91	0.102	495.10	0.102	494.97
0.102	494.93		494.98	Pause $1\frac{1}{2}$ hours			494.92
	494.95		494.98	0.102	495.04		494.85
	494.98	0.102	495.08		494.96	0.102	495.00
0.102	494.94				495.12		
				0.102	494.99		
$L = 494.943$		$L = 494.987$		$L = 495.044$		$L = 494.927$	
$M = \pm 0.026 \pm 0.006$		$M = \pm 0.019 \pm 0.004$		$M = \pm 0.022 \pm 0.005$		$M = \pm 0.020 \pm 0.005$	
$m = \pm 0.068 \pm 0.015$		$m = \pm 0.050 \pm 0.011$		$m = \pm 0.061 \pm 0.014$		$m = \pm 0.053 \pm 0.012$	
$\vartheta = \pm 0.050 \pm 0.012$		$\vartheta = \pm 0.034 \pm 0.008$		$\vartheta = \pm 0.056 \pm 0.013$		$\vartheta = \pm 0.044 \pm 0.011$	

A difficulty in obtaining accurate values of the limiting viscosity numbers is connected with the non-Newtonian behaviour of polymer solutions even of low concentration (de Wind and Hermans (127)). This makes reliable extrapolations to zero concentration difficult, especially for polymers of high molecular weight. The non-Newtonian behaviour, however, is not an intrinsic property of the macromolecules but dependent upon interaction between molecules. Further, this behaviour is more pronounced at high shear rates. Therefore in the present case the viscometer was constructed to give a moderate shear rate. For chloroform the maximum rate was 2800 sec.$^{-1}$ The values obtained in this way are in any case accurate enough to permit a comparison of the investigated substances.

Complete series of viscosity measurements are presented in Table 13 for a low, a medium and a high molecular weight fraction; P2a1SVI, P2b6HII and P2d1TIa respectively. The $[\eta]$ and k'-values given at $c = 0$ were calculated using the method of least squares. The k'-values for the other concentrations were calculated from $[\eta]$ using Equation (128).

The limiting viscosity numbers (expressed in 100 ml./g.) of the fractions measured are given in Table 14. The constant k' defined by the equation

$$\frac{\eta_{sp}}{c} = [\eta](1 + k'[\eta]c) \tag{128}$$

has been calculated and included in the table.

TABLE 13

Viscosity measurements of fractions (concentration in g./100 g., time in sec.)

Liquid	Efflux time					Mean value	η_{sp}/c	k'
	P2a1SVI (25.7.52)							
Solvent	200.78	200.79	200.79	200.79	200.79	200.79		
$c_0 = 0.4988$	222.77	222.76	222.74	222.74	222.74	222.75	0.2193	0.640
Solvent	200.79	200.78	200.79	200.76	200.76	200.78		
$c_1 = 0.4000$	218.13	218.13	218.18	218.14	218.24	218.16	0.2164	0.627
Solvent	200.84	200.88	200.83	200.81	200.77	200.83		
$c_2 = 0.3015$	213.74	213.82	213.80	213.84	213.76	213.79	0.2140	0.643
Solvent	200.83	200.78	200.82	200.78	200.77	200.80		
$c_3 = 0.2013$	209.33	209.32	209.35	209.38	209.38	209.34	0.2112	0.635
$c = 0$							**0.2058**	**0.636**
	P2b6HII (5.6.52)							
Solvent	201.21	201.22	201.21	201.16	201.22	201.20		
$c_0 = 0.5119$	591.92	592.06	592.24			592.07	3.795	0.333
Solvent	201.19	201.20	201.17	201.22	201.24	201.20		
$c_1 = 0.2228$	341.77	341.75	341.88	341.88	341.88	341.83	3.137	0.336
Solvent	201.21	201.25	201.19	201.23	201.23	201.22		
$c_2 = 0.1794$	310.81	310.83	310.91	310.96	310.95	310.91	3.038	0.337
Solvent	201.19	201.22	201.21	201.18	201.22	201.20		
$c_3 = 0.1285$	276.65	276.68	276.65	276.66	276.74	276.68	2.919	0.336
Solvent	201.23	201.15	201.17	201.16	201.12	201.17		
$c_4 = 0.0996$	258.29	258.26	258.22	258.31	258.31	258.28	2.850	0.333
Solvent	201.13	201.19	201.27	201.21	201.14	201.19		
$c_5 = 0.0624$	235.79	235.84	235.86	235.77	235.87	235.83	2.759	0.312
$c = 0$							**2.622**	**0.334**
	P2d1TIa (11.6.52)							
Solvent	201.11	201.15	201.10	201.13	201.03	201.10		
$c_0 = 0.1024$	696.06	697.47	697.67			697.07	24.08	0.503
Solvent	201.15	201.09	201.11	201.11	201.10	201.11		
$c_1 = 0.0565$	421.72	421.71	421.72	421.97	422.06	421.84	19.43	0.492
Solvent	201.10	201.06	201.15	201.09		201.10		
$c_2 = 0.0382$	338.18	337.95	338.03	337.94	337.83	337.99	17.82	0.512
Solvent	201.26	201.24	201.20	201.19	201.19	201.22		
$c_3 = 0.0243$	281.41	281.30	281.28	281.30	281.36	281.33	16.38	0.502
$c = 0$							**13.99**	**0.502**

Table 14

Viscosity data of polymethyl methacrylates

Sample	$[\eta]$	k'	Sample	$[\eta]$	k'
P2a1	0.689	0.373	P2b6	1.180	0.351
P2a1GII	1.687	0.338	P2b6HI	2.524	0.341
GIII	0.980	0.358	HII	1.774	0.334
GIV	0.661	0.397	HIII	1.250	0.353
GV	0.424	0.417	HIV	0.888	0.378
SI	0.922	0.411	HV	0.543	0.401
SIV	0.380	0.495	LI	0.789	0.364
SVI	0.140	0.636	LII	0.375	0.560
P2c1	0.593	0.386	P2d1TIa	9.486	0.502

Other Materials

Besides the materials already discussed, a lot of other substances have been necessary. These are listed below.

Chloroform, solvent used in viscosity, ultraviolet and infrared measurements. The crude product was distilled at ordinary pressure. The purity was tested by refractive index and density determinations.

Benzene, analytical grade, free of thiophene, used for wave-length scale calibration of the infrared spectrophotometer.

A coarser quality was used for fractionation of the polymer samples.

n-Hexane, practical, used in fractionation.

Cyclohexane, practical, used in fractionation.

Methanol, practical, used in fractionation.

Acetone, analytical grade, distilled, used as solvent for infrared measurements.

Carbon tetrachloride, analytical grade, distilled, used as solvent in infrared measurements and as a reference in intensity determinations of raman lines.

Carbon disulphide, analytical grade, distilled, used as solvent in infrared measurements.

Methyl benzoate, for chemical purposes, not further purified, used in infrared measurements.

Ethyl benzoate, for chemical purposes, not further purified, used in infrared measurements.

Benzyl benzoate, for chemical purposes, not further purified, used in infrared measurements.

o-Dichloro benzene, practical, used in infrared measurements.

Methyl isobutyrate[1], produced in the laboratory, distilled, used in raman measurements.

[1] I am much indebted to Fil. mag. F. Eriksson for placing this sample at my disposal.

Chapter 3

Raman Spectra of Polymerizing Mixtures

In addition polymerization the formation of polymer molecules occurs in a radical chain reaction. To-day, this is a well-established fact. The radicals are formed from the unsaturated monomer by an opening of the carbon–carbon double bond, a process initiated by heat, light or easily-split compounds such as peroxides. A polymerizing mixture will evidently contain, apart from molecules of the monomer and the formed polymer, excited molecules of different sizes — the growing macromolecules. The raman spectrum of such a mixture will be composed of lines from both the monomer and the polymer. A study of the spectrum will undoubtedly give valuable information about the polymerization process.

This chapter gives a brief review of the use of raman spectroscopy in the study of high polymers, followed by a description of the work carried out in the present investigation.

Previous Work

The raman investigations on high polymeric systems published since the discovery of the raman effect, are very few. Only about twenty papers have appeared on this subject compared to several thousand on low molecular-weight compounds. The interesting problem has been the elucidation of the structure of the polymer by comparing its spectrum with spectra from the monomer and various other compounds containing structural elements similar to those of the polymer. The results have given strong evidence both for the existence of macromolecules and for the mechanism of their formation.

The following review is concerned first with compounds formed from monomers having a single double bond and then with substances formed from monomers having a diene structure. A survey up to 1941 is given by Simon (128).

A. Vinyl Compounds

The first raman investigation on high polymeric substances was carried out by Signer and Weiler (129). They compared the spectra of styrene, polystyrene and ethyl benzene. The polymer was made by thermal polymerization. The spectrum

of polystyrene was of the same nature as those of organic compounds with low molecular weight. Further, the complete coincidence of the lines from solid polystyrene with those from a fifteen per cent solution in carbon tetrachloride showed that in the solid state no intermolecular forces existed. Therefore it was concluded that the polystyrene molecule was a real macromolecule in the sense proposed by Staudinger.

A similar investigation of the raman spectrum of polystyrene has recently been carried out by Palm (130). She has made a comparison with the spectra of benzene and styrene, and has also measured the depolarization factors.

An attempt to follow the polymerization reaction when converting styrene to the corresponding polymer has been made by Mizushima, Morino and Inoue (131). The only result was the conclusion that a solution of the polymer in the monomer had a very high viscosity because of micelles built up from monomer molecules held together by van der Waals forces. From the spectra of polymers with a low degree of polymerization (molecular weight 1150) they concluded that the macromolecule had double bonds in the end groups.

Measurements on polymethyl methacrylate were made in 1937 by Hibben (132) and by Monnier *et al.* (133, 134). Hibben compared the spectra of the monomer and the polymer with spectra of diethyl maleate, diethyl fumarate, methyl crotonate, and methyl isocrotonate (the data of the last two compounds taken from Dadieu, Pongratz and Kohlrausch (135)) and concluded that the absence of an ethylenic double-bond frequency is a strong evidence for the coupling of molecules by the breaking of the double bond. He has also taken spectra of partially polymerized methyl methacrylates. These mixtures had very different viscosities but, even so, their spectra were very much the same as that of the monomer. Hibben concludes that a small amount of polymer (less than 5–10 per cent) has an enormous effect on the viscosity. Monnier *et al.* have included acrylic acid and ethyl methacrylate in their investigation. They have reached the same conclusions about the polymerization reaction as Hibben. The lines in a partially polymerized ethyl methacrylate are given.

Yasumi (136, 137) has studied the spectrum of methyl methacrylate in the liquid and the solid state and also taken spectra from various stages in the polymerization reaction. He found that at low degrees of polymerization the double-bond frequency does not entirely disappear. The spectrum of the partially polymerized monomer generally consisted of the lines of the monomer and those of the final product. Kojima (138, 139, 139 a) has made investigations on polymethyl methacrylate and its copolymer with acrylonitrile. The polymers were studied in various stages of polymerization. Finally Patel (140) has given the raman lines of polymethyl methacrylate.

B. Diene Compounds

Raman spectroscopy has also been used in the elucidation of the structure of rubber and rubber-like compounds. Thus Gehman (141, 142) has compared the spectra of rubber and balata with those of isoprene, myrcene and trimethylethylene. He concludes that the rubber molecule is built up of isoprene units in long chains. Kubota (143) has found that in the polymerization of chloroprene, the intensity of the double-bond frequency decreases slightly, but, simultaneously, another double-bond frequency appears corresponding to the same frequency in 2-chlorobutene-(2). The conclusion is that the polymerization proceeds linearly but to no great extent. In its solid state the larger part of the chloroprene does not polymerize by primary linkages but is held together by van der Waals forces. A comparison of the raman spectra of chloroprene and isoprene has been made by Gantmacher and Medvedev (144, 145). The changes in the spectrum of polymerized isoprene are smaller and less numerous than in the corresponding chloroprene spectrum. As to the background, which many times renders the investigations more difficult, they have found that the formation of high molecular-weight compounds does not increase the intensity. Chloroprene has also been studied by Perumova (146) but due to the turbidity of the polymerizing mixture no detailed investigation could be made. A comparison of the structure of polystyrene, rubber, balata, and various low molecular-weight compounds has been made by Putilova (147).

Present Work

From the foregoing review it is evident that the raman spectra of the monomer and its corresponding polymer have, in many cases, given strong evidence that the carbon–carbon double bond in vinyl compounds is opened during polymerization and that the carbon atoms of this bond constitute the skeleton of the macromolecules formed. The structural changes during the conversion of the monomer to the polymer, as far as other atomic groupings in the molecules are concerned, have been studied by comparison with "model" substances. Convincing results have been obtained even here. There is, however, one point where the previous work can be given an important complement, namely, in an accurate determination of the intensities of the raman lines of the monomer and the polymer, and also of the change in intensity of certain lines during the course of the polymerization. The results obtained may be of value to a more thorough interpretation of what is taking place during the formation of the macromolecules.

The present study may be regarded as an introduction to an investigation of this kind. So many problems of various nature are involved, that a first orientation about the possibilities is very necessary.

A. Polymerization Technique

The purification of the monomer and the initiator used was described in Chapter 2.

The polymerization was performed at 50 and 60 °C. with different amounts of initiator. In the first experiments, made directly in the raman tube, it was difficult to avoid the formation of bubbles in the polymer at higher degrees of conversion. Later, a pre-polymerization was done in an Erlenmeyer flask until a very viscous syrup was obtained; this was poured into the raman tube and the polymerization continued. Even in this case, however, it was sometimes difficult to avoid the formation of bubbles during the later stage of the polymerization. In this stage, very easily refractive index gradients were formed, due to strong contraction in the middle of the tube. The upper layer in the tube, which often had a lower degree of conversion, was sucked down. This optical inhomogeneity caused an increase in the rayleigh scattering and hence a higher background. No systematic experiments at different amounts of initiator have been made. The only aim so far has been to correlate the measured intensities with the degree of conversion. This has been determined gravimetrically or photometrically as described in Chapter 2. In the first experiments ampoules with small amounts of monomer were polymerized simultaneously with the main lot in the raman tube. They were taken up from the thermostat at the same time as the raman tube and kept at the same temperature as the tube during the running of the spectrum. Then the remaining ampoules were put down in the thermostat with the raman tube. It was, however, uncertain to what extent the degree of conversion in the ampoules really coincided with that in the raman tube. Therefore in the later experiments, determinations were always made on the content in the raman tube. This involved more experiments.

It should be emphasized that the conditions under which these experiments have been made do not invite a thorough discussion of the results obtained. With the present spectrograph it takes about one hour to record the whole spectrum. During this time the tube cools down to a temperature of about 20 °C. and the speed of the reaction will decrease. The tube is then reheated and so on. Further the reaction will continue during the recording and therefore different parts of the spectrum may not correspond to the same degree of conversion. To prevent too great influences of this kind the polymerization has been performed at a fairly low temperature and generally at a low amount of initiator giving a low over-all rate.

The raman tube was made of fused silica glass and could be closed at the upper end by means of a ground joint.

Data about the polymerization experiments are given below.

Experiment P4a. Monomer: $n_D^{20} = 1.4143$; boiling point: 27–29 °C. at 38–41 mm. Hg, amount of initiator: 0.267 mg./g. Temperature of thermostat: 60 °C. Spectra taken: 0^h (monomer) No. 36; 2^h No. 37 (degree of conversion: gravimetrically 3.3 %; photometrically 3.9 %); 5^h No. 38 (6.5 %; 5.7 %); 8^h30^m No. 39 (7.5 %; 11.3 %).

Experiment P4b. Monomer: $n_D^{20} = 1.4143$; boiling point: 27.5–29 °C. at 39–41 mm. Hg. Amount of initiator: 0.406 mg./g. Temperature of thermostat: 60 °C. Spectra taken: 0^h (monomer) No. 41; 2^h30^m No. 42 (6.7 %; —); 7^h30^m No. 43 (18.0 %; —).

Experiment P4c. Monomer: $n_D^{20} = 1.4143$; boiling point: 27–29 °C. at 38–41 mm. Hg. Amount of initiator: 0.300 mg./g. Temperature of thermostat: 60 °C. Spectra taken: 0^h (monomer) No. 45.

Experiment P4d. Monomer: the same as for P4a. Amount of initiator: 0.260 mg./g. Temperature of thermostat: 60 °C. Spectra taken: 7^h30^m No. 46 (—; —).

Experiment P4e. Monomer: $n_D^{20} = 1.4146$; boiling point: —. Amount of initiator: 3.265 mg./g. Temperature of thermostat: 40 °C. Spectra taken: 7^h No. 65 (11.8, 11.4, 11.7 % mean value 11.6 %; 11.6, 11.1, 11.3 % mean value 11.3 %); $> 10^h$ No. 66 (26.7, 39.8, 79.9 %; 25.0, 40.6, 83.3 %).

Experiment P4f. Monomer: $n_D^{20} = 1.4145$; boiling point: 25–28 °C. at 35–41 mm. Hg. Amount of initiator: 5.027 mg./g. Temperature of thermostat: 50 °C. Spectra taken: 4^h No. 75 (—; 14.0 %).

The following comments should be made. Already at the lowest degrees of conversion the viscosity of the liquid in the tube became very high. At the end of expt. P4a it was still fluid. After the last spectrum was taken in expt. P4b the tube was left in the thermostat overnight. Next day, however, the polymer was hard and filled with bubbles. In expt. P4c bubbles were formed after about eight hours. Experiments P4a–d were done directly in the raman tube. The values of the degree of conversion in expt. P4e after 10 hours polymerization, refer to different parts of the raman tube. The lowest value was obtained in the uppermost layer (total height of the polymer was 21 cm.), the next value 1 cm. and finally the highest value, about 4 cm. from the top. Here the polymer was very hard. The highest value of the degree of conversion is probably representative of the greater part of the polymer. In expt. P4f it was observed that the polymerization in its latest stages proceeded to completion within half an hour beginning at the bottom.

The polymerization technique used is less suitable for an investigation of this kind. Therefore, it was judged sufficient to make only a few polymerization runs in order to get some preliminary results, and to postpone using a more refined technique until a better spectrograph was available. In another work (unpublished), it was found that polymerization at room temperature, initiated by γ-quanta from Co^{60}, gives a solid polymer which is optically homogeneous and free of bubbles. This technique seems to be very suitable for spectrophotometric work.

B. Raman Spectrum of Monomeric Methyl Methacrylate

The raman spectra were recorded in the range 0–1800 $cm.^{-1}$ only. The reason for this was the many foreign lines from the mercury spectrum present in the region around 3000 $cm.^{-1}$ (p. 78). In the following, the spectra of the monomer recorded in experiments P4a–d are not discussed. A new series of four monomer spectra was run before expt. P4f. The technique was the same as that used for methyl isobutyrate.

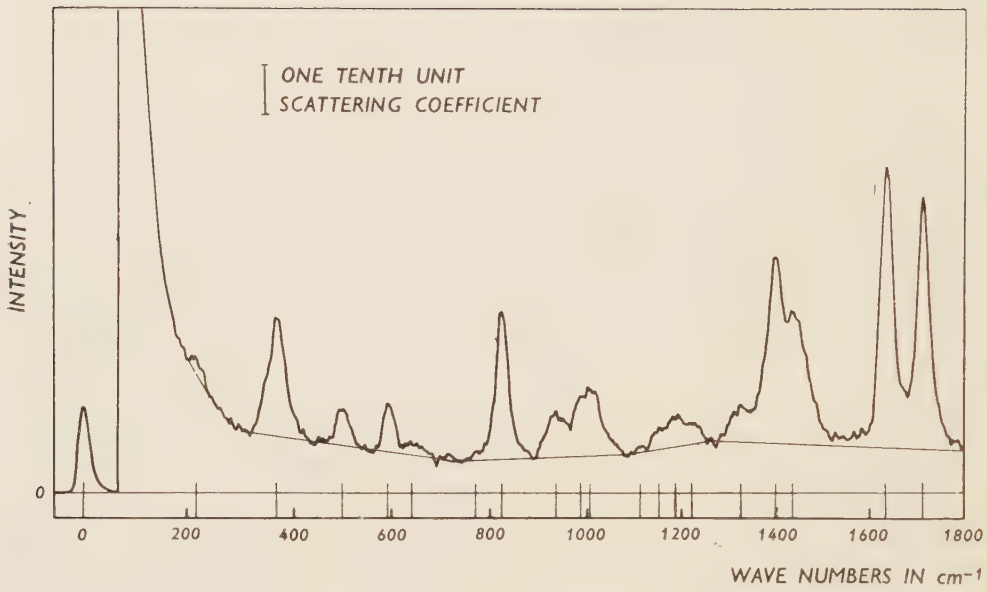

FIGURE 36. Raman spectrum of methyl methacrylate. (Spectrum No. 73 d.)

The position, Δl, of the lines and their maximum heights were measured. The positions were converted to wave numbers using Equation (124) and the heights to scattering coefficients as described earlier. No correction was applied for the difference in refractive indices. The results are given in Tables 15 and 16. The way in which the base lines have been drawn is shown in Figure 36. In Table 15 are also given the wave numbers obtained by HIBBEN (132) and MONNIER *et al.* (134). Spectrum No. 73 d in Table 16 was run at a higher gain than the other ones. In Table 17 the relative intensities obtained in different laboratories have been collected. The reference is the $\Delta\nu$ 1720 cm.$^{-1}$ line.

All the spectra were run under the same conditions, namely:

Amount of liquid: 60 ml.
Filter: sodium nitrite.
Entrance slit: 10 cm.$^{-1}$
Exit slit: 5 cm.$^{-1}$
Height of slit: 10 mm.
Dynode voltage: 65 V.
Scanning rate: 20 cm.$^{-1}$/min.
Chart rate: 4 cm.$^{-1}$/mm.
Time constant: 18 sec.
Zero depression: 0.
Cooling of the photo-tube: none.

The precision in the determination of wave numbers is better than that reported for methyl isobutyrate (Table 7). As is seen from Figure 36 the resolution of the lines in the regions at 1000 cm.$^{-1}$ and 1200 cm.$^{-1}$ is not very good. In the last region the $\Delta\nu$ 2934 cm.$^{-1}$ line excited by λ 4047 Å may contribute to the complexity.

TABLE 15

Position of raman lines in methyl methacrylate

Δl, mm.	M, mm.	M per cent	Wave numbers, cm.$^{-1}$			Structure of lines
			This investigation	HIBBEN (132)	MONNIER (134)	
53.9	±0.7	±1.3	219±3	—	—	broad
—	—	—	—	—	263	—
—	—	—	—	—	338	—
91.8	±0.4	±0.4	376±2	377	377	sharp
—	—		—	—	476	—
122.4	±0.4	±0.3	504±2	507	501	sharp
144.3	±0.5	±0.3	597±2	599	590	sharp
155.9	±1.5	±1.0	646±6	656	647	broad
185.4	±0.2	±0.1	772±1	—	—	broad
198.1	±0.35	±0.2	827±1.5	835	836	sharp
223.2	±0.4	±0.2	937±2	940	937	sharp
235.1	±0.6	±0.3	989±3	—	995	not resolved
240.3	±0.45	±0.2	1011±2	1008	1018	
263.3	±0.3	±0.1	1113±1	—	—	uncertain
273.7	±1.1	±0.4	1159±4.5	—	1163	not resolved
280.1	±0.7	±0.25	1188±3	—	—	
—	—	—	—	—	1217	—
289.4	±0.9	±0.3	1229±4	—	1235	broad
311.6	±0.7	±0.25	1329±3	1332	1322	sharp
327.6	±0.5	±0.15	1402±2	1404	1403	sharp
336.2	±0.7	±0.2	1440±3	1451	1442	sharp
379.2	±0.2	±0.1	1637±1	1638	1634	sharp
396.8	±0.3	±0.1	1719±1.5	1722	1722	sharp

The wave number difference from λ 4358 Å is 1167 cm.$^{-1}$. The correspondence with the spectra given by HIBBEN and MONNIER is good. All the lines reported by HIBBEN have been found. The very strong line $\Delta\nu$ 263 cm. $^{-1}$ obtained by MONNIER has not appeared and its existence may be doubtful. The lines $\Delta\nu$ 338, 476 and 1217 cm.$^{-1}$ in MONNIER's spectrum are very weak. The line $\Delta\nu$ 772 cm.$^{-1}$ found in the present work is weak but appears in all recorded spectra. There is no corresponding line in the infrared spectrum of methyl methacrylate. The two lines $\Delta\nu$ 1113 cm.$^{-1}$ and 1188 cm.$^{-1}$ are not reported by HIBBEN or MONNIER. There are, however, corresponding lines in the polymer (*v. infra*) and further the infrared spectrum has a strong double band at 1162 cm.$^{-1}$ and 1197 cm.$^{-1}$. The line $\Delta\nu$ 1113 cm.$^{-1}$ has been found only in two of the spectra.

The scattering coefficients in Table 16 have about the same precision as those determined for methyl isobutyrate. The spectrum No. 73 d recorded at a higher

TABLE 16

Scattering coefficients of raman lines in methyl methacrylate

Wave numbers cm.$^{-1}$	Scattering coefficients						
	Spectrum No. 73 a	Spectrum No. 73 b	Spectrum No. 73 c	Spectrum No. 73 d	Mean value	M	M per cent
219	0.027	0.004	0.018	0.022	0.018	$\pm$ 0.005	$\pm$ 27.4
376	0.186	0.210	0.191	0.192	0.195	$\pm$ 0.005	$\pm$ 2.7
504	0.058	0.074	0.059	0.058	0.062	$\pm$ 0.004	$\pm$ 6.3
597	0.081	0.087	0.089	0.077	0.084	$\pm$ 0.003	$\pm$ 3.2
646	0.023	0.020	0.018	0.015	0.019	$\pm$ 0.002	$\pm$ 8.3
772	0.019	0.009	0.011	0.012	0.013	$\pm$ 0.002	$\pm$ 16.4
827	0.233	0.227	0.225	0.240	0.231	$\pm$ 0.003	$\pm$ 1.47
937	0.070	0.072	0.073	0.070	0.071	$\pm$ 0.001	$\pm$ 1.13
989	0.099	0.085	0.068	0.099	0.088	$\pm$ 0.007	$\pm$ 8.4
1011	0.112	0.106	0.105	0.108	0.108	$\pm$ 0.002	$\pm$ 1.6
1113	0.006	—	—	0.009	0.008	$\pm$ 0.001	$\pm$ 14.7
1159	0.047	0.036	0.027	0.036	0.037	$\pm$ 0.004	$\pm$ 11.0
1188	0.055	0.050	0.039	0.053	0.049	$\pm$ 0.004	$\pm$ 7.5
1229	0.038	0.029	0.023	0.036	0.032	$\pm$ 0.004	$\pm$ 11.4
1329	0.070	0.056	0.064	0.058	0.062	$\pm$ 0.003	$\pm$ 5.1
1402	—	0.289	0.312	0.307	0.302	$\pm$ 0.007	$\pm$ 2.3
1440	—	0.217	0.216	0.218	0.217	$\pm$ 0.005	$\pm$ 0.2
1637	0.451	0.444	0.434	0.459	0.447	$\pm$ 0.005	$\pm$ 1.2
1719	0.417	0.428	0.418	0.413	0.419	$\pm$ 0.003	$\pm$ 0.8

gain does not show any systematic deviations from the three other ones. This means that the rate of voltage increase at the input of the amplifier has never been too high with regard to the time constant of the system. The two lines $\Delta\nu$ 1402 cm.$^{-1}$ and 1440 cm.$^{-1}$ in spectrum No. 73 a could not be measured because of accidental troubles with the amplifier.

The relative intensities in Table 17 are quite interesting. Evidently the correspondence between the present work and HIBBEN's is rather good. Only $\Delta\nu$ 504 cm.$^{-1}$, 597 cm.$^{-1}$, 835 cm.$^{-1}$ and 937 cm.$^{-1}$ show large differences. As regards these particular lines, however, there is a marked agreement between HIBBEN's and MONNIER's intensities. With regard to the arbitrariness in drawing the base lines no thorough discussion can be given but it follows from a comparison between HIBBEN's microphotometer curves and the present records that the base lines have probably been drawn in about the same way. MONNIER has estimated the intensities on the microphotogram. Certain differences are also to be expected due to the influences of the optical instrument as regards resolution and transmittancy of polarized light (*cf.* RANK (148, 149)).

Table 17

Relative intensities of raman lines in methyl methacrylate

Wave numbers cm.$^{-1}$	Relative intensity		
	Monnier (134)	Hibben (132)	This investigation
219	—	—	4
263	110	—	—
338	10	—	—
377	70	45	47
476	10	—	—
504	30	30	15
597	30	30	20
646	6	0	5
772	—	—	3
835	100	85	55
937	30	30	17
989	20	—	21
1011	40	30	26
1113	—	—	2
1159	10	—	9
1188	—	—	12
1217	0	—	—
1229	10	—	8
1329	20	15	15
1402	100	70	72
1440	40	43	52
1637	140	114	107
1719	100	100	100

C. Raman Spectrum of Polymeric Methyl Methacrylate

The sample used to obtain the spectra of completely polymerized methyl methacrylate was a rod of perspex having approximately the same diameter and length as the raman tube. One of the ends was polished clear. The conditions under which this rod was polymerized are not known. It may contain some softeners. Only the region 0–1800 cm. ^{1} was studied. The reference was, as before, the three strongest carbon tetrachloride lines. Five spectra (Nos. 71 a–c and 72 a, b) were run under the same conditions as the spectra of the monomer. In run No. 71 the gain was twice as high as in run No. 72. The results are given in Tables 18–20 and in Figure 37. The values of the scattering coefficients are not corrected to the same refractive index basis. The relative intensities are given with $\Delta\nu$ 1725 cm.$^{-1}$ as a reference. The

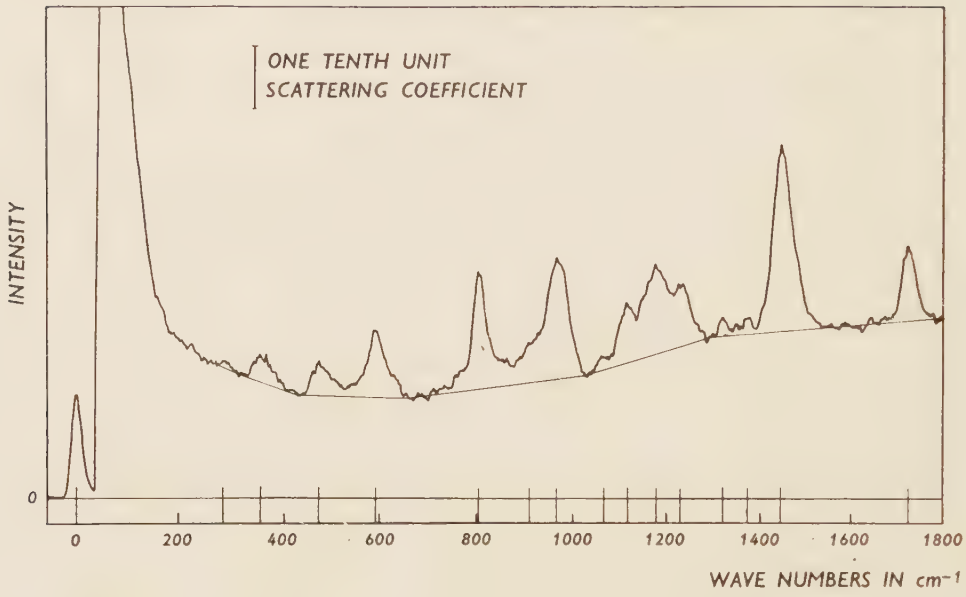

FIGURE 37. Raman spectrum of polymethyl methacrylate. (Spectrum No. 71 c.)

positions of the lines have been measured in the same way as before and converted to wave numbers by means of Equation (124).

Most of the lines are well defined and no broadening as a consequence of the high molecular weight can be detected. MONNIER reports a strong line $\Delta\nu$ 293 cm.$^{-1}$; this line is also found by HIBBEN and PATEL and in this investigation but it is much weaker. The new line $\Delta\nu$ 910 cm.$^{-1}$ is not completely resolved. It has a medium intensity and its existence as a line from the polymer may be doubtful. There is a possibility that it originates from a softener. However, the infrared spectrum contains a line 913 cm.$^{-1}$ (*v. infra*). MONNIER has three lines in the region of $\Delta\nu$ 970 cm.$^{-1}$. As far as the lines $\Delta\nu$ 968 cm.$^{-1}$ and $\Delta\nu$ 990 cm.$^{-1}$ are concerned they correspond to infrared lines at 966 cm.$^{-1}$ and 988 cm.$^{-1}$ respectively. The line $\Delta\nu$ 1379 cm.$^{-1}$ found here is not well resolved and may be attributed to a possible softener. But even this line can have a correspondence in the infrared spectrum where two fairly weak lines 1366 cm.$^{-1}$ and 1385 cm.$^{-1}$ exist. The strong lines $\Delta\nu$ 3127 cm.$^{-1}$ excited by λ 4047 Å and $\Delta\nu$ 2939 cm.$^{-1}$ excited by λ 4078 Å should give a line $\Delta\nu$ 1361 cm.$^{-1}$. MONNIER has reported a very weak line $\Delta\nu$ 1628 cm.$^{-1}$ and PATEL a fairly strong line $\Delta\nu$ 1598 cm.$^{-1}$. The large shift of about 25 cm.$^{-1}$ in the line reported by PATEL is not explained.

The agreement between the scattering coefficients calculated from different spectra is rather satisfactory. The average value of M is $\pm$ 0.0022 compared to $\pm$ 0.0034 for the monomer and $\pm$ 0.0033 for methyl isobutyrate. This shows that

Table 18

Position of raman lines in polymethyl methacrylate

Δl, mm.	M, mm.	M per cent	Wave numbers, cm.$^{-1}$				Structure of lines
			This investigation	Hibben (132)	Monnier (134)	Patel (140)	
54.4	± 1.8	± 3.4	221 ± 8	—	—	231	broad
71.35	± 0.4	± 0.6	291 ± 2	299	293	295	broad
88.7	± 0.25	± 0.3	363 ± 1	367	—	360	sharp
117.7	± 0.5	± 0.45	484 ± 2	487	470–85	491	sharp
143.8	± 0.15	± 0.1	594 ± 1	599	590	606	sharp
192.9	± 0.25	± 0.1	805 ± 1	806	807–16	817	sharp
217.2	± 0.4	± 0.2	910 ± 2	—	—	—	broad
—	—	—	—	—	956	—	
230.6	± 0.2	± 0.1	969 ± 1	974	968	982	sharp
—	—	—	—	—	990	—	
251.3	± 0.5	± 0.2	1060 ± 2	—	1058	—	not resolved
265.6	± 0.5	± 0.2	1123 ± 2	1116	1118	1129	
277.9	± 0.2	± 0.1	1178 ± 1	—	1172–95	1176	broad
288.9	± 0.15	± 0.05	1227 ± 1	—	1235	—	broad
310.7	± 0.34	± 0.1	1325 ± 1.5	1335	—	—	not well resolved
322.6	± 0.8	± 0.25	1379 ± 4	—	—	—	
337.6	± 0.1	± 0.05	1447 ± 1	1448	1452–68	1455	sharp
—	—	—	—	—	1628	1598	
398.3	± 0.2	± 0.05	1726 ± 1	1725	1710–26	1729	sharp

the polymer spectrum does not offer any greater difficulties as regards intensity measurements than spectra of organic compounds of low molecular weight. The values obtained at different gains of the amplification system do not show any systematic deviations. The magnitude of the scattering coefficients is of the same order as that for the other spectra investigated. Thus even in this respect the high polymer shows the same behaviour as low molecular-weight substances.

The relative intensities of the lines obtained at different laboratories do not show the same correspondence as was found for the monomeric methyl methacrylate. Only two lines in Hibben's, Monnier's and the present spectra agree within 10 per cent compared to three or five for the monomer. Patel's estimations seem to be the most unreliable. Undoubtedly it can be stated that the good conformity between the deviations (M-values) in Table 19 shows that the photo-electric recording method gives a rather reliable measure of the intensities of the lines.

A problem which has concerned most of the earlier investigators of raman spectra of high polymers is the diffuse background radiation which very often occurs. Singer and Weiler (129) attributed the background to fluorescent by-products formed in minute amounts during the polymerization or to the presence of small

Table 19

Scattering coefficients of raman lines in polymethyl methacrylate

Wave numbers cm.$^{-1}$	Scattering coefficients							
	Spectrum No. 71 a	Spectrum No. 71 b	Spectrum No. 71 c	Spectrum No. 72 a	Spectrum No. 72 b	Mean value	M	M per cent
221	0.009	0.006	—	0.006	0.010	0.008	$\pm$ 0.001	$\pm$ 13.0
291	0.012	—	0.006	0.014	0.016	0.012	$\pm$ 0.002	$\pm$ 17.4
363	0.036	0.045	0.040	0.045	0.035	0.040	$\pm$ 0.002	$\pm$ 5.2
484	0.043	0.041	0.047	0.048	0.0415	0.044	$\pm$ 0.0015	$\pm$ 3.4
594	0.105	0.096	0.105	0.111	0.109	0.105	$\pm$ 0.003	$\pm$ 2.5
805	0.188	0.192	0.1825	0.1815	0.185	0.186	$\pm$ 0.002	$\pm$ 1.0
910	0.064	0.068	0.063	0.049	0.054	0.060	$\pm$ 0.003	$\pm$ 5.7
969	0.190	0.191	0.188	0.180	0.204	0.191	$\pm$ 0.004	$\pm$ 2.0
1060	0.008	0.016	0.019	0.012	0.013	0.0135	$\pm$ 0.002	$\pm$ 14.1
1123	0.083	0.092	0.089	0.082	0.083	0.086	$\pm$ 0.002	$\pm$ 2.2
1178	0.124	0.134	0.136	0.1265	0.128	0.130	$\pm$ 0.002	$\pm$ 1.8
1227	0.106	0.104	0.097	0.103	0.099	0.102	$\pm$ 0.002	$\pm$ 1.7
1325	0.031	0.0285	0.026	0.027	0.019	0.026	$\pm$ 0.002	$\pm$ 7.3
1379	0.026	0.032	0.026	0.027	0.029	0.027	$\pm$ 0.001	$\pm$ 4.0
1447	0.2785	0.2805	0.292	0.2745	0.275	0.280	$\pm$ 0.003	$\pm$ 1.1
1726	0.114	0.116	0.117	0.094	0.1245	0.113	$\pm$ 0.005	$\pm$ 4.5

amounts of initiator. The suggestion put forward by Venkateswaran (150, 151). that the background should increase with increasing viscosity of the scattering medium was shown to be unjustified. Signer and Weiler could prepare polystyrenes almost free of any background. Further Palm (130) and Hibben (132) have shown that a small extent of polymerization does not change the spectrum of the monomer very much but it increases the viscosity enormously. The same has been found in the present investigation. The background of the polymer spectra obtained here is not low. However, it does not seem to have any influence on the raman spectrum. From a minimum value at about 600 cm.$^{-1}$ it increases slightly and reaches at about 1800 cm. ^{1} a value 75 per cent higher than at the minimum. The scattering coefficient of the background at $\Delta\nu$ 1060 cm.$^{-1}$ is about 0.19. The contribution from the rayleigh scattering and stray light from the lamp-house can be calculated from the scattering coefficient, 545, of the exciting line, and the ratio, $5.5 \cdot 10^{-5}$, of the λ 4358 Å intensity and the background at $\Delta\nu$ 1060 cm.$^{-1}$ in the mercury spectrum (obtained from the spectrum in Figure 27). The scattering coefficient 0.030 is obtained. This is only 15 per cent of the total background. For the monomer the scattering coefficient of the exciting line is 490 and this gives a background scattering coefficient at $\Delta\nu$ 1060 cm. ^{1} of 0.025 which is about 35 per cent of the actual value 0.075. The

Table 20

Relative intensities of raman lines in polymethyl methacrylate

Wave numbers cm.$^{-1}$	Relative intensities			
	Hibben (132)	Monnier (134)	Patel (140)	This investigation
221	—	—	0	7
295	35	140	0	11
363	65	—	20	35
485	65	30	20	39
594	100	100	60	93
805	200	180	140	165
910	—	—	—	53
956	—	160	—	—
970	165	140	80	169
990	—	40	—	—
1060	—	20	—	12
1120	35	20	20	76
1178	—	60	0	115
1230	—	20	—	90
1330	0	—	—	23
1379	—	—	—	24
1450	?	200	100	248
1620	—	0	20	—
1725	100	100	100	100

main part of the background, therefore, has other causes than rayleigh scattering and stray radiation.

The raman spectrum of polymethyl methacrylate has many similarities with the spectrum of methyl isobutyrate (*cf.* Figure 30). This is to be expected because isobutyric acid is the saturated methacrylic acid. Further, it is interesting to note the differences in intensity of the $\Delta\nu$ 1720 cm.$^{-1}$ line between the unsaturated methyl methacrylate, the saturated polymethyl methacrylate and methyl isobutyrate. The scattering coefficients are respectively: 0.419; 0.113 and 0.098. The corresponding wave numbers are $\Delta\nu$ 1719 cm.$^{-1}$, $\Delta\nu$ 1726 cm.$^{-1}$ and $\Delta\nu$ 1725 cm.$^{-1}$; therefore it may be a shift in frequency too. The following values on methyl esters of some unsaturated and corresponding saturated acids are taken from Kohlrausch (121):

Methyl acrylate: $CH_2{=}CH \cdot CO \cdot O \cdot CH_3$ ..... $\Delta\nu$ 1722 cm.$^{-1}$
Methyl propionate: $CH_3 \cdot CH_2 \cdot CO \cdot O \cdot CH_3$ ..... $\Delta\nu$ 1734 cm.$^{-1}$
Methyl α-crotonate: $CH_3 \cdot CH{=}CH \cdot CO \cdot O \cdot CH_3$ ..... $\Delta\nu$ 1715 cm.$^{-1}$
Methyl *n*-butyrate: $CH_3 \cdot CH_2 \cdot CH_2 \cdot CO \cdot O \cdot CH_3$ ..... $\Delta\nu$ 1731 cm.$^{-1}$
Methyl $\beta\beta'$-dimethyl acrylate: $(CH_3)_2C{=}CH \cdot CO \cdot O \cdot CH_3$ ..... $\Delta\nu$ 1715 cm.$^{-1}$
Methyl isovalerate: $(CH_3)_2CH \cdot CH_2 \cdot CO \cdot O \cdot CH_3$ ..... $\Delta\nu$ 1727 cm.$^{-1}$

These values show a shift of 10–15 cm.$^{-1}$. The explanation for the large differences in intensity is the conjugation between the double bond in the carbonyl group and the carbon–carbon double bond. Such conjugation phenomena have been studied by HARRAND (152). She has compared unsaturated and saturated aldehydes and found a much more intense spectrum for unsaturated aldehydes with a conjugated double bond system. A similar phenomenon occurs if the carbonyl double bond or the carbon–carbon double bond is conjugated with a benzene nucleus: styrene compared to ethyl benzene (HARRAND (153)) and methyl benzoate compared to methyl phenylacetate (KOHLRAUSCH and PONGRATZ (154)). Precise measurements of the change in intensity for such compounds do not exist.

D. Bond Frequencies in Monomeric and Polymeric Methyl Methacrylates

For the further discussion it is necessary to give the structural assignments which have been found for the spectra of monomeric and polymeric methyl methacrylates, *i.e.* the characteristic bond frequencies of these molecules. In this section only those frequencies which are of interest in the interpretation of spectra of polymerizing mixtures will be discussed. It is not possible to make a complete assignment of fundamental, overtone and combination frequencies for these very complex molecules. For a detailed discussion about characteristic bond frequencies reference is made to the monograph of HERZBERG (155). The underlying principle is the invariance of the force constant of a bond in similar surroundings in different molecules. We are here concerned with the bond-stretching and the bond-bending force constants and shall, in accordance with HERZBERG, refer to the corresponding oscillations as bond-stretching and bond-bending vibrations. Vibrations of the last type can be divided in subgroups, namely 1) deformation vibration producing a change in the angles between atoms in the structure group itself; 2) wagging vibration of the structure group as a rigid unit in a plane perpendicular to the symmetry plane of the whole molecule; 3) rocking vibration as 2) but with swingings in the plane of symmetry; 4) twisting vibration consisting of a rotation of the structure group around the bond joining it with the rest of the molecule. Then the notation bending vibration is used only when the structure group is so simple that any more specialized description would not be useful, or if a more detailed assignment cannot be made owing to lack of data (*cf.* RANDALL, FOWLER, FUSON, and DANGL (156)).

The structural groups characteristic of the present compounds are:

The carbonyl group: $\rangle C=O$

The carbon–carbon double bond: $\rangle C-C\langle$

The methylene group: and

The methyl group: 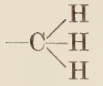

The carbon–carbon single bond: 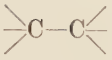

The ester group: 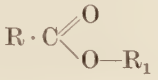

The most striking differences between the spectrum of the monomer and the polymer are the disappearance of the lines $\Delta\nu$ 1637 cm.$^{-1}$ and $\Delta\nu$ 1402 cm.$^{-1}$ and the marked decrease in intensity of the line $\Delta\nu$ 1720 cm.$^{-1}$. The line $\Delta\nu$ 1637 cm.$^{-1}$ is ascribed to bond-stretching vibrations in the C=C group and the $\Delta\nu$ 1720 cm.$^{-1}$ line to similar vibrations in the C O group. Then these assignments are in accordance with the decrease in the carbonyl bond-frequency due to the disappearance of the conjugated double bond system. The frequency $\Delta\nu$ 1402 cm.$^{-1}$ corresponds to a deformation vibration of the CH-groups of the carbon–carbon double bond and the lines $\Delta\nu$ 1440 cm.$^{-1}$ and $\Delta\nu$ 1447 cm.$^{-1}$ respectively, to similar oscillations in the methylene and methyl groups. The monomer frequencies $\Delta\nu$ 989 cm.$^{-1}$ and $\Delta\nu$ 1011 cm.$^{-1}$ and the polymer frequency $\Delta\nu$ 969 cm.$^{-1}$ are ascribed to bond-stretching vibrations of the C—C bonds. It should be noted that the bond-stretching vibrations of the C—H linkages are not recorded in the present spectra because they give frequency shifts in the region of 3000 cm.$^{-1}$. The assignments given are the most important for the discussions in the next section. They correspond to the interpretation given by Hibben and Monnier.

E. Raman Spectra of Partially Polymerized Methyl Methacrylates

A most striking fact in a spectrophotometric investigation of this kind is the very small change of the raman spectrum after an enormous increase in viscosity of the polymerizing mixture. The true state of affairs is, however, clear as soon as the degree of conversion has been determined. Experience of work with solutions of high polymers also shows that already fairly low concentrations of the solute give highly viscous solutions.

The spectra obtained have been run under the conditions given on p. 106. Table 21 contains the scattering coefficients calculated from spectra taken in expts. P4a, P4b, P4e, and P4f. Mean values of the corresponding degrees of conversion are also given. As the scattering coefficients have been calculated from one single spectrum

TABLE 21

Scattering coefficients of partially polymerized methyl methacrylate

Wave numbers cm.$^{-1}$	Scattering coefficients								
	Monomer (Table 16)	Expt. P4a			Expt. P4b		Expt. P4e		Expt. P4f
		Spectrum No. 37	Spectrum No. 38	Spectrum No. 39	Spectrum No. 42	Spectrum No. 43	Spectrum No. 65	Spectrum No. 66	Spectrum No. 75
219	0.018	—	—	—	0.027	0.036	0.035	0.018	0.022
376	0.195	—	—	—	0.185	0.198	0.132	0.075	0.139
504	0.062	—	—	—	0.052	0.057	0.044	0.036	0.046
597	0.084	—	—	—	0.088	0.111	0.086	0.102	0.087
646	0.019	—	—	—	—	—	—	—	0.027
772	0.013	—	—	—	0.027	0.036	0.013	0.043	0.022
827	0.231	—	—	—	0.232	0.244	0.188	0.144	0.181
937	0.071	—	—	—	0.077	0.087	0.056	0.038	0.065
989	0.088	—	0.125	0.134	0.131	0.141	0.077	0.186	0.097
1011	0.108	—	—	—	0.111	0.107	0.088	—	0.087
1113	0.008	—	—	—	—	—	-	-	-
1159	0.037	—	—	—	0.041	—	0.033	0.068	0.031
1188	0.049	—	—	—	0.046	0.057	0.047	0.106	0.046
1229	0.032	—	—	—	0.056	0.066	0.029	0.129	0.036
1329	0.062	—	—	—	0.052	0.050	0.044	0.050	0.051
1402	0.302	0.288	0.317	0.294	0.287	0.284	0.245	0.104	0.245
1440	0.217	0.211	0.222	0.220	0.218	0.241	0.193	0.242	0.192
1637	0.447	0.424	0.433	0.435	0.394	0.393	0.338	0.113	0.350
1719	0.419	0.406	0.402	0.408	0.401	0.381	0.328	0.182	0.348
Degree of conversion	0	0.036	0.061	0.094	0.067	0.180	0.115	0.816	0.140

only, the uncertainty in the values is great. Spectra Nos. 65 and 75, run under almost the same conditions, show the magnitude of the variations. Figures 38 and 39 show reproductions of the original spectra of partially polymerized methyl methacrylates (spectra Nos. 65 and 66). In Figure 40 the scattering coefficients are plotted against the corresponding wave numbers for spectra of methyl methacrylate, partially polymerized methyl methacrylate, polymethyl methacrylate and methyl isobutyrate. Finally Figures 41 a–d show the variation of the scattering coefficients of certain bond-frequencies as a function of the degree of conversion. The uncertainty in the scattering coefficients indicated in the last figures corresponds to ± 0.010 unit scattering coefficient.

It should be kept in mind in the following discussion that no corrections have been made for the different refractive indices of the substances investigated. During polymerization the refractive index increases: hence the effective, scattering volume

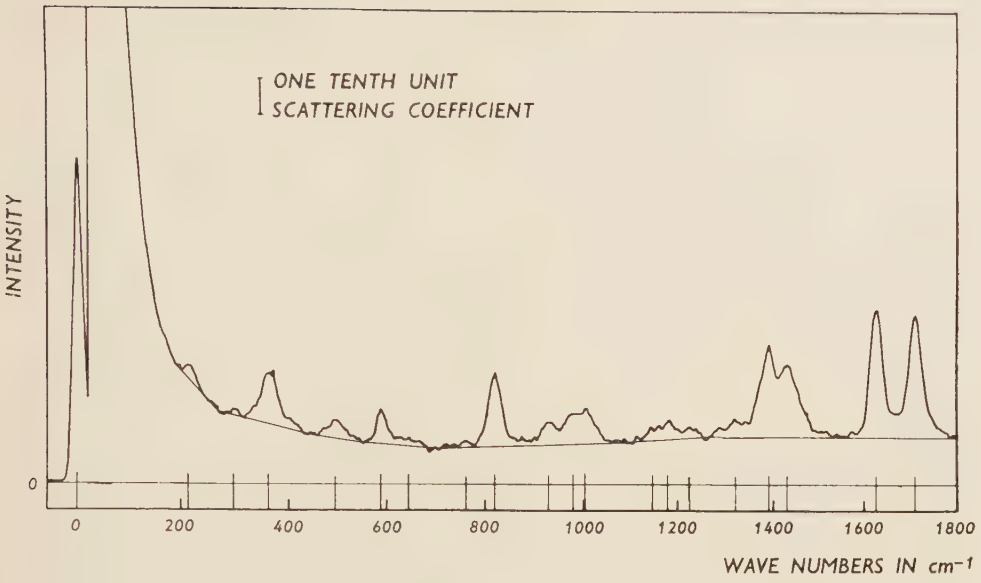

FIGURE 38. Raman spectrum of partially polymerized methyl methacrylate at a degree of conversion of 11.5 per cent. (Spectrum No. 65.)

seen by the spectrograph will decrease. The refractive indices 1.41 and 1.50 for the monomer and the polymer respectively and 1.46 for carbon tetrachloride give the correction factors 0.93 and 1.06 respectively. The changes in intensity discussed below are so great that the conclusions are valid without taking the corrections into account.

A clear impression of what is happening during the polymerization is obtained from Figure 40. The regular decrease in intensity of the carbonyl bond-frequency and the disappearance of the carbon–carbon double bond are obvious, as are also the increase of the $\Delta\nu$ 1440 cm.$^{-1}$ line and the disappearance of $\Delta\nu$ 1402 cm.$^{-1}$. This is in agreement with the fact that the double bond is opened during the reaction. Then the deformation vibrations of the hydrogen atoms in the group $C\begin{matrix}H\\H\end{matrix}$ will disappear and, instead, similar vibrations in the group $>C\begin{matrix}H\\H\end{matrix}$ occur. The increase in scattering coefficents of the band system at $\Delta\nu$ 1150–1230 cm.$^{-1}$ is evident. The reason is partly due to the presence of lines excited by λ 4047 Å and λ 4078 Å and corresponding to bond-stretching vibrations of the C—H linkages. A marked increase in intensity of the lines in the 3000 cm.$^{-1}$ region has been observed but not quantitatively interpreted. The two lines $\Delta\nu$ 1159 cm.$^{-1}$ and $\Delta\nu$ 1229 cm.$^{-1}$ are attributed by MONNIER to bond-stretching vibrations of C—C groups. Due to the low resolving power of the spectrograph used here the separation of the lines in this

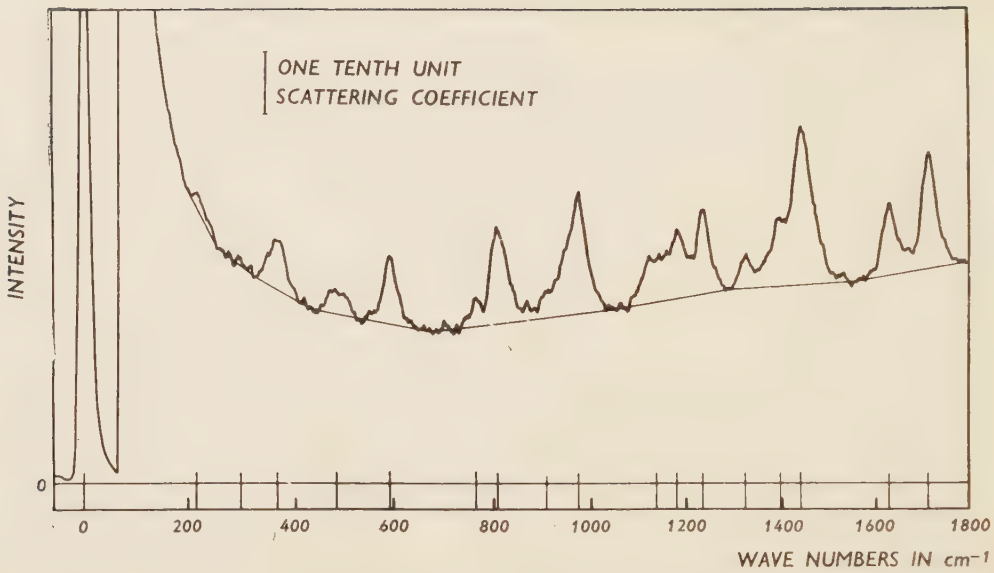

FIGURE 39. Raman spectrum of partially polymerized methyl methacrylate at a degree of conversion of 82 per cent. (Spectrum No. 66.)

band is bad and therefore a more thorough discussion is excluded. The same is partly true of the band system at 1000 cm.$^{-1}$. This band also contains bond-frequencies of the C—C groups. The increase of the scattering coefficient of $\Delta\nu$ 989 cm.$^{-1}$ is, however, quite obvious. At the same time it shifts towards shorter wave-lengths. HIBBEN says that the disappearance of the lines $\Delta\nu$ 937 and 1011 cm.$^{-1}$ and the appearance of the line $\Delta\nu$ 969 cm.$^{-1}$ may possibly be an accidental degeneracy indicating an increase in symmetry of the molecule. However, in his work, the line $\Delta\nu$ 989 cm.$^{-1}$ of the monomer spectrum is absent (Table 15). From the present investigation it also follows that the line $\Delta\nu$ 910 cm.$^{-1}$ of the polymer may correspond to $\Delta\nu$ 937 cm.$^{-1}$. Thus the only line which should have disappeared is $\Delta\nu$ 1011 cm.$^{-1}$. However, both MONNIER and the present author have a line $\Delta\nu$ 1060 cm.$^{-1}$. Therefore it is not at all clear that this band system should change in a way indicative of an increase in symmetry. Methyl isobutyrate has a line $\Delta\nu$ 976 cm. $^{-1}$ of about half the intensity of the polymer line. The higher intensity in the polymer should then indicate that this line has a direct relation to the long chain. The line $\Delta\nu$ 881 cm. $^{-1}$ is a possible correspondence to the line $\Delta\nu$ 910 cm.$^{-1}$ of the polymeric methyl methacrylate. The lines $\Delta\nu$ 827 cm. $^{-1}$ and $\Delta\nu$ 597 cm. $^{-1}$ in the monomer do not change appreciably; there is, however, an evident shift in frequency of the first line. Finally a decrease in intensity occurs for the line $\Delta\nu$ 376 cm.$^{-1}$. This is rather interesting because the line falls in a region of bond-bending vibrations of larger structural elements such as C- -C chains. However, methyl isobutyrate has a band in the same

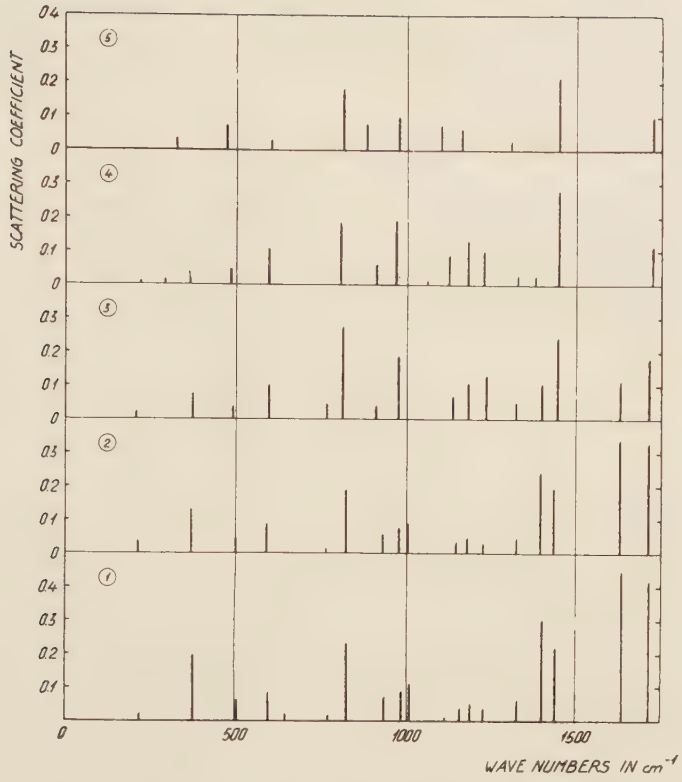

FIGURE 40. Scattering coefficients of the raman lines of methyl methacrylate 1); partially polymerized methyl methacrylates 2) 11.5 per cent, 3) 82 per cent; polymethyl methacrylate 4), and methyl isobutyrate 5).

region and of about the same intensity as in the polymer. Therefore it is improbable that this band has anything to do with the very long carbon chain. It is possible that its appearance should be attributed to such structural elements as C $\begin{matrix} C \\ \diagup \\ \diagdown \\ C \end{matrix}$ and C—C$\begin{matrix} C \\ \diagup \\ \diagdown \\ C \end{matrix}$. Nothing can be definitely stated, however, without further data.

Another interesting point is to what extent the change in scattering coefficient can be correlated with the degree of conversion. A distinction must be made between two cases, namely, 1) the raman shift under discussion exists in the monomer but not in the polymer and 2) the raman shift exists both in the monomer and in the polymer and has nearly the same frequencies (they can not be resolved by the instrument).

The intensity of a raman shift depends upon the number of molecules, N_n, in the initial state, n, and of the EINSTEIN transition probabilities of the transition

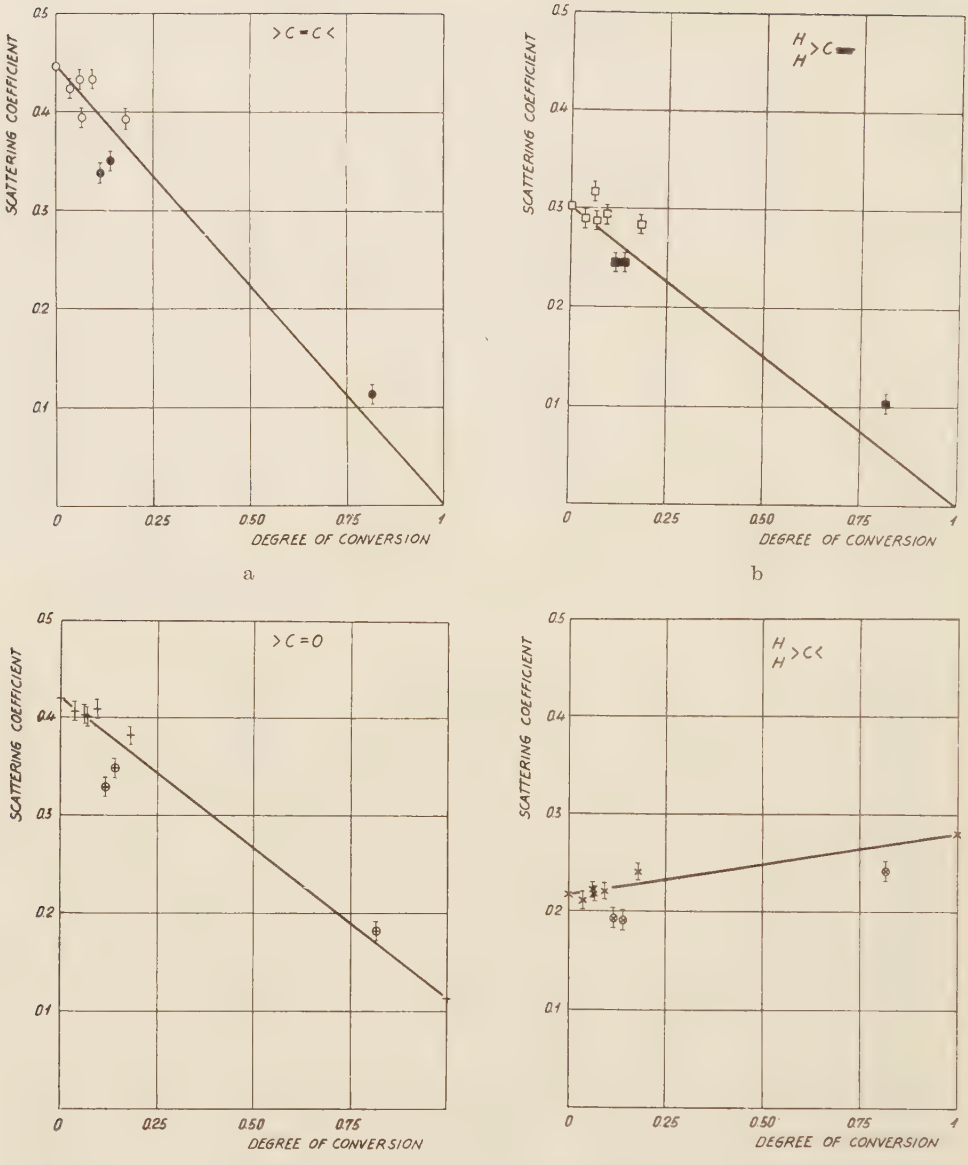

FIGURE 41. Scattering coefficients at different degrees of conversion:

a) bond-stretching vibrations of the >C C< bond;

b) deformation vibrations in the H, H >C= group;

c) bond-stretching vibrations of the >C= O bond;

d) deformation vibrations in the H, H >C< group.

$n \rightarrow m$. These probabilities are functions of the dipole moment $\boldsymbol{P} = \alpha \boldsymbol{F}$ induced in the molecules (α is the polarizability tensor and $\boldsymbol{F}$ the perturbing electric field). The quantum mechanical expression for the transition probability contains matrix elements of the form

$$[\boldsymbol{P}^0]^{nm} = |\boldsymbol{F}| \int \psi_n^* \alpha \psi_m \, \mathrm{d}\tau \tag{129}$$

where ψ_n and ψ_m are the time-independent wave functions of the two states of the system (*cf.* HERZBERG (155, 157)); the integral is taken over the whole configuration space. In case 1) the number of not converted molecules can be expressed as a simple function of the degree of conversion, q. Let N_n^0 be the initial number of molecules per volume in state n; then

$$\frac{N_n}{N_n^0} = \frac{1-q}{1-q\left(1-\frac{\varrho_1}{\varrho_2}\right)} \tag{130}$$

where ϱ_1 and ϱ_2 are the densities of the monomer and the polymer respectively. Methyl methacrylate has $\varrho_1 = 0.94$ and the polymer has $\varrho_2 = 1.20$ hence $\varrho_1/\varrho_2 < 1$ and $N_n/N_n^0 > 1-q$. At $q = 0.5$ we have $N_n/N_n^0 = 0.56$ and the scattering coefficient equal to 0.250 instead of 0.223. The last value corresponds to the heavy line in Figure 41 a, which is drawn under the assumption $\varrho_1 = \varrho_2$. Consequently the true, theoretical relation between scattering coefficient and degree of conversion should follow a curve situated above the lines in Figures 41 a and b and coinciding with them only at the degrees of conversion zero and one. However, the refractive index of the medium increases during the polymerization. This causes a decrease of the amount of luminous flux through the spectrograph. The refractive indices 1.41 and 1.50 for the monomer and the polymer respectively give a maximum correction factor of 0.885 (*cf.* Equation (31)). The influence of density and refractive index will, therefore, to a certain extent compensate each other. No exact measurements of the changes in density and refractive index during the polymerization have been made here. Therefore, no quantitative estimations of the fitting of the measured points to a theoretical relation can be done. The data obtained follow the straight lines fairly well.

The situation is quite different in case 2). Now two types of molecules contribute to the intensity of the bond-frequency. The total intensity is a sum of expressions containing the number of each of the molecular species in their original states multiplied with the corresponding transition probabilities. Only when the two molecular species have the same polarizability and are described by the same set of eigenfunctions the same matrix elements, $[\boldsymbol{P}^0]^{nm}$, will be obtained and the relative change in intensity can, in a simple way, be correlated with the degree of conversion. In Figure 41 c the scattering coefficient of the carbonyl bond-frequency of the reaction mixture is plotted *versus* the degree of conversion. The number of these bonds per

volume changes only as the density of the medium changes. This would tend to increase the scattering coefficients. Instead, a pronounced decrease occurs. This is caused by the difference in polarizability of molecules containing the conjugated system $O=C-C=C\diagdown\!\diagup$ and molecules containing only the bond $\diagup C=O$. In the case of deformation vibrations of hydrogen atoms a slight increase of the scattering coefficients occurs (Figure 41 d). The polarizability properties of the molecules do not change very much during the polymerization. An instrument of higher resolving power renders a separate study of the phenomena in the two molecular species possible.

A further question of importance in this discussion is the influence of the free radicals. A large number of these radicals will make the raman spectrum of a polymerizing mixture to something more than a pure superposition of the spectra of the monomer and the polymer. An interpretation is impossible, however, without a more complete knowledge of the conditions governing the polymerization process. From Figure 41 it is evident that experiments made at a higher amount of initiator (●, ■, ⊕, ⊗) have given lower scattering coefficients for degrees of conversion between 0 and 0.25. This discrepancy is difficult to explain. It may have some connection with different states in the polymerizing mixtures.

Chapter 4

Ultra Violet Studies of End Groups

In the radical chain polymerization of vinyl compounds three types of reactions occur, namely: the initiation of the reaction, the propagation of the chain and the termination reaction. In a peroxide-initiated process the original free radicals are produced through a decomposition of the initiator. The fragments are added to the monomer and large radicals of different size are successively formed. In the termination the growing chains are deactivated to the final macromolecules. The reaction mechanism can be complicated by the occurrence of chain transfer, *i.e.* the radical character is transferred from the growing chain to a monomer, a polymer or an intentionally added transfer agent. Finally the termination reaction can be of different nature: two growing molecules can add (combination) or they can exchange an atom (disproportionation).

A study of the ends of a macromolecule is mainly concerned with the structure of the end groups and their number. A knowledge about the structure gives information about the type of radicals formed from the initiator, a knowledge of the number tells something about the type of termination reaction. An investigation of this kind is far from simple. The presence of chain transfer, the possibility of obtaining several types of radicals from the same initiator *etc.* render the interpretation of experimental data difficult. For a study of this kind, several methods have been employed. In the present case the possibilities offered by ultraviolet absorption have been utilized.

Previous Work

The thermal decomposition of diacid peroxides have been studied by several investigators. (For a short review reference is made to Mark *et al.* (158).) Both carboxyradicals and hydrocarbon radicals can be formed

$$(\mathrm{R.COO})_2 \rightarrow 2\,\mathrm{RC}\!\left(\!\begin{array}{l}\!\!\!

Thus the polymerization reaction can be initiated by two types of radicals giving the polymers two kinds of end groups. The amount of the different radicals depends upon the reaction conditions. Some of the most important investigations concerning the end groups will briefly be discussed below.

Price, Kell and Krebs (159) have polymerized styrene and methyl methacrylate with *p*-bromobenzoyl peroxide, anisoyl peroxide and chloroacetyl peroxide. In the polymers formed, they have found from determinations of bromine, methoxygroups and chlorine about one initiator fragment per macromolecule. Hydrolysis of the polymer did not yield anything and therefore they concluded that the initiator fragment was a *p*-bromophenyl group. Price and Durham (160) showed that *p*-bromobenzene diazonium hydroxide initiates styrene polymerization by *p*-bromophenylradicals. Price and Tate (161) found 3,4,5-tribromophenyl fragments in polystyrene. Finally Price and Durham (162) and Price (163) have shown that retarders like nitrobenzene, 2,4-dinitrochlorobenzene and nitrothiophene, and chain transfer agents like chloranil are combined with the polymer.

Kern and Kämmerer (164) used *p*-bromobenzoyl peroxide to polymerize styrene and found from bromine determinations that each polymer molecule contained on an average four bromine atoms, corresponding to the addition of two complete initiator molecules to each chain.

Bartlett and Cohen (165) also used *p*-bromobenzoyl peroxide in the polymerization of styrene. They found that the polymer contained both benzoic and phenyl groups. The failure of Price *et al.* to obtain benzoic acid through hydrolysis depended upon their use of too weak a hydrolysing agent. Bartlett and Altschul (166) found in polymers from allyl acetate polymerized with *p*-chlorobenzoyl peroxide 72.5 per cent of the total chlorine in the end groups. Of this amount 52 per cent was contained as benzoic groups and 12 per cent as phenyl groups.

Blomquist, Johnson and Sykes (167) used bromine derivatives of N-nitrosoacylarylamines as initiators and found in polystyrene, polymethyl methacrylate and polyacrylonitrile between one and two arylradicals per polymer molecule.

Pfann, Salley and Mark (168) found by bromine analysis between one and three bromine atoms per chain when styrene was polymerized with *m*-bromobenzoyl peroxide. Measurement of induced radioactivity after bombardment with slow neutrons gave the same figure. Later Pfann, Williams and Mark (158) showed that the polystyrene samples prepared had a measurable absorption at 1720 cm.$^{-1}$ in the infrared. This band is a carbonyl bond frequency. The result supports previous evidence for the existence of benzoate ester groupings in the polymer molecule.

Dainton and Sutherland (169) have applied the infrared technique to elucidate the end group structure in polyisobutene prepared with boron trifluoride as an initiator. They could prove the presence of two end groups: $(CH_3)_3C-$ and $CH_2=C<$.

In this case the trifluoride behaves as a catalyst. Flett and Plesch (169 a) have found that trichloroacetic acid, added as a co-catalyst, gives the polymer trichloroacetate end groups.

In a recent work Arnett (170) and Arnett and Peterson (171) have studied the initiation of vinylpolymerization with aliphatic azobisnitriles containing C^{14}. For polymethyl methacrylate they found, from radioactivity measurements, one initiator fragment attached to each end of the polymer molecule.

Finally Katchalsky and Wechsler (172) have studied the transparency of polymethyl methacrylate in the ultraviolet and found a benzoyl peroxide polymerized polymer transparent to waves longer than 300 mμ and an acetyl peroxide polymer transparent to waves longer than 250 mμ. The difference is attributed to the presence of aromatic compounds and thus supports the evidence for aromatic end groups.

Present Work

A. General Considerations

A study of ultraviolet spectra of compounds containing benzoate groups shows that the absorption curve has three main maxima: a large maximum at about 230 mμ and two small at about 274 mμ and 282 mμ (Ref. 173). These maxima are rather characteristic and it was thought of interest to extend the work of Katchalsky and Wechsler (172) and make a detailed study of benzoyl peroxide polymerized methyl methacrylates in this ultraviolet region and see if any absorption due to benzoate groups existed. At the same time an infrared study was started (Chapter 5).

Besides information about the structure of the end groups such an investigation also gives the number of these groups. The following notations are introduced:

M_A molecular weight of the monomer unit
ε_A specific extinction coefficient of the monomer unit
i degree of polymerization of molecule i
j number of end groups in molecule i
M_B molecular weight of the end group
ε_B specific extinction coefficient of the end group
c_{ij} concentration of molecules having the molecular weight $M_{ij} = i \cdot M_A + j \cdot M_B$
D_{ij} optical density at concentration c_{ij}.

Assuming Beer's law to be valid we get:

$$D_{ij} = \varepsilon_A \frac{i M_A}{M_{ij}} c_{ij} + \varepsilon_B \frac{j M_B}{M_{ij}} c_{ij} \tag{131}$$

and after summation

$$D_{\text{tot}} = \varepsilon_A c + (\varepsilon_B - \varepsilon_A) M_B \sum_{ij} j \frac{c_{ij}}{M_{ij}} \tag{132}$$

or

$$D_{\text{tot}} = \varepsilon_A c + (\varepsilon_B - \varepsilon_A) M_B \frac{\bar{j}_n}{\bar{M}_n} c \tag{133}$$

where $\bar{j}_n$ and $\bar{M}_n$ are the number averages of the number of end groups and the molecular weight respectively. Dividing by c we get

$$\varepsilon_{\text{tot}} = \varepsilon_A + (\varepsilon_B - \varepsilon_A) M_B \frac{\bar{j}_n}{\bar{M}_n} \tag{134}$$

and finally

$$\bar{j}_n = \frac{\bar{M}_n}{M_B} \frac{\varepsilon_{\text{tot}} - \varepsilon_A}{\varepsilon_B - \varepsilon_A} \tag{135}$$

This is, in fact, a determination of the molecular weight of the branches of the polymer molecule. About twenty years ago SMAKULA (174) claimed to have used absorption in ultraviolet as a method for molecular weight determinations on polystyrenes. What he has shown is, however, that the absorption per monomer unit is independent of the degree of polymerization.

B. Experimental Work

a. Experimental Technique

The preparation and purification of the samples used is described in Chapter 2. Measurements were done on polymer samples P2a1, P2b6, P2c1, on fractions of P2a1 and P2b6 and on the fraction P2d1TIa. Further methyl methacrylate, benzoyl peroxide and methyl isobutyrate were measured. As a solvent, freshly distilled chloroform was used. Unfortunately, chloroform has a high transparency only down to 245 mμ which makes a study of the 230 mμ maximum of the benzoate group impossible. Attempts were made to use isopropyl chloride which is transparent to 225 mμ. Due to its high volatility it was difficult to avoid evaporation and changes in concentration during the measurements. Further, it was a rather bad solvent for higher molecular weight samples. The measurements were always done at a polymer concentration of about 2 g./100 g.

The instrument used was a Beckman Model DU Quartz Spectrophotometer. Matched quartz cells were used. The compartment for the cells was thermostated at 20 °C. by circulating water. Cell corrections were determined before each measuring series and over the whole wave-length region to be used. To secure a complete dissolution of the polymer the solutions were made one day in advance.

b. Sources of Error

1. Losses due to Scattering

The scattering power of a solution increases with the molecular weight of the solute, with the frequency of the incident light, and with the amount of solute (*cf.* MARK (175)). At the rather high concentration and the low wave-length used it is to be expected that the losses due to scattering are noticeable. The turbidity, τ, defined by $I = I_0 \exp(-\tau l)$ is determined from $\tau = HMc$ (second order terms in concentration neglected) where $H = 32\pi^3\gamma^2 n^2/(3N_0\lambda^4)$ ($\gamma = \mathrm{d}n/\mathrm{d}c$, n = refractive index of solvent, N_0 = Avogadro's number). $\gamma = 10^{-3}\,100$ g./g.; $n = 1.5$ and $\lambda = 250\,\mathrm{m}\mu$ give $H = 3 \cdot 10^{-9}$. Then at $c = 2$ g./100 g. $\tau > 0.006$ when $M > 10^6$.

2. Presence of Stray Light

The presence of stray light will introduce an error in the determined optical densities. These can be larger or smaller than the true value, depending upon the absorption properties of the medium. The influence of stray radiation is greatest in those regions of the spectrum where the emission from the light-source is weak; with the present instrument between 200–230 mμ, as has been pointed out by HOLIDAY and BEAVEN (176) and by SAIDEL, GOLDFARB and KALT (177). An indirect test that stray radiation does not disturb the measurements is the validity of Beer's law. Therefore density measurements were made on the two unfractionated samples P2b6 and P2c1. The results are given in Figures 42 and 43. On P2b6 two series of measurements were done (the full drawn and dashed lines in Figure 42). In Tables 22 and 23 an analysis of the measured data by means of the method of least squares has been done. The concentration is expressed in g./100 g. and the specific extinction coefficients are given in cm.$^{-1}$. In Table 22 the two series of measurements have

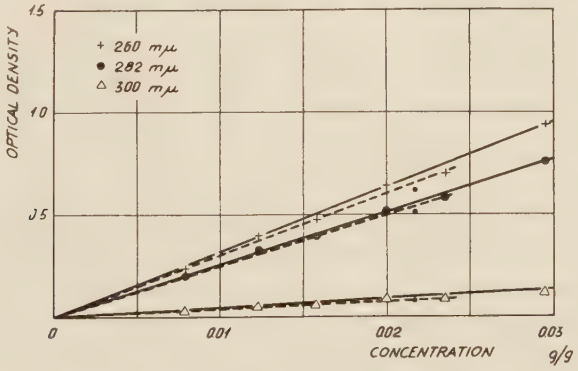

FIGURE 42. Optical density of P2b6 in chloroform at different wave-lengths as a function of concentration.

Table 22

Validity of Beer's law for P2b6

c	D	D^*_{cal}	ΔD^*	D^{**}_{cal}	ΔD^{**}	D_{cal}	ΔD
			λ 260 mμ; $\varepsilon^* = 31.9$; $\varepsilon^{**} = 29.8$; $\varepsilon = 31.1$.				
2.952	0.939	0.941	+ 0.002	—	—	0.918	− 0.018
2.348	0.698	—	—	0.700	+ 0.002	0.730	+ 0.032
1.990	0.637	0.635	− 0.002	—	—	0.619	− 0.018
1.579	0.473	—	—	0.471	− 0.002	0.491	+ 0.018
1.236	0.396	0.394	− 0.002	—	—	0.384	− 0.012
0.790	0.237	—	—	0.235	− 0.002	0.286	+ 0.009
			λ 274 mμ; $\varepsilon^* = 31.2$; $\varepsilon^{**} = 29.7$; $\varepsilon = 30.65$.				
2.952	0.918	0.922	+ 0.004	—	—	0.905	− 0.013
2.348	0.696	—	—	0.698	+ 0.002	0.720	+ 0.024
1.990	0.624	0.621	− 0.003	—	—	0.610	− 0.012
1.579	0.472	—	—	0.469	− 0.003	0.484	+ 0.012
1.236	0.390	0.386	− 0.004	—	—	0.379	− 0.011
0.790	0.235	—		0.235	± 0.000	0.242	+ 0.007
			λ 282 mμ; ε^* 25.7; ε^{**} 24.7; ε - 25.3.				
2.952	0.754	0.759	+ 0.005	—	—	0.747	− 0.007
2.348	0.579	—	—	0.579	± 0.000	0.595	+ 0.016
1.990	0.515	0.512	− 0.003	—	—	0.504	− 0.011
1.579	0.390	—	—	0.390	± 0.000	0.400	+ 0.010
1.236	0.324	0.318	− 0.006	—	—	0.313	− 0.011
0.790	0.195	—	—	0.195	± 0.000	0.200	+ 0.005
			λ 300 mμ; $\varepsilon^* = 4.1$; $\varepsilon^{**} = 3.7$; $\varepsilon = 3.95$.				
2.952	0.120	0.122	+ 0.002	—	—	0.117	− 0.003
2.348	0.085	—	—	0.086	+ 0.001	0.092	+ 0.007
1.990	0.083	0.082	− 0.001	—	—	0.079	− 0.004
1.579	0.059	—	—	0.058	0.001	0.062	+ 0.003
1.236	0.054	0.051	− 0.003	—	—	0.049	− 0.005
0.790	0.029			0.029	+ 0.000	0.031	+ 0.002

been treated both separately (ε^*, ε^{**}) and as a whole (ε). From the ε-values, D-values have been calculated. The comparison of these with the measured values gives strong evidence for the validity of Beer's law within each series (ΔD^* and ΔD^{**}). The deviations, ΔD, are much larger than could be expected with respect to the variance in the density readings.[1] For P2c1 the ΔD-values in Table 23 are higher. For the

[1] A reasonable explanation of the systematic differences between the two series was not found. In the discussion of the results the corresponding uncertainty of the ε-values was kept in mind.

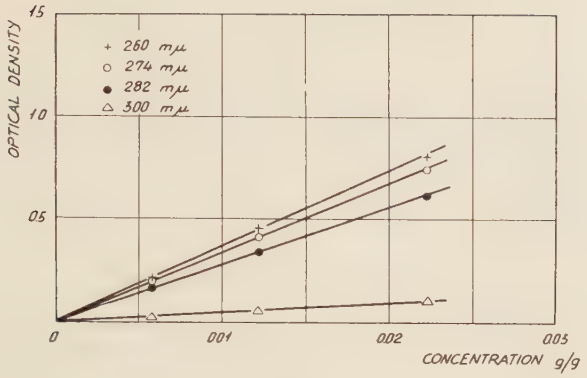

FIGURE 43. Optical density of P2c1 in chloroform at different wave-lengths as a function of concentration.

purpose of the present work, however, the deviations can be tolerated. It should be pointed out that at wave-lengths lower than 250 mμ the deviations from Beer's law were considerable.

TABLE 23

Validity of Beer's law for P2c1

c	D	D_{cal}	ΔD
	λ 260 mμ; $\varepsilon = 36.8$.		
2.220	0.810	0.817	+0.007
1.215	0.459	0.447	−0.012
0.578	0.217	0.213	−0.004
	λ 274 mμ; $\varepsilon = 33.7$.		
2.220	0.744	0.749	+0.005
1.215	0.417	0.410	−0.007
0.578	0.200	0.195	−0.005
	λ 282 mμ; $\varepsilon = 27.7$.		
2.220	0.613	0.616	+0.003
1.215	0.341	0.337	−0.004
0.578	0.164	0.160	−0.004
	λ 300 mμ; $\varepsilon = 4.6$.		
2.220	0.102	0.103	+0.001
1.215	0.058	0.056	−0.002
0.578	0.027	0.027	±0.000

3. Influence of Finite Wave Band

It was pointed out on p. 73 that the light bundles emerging from a dispersing instrument were not completely monochromatic. Further, the detecting system had different sensitivity for different wave-lengths. Consequently the measured density does not give the true density for the nominal wave-length (*cf.* Lothian (178)). No corrections were applied for this effect. In order to make all measurements comparable the same slit width was used in each series.

4. Other Influences

A lot of other factors can influence the measurements, as has been pointed out by Caster (179). As far as possible all influences of this kind were minimized.

c. Results

1. Benzoyl Peroxide and Methyl Methacrylate

The optical densities of benzoyl peroxide and methyl methacrylate measured in chloroform at different concentrations as function of the wave-length in the region 250–310 mμ are given in Figures 44 and 45. As in isooctane solution, benzoyl peroxide has two small maxima also in chloroform solution (the large maximum cannot be studied owing to the low transparency of chloroform below 245 mμ). The wave-lengths are 282.5 and 275.5 mμ compared to 282 and 274.5 mμ in isooctane. In chloroform the maximum at 282 mμ is not so well resolved as in isooctane. The

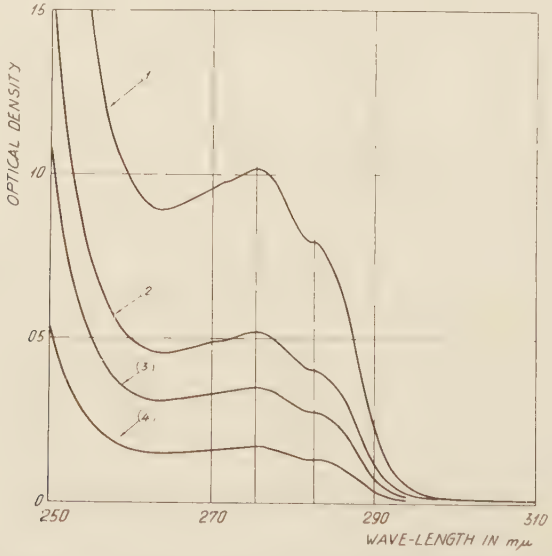

Figure 44. Optical density of benzoyl peroxide in chloroform at different concentrations as a function of wave-length. 1) 0.06705 mg./g.; 2) 0.03384 mg./g.; 3) 0.02287 mg./g.; 4) 0.01124 mg./g.

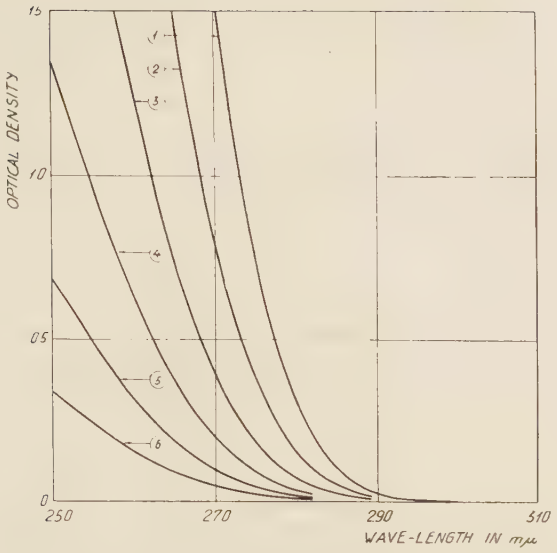

FIGURE 45. Optical density of methyl methacrylate in chloroform at different concentrations as a function of wave-length. 1) 7.361 mg./g; 2) 3.677 mg./g.; 3) 1.832 mg./g.; 4) 0.916 mg./g.; 5) 0.458 mg./g.; 6) 0.229 mg./g.

spectrum obtained in isooctane contains a flat maximum at 269 mμ, whose existence in the chloroform solution is doubtful. Methyl methacrylate does not show any absorption maxima in the measured region. GOODEVE (180) has done measurements down to 210 mμ and found a flat niveau at 240 mμ. She ascribes the absorption to the conjugation of the double bonds.

2. Unfractionated Samples

In Figure 46 the specific extinction coefficients (expressed in $cm.^{-1}$) of samples P2a1, P2b6 and P2c1 are plotted as a function of the wave-length between 250 and 310 mμ. The dotted curve is the values found for fraction P2d1TIa. The curves for P2b6 and P2c1 have maxima at 281.5, 274.5, 269 and 265 mμ. The curves for P2a1 and P2d1TIa do not show any pronounced maxima, but at 280 and 274 mμ they show a tendency to flatten out.

3. Fractionated Samples

Only fractions from the preparations P2a1 and P2b6 were investigated. The variation of the specific extinction coefficient with the wave-length is shown in Figures 47 and 48 respectively. The curves for P2a1-fractions do not give a completely true picture of the variation because most of the samples were found to contain

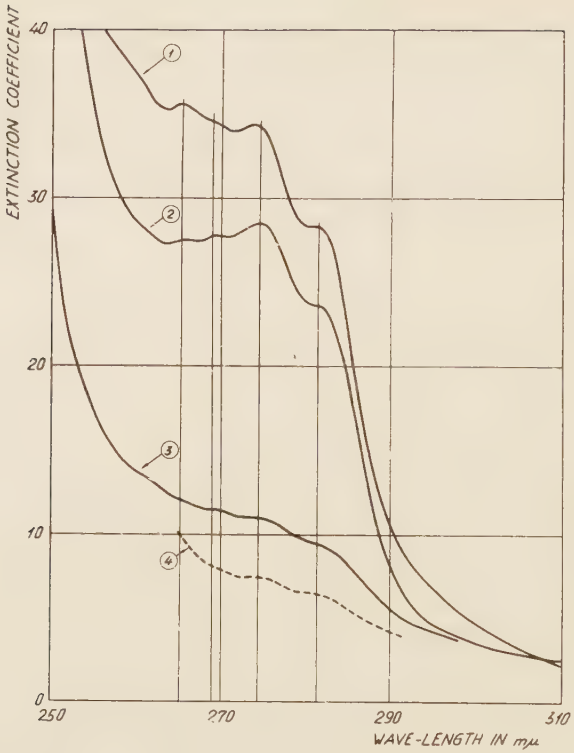

FIGURE 46. Specific extinction coefficient of polymethyl methacrylates in chloroform as a function of wave-length. 1) P2c1; 2) P2b6; 3) P2a1; 4) P2d1TIa.

minute amounts of benzene, about 1 pro mille. This means that the true extinction coefficients are a few per cent higher in the region 270–290 mμ. The curves in Figure 48 show the same maxima as Nos. 1 and 2 of Figure 46.

C. Discussion

The results obtained appear to be rather interesting. It must be remembered, however, that the differences between the curves could depend upon various amounts of benzoyl peroxide adsorbed on the macromolecules. Especially for P2b6 and the fraction P2b6HI with the highest molecular weight there is a great chance for adsorption. Two benzoate groups on each of these molecules correspond to 0.08 and 0.03 per cent benzoyl peroxide respectively. In the polymerization of polymer P2b five per cent benzoyl peroxide was used. However, the fairly high molecular weight shows that only a minute amount has been used up for the polymerization reaction. The main part of the peroxide is either unchanged or has been decomposed. Probably some of it has dissolved in the water phase as benzoic acid. It seems reasonable to assume that 25 per cent of the original peroxide contaminate the polymer in

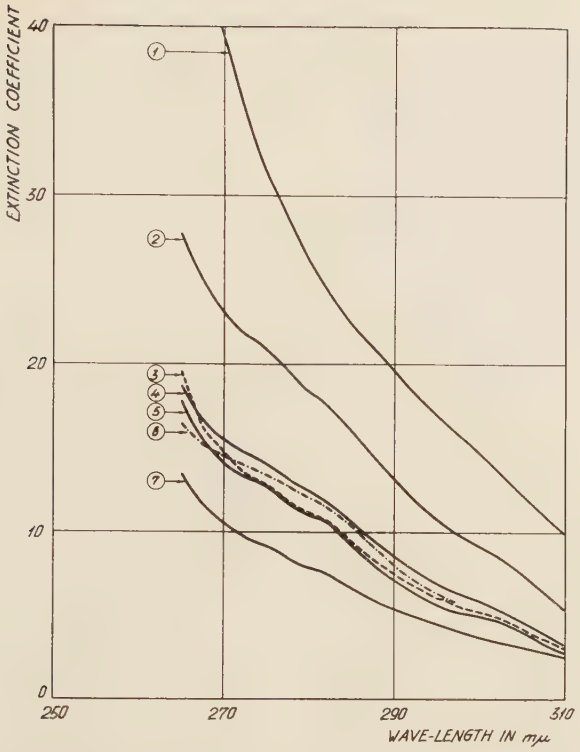

FIGURE 47. Specific extinction coefficient of P2a1-fractions in chloroform as a function of wavelength. 1) P2a1GIV; 2) P2a1GV; 3) P2a1SI; 4) P2a1SIV; 5) P2a1GII; 6) P2a1SVI; 7) P2a1GIII.

the form of pure peroxide or its decomposition products. The long extraction with methanol was estimated to remove at least 90 per cent of the contamination. Then the polymer was cleansed by dissolution in benzene and precipitation with cyclohexane and the precipitate thoroughly washed with cyclohexane. According to KERN and KÄMMERER (164) the adsorbed amount of peroxide decreases to about one third for each reprecipitation. Thus the amount of benzoyl peroxide and its decomposition products is for P2b6 estimated to be less than 0.04 per cent. For the fraction P2b6HI the amount is about three quarters of that of the starting material (KERN and KÄMMERER). Then the fraction is reprecipitated. Thus it will contain less than 0.01 per cent. The content of dissolvable materials in P2b6HI was checked through extraction with *n*-hexane in a Soxhlet apparatus for 12 h.; this decreased the specific extinction coefficient about five per cent. No weighable amounts of extract were obtained.

This consideration shows that the original material and the first fractions may contain some absorbing materials adsorbed by the molecules. The amount is, however, not too large to make a discussion irrelevant.

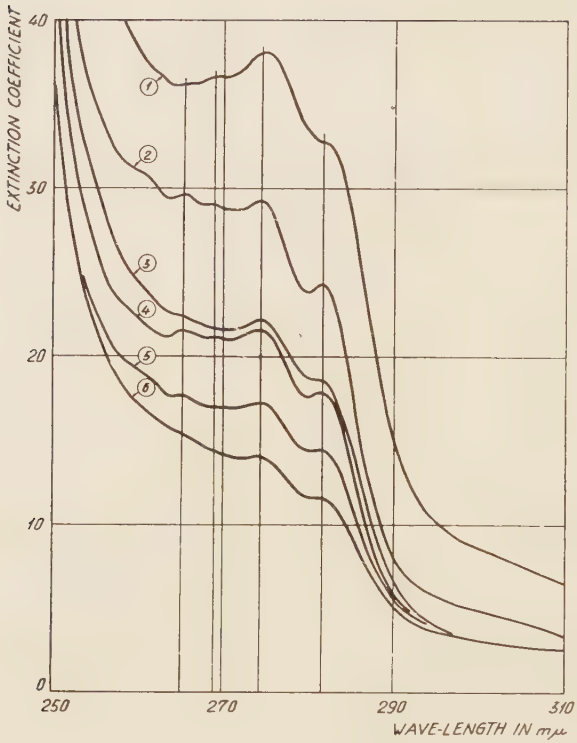

FIGURE 48. Specific extinction coefficient of P2b6-fractions in chloroform as a function of wavelength. 1) P2b6HI; 2) P2b6LII; 3) P2b6HIV; 4) P2b6HV; 5) P2b6LI; 6) P2b6HII.

There are strong evidences for a difference in structure between samples P2b6 and P2c1 and sample P2a1. With the initiator (azo dimethyl isobutyrate) used for P2a1 the ends of the molecules would consist of methyl isobutyrate groups

$((CH_3)_2 \cdot \overset{|}{C} \cdot CO \cdot O \cdot CH_3)$. These have no absorption in the region investigated as checked with methyl isobutyrate. On the other hand the presence of chain transfer agents may give end groups having some absorption. A comparison of the spectrum of P2b6 and its fractions and P2c1 with the spectra of compounds containing benzoate groups reveals striking similarities as is demonstrated in Table 24. The maxima at 275 and 282 mμ are common for all compounds. The other maxima do not occur regularly in benzoates. They may be attributed to the existence of phenyl groups in the macromolecules. The absorption of such groups would be similar to that of alkyl benzenes presupposed that there is no interaction between the π-electrons of the benzene rings and of the carbonyl bond. The separation between the two π-electron systems is two or three σ-bonds depending upon the arrangement in the chain. According to SCHEIBE and FAUSS (181) this gives a sufficient isolation. Alkyl ben-

Table 24

Comparison of ultraviolet spectra of benzoate compounds and benzoyl peroxide polymerized polymethyl methacrylates

Compound, solvent	Wave-length, at absorption maxima (mμ)			
P2c1 (chloroform)	281.5	274.5	269	265
P2b6 (chloroform)	281.5	274.5	269	265
P2b6HI (chloroform)	281.5	274.5	269	265
P2b6HII (chloroform)	281.5	274.5	—	—
P2b6HIV (chloroform)	281.5	274.5	—	?
P2b6HV (chloroform)	281.5	274.5	269	265
P2b6LI (chloroform)	281.5	274.5	269	265
P2b6LII (chloroform)	281.5	274.5	269	265
Benzoyl Peroxide (chloroform)	282.5	275.5	—	—
Benzoyl Peroxide (isooctane)	282	274.5	269	- -
Benzoic Acid (isooctane)	283	275	—	266(?)
Benzoic Acid (methanol)	280	272	—	267
Benzoic Acid (chloroform)	282	274	?	?
Ethyl Benzoate (isooctane)	280	273	267	264
Ethyl Benzoate (chloroform)	282	274	—	267
Phenyl Benzoate (isooctane)	282	274	—	—

zenes have a fairly strong absorption in this region with absorption maxima at 258–260, 262, 264–265, 268–269 mμ (182).

The absorption of thermally polymerized methyl methacrylate has been studied by Goodeve (180). She found an increase in absorption with decreasing wave-length. The polymer was, however, more transparent in the far ultraviolet than the monomer. The absorption can be attributed to the carboxyl groups and to a possible, conjugated end group:

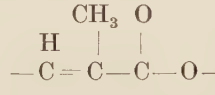

The order of magnitude of this absorption is illustrated by sample P2d1TIa (curve No. 4 in Figure 46). This polymer has a molecular weight higher than 4000000. The presence of two benzoate end groups would give a specific extinction coefficient of 0.5–1 at 275 mμ. The measured value is about 7.5.

In Table 25, data on the investigated samples are collected. The molecular weights have been calculated from the limiting viscosity numbers (p. 100) using the relation $[\eta] = 4.85 \cdot 10^{-5} M^{0.80}$ (*cf.* Meyerhoff and Schulz (183) and Bischoff and Desreux (184)). If the absorption of a polymer molecule is due to the whole molecular chain, the specific extinction coefficient would be independent of the degree of polymeriza-

Table 25

Viscosity and ultraviolet data for samples P2a1 and P2b6

Sample	Molecular weight, M	k'	ε_{tot} λ 274.5 mμ	$M(\varepsilon_{tot}-\varepsilon_A)$ $\times 10^{-5}$	$\bar{j}_n$
P2b6	300000	0.351	28.5	—	5.3
P2b6 HI	790000	0.341	38.1	246	20
HII	500000	0.334	14.1	35.5	2.9
HIV	210000	0.378	22.2	31.9	2.6
LI	180000	0.364	17.3	18.5	1.5
HV	115000	0.401	21.6	16.8	1.4
LII	72000	0.560	29.3	16.1	1.3
P2a1	155000	0.373	11.0	—	—
P2a1 GII	475000	0.338	12.8	27.6	—
GIII	240000	0.358	9.3	5.5	—
SI	225000	0.411	12.9	13.3	—
GIV	150000	0.397	31.9	37.3	—
GV	84500	0.417	21.1	11.9	—
SIV	74000	0.495	14.3	5.4	
SVI	21000	0.636	13.5	1.4	—

tion. From Table 25 it is evident that for both samples ε_{tot} varies with the molecular weight. Hence the absorption must to a large extent be determined from the amount of end groups. For sample P2b6 the number, $\bar{j}_n$, of these groups has been calculated from Equation (135) using $\varepsilon_A = 7$, $\varepsilon_B = 10000$ and $M_B = 121$ (ε_B is estimated from data in ref. (173): in chloroform solution benzoic acid has $\varepsilon = 12000$, ethyl benzoate $\varepsilon = 9250$; from the measurements here benzoyl peroxide in chloroform has $\varepsilon = 15700$). The figures are quite reasonable except for the high value on fraction HI. This, however, may be due to the possible adsorption of benzoyl peroxide. The fractions LI, HV and LII with low $\bar{j}_n$-values have the maxima at 265 and 269 mμ most welldefined. For sample P2a1 only the quantity $M(\varepsilon_{tot} - \varepsilon_A)$ has been calculated. This is proportional to the number of end groups. The values obtained vary much more than for sample P2b6.

In Table 25 the constant k' is also given. It has been found (*cf.* Ewart (185) and Manson and Cragg (185 a)) that k' has a value of 0.38 for linear polymers in good solvents. Chloroform is an excellent solvent for polymethyl methacrylate. The k'-values found are less than 0.38 for fractions with a high molecular weight and higher then 0.38 for low molecular weight fractions. A comparison between the k'-values and $M(\varepsilon_{tot} - \varepsilon_A)$ as a measure of the number of branches in the chains shows for P2b6 that the k'-value can increase without a corresponding change in branching. On the other hand, for the last fractions of P2a1 k' increases when the

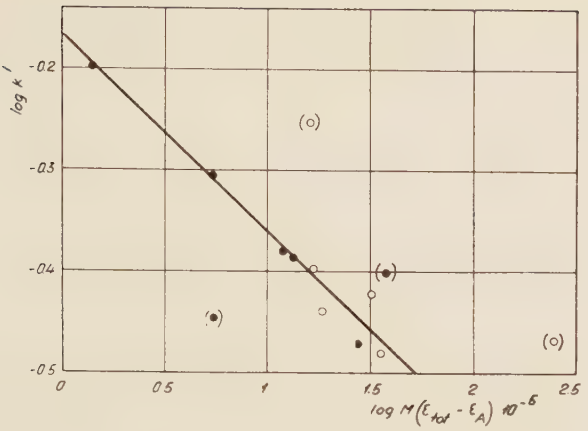

FIGURE 49. Relation between k' and $M(\varepsilon_{tot}-\varepsilon_A)$ for different fractions: P2a1 ●; P2b6 ○.

number of branches decreases. If the values for fractions P2b6HI and LII, P2c1GIII and GIV are deleted, the remaining nine values fit fairly well into a relationship of the form (Figure 49):

$$k' \approx \left(\frac{1}{j_n}\right)^{\frac{1}{5}} \tag{136}$$

A judgement about the real value of these findings cannot be given on the basis of the present data.

Chapter 5

Some Infra Red Measurements

In the previous chapter it has been shown that the end groups of a high polymer molecule have a characteristic ultraviolet absorption. This shows that the end groups have a structure different from that of the repeating unit of the molecular chain. Information about the structure of these groups can also be obtained by means of measurements in the infrared. An investigation of polymethyl methacrylates in this spectral region is also of interest with respect to the previous study of the raman spectra of the polymer and its monomer.

Previous Work

Infrared absorption has been used in connection with raman measurements to elucidate the structure of a large number of small molecules (*cf.* Herzberg (155, 157)). An increased number of atoms in the molecules will render complete structural assignments more difficult. For poly-atomic molecules, therefore, the infrared technique has become more chemical in nature: investigations on a large number of compounds having some particular atomic groupings in common have shown that certain of the infrared vibrations do not change very much between different compounds. These bond-frequencies (*v. supra*) are used for structural diagnosis work. In this way the infrared technique can be applied even to high polymer chemistry (*cf.* Thompson (186, 187) and Sutherland (188)). A review of some of the investigations made on high polymer problems is given below. None of these is particularly concerned with the problems which will be discussed in this chapter but it was thought of value to give some hints about the general trends in this rather new field. Reviews of general work in infrared spectroscopy done during the last years may be found in papers by Gore (189–191), by Barnes and Gore (192) and in the monograph by Barnes, Gore, Liddel and Williams (193).

One of the first successful applications of the infrared technique to structural problems in high polymer chemistry was the observation by Fox and Martin (194) that the bands of the spectrum of polythene in the region of 3 μ indicated the presence of methyl groups in the polyethylene chain. Independent confirmation was later provided by Thompson

and Torkington (195, 196) who observed a band at 1375 cm.$^{-1}$ characteristic of symmetrical deformation vibrations in a methyl group. They were also able to estimate the number of methyl groups to one per fifty methylene groups. Another new feature of the polythene molecule revealed by its infrared spectrum was the presence of C=O groups (shown by a weak absorption at 1720 cm.$^{-1}$). A comprehensive study of the structure of ethylene polymers has recently been made by Cross, Richards and Willis (197) who have determined the number of methyl groups, the type and amount of unsaturation and the nature and quantity of oxygen containing groups. — The paper by Thompson and Torkington (196) contains structural studies of many other polymers, both of the vinyl and diene type. Spectra of polyamides, polyesters, condensation polymers from phenol and formaldehyde, and of cellulose derivatives have also been discussed (Thompson and Torkington (195)). These investigators have also studied spectra of polymers containing chlorine, *e.g.* polyvinyl chloride, polyvinylidene chloride, halothene and neoprene (Thompson and Torkington (198)).

The possibility of adopting infrared spectroscopy to reveal the structure of natural and synthetic rubbers is often used to advantage. Williams (199) in 1936 studied natural rubber between 1 and 15 μ and found a striking resemblance between its spectrum and that of isoprene. He also investigated polybutadiene and rubber hydrochloride. Later Williams and Dale (200) found that linear extension of rubber to high elongations increases the frequency of C—C vibrations. Barnes *et al.* (201, 202) in 1943 and 1944 made important contributions to the application of the infrared technique to analytical problems in rubber chemistry. Similar methods were later used by Dinsmore and Smith (203) and by Saunders and Smith (204). The latter authors have studied several elastomers and found that a classification can be done in hevea and gutta types, probably related to *cis-* and *trans*-polyisoprenes respectively. Some changes in carbon–carbon double bond frequencies and in CH_3 bending vibrations produced by the chlorination of natural rubber have been revealed by Salomon, van der Schee, Ketelaar and van Eyk (205). Spectral changes during crystallization of neoprenes have been discussed by Mochel and Hall (206). They stress the importance of these changes because of their relation to the order in the polymer. Finally it may be mentioned that Thompson and Torkington (207) have studied the vibrational spectrum of perbunan.

An analytical problem, closely related to the production of synthetic rubbers, is the determination of the amount of 1,2- and 1,4-structures in addition polymerizates of butadiene. The quantitative estimation is based on different absorption properties of molecules having the structures CH_2—CHR and R_1CH=CHR_2. Work along such lines has been done by Hart and Meyer (208), Hampton (209), Treumann and Wall (210), and Burgova and Korotkov (211) (*cf.* also Thompson and Torkington (195)).

The vulcanization of natural rubber with sulphur has been investigated by Sheppard and Sutherland (212). They state that two new bands appear, namely at 10.4 μ and 17 μ. The latter is tentatively assigned to C—S vibrations. No appreciable changes occur in the 6 μ C=C bond frequency. Soft and hard vulcanized rubber has been studied by Sears (213) and the presence of accelerators and antioxidants in rubber by Mann (214).

During the last few years the phenomenon of infrared pleochroism has been found of great value in elucidating molecular structures. Thus Glatt and Ellis (215–219) have studied polythene, nylon, polyvinyl alcohol, polyvinyl chloride and polyvinylidene chloride by using polarized infrared radiation. Similar studies have been made by Elliot, Ambrose and Temple (220) and by Thompson and Torkington (196). Sutherland and Jones (221) have measured dichroic ratios of bands in the spectra of rubber and α- and β-gutta-percha.

Spectra of polythene, rubber, polystyrene and polyvinyl chloride at 4 °K. have been recorded by King, Hainer and McMahon (222). Some sharpening and improvement in resolution was observed.

Finally it can be mentioned that the infrared transmission of thin films of various polymers has been measured by Wells (223). Spectra of carbohydrates and amino acids are discussed by Thompson, Nicholson, and Short (224). Magat, Chandler, Faris, Reith, and Salisbury (225) have found that polyamides from dinitriles and formaldehyde contain several branches with C≡N end groups. The degradation of polystyrene, induced by ultraviolet irradiation and heat treatment, has been followed by Achhammer, Reiney, and Reinhart (226). Nuclear-methylated styrenes and their polymers have been studied by Bryant, Kennedy, and Tanner (227). An infrared investigation of arcylic fibers has been made by Houtz (228). Analysis of softeners in polyvinyl chloride has been performed by Haslam, Soppet, and Willis (229). Hausdorff (230) has presented spectra of some vinyl polymers and softeners. The polymerization of styrene in the presence of drying oils has been studied by Kronstein (231) and by Bezman and Browning (232).

A work of considerable importance in the interpretation of infrared (and raman) spectra of high polymers has recently been made by Kellner (233, 234) and Barrow (235). They have calculated the frequencies for the fundamental vibrations of an infinite *n*-paraffin chain and found a very good coincidence between the theoretical values and those determined experimentally for polythene. Kellner states that a polythene of molecular weight 7000 still has the properties of a "finite" molecule. At 13000 the periodic structure is fully established.

Present Work

A. General Considerations

In the search for non-recurring structures in polymer chains a comparison is made between spectra from samples of very high and low molecular weight respectively. The former has such a large number of recurring units that absorption bands from end groups *etc.* are not detectable. This, of course, presupposes that the polymers belong to the same homologous series. Thompson and Torkington (195, 196) found no significant differences in the bond-frequencies of polyisobutenes having molecular weights between 1000 and 100000. The same was true of polythenes of molecular weight 1000 and higher. Therefore, differences only in the intensities of the bands are to be expected. The study of end groups in polyisobutene made by Dainton and Sutherland (169) was made on a polymer having a degree of polymerization of only 10 (molecular weight less than 600). (It may be mentioned that Thompson (187) has obtained results on normal paraffins, showing that the intensity of a band at 725 cm.$^{-1}$ depends upon the length of the hydrocarbon chain; thus, accurate measurements on this band might possibly give the molecular weights of lower polythenes.)

In the present case, an investigation has been made on certain polymers having a high molecular weight to establish the general features of their spectra between 1 and 15 μ. These spectra have then been compared with those obtained from fractions of polymers having a very low molecular weight. As already discussed in Chapter 4, the end groups of interest in this work are those originating from the splitting of benzoyl peroxide into benzoate or phenyl groups. A comparison has therefore been made with spectra of compounds containing these groups, *i.e.* various benzoates and benzene homologues.

B. Experimental Work

a. Experimental Technique

The preparation and purification of the samples used have been described in Chapter 2. Measurements were made on polymer samples P2a1, P2c1, P2d1TIa, P2a1SVI and P2c1AVIII. Further methyl-, ethyl- and phenyl benzoate, and benzoyl peroxide were studied. Some runs were also made on methyl methacrylate and methyl isobutyrate. The measurements were made both in solution and on films. Freshly distilled acetone and chloroform were used as a solvent for the polymers. The benzoates, benzoyl peroxide, methyl methacrylate and methyl isobutyrate were investigated in carbon tetrachloride or carbon disulphide solutions. The films were prepared from chloroform and *o*-dichlorobenzene (*cf.* Hausdorff (230)) solutions by evaporating the solvent from a rock-salt plate. The evaporation of *o*-dichlorobenzene was followed at the 9.7 μ band. Heating at 150–170 °C. for 1–2 h. was necessary to remove the solvent. The average thickness of the films was determined by weighing.

The instrument used was a Beckman Infra Red Spectrophotometer IR-2 with a rock-salt prism covering the range 1 to 15 μ. The instrument has facilities for direct recording of the spectra or for manual transmission (and optical density) readings. The latter procedure was mainly employed. Measurements were done at every 0.01 or 0.02 μ. The films were measured with air as the reference; for solutions the reference was the solvent in a layer of the same thickness (0.1 mm.). The slit widths used were the following: 1 μ/0.1 mm., 1.36/0.05, 3.00/0.10, 4.00/0.15, 5.99/0.20, 7.30/0.25, 7.51/0.30, 8.11/0.35, 9.93/0.45, 10.63/0.55, 12.00/0.80, 13.10/0.90, 13.50/1.10, 14.01/1.50, and 14.50/2.00. The calibration of the wave-length scale was made with benzene using the bands 2.45, 2.71, 3.26, 5.10, 5.51, 8.50, 9.65, 11.76 and 12.90 μ (Ref. (236)).

The instrument had to be warmed up for at least three hours before the readings on the wave-length scale gave true values. The wave-lengths given in the following are accurate to 0.02 μ. (It may be mentioned that Plyer and Peters (237) have determined the wave-lengths of certain absorption bands of polystyrene, 1,2,4-

trichlorobenzene, toluene and methylcyclohexane for calibration purposes. These determinations were made in a grating instrument and are therefore much more accurate than the benzene bands given above.) The wave-length calibration was between whiles checked at the carbon dioxide bands at 4.22 μ and 13.89 μ.

In order to avoid the appearance of foreign bands great care was always taken to remove traces of substance and solvent from the liquid absorption cells. Before filling the cells with new substance and/or solvent they were always checked for absorption bands originating from the previous fillings. The solvents were also checked for evaporation residues.

b. Sources of Error

The various sources of error which may influence measurements of optical density are 1) stray light; 2) uncertainty of radiation measurements; 3) mismatch of absorption cells, and 4) non-linearity of the measuring system (*cf.* MARTIN (238)). As the optical densities were not of primary interest no special precautions were taken to eliminate errors of this kind.

c. Results

1. Polymers of High Molecular Weight

The spectra obtained on films of the polymers P2a1, P2c1 and P2d1TIa having the molecular weights 155000, 120000 and 4000000 respectively are given in Figure 50. All films were made from solutions in chloroform with the exception of the one corresponding to the full-drawn curve of P2c1. This was made from *o*-dichlorobenzene. When making the films from chloroform solutions the necessity of prolonged heating to remove the last residues of the solvent had not been realized. Therefore the 13.3 μ band in these cases to a considerable extent consists of the very strong 13.2 μ band of chloroform. None of the other absorption bands of chloroform interfere with the polymer spectrum. No significant differences have been found between the spectra from the various polymers. Some parts of the spectra of samples P2a1 and P2c1 were also investigated in acetone and chloroform solutions. Then it appeared that in chloroform the 6.9 μ band was resolveable into the components 6.92 μ and 6.98 μ (Figure 51). A similar resolution of the 7.3 μ band was not possible. The 10.12 μ band showed a tendency to separate in components 10.10 μ and 10.17 μ when the polymers were studied in acetone solutions. Further, it was found that great differences existed between spectra obtained from films and solutions in the region 2.5–3.5 μ as is shown in Figure 52. The absorption band at 2.8 μ increases considerably in intensity. At the same time the intensity of the 3.4 μ band decreases. The effect is most pronounced in acetone solutions. A slight difference may exist between samples P2a1 and P2c1.

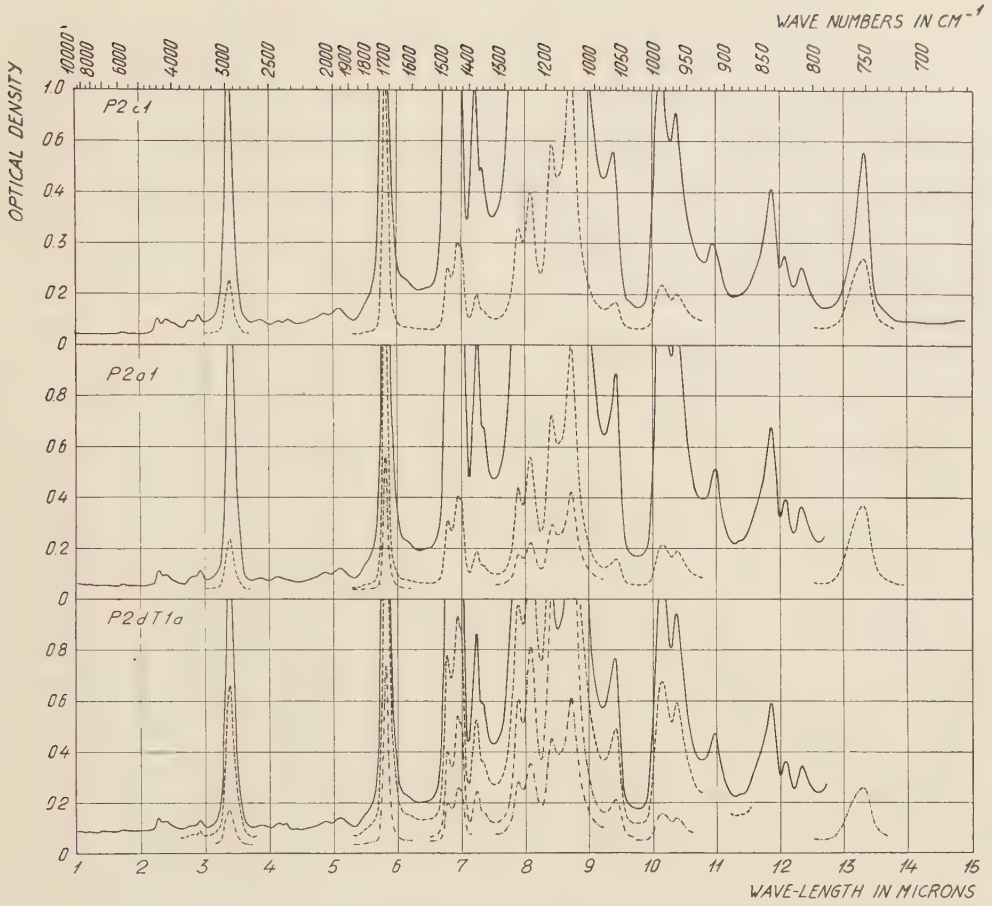

FIGURE 50. Absorption of polymethyl methacrylate films between 1 and 15 μ.
Thickness of films:

P2c1 ———— 50 μ, — — — — 10 μ;
P2a1 ———— 50 μ, — — — — 10 μ, — · — · — 5 μ;
P2d1TIa ———— 50 μ, — — — — 25 μ, — · — · — 15 μ, — · · — · · — 7 μ.

2. Polymers of Low Molecular Weight

The spectra of the two fractions P2a1SVI and P2c1AVIII were recorded between 1 and 15 μ. The first sample has a molecular weight of 21000 (Table 25). The second one was not investigated in this respect. P2c1AVIII, however, is that fraction of P2c1 which probably has the lowest molecular weight; it may be estimated to less than 20000. The films were made from *o*-dichlorobenzene solutions and had a thickness of about 25 μ. No traces of solvent could be found after the evaporation. In the region 1–13 μ the spectra were completely identical with those given in Figure

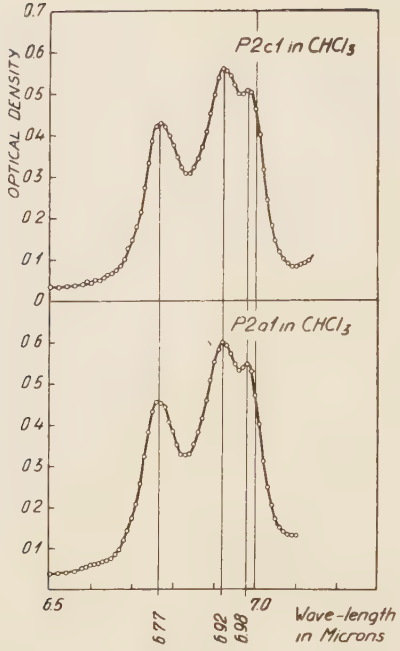

FIGURE 51. Optical density of polymethyl methacrylates in chloroform as a function of wave-length in the region 6.5–7.3 μ.

FIGURE 52. Optical density of polymethyl methacrylates in different solvents as a function of wave-length between 2 and 4 μ. I: 50 μ film; II: solution in chloroform; III: solution in acetone.

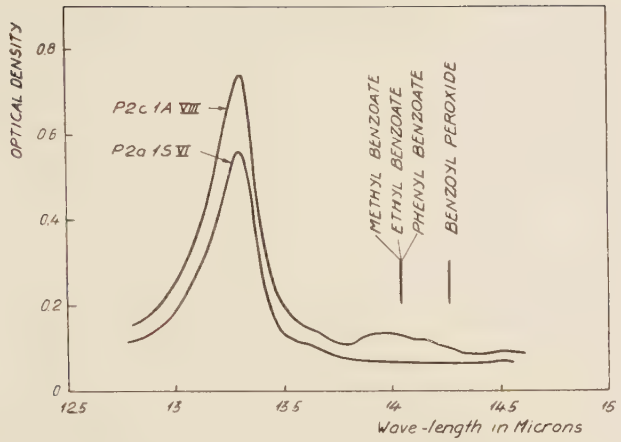

FIGURE 53. Comparison of fractions P2a1SVI and P2c1AVIII at the 13.3 μ absorption band.

50. The 13.3 μ bands correspond to that of P2c1. At 13.96 μ the spectrum of P2c1AVIII has a broad absorption band, not present in the spectrum of P2a1SVI (Figure 53). It was uncertain as to what extent changes could be produced in the polymers during the long heating of the samples at high temperature to remove the solvent. Therefore sample P2c1AVIII was heated at 150–170 °C. for several hours. No changes in the spectrum could be found. The strongest absorption band of the benzoates was localized to 14.05 μ and that of benzoyl peroxide to 14.25 μ. The optical densities of the bands at 13.3 μ are 0.5 and 0.7 for P2a1SVI and P2c1AVIII respectively compared to 0.6 for P2c1 in a layer twice as thick. This is an indication that the intensity of this band depends upon the molecular weight of the samples. A further study of this phenomenon had to be postponed.

C. Discussion

The wave-length and the corresponding wave number of the absorption bands of polymethyl methacrylates are collected in Table 26. There are also given the raman shifts (from Table 18 and the works of HIBBEN (132) and MONNIER (134)) and estimations of the intensities of the lines (*w* weak, *m* medium, *s* strong, *v* very). In the region 4.5–14 μ the infrared bands correspond to those given by THOMPSON and TORKINGTON (195) with the following exceptions: they do not report two components at 6.9 μ, and the very weak line at 11.34 μ, they have two very weak lines at 9.7 μ and 12.9 μ, and a weak line at 14.3 μ. In the region <4.5 μ the lines at 3.3 μ are common. THOMPSON and TORKINGTON have not made any measurements below 3.25 μ.

A thorough interpretation of the spectrum cannot be made. Only a few remarks complementary to the discussion in Chapter 3 will be given.

TABLE 26

Infrared and raman lines of polymethyl methacrylate

Infrared		Raman	Infrared		Raman	Infrared		Raman
μ	cm.$^{-1}$	cm.$^{-1}$	μ	cm.$^{-1}$	cm.$^{-1}$	μ	cm.$^{-1}$	cm.$^{-1}$
—	—	221 (v.w.)	8.69	1151 (v.s.)	1123 (m.)	4.12	2427 (v.w.)	—
—	—	291 (v.w.)	8.39	1192 (v.s.)	1178 (m.)	3.88	2577 (v.w.)	—
—	—	363 (w.)	8.06	1241 (s.)	1227 (m.)	—	—	2860 (m.)
—	—	484 (w.)	7.87	1270 (s.)	—	3.37	2967 (s.)	2947 (v.s.)
—	—	594 (m.)	7.32	1366 (m.)	1325 (w.)	3.32	3012 (s.)	3005 (w.)
13.38	747 (s.)	—	7.22	1385 (m.)	1379 (m.)	—	—	3127 (s.)
12.32	812 (m.)	805 (s.)	6.98	1435 (s.)	—	2.90	3448 (w.)	—
12.06	829 (m.)	—	6.92	1445 (s.)	1447 (v.s.)	2.79	3584 (w.)	—
11.84	845 (m.)	—	6.77	1479 (s.)	—	2.37	4219 (w.)	—
11.34	882 (v.w.)	—	6.14	1629 (v.w.)	1628 (v.w.)	2.27	4405 (w.)	—
10.95	913 (m.)	910 (m.)	5.80	1724 (v.s.)	1726 (m.)	1.70?	5882 (v.w.)	—
10.35	966 (s.)	969 (s.)	5.09	1965 (w.)	—	1.38?	7246 (v.w.)	—
10.12	988 (s.)	990 (m.)	4.87	2053 (w.)				
9.40	1064 (m.)	1060 (v.w.)	4.25	2353 (v.w.)				

The 1724 cm.$^{-1}$ band is ascribed to bond-stretching vibrations in the carbonyl group but also symmetrical stretching vibrations of the adjacent C—C and C—O groups may contribute (*cf.* FRANCIS (239)). The weak band at 3448 cm.$^{-1}$ is the first overtone band of 1724 cm.$^{-1}$.

The bands in the region 1151–1270 cm.$^{-1}$ are probably connected to vibrations in the ester groups in accordance with a suggestion by THOMPSON and TORKINGTON (240) who have found that esters of fatty acids have very characteristic bands around 1200 cm.$^{-1}$. The strongest of the present bands are 1151 cm.$^{-1}$ and 1192 cm.$^{-1}$. Methyl isobutyrate (in carbon tetrachloride solution) has an almost identical pair of bands: 1159 cm.$^{-1}$ and 1200 cm.$^{-1}$. Monomeric methyl methacrylate (in carbon tetrachloride solution) has similar bands at 1162 cm.$^{-1}$ and 1197 cm.$^{-1}$ (personal investigations and Ref. (241)). The polymer has two strong bands at 1241 cm.$^{-1}$ and 1270 cm.$^{-1}$ corresponding to one band at 1264 cm.$^{-1}$ in methyl isobutyrate and two bands at 1300 cm.$^{-1}$ and 1322 cm.$^{-1}$ in the monomer. FRANCIS (239) has shown that the bond-stretching vibrations of the carbonyl group is accompanied by an appreciable amount of deformation of the carbonyl bond. The complete vibrational motion associated with the 1200 cm.$^{-1}$ band is then a deformation vibration of the O $C\begin{smallmatrix}O\\C\end{smallmatrix}$ linkage and asymmetrical bond-stretching vibrations of the C –C and C—O groups. The other bands in this region are ascribed by THOMPSON and TORKINGTON to vibrations in the C—O link derived from the alcohol and to

C—C bond vibrations. The displacement of two of the bands in the unsaturated methyl methacrylate may probably be related to the conjugated double bond system.

Another set of bands which occurs in all three compounds is the following:

Polymer	Monomer	Methyl isobutyrate
1366 cm.$^{-1}$	—	1348 cm.$^{-1}$
1385	1375 cm.$^{-1}$	1385
—	1400	—
1435	1440	1435
1445	1450	—
1479	—	1464

These bands are due to vibrations in CH_2 and CH_3 groups. In all compounds there are two kinds of methyl groups, namely, one attached to the α-carbon atom and the other attached to the oxygen atom of the ester linkage. The 1400 cm.$^{-1}$ band of the monomer is ascribed to deformation vibrations of hydrogen atoms in the group $=C\begin{smallmatrix}H\\H\end{smallmatrix}$. The —O—$CH_3$ group has the same position relative to the α-carbon atom in all compounds. Hence its vibrational behaviour ought to be only slightly influenced by structures contiguous to the α-carbon atom. The other methyl group is more exposed to structural changes in its surroundings. Besides the bands at 1348 and 1385 cm.$^{-1}$ in methyl isobutyrate Thompson and Torkington (240) report a band at 1373 cm.$^{-1}$; an assignment of the double band 1373, 85 cm.$^{-1}$ to the two methyl groups on the α-carbon atom may be doubtful, judged from their spectra on isobutyrates. According to Francis (239) esters of fatty acids have bands corresponding to symmetrical deformation vibrations of the methyl groups in the region at 1435–40 cm.$^{-1}$ for —O—CH_3 and around 1375 cm.$^{-1}$ for —C—CH_3. The deformation vibration of CH_2 groups and the doubly degenerate deformation vibration of CH_3 groups are expected in the region 1450 cm.$^{-1}$. The latter will be split since the molecules have low symmetry. Unambiguous assignments cannot be done.

The 3000 cm.$^{-1}$ region corresponds to symmetrical and asymmetrical bond-stretching vibrations of CH, CH_2 and CH_3 groups. These bands could not be resolved with the rock-salt optics used.

Any further discussion of these spectra is not possible on the basis of the present material. Thus, knowledge about the vibrational behaviour of model substances like methyl glutarates and succinates is necessary for a study of skeletal frequencies of the macromolecular chain *etc.*

The observations illustrated in Figure 52 may be taken as an indication that the interaction between solvent and solute in high polymer solutions can be studied in the infrared. The difference between the film and the solutions may correspond to the possibilities of forming intra- and intermolecular hydrogen bonds. In a film,

the molecules, during the drying procedure, will be less movable than in a solution, hence the number of contacts between chains and chain elements will be low and so also the number of hydrogen bonds. When dissolving the polymer in chloroform the mobility of the molecules increases and also their chances of forming hydrogen bonds both intra- and intermolecularly. The hydrogen atom in chloroform may also contribute to the bond formation. When using acetone as the solvent, intramolecular hydrogen bonding may increase due to the denser coiling of the macromolecules in bad solvent. Also, intermolecular bonds may be formed between hydrogen atoms of the macromolecules and the oxygen atoms of the solvent. Further studies of these phenomena had to be postponed.

Finally, the difference between the spectra of fractions P2a1SVI and P2c1AVIII in the region of 14 μ (Figure 53) may show that the polymer P2c1 contains end groups of benzoate character. The possibility that the absorption band should be due to adsorbed benzoyl peroxide seems to be excluded. To what extent, also, phenyl groups may be present in the molecules can be judged from the following absorption maxima of benzene homologues (Ref. (242)):

Toluene		13.74	14.35 μ
n-Propyl benzene	13.49		14.35 μ
Isopropyl benzene	13.17		14.33 μ
n-Butyl benzene	13.43	13.68	14.34 μ
Isobutyl benzene		13.57	14.31 μ
sec-Butyl benzene	13.17	13.67	14.30 μ
tert-Butyl benzene	13.11		14.32 μ
n-Hexyl benzene	13.40	13.75	14.34 μ
n-Octyl benzene	13.5		14.25 μ

All of these bands are very strong. There is no obvious correlation between any of them and the broad band in Figure 53. The two fractions have been prepared in the same way using the same solvents and non-solvents; therefore it seems unlikely that only one of them should contain some impurities. The most probable conclusion is that the absorption maximum at 13.96 μ really originates from benzoate groups formed from the benzoyl peroxide used in preparing polymer P2c1. Then this result supports the statement in Chapter 4, that the ultraviolet absorption at 270–280 mμ is due to benzoate groups.

Summary

The purpose of this work has been to show the possibilities offered by spectrophotometric methods in the study of high polymers. The performance of the investigation necessitated the construction of a recording raman spectrograph.

1. The requirements which mercury vapour discharge lamps have to fulfil in order to be suitable light-sources for raman spectroscopy have been discussed.

2. It has been found that a good light-source can be obtained by removing the protecting glass envelope from an ordinary mercury discharge lamp designed for illuminating purposes and then cooling the discharge tube in a stream of air.

3. The spectral characteristics of this lamp are the same as those of a low-pressure lamp. The stability and constancy of the luminous flux are good. The purity of the spectrum is excellent in the range $\Delta\nu$ 0–1800 cm.$^{-1}$ from λ 4358 Å.

4. A lamp-house containing the raman tube, space for polarizing media, filter-jackets, and six mercury lamps have been constructed. It is provided with water and air-cooling systems, and precautionary measures against accidental disturbancies.

5. The conditions which must be fulfilled in order to secure a maximum amount of luminous energy through the spectrograph have been studied for a cylindrical light-source.

6. It was found that a correction had to be applied for the difference in refractive indices between various media; otherwise, raman line intensities could not be compared. This correction originates from the fact that the volume, effective in sending light into the spectrograph, changes with the refractive index.

7. The influence of absorption in the liquid to be studied has also been discussed. The absorption does not change the conditions for maximum illumination.

8. The raman spectra are recorded by moving the multiplier photo-tube system. The principles of the mechanical and optical systems are outlined.

9. A detailed description of the construction of these systems is given. The scanning of spectra could be done with a sufficient accuracy for the purposes in view.

10. The properties of multiplier photo-tubes have been discussed in detail, as well as different sources of input noise of vacuum tube amplifiers.

11. The photo-tube system, including the photo-tube, voltage divider for the dynode voltages and the high-tension supply has been discussed, especially with regard to stability of operation. It has been shown that the amplification of the photo-tube is constant only when the output current is low compared to the total current through the bleeder resistances.

12. The amplifier system with necessary filament-current and anode-voltage supplies have been discussed.

13. Rectification of the 100 cycles signal from the amplifier is made by applying a homodyne principle. The operation of this rectifier has been studied experimentally.

14. A discussion of the interpretation of the recorded spectra is given.

15. The spectrophotometer has been found to have a linear response within $\pm$ 1 per cent in a range covering light intensities from raman lines to lines in ordinary emission spectra.

16. The signal-to-noise ratio is only slightly dependent on the dynode voltage.

17. Wave number determinations can be made within $\pm$ 5 cm.$^{-1}$.

18. The accuracy of intensity determination is about $\pm$ 1 per cent for strong raman lines and $\pm$ 5 per cent ($\pm$ 0.003 unit scattering coefficient) for weak and medium raman lines.

19. The selectivity of the photo-electric recording method, compared to the photographic in recording very weak and very strong raman lines simultaneously, is examplified on carbon tetrachloride and carbon disulphide.

20. The use of the spectrograph for the study of ordinary emission spectra has been demonstrated, using a cesium discharge lamp.

21. The spectrograph has been used to study changes occurring during polymerization of methyl methacrylate.

22. The spectra of monomeric and polymeric methyl methacrylates have been compared with those of polymerizing mixtures. The changes in certain bond-frequencies have been discussed with special reference to the decrease in unsaturation and conjugation during the polymerization.

23. A discussion has also been given concerning the possibility of correlating the change in scattering coefficients with the degree of conversion. This depends upon the possibility of resolving the lines under discussion. Further corrections must be applied for the changes in density and refractive index occurring during the polymerization.

24. Measurements in the ultraviolet region 250–300 mμ on several fractionated and unfractionated samples of polymethyl methacrylate have shown that fragments originating from benzoyl peroxides can be detected. The specific extinction coefficients have been measured and used to calculate the number of end groups in the samples. A tentative correlation with the k'-constant obtained from viscosity measurements has been made. There is an indication that phenyl end groups may also be present in some of the polymers.

25. The absorption bands of polymethyl methacrylates in the infrared region 1–15 μ have been thoroughly investigated. A discussion of the structural assignments of these bands is given. It is pointed out that more data on model substances are necessary for unambiguous assignments.

26. The spectra of two polymer samples having low molecular weights show a difference in the 14 μ region, indicating the presence of benzoate groups in the polymer sample made through initiation with benzoyl peroxide. In spectra of benzoates, a strong absorption band is found at 14.05 μ, whereas the polymer sample has a maximum at 13.96 μ.

Appendix I

List of Symbols

A Constant in Richardson's formula.

a Width of light beam; distance from nodal point to axis of screw.

B Amount of radiation (luminous energy) in unit time, unit volume and unit solid angle; mean square deviation of amplification factor.

b Height of light beam; relative mean square deviation of amplification factor.

C Capacitor, capacitance.

c Concentration; as a subscript: cathode.

D Optical density.

d Thickness of lens.

E Energy; electromotive force.

e Voltage; distance of nodal point from lens' surface; modulus of electronic charge; base of natural logarithms.

F Luminous energy entering spectrograph.

$\boldsymbol{F}$ Electric field vector.

f Focal distance; frequency.

g Number of secondary electrons; as a subscript: grid.

g_m Transconductance.

H Light scattering factor.

h Planck constant; height of light source cross-section.

I Light intensity; quantum number (nuclear angular momentum); electric current.

i Electric current; degree of polymerization; as a subscript: internal, input.

J Quantum number (total resultant angular momentum).

j Current density; number of end groups.

K Kelvin.

k Boltzmann constant.

k' Constant in viscosity formula.

L Quantum number (total angular momentum); inductance; mean value; as a subscript: load.

l Length of light source; position of spectral line on chart.

l_i Observed data.

M Molecular weight; standard deviation of the mean.

m Standard deviation; multiplication factor.

N_0 Avogadro's number.

n Refractive index.

o As a subscript: output.

P Reciprocal difference of short-circuit and transfer conductance of stabilizer under load and non zero supply resistance condition.

P Induced dipole moment.

p Probability; reciprocal difference of short-circuit and transfer conductance of stabilizer under no load and zero supply resistance conditions; as a subscript: anode (plate).

Q Open circuit input resistance.

q Reflectivity; open circuit input resistance; degree of conversion.

R Resistor; resistance; radius of light source cross-section; as a subscript: resistance.

r Resistance.

S Quantum number (spin angular momentum); statistical spectrum of noise variables; signal-to-noise ratio; stabilizing ratio; spectral sensitivity function; as a subscript: signal.

s Height of slit; stabilizing ratio; as a subscript: supply, signal.

sp As a subscript: specific.

T Absolute temperature; time; transmission; transmittancy function.

t Time; as a subscript: true, total.

V Voltage.

v Voltage; electromotive force; angle; speed of scanning.

w Work function.

Z Impedance.

z Distance along optical axis.

α Resistance ratio; coefficient of resistivity; angular aperture; polarizability.

β Angular aperture; constant characterizing secondary emission surfaces.

γ Total transition probability per unit time; refractive index increment per unit concentration.

Δ Difference.

δ Slit width.

ε Specific extinction coefficient.

η Viscosity.

θ Angle; space charge factor.

$\varkappa$ Absorption coefficient.

λ Wave-length.

μ Wave-length unit (microns); amplification factor of vacuum tube.

ν Wave number; frequency.

ϱ Depolarization factor; radius vector; density.

σ Geometrical factor to characterize shot effect noise.

τ Time constant; turbidity.

φ Phase angle.

ψ Time-independent wave function.

ω Angular frequency.

Appendix II

Details of Coupling Elements in Electronic Circuits

This Appendix contains details about the various coupling elements *etc.* of the electronic circuits described in Chapter 1. The tube notations follow RCA Tube Handbook except for the voltage stabilizer tube 85A1 (Philips). (HT = high tension, w.w. = wire wound.)

I. High Tension Supply (Figure 16, p. 62)

V_1	2X2/879	R_6	400 kΩ
V_2	6V6	R_7	1 MΩ
V_3	6AU6	R_8	1 MΩ
V_4	6SC7	R_9	200 kΩ
V_5	85A1	R_{10}	15 kΩ, w.w.
V_6	85A1	R_{11}	10 × 5 kΩ, w.w.
V_7	85A1	R_{12}	5 × 50 kΩ, w.w.
V_8	85A1	R_{13}	130 kΩ, w.w.
V_9	Birka relay: type 900, 45 sec. delay	R_{14}	100 kΩ
		R_{15}	75 kΩ, w.w.
T_1	Transformer 220/2.5; 6.3	R_{16}	10 × 10 kΩ, w.w.
T_2	Transformer 220/6.3; 6.3	R_{17}	5 × 100 kΩ, w.w.
T_3	Transformer 220/6.3	R_{18}	10 MΩ
T_4	Transformer 220/high tension	R_{19}	15 kΩ
M_1	mA-meter: 0–10	R_{20}	15 kΩ
M_2	μA-meter: 0–200	C_1	2 μF
M_3	kV-meter: 0–2	C_2	2 μF
S_1	Switch for HT, coarse; 200 V./step.	C_3	2000 pF
S_2	Switch for HT, fine; 20 V./step.	C_4	0.1 μF
S_3	Main switch	C_5	0.25 μF
S_4	HT-switch	C_6	0.1 μF
S_5	Switch for M_3	C_7	0.1 μF
R_1	200 kΩ	L_1	Choke: 6000 Ω, 600 H, 15 mA
R_2	1 MΩ	F_1	Main fuse
R_3	10 MΩ	F_2	HT fuse
R_4	100 kΩ	P_1	Pilot-lamp: filament current
R_5	250 kΩ	P_2	Pilot-lamp: HT

II. Amplifier (Figure 17, p. 64)

V_1	5693	V_6	1P21
V_2	5693	R_1	1 MΩ, w.w.
V_3	5693	R_2	1 MΩ
V_4	5693	R_3	3 kΩ, w.w.
V_5	5693	R_4	500 kΩ, w.w.

R_5	2 MΩ	R'	100 kΩ, w.w.
R_6	1 MΩ, w.w.	C_1	0.08 μF
R_7	900 Ω	C_2	25 μF
R_8	330 kΩ	C_3	5000 pF
R_9	100 kΩ, w.w.	C_4	0.02 μF
R_{10}	270 kΩ + 27 kΩ + 2.7 kΩ + 270 Ω + 30 Ω	C_5	0.1 μF
		C_6	50 μF
R_{11}	800 kΩ	C_7	1000 pF
R_{12}	500 kΩ	C_8	0.05 μF
R_{13}	500 kΩ	C_9	0.5 μF
R_{14}	800 kΩ	C_{10}	0.02 μF
R_{15}	1 kΩ, w.w.	C_{11}	0.02 μF
R_{16}	750 kΩ	C_{12}	0.1 μF
R_{17}	150 kΩ	C_{13}	500 pF
R_{18}	1 MΩ	C_{14}	10000 pF
R_{19}	200 kΩ	C_{15}	1000 pF
R_{20}	160 kΩ	C_{16}	1000 pF
R_{21}	1 kΩ, w.w.	C_{17}	0.1 μF
R_{22}	500 kΩ	C_{18}	0.05 μF
R_{23}	100 kΩ	C_{19}	0.025 μF
R_{24}	330 kΩ	C_{20}	0.01 μF
R_{25}	10 × 30 kΩ	C_{21}	0.05 μF
R_{26}	500 kΩ	C_{22}	0.05 μF
R_{27}	100 kΩ	C_{23}	8 μF
R_{28}	500 Ω, w.w.	C_{24}	16 μF
R_{29}	150 kΩ	C_{25}	8 μF
R_{30}	25 kΩ	C_{26}	8 μF
R_{31}	10 kΩ	C_{27}	8 μF
R_{32}	10 kΩ	h_1	Connection to filament-current supply
R_{33}	25 kΩ		
R_{34}	50 kΩ	h_2	Connection to filament-current supply
R_{35}	50 kΩ		
R	9 × 250 kΩ, w.w.	A	Connection to homodyne rectifier

III. Anode Voltage Supply of Amplifier (Figure 18, p. 65)

V_1	5U4G	M_1	mA-meter: 0–100
V_2	6L6	M_2	μA-meter: 0–200
V_3	6L6	S_1	Main switch
V_4	1N5GT/G	R_1	0.5 MΩ
V_5	85A1	R_2	100 Ω each
V_6	85A1	R_3	100 Ω
V_7	VR75	R_4	25 kΩ
V_8	VR75	R_5	1.7 kΩ
V_9	VR75	R_6	0.5 MΩ
V_{10}	VR75	R_7	0.5 MΩ
T_1	Transformer 220/2 × 3.15; 5; 2 × 350	R_8	2 MΩ
		R_9	0.5 MΩ
T_2	Transformer 220/6.3	R_{10}	60 kΩ

R_{11}	2 MΩ	C_4	0.02 μF
R_{12}	1000 Ω	C_5	0.1 μF
R_{13}	1000 Ω	L_1	Choke: 300 Ω, 19 H, 75 mA
R_{14}	1000 Ω	L_2	Choke: 300 Ω, 19 H, 75 mA
C_1	6 μF	F_1	Main fuse
C_2	6 μF	P_1	Pilot-lamp
C_3	6 μF		

IV. Filament Current Supply (Figure 19, p. 66)

V_1, V_2	5U4G	R_{10}	20 kΩ
V_3, V_4	6AS7	R_{11}	300 Ω
V_5	6SC7	R_{12}	75 Ω
V_6	6SF5	R_{13}	75 Ω
V_7, V_8	85A1	R_{14}	10 Ω
T_1	Transformer 220/2 × 3.15; 2 × 3.15	R_{15}	200 Ω
T_2	Transformer 220/2 × 2.5	R_{16}	1 kΩ
T_3	Transformer 220/2 × 300; 6.3	R_{17}	1 kΩ
M_1	mA-meter: 0–500	C_1	16 μF
M_2	mA-meter: 0–500	C_2	16 μF
S_1	Main switch	C_3	500 pF
S_2	HT-switch	C_4	200 pF
R_1	25 Ω each	L_1	Choke: 60 Ω, 8.5 H, 400 mA
R_2	25 Ω each	F_1	Main fuse
R_3	1 MΩ	P_1	Pilot-lamp: filament current
R_4	100 kΩ	P_2	Pilot-lamp: voltage
R_5	0.5 MΩ	h_1, h_2	Connection to amplifier
R_6	60 kΩ	h_3	Connection to homodyne rectifier
R_7	0.4 MΩ	h_4	Connection to anode-voltage
R_8	20 kΩ		supply of homodyne rectifier
R_9	0.5 MΩ		

V. Homodyne Rectifier and Cathode Follower (Figure 20, p. 68)

V_1	6C5	R_1	100 kΩ
V_2	6L7	R_2	1 MΩ
V_3	6L7	R_3	50 kΩ, w.w.
V_4	6SN7-GT	R_4	1 kΩ, w.w.
V_5	6H6	R_5	50 kΩ, w.w.
V_6	6C5	R_6	100 kΩ
T_1	Transformer 220/2 × 0, 5, 10, 20, 30, 50	R_7	(200 + 100 + 200) Ω, w.w.
		R_8	220 Ω, w.w.
T_2	Transformer 220/2 × 3.15; 2 × 3.15	R_9	220 Ω, w.w.
M_1	mA-meter: 0–20 mA	R_{10}	220 Ω, w.w.
S_1	Switch for band width	R_{11}	100 kΩ
S_2	Switch for recorder	R_{12}	60 kΩ
S_3	Switch for synchronous voltage	R_{13}	40 kΩ, w.w.
S_4	Switch for phase adjustment	R_{14}	40 kΩ, w.w.
S_5	Control switch	R_{15}	500 kΩ
S_6	Main switch	R_{16}	500 kΩ

R_{17}	500 kΩ	C_8	0.1 μF
R_{18}	500 kΩ	C_9	0.25 μF
R_{19}	1 MΩ	C_{10}	1 μF
R_{20}	30 kΩ	C_{11}	4 μF
R_{21}	50 kΩ, w.w.	C_{12}	8 μF
R_{22}	50 kΩ	C_{13}	0.1 μF
R_{23}	30 kΩ	C_{14}	0.25 μF
R_{24}	1 MΩ	C_{15}	1 μF
R_{25}	2 × (1 + 9 + 90 + 900) Ω, w.w.	C_{16}	4 μF
R_{26}	2.5 + 7.5 kΩ, w.w.	C_{17}	8 μF
R_{27}	10 kΩ, w.w.	C_{18}	0.2 μF
R_{28}	50 kΩ	C_{19}	0.2 μF
R_{29}	50 kΩ	C_{20}	0.01 μF
R_{30}	50 kΩ	C_{21}	0.01 μF
R_{31}	500 kΩ	C_{22}	0.25 μF
R_{32}	5 kΩ, w.w.	C_{23}	0.25 μF
R_{33}	500 Ω, w.w.	C_{24}	0.01 μF
R_{34}	5 kΩ, w.w.	C_{25}	8 μF
R_{35}	50 kΩ, w.w.	C_{26}	8 μF
R_{36}	20 kΩ	C_{27}	8 μF
R_{37}	20 kΩ, w.w.	C_{28}	8 μF
C_1	2000 pF	L_1	Choke: 25 kΩ, 100 H, 50 mA
C_2	0.1 μF	F_1	Main fuse
C_3	0.1 μF	P_1	Pilot-lamp
C_4	0.25 μF	h_3	Connection from filament-current supply
C_5	0.25 μF		
C_6	0.2 μF	a, b, c	Connections to voltmeter or oscillograph
C_7	0.2 μF		

VI. Anode Voltage Supply of Homodyne Rectifier (Figure 22, p. 71)

V_1	5U4G	R_6	1 MΩ
V_2	6L6	R_7	80 kΩ
V_3	6L6	R_8	100 kΩ
V_4	6SJ7	R_9	0.5 MΩ
V_5	VR75	R_{10}	10 kΩ
V_6	VR150	R_{11}	2 MΩ
V_7	VR75	R_{12}	1 kΩ
V_8	VR75	C_1	6 μF
T_1	Transformer 220/2 × 3.15; 5; 2 × 350	C_2	6 μF
T_2	Transformer 220/6.3	C_3	6 μF
M_1	mA-meter: 0–100	C_4	0.02 μF
M_2	μA-meter: 0–200	C_5	0.1 μF
S_1	Main switch	L_1	Choke: 300 Ω, 19 H, 75 mA
R_1	0.5 MΩ	L_2	Choke: 300 Ω, 19 H, 75 mA
R_2	100 Ω each	F_1	Main fuse
R_3	100 Ω	P_1	Pilot-lamp
R_4	10 kΩ	h_1	Connection from filament-current supply
R_5	30 kΩ		

References

An asterisk (*) after the number means that the reference has been available only as an abstract.

1. Kinell, P.-O., On the Determination of Polydispersity from Ultracentrifugal Sedimentation. — Acta Chem. Scand. *1* (1947) 335.
2. Kinell, P.-O., The Distribution of Sizes of Particles in Some Polymeric Methyl Methacrylates. — Acta Chem. Scand. *1* (1947) 832.
3. Kudrjawzewa, V., Über die Untersuchung von Ramanspektren mit Hilfe des photoelektrischen Zählers. — Acta Physicochim. U.R.S.S. *3* (1935) 613.
4. Menzies, A. C., Infra-Red and Raman Spectra — Recent Advances in Great Britain. — Instruments and Measurements Conference, Stockholm, Transactions (1949) 29.
5. Rank, D. H., Pfister, R. J., and Coleman, P. D., Photoelectric Detection and Intensity Measurement in Raman Spectra. — J. Optical Soc. Am. *32* (1942) 390.
6. Rank, D. H., Pfister, R. J., and Grimm, H. H., A Method for Determining Depolarization Factors in Raman Spectra. — J. Optical Soc. Am. *33* (1943) 31.
7. Rank, D. H., and Wiegand, R. V., A Photoelectric Raman Spectrograph for Quantitative Analysis. — J. Optical Soc. Am. *36* (1946) 325.
8. Fenske, M. R., Braun, W. G., Wiegand, R. V., Quiggle, D., McCormick, R. H., and Rank, D. H., Raman Spectra of Hydrocarbons. — Anal. Chem. *19* (1947) 700.
9. Braun, W. G., Spooner, D. F., and Fenske, M. R., Raman Spectra. Hydrocarbons and Oxygenated Compounds. — Anal. Chem. *22* (1950) 1074.
10. Chien, J.-Y., and Bender, P., Photoelectric Intensity Measurements of Raman Spectra. — J. Chem. Phys. *15* (1947) 376.
11. Kinell, P.-O., and Traynard, Ph., Utilisation des Cellules Multiplicateurs d'Electrons en Spectrographie Raman. — Acta Chem. Scand. *2* (1948) 193.
12. Miller, C. H., Long, D. A., Woodward, L. A., and Thompson, H. W., A recording Spectrometer for Raman Spectroscopy. — Proc. Phys. Soc. (London) *A 62* (1949) 401.
13. Sushchinskii, M. M., Self Recording Photo Electric Spectrograph for Investigations of Optical Raman Spectra (in Russian). — Doklady Akad. Nauk. S.S.S.R. *70* (No. 2) (1950) 221.
14. Sushchinskii, M. M., Photo Electric Method of Investigating Raman Spectra (in Russian). — J. Exptl. Theoret. Phys. U.S.S.R. *20* (1950) 304.
15. Heigl, J. J., Black, J. F., and Dudenbostel, Jr., B. F., Determination of Total Olefins and Total Aromatics in Hydrocarbon Mixtures by Raman Spectrometry. — Anal. Chem. *21* (1949) 554.
16. Heigl, J. J., Dudenbostel, Jr., B. F., Black, J. F., and Wilson, J. A., Direct-Recording Raman Spectrometer. — Anal. Chem. *22* (1950) 154.
17. Tolansky, S., High Resolution Spectroscopy, London (1947).
18. Zworykin, V. K., and Ramberg, E. G., Photoelectricity and its Application, New York (1949) 99.
19. Schwetzoff, V., and Robin, S., Cellule photoélectrique à multiplicateur d'électrons pour l'ultraviolet lointain. — Compt. rend. *230* (1950) 1759.
20. Morrish, A. H., Williams G. W., and Darby, E. K., Ultraviolet Photon Counting with an Electron Multiplier. — Rev. Sci. Instruments *21* (1950) 884.

21. Görlich, P., and Lau, E., Quantitative Messungen mit dem Multiplexinterferenzspektroskop. — Z. Physik *77* (1932) 746.
22. Glansholm, D., and Kleman, B., The use of photomultipliers in spectroscopy. — Arkiv Fysik *2* (1950) 305.
23. Rank, D. H., and McCartney, J. S., Some Spectral Characteristics of Mercury Arcs for Use in Study of the Raman Effect. — J. Optical Soc. Am. *38* (1948) 279.
24. Menzies, A. C., and Skinner, J., A New Source for Raman Spectroscopy. — J. Sci. Instruments *26* (1949) 299.
25. Kemp, J. W., Recent Advances in Raman Equipment. — J. Optical Soc. Am. *41* (1951) 868.
26. Simon, A., and Jentzsch, D., Untersuchungen über die quantitative ramanspektroskopische Bestimmung der γ-Isomeren in technischen Hexachlorcyclohexan. — Z. anorg. allgem. Chem. *266* (1951) 193.
27. Uyterhoeven, W., Elektrische Gasentladungslampen, Berlin (1938).
28. Uyterhoeven, W., Elektrische Erscheinungen in der positiven Säule bei niedrigem Druck. — Philips techn. Rundschau *3* (1938) 161. — Lichtemission der positiven Säule bei niedrigem Druck. — *Ibid.* *3* (1938) 201. — (with Zecher, G.) Niederdruck-Quecksilberentladung in lumineszierenden Röhren. — *Ibid.* *3* (1938) 277.
29. Elenbaas, W., The High Pressure Mercury Vapour Discharge, Amsterdam (1951).
30. Heller, G., Vergleich zwischen den Entladungsformen in Natrium- und Quecksilberdampflampen. I–II. — Philips techn. Rundschau *1* (1936) 2, 70.
31. Holstein, T., Imprisonment of Resonance Radiation in Gases. — Phys. Rev. *72* (1947) 1212.
32. Alpert, D., McCoubrey, A. O., and Holstein, T., Imprisonment of Resonance Radiation in Mercury Vapour. — Phys. Rev. *76* (1949) 1257.
33. Holstein, T., Imprisonment of Resonance Radiation in Gases. II. — Phys. Rev. *83* (1951) 1159.
34. Borchert, R., Die Entstehung des Kontinuums in der Quecksilberhochdruckentladung und die Grösse ihrer mittleren "Anregungsspannung". — Ann. Physik *7* (1950) 332.
35. Heitler, W., The Quantum Theory of Radiation, Second Edition, Oxford (1944) 113.
36. Ishida, Y., and Hiyama, S., On the Stark Effect of Hg I. — Sci. Papers Inst. Phys. Chem. Research (Tokyo) *36* (1939) 390.
37. Rompe, R., and Schultz, P., Die Breite der Spektrallinien in der Quecksilberhochdruckentladung. — Z. Physik *108* (1938) 654.
38. Landolt-Börnstein, Zahlenwerte und Funktionen aus Physik, Chemie, Astronomie, Geophysik und Technik, Sechste Auflage, Band *I: 1*, Berlin (1950) 259.
39. Blet, M. G., Étude thèorique et expérimentale de l'Élargissement et du Renversement de Raies de l'arc au Mercure Haute Pression. — Congr. groupement avance. méthodes anal. spectrograph. produits mét. (Paris) *11* (1949) 65.
40. Kastha, G. S., The structure of the resonance line of mercury filtered through mercury vapour. — Indian J. Phys. *23* (1949) 247.
41. Brillouin, L., Diffusion de la lumière et des rayons X par un corps transparent homogène. Influence de l'agitation thermique. — Ann. phys. *17* (1922) 88.
42. Gross, E., Über die Veränderung der Wellenlänge durch elastische Wärmewellen bei Lichtzerstreuung in Flüssigkeiten. — Naturwissenschaften *18* (1930) 718.
43. Rank, D. H., McCartney, J. S., and Szasz, G. J., Intensity and Polarization of Brillouin Spectra. — J. Optical Soc. Am. *38* (1948) 287.

44. Elenbaas, W., and Riemens, J., Light Sources for Line Spectra. — Philips Techn. Rev. *11* (1950) 299.
45. Dorgelo, E. G., Wechselstromschaltungen für Entladungslampen. — Philips techn. Rundschau *2* (1937) 103.
46. Bouma, P. J., Das Flimmern elektrischer Lichtquellen. — Philips techn. Rundschau *6* (1941) 299.
47. Carr, C. I., and Zimm, B. H., Absolute Intensity of Light Scattering from Pure Liquids and Solutions. — J. Chem. Phys. *18* (1950) 1616.
48. Harrison, V. G. W., The light-diffusing properties of magnesium oxide. — Proc. Phys. Soc. (London) *58* (1946) 408.
49. Benford, F., Lloyd, G. P., and Schwarz, S., Coefficients of Reflection of Magnesium Oxide and Magnesium Carbonate. — J. Optical Soc. Am. *38* (1948) 445.
50. Benford, F., Schwarz, S., and Lloyd, G. P., Coefficients of Reflection in the Ultraviolet of Magnesium Carbonate and Oxide. — J. Optical Soc. Am. *38* (1948) 964.
51. Edsall, J. T., and Wilson, Jr., E. B., A Simple Method for Determining the Polarization of Raman Lines. — J. Chem. Phys. *6* (1938) 124.
52. Crawford, Jr., B. L., and Horwitz, W., A Raman Apparatus for Quantitative Polarization Measurements. — J. Chem. Phys. *15* (1947) 268.
53. Douglas, A. E., and Rank, D. H., Determination of the Depolarization Factors of Highly Polarized Raman Lines. — J. Optical Soc. Am. *38* (1948) 281.
54. Rank, D. H., and Kagarise, R. E., Empirical Convergence Correction of Depolarization Measurements. — J. Optical Soc. Am. *40* (1950) 89.
55. Otting, W., Der Raman-Effekt und seine analytische Anwendung. Anleitungen für die chemische Laboratoriumspraxis, Band V, Berlin (1952) 66.
56. Nielsen, J. R., The Filling of a Spectrograph with Light Considered as a Geometrical Radiation Problem. — J. Optical Soc. Am. *20* (1930) 701.
57. Slyusarev, G. G., and Chulanovsky, V. M., Illumination of the slits of a spectrograph with an extended non-absorbing source of light (in Russian). — J. Tech. Phys. U.S.S.R. *18* (1948) 665.
58. Donzelot, P., and Barriol, Notes sur l'éclairement d'un spectrographe pour l'étude de l'effet Raman. — J. phys. radium *VII* (*VII*) (1936) 36 S.

58a. Woodward, L. A., and George, J. H. B., Refractive Index Correction in Relative Raman Intensity Measurements. — Nature *167* (1951) 193. — Light Flux received by a Spectrograph from a Spatially Extended Refracting Source. — Proc. Phys. Soc. (London) *B64* (1951) 780.

59. Sawyer, R. A., Experimental Spectroscopy, Second edition, New York (1951).
60. Zimm, B. H., Apparatus and Methods for Measurement and Interpretation of the Angular Variation of Light Scattering: Preliminary Results on Polystyrene Solutions. — J. Chem. Phys. *16* (1948) 1099.
61. Zworykin, V. K., and Ramberg, E. G., Photoelectricity and its Application, New York (1949).
62. Engstrom, R. W., Multiplier Photo-Tube Characteristics: Application to Low Light Levels. — J. Optical Soc. Am. *37* (1947) 420.
63. Rodda, S., Photoelectric Multipliers. — J. Sci. Instruments *26* (1949) 65.
64. Winans, R. C., and Pierce, J. R., Operation of Electrostatic Photo-Multipliers. — Rev. Sci. Instruments *12* (1941) 269.
65. Sommer, A., and Turk, W. E., New Multiplier Phototubes of High Sensitivity. — J. Sci. Instruments *27* (1950) 113.

66. Lallemand, A., Les cellules a multiplicateurs d'électrons. Développements. Utilisation. — J. phys. radium *VIII* (*X*) (1949) 235.
67. Dieke, C. H., Progress Report on a Study of Standard Methods for Spectrographic Analysis. VI. The Use of Multiplier Phototubes in Spectrographic Analysis. — Research Report W-193, Office of Production Research and Development, War Production Board, Washington, D. C., U.S.A. (1945).
68. Dieke, C. H., Photoelectric Intensity Measurements in Spectra. — Instruments and Measurements Conference, Stockholm, Transactions (1947) 17.
69. Morton, G. A., and Mitchell, J. A., Performance of 931-A Type Multiplier in a Scintillation Counter. — RCA Review *9* (1948) 632 and Nucleonics *4* (1949) Jan. 16.
70. Morton, G. A., Photomultipliers for Scintillation Counting. — RCA Review *10* (1949) 525.
71. Westöö, R., and Wiedling, T., Investigations of the pulse-distribution of an RCA multiplier phototube. — Arkiv Fysik *1* (1949) 269.
72. Drigo, A., Sulla nuova Tecnica dei Contatori a Scintillazione. — Tecn. Ital. *5* (1950) 2.
73. Ageno, M., Chiozzotto, M., and Querzoli, R., Sulle caratteristiche dei fotomoltiplicatori elettronici, usati come rivelatori di Scintillazioni. Nota I. — R. C. Ist. Super. Sanità *12* (1949) 265.
74. Corson, D. R., and Wilson, R. R., Particle and Quantum Counters. — Rev. Sci. Instruments *19* (1948) 207.
75. Stone, R. P., A Secondary-Emission Electron Multiplier Tube for the Detection of High Energy Particles. — Rev. Sci. Instruments *20* (1949) 935.
76. Schremp, E. J., Amplifier Sensitivity. — Valley, Jr., G. E., and Wallman, H., editors, Vacuum Tube Amplifiers, Massachusetts Institute of Technology Radiation Laboratory Series *18*, New York (1948) 496.
77. Shockley, W., and Pierce, J. R., A Theory of Noise for Electron Multipliers. — Proc. Inst. Radio Engrs. *26* (1938) 321.
78. Zworykin, V. K., Morton, G. A., and Malter, L., The Secondary Emission Multiplier — A New Electronic Device. — Proc. Inst. Radio Engrs. *24* (1936) 351.
79*. Rajchman, J., Residual Current in Electrostatic Electron Multipliers. — Arc. Sci. Phys. Nat. (5) *20* (1938) 231 and (5) *21* (1939) 5.
80. Richtmyer, F. K., and Kennard, E. H., Introduction to Modern Physics, New York (1942) 117.
81. de Boer, J. H., and Teves, M. C., Sekundärerscheinungen, die auf den primären photoelektrischen Effekt bei an Salzschichten adsorbierten Cäsiumatomen folgen. — Z. Physik *74* (1932) 604.
82. Engstrom, R. W., Refrigerator for a Multiplier Photo-Tube. — Rev. Sci. Instruments *18* (1947) 587.
83. Drigo, A., Sulla possibilità di ridurre gli impulsi di fondo dei fotomoltiplicatori "931 A" mediante un elettrodo esterno. — Nuovo Cim. *7* (1950) 267.
84. Taylor, C., Sur la variation du bruit de fond d'un photomultiplicateur RCA 931 A avec le potentiel de l'enveloppe en verre. — J. phys. radium *VIII* (*X*) (1949) 255.
85. Marshall, F.-H., Coltman, J. W., and Bennett, A. I., The Photo-Multiplier Radiation Detector. — Rev. Sci. Instruments *19* (1948) 744.
86. Marshall, F.-H., Coltman, J. W., and Hunter, L. P., The Photomultiplier X-Ray Detector. — Rev. Sci. Instruments *18* (1947) 504.
87. Moullin, E. B., Spontaneous Fluctuations of Voltage, Oxford (1938) 155.

88. Godfrey, T. N. K., Harrison, F. B., and Keuffel, J. W., Satellite Pulses from Photomultipliers. — Phys. Rev. *84* (1951) 1248.
89. Normand, C. W. B., and Kay, R. H., Notes on the design, adjustment and calibration of spectrophotometers. — J. Sci. Instruments *29* (1952) 33.
90. Peterson, E. W., and Holland, D. H., On the Shape of the Sensitive Cathode Area of Electron Multiplier Photo-Tubes. — J. Optical Soc. Am. *40* (1950) 253.
91. Clancy, E. P., Polarization Effects in Photomultiplier Tubes. — J. Optical Soc. Am. *42* (1952) 357.
92. Brice, B. A., Halwer, M., and Speiser, R., Photoelectric Light-Scattering Photometer for Determining High Molecular Weights. — J. Optical Soc. Am. *40* (1950) 768.
93. Lubszynski, H. G., Photo-Cells for the Visible and Ultra-Violet. — B. Lovell, editor, Electronics and their application in Industry and Research, London (1947) 53.
94. Johnson, J. B., Thermal Agitation of Electricity in Conductors. — Phys. Rev. *32* (1928) 97.
95. Nyquist, H., Thermal Agitation of Electric Charge in Conductors. — Phys. Rev. *32* (1928) 110.
96. Elmore, W. C., Electronics for the Nuclear Physicist II. — Nucleonics *2* (1948) March 16.
97. Valley, Jr., G. E., and Wallman, H., Vacuum Tube Amplifiers, Massachusetts Institute of Technology Radiation Laboratory Series *18*, New York (1948).
98. Miller, S. E., Sensitive D. C. Amplifier with A. C. Operation. — Electronics *14* (1941) Nov. 27.
99. Greenwood, I. A., Holdam, J. V., and MacRae, Jr., D., Electronic Instruments, Massachusetts Institute of Technology Radiation Laboratory Series *21*, New York (1948) 512.
100. Jurriaanse, T., A voltage stabilizing tube for very constant voltage. — Philips Techn. Rev. *8* (1946) 272.
101. Boers, C. J., The "Miniwatt" stabilizing tube 85A1 as a voltage reference. — Electronic Application Bulletin *10* (1949) 33.
102. Benson, F. A., Variations in extinction voltages of glow-discharge voltage-regulator tubes. — J. Sci. Instruments *28* (1951) 186.
103. Benson, F. A., Cain, W. E., and Clucas, B. D., Variations in the Characteristics of some Glow-Discharge Voltage-Regulator Tubes. — J. Sci. Instruments *26* (1949) 399.
104. Benson, F. A., Initial Drifts in Running Voltage of Glow-Discharge Regulator Tubes. — J. Sci. Instruments *27* (1950) 71.
105. Benson, F. A., and Bache, H., A note on the temperature coefficients of running voltage of glow-discharge tubes. — J. Sci. Instruments *29* (1952) 25.
106. Titterton, E. W., Some Characteristics of Glow-Discharge Voltage Regulator Tubes. — J. Sci. Instruments *26* (1949) 33.
107. Gilvarry, J. J., and Rutland, D. F., General Theory of Voltage Stabilizers. — Rev. Sci. Instruments *22* (1951) 464.
108. Hunt, F. V., and Hickman, R. W., On Electronic Voltage Stabilizers. — Rev. Sci. Instruments *10* (1939) 6.
109. Gustafson, W. G., Magnetic Shielding of Transformers at Audio Frequencies. — Bell Syst. Tech. J. *17* (1938) 416.
110. Lyons, W., Experiments on Electromagnetic Shielding at Frequencies Between One and Thirty Kilocycles. — Proc. Inst. Radio Engrs. *21* (1933) 574.

111. Ellwood, W. B., Magnetic Shields. — Bell Lab. Rec. *17* (1938) 93.
112. Roess, L. C., Vacuum Tube Amplifier for Measuring Very Small Alternating Voltages. — Rev. Sci. Instruments *16* (1945) 172.
113. Tucker, D. G., The "Synchrodyne". A New Type of Radio Receiver for A.M. Signals. — Electronic Engng *19* (1947) 75.
114. Tucker, D. G., The Design of a Synchrodyne Receiver. Part 1 — Design Principles. — Electronic Engng *19* (1947) 241.
115. Tucker, D. G., and Ridgway, J. F., The Design of a Synchrodyne Receiver. Part 2 — Some Suitable Design. — Electronic Engng *19* (1947) 276.
116. Tucker, D. G., The Synchrodyne. Further Notes on the Receiver shown at Radiolympia. — Electronic Engng *19* (1947) 366.
117. Tucker, D. G., and Garlick, J., The Synchrodyne: Refinements and Extensions. 1. Control of the Phase Angle between the Output and Injected Signal of the Synchronized Oscillator. — Electronic Engng *20* (1948) 49.
118. Herold, E. W., The Operation of Frequency Converters and Mixers for Superheterodyne Reception. — Proc. Inst. Radio Engrs. *30* (1942) 84.
119. Villard, Jr., O. G., Tunable A–F Amplifier. — Electronics *22* (1949) July p. 77.
120. Doetsch, G., Theorie und Anwendung der Laplace-Transformation, New York (1943).
121. Kohlrausch, K. W. F., Ramanspektren. — Eucken, A., and Wolf, K. L., editors, Hand- und Jahrbuch der chemischen Physik, Band 9, Leipzig (1943).
122. Kohlrausch, K. W. F., Köppl, F., and Pongratz, A., Studien zum Raman-Effekt. Mitteilung XXVI. Das Raman-Spektrum der Methyl- und Äthylester einbasischer Fettsäuren. — Z. physik. Chem. *B 22* (1933) 359.
123. Reitz, A. W., Studien zum Raman-Effekt. Mitteilung LXXIX. Der fünfgliedrige Ring (3. Teil a, Polarisationsmessungen an Pyrrol, Furan, Thiophen). — Z. physik. chem. *B 38* (1937) 275.
124. Ekegren, S., Öhrn, O., Granath, K., and Kinell, P.-O., Heat of Polymerization of Chloroprene. — Acta Chem. Scand. *4* (1950) 126.
125. Grassie, N., Determination of the Concentration of High Polymer Solutions. — J. Polymer Sci. *6* (1950) 643.
126. Washburn, E. W., and Williams, G. Y., A Precision Viscosimeter for the Measurement of Relative Viscosity, and the Relative Viscosities of Water at 0°, 18°, 25° and 50°. — J. Am. Chem. Soc. *35* (1913) 737.
127. de Wind, G., and Hermans, J. J., Non-Newtonian Flow of Dilute Polymer Solutions. I–II. — Rec. trav. chim. *70* (1951) 521, 615.
128. Simon, A., Über Raman-Spektroskopie und ihre Anwendung auf Gläser und glasartige Kunststoffe. — Kolloid-Z. *96* (1941) 169.
129. Signer, R., and Weiler, J., Raman-Spektrum und Konstitution hochmolekularer Stoffe. — Helv. Chim. Acta *15* (1932) 649.
130. Palm, A., Raman Spectrum of Polystyrene. — J. Phys. Colloid Chem. *55* (1951) 1320.
131. Mizushima, S., Morino, Y., and Inoue, Y., A Note on the Polymerisation of Styrene as revealed by the Raman Effect. — Bull. Chem. Soc. Japan *12* (1937) 136.
132. Hibben, J. H., Chemical Applications of the Raman Effect: I. Polymerization. — J. Chem. Phys. *5* (1937) 706.
133*. Monnier, D., Susz, B., and Briner, E., Raman Spectra of Acrylic Acid and of Unpolymerized and Polymerized Methyl Methacrylate (in French). — Compt. rend. soc. phys. hist. nat. Genève *54* (1937) 104 (in Arch. sci. phys. nat. *19* (1937) July–Aug.).

134. Monnier, D., Susz, B., and Briner, E., Spectres Raman de l'acide acrylique et des méthacrylates de méthyle et d'étyle à divers degrés de polymérisation. — Helv. Chim. Acta *21* (1938) 1349.

135. Dadieu, A., Pongratz, A., and Kohlrausch, K. W. F., Studien zum Ramaneffekt. XV. Das Ramanspektrum organischer Substanzen (Cis-Trans-Isomerie). Monatsh. *60* (1932) 205.

136*. Yasumi, M., Raman spectra of monomeric methyl methacrylate in liquid and solid states. The relation between the doublet lines and the intermolecular rotation (in Japanese). — J. Chem. Soc. Japan *63* (1942) 983.

137*. Yasumi, M., Studies on the polymerization of methyl methacrylate by means of Raman effect (in Japanese). — J. Chem. Soc. Japan *63* (1942) 988.

138*. Kojima, K., Polymerization. I. Raman spectra and dipole moment of methacrylate and its polymer (in Japanese). — J. Chem. Soc. Japan *62* (1941) 903.

139*. Kojima, K., Studies on polymerization. II. Copolymerization of methyl methacrylate and acrylonitrile as revealed by their Raman spectra (in Japanese). — J. Chem. Soc. Japan *64* (1943) 496.

139a*. Kojima, K., Studies on polymerization. III. Raman scattering of methyl methacrylate in the different stages of polymerization (in Japanese). — J. Chem. Soc. Japan, Pure Chem. Sect., *70* (1949) 147.

140*. Patel, M. M., Raman spectrum of methyl methacrylate glass. — Current Sci. (India) *18* (1949) 436.

141. Gehman, S. D., The Raman Spectrum of Rubber. — J. Am. Chem. Soc. *57* (1935) 1382.

142. Gehman, S. D., and Osterhof, H. J., Raman Spectrum of Rubber and Some Related Hydrocarbons. — J. Am. Chem. Soc. *58* (1936) 215.

143. Kubota, T., On the Polymerization of Chloroprene as Revealed by the Raman Effect. — Bull. Chem. Soc. Japan *13* (1938) 678.

144*. Gantmacher, A. R., and Medvedev, S., Change in the Raman spectra of chloroprene and isoprene in the polymerization process. — Acta Physicochim. U.R.S.S. *16* (1942) 1.

145*. Gantmacher, A. R., and Medvedev, S. S., Changes in the Raman spectra of chloroprene and isoprene during the process of polymerization (in Russian). — J. Phys. Chem. (U.S.S.R.) *17* (1943) 12.

146*. Perumova, E. D., Raman effect of chloroprene in the course of polymerization (in Russian). — J. Phys. Chem. (U.S.S.R.) *14* (1940) 346.

147*. Putilova, I. N., Raman spectra and the structure of highly polymerized substances (Rubber, balata and synthetic polymers) (in Russian). — Uspekhi Khim. *8* (1939) 75.

148. Rank, D. H., Polarization and Intensity Measurement in Raman Spectra by Photoelectric Method. — J. Optical Soc. Am. *37* (1947) 798.

149. Rank, D. H., Correlation of Intensity Measurements in Raman Spectra Obtained with Different Instruments. — Anal. Chem. *19* (1947) 766.

150. Venkateswaran, S., The Raman Effect in Highly Viscous Liquids. — Nature *122* (1928) 506.

151*. Venkateswaran, S., A study of the Raman effect in glycerol and glycerol-water mixtures. — Indian J. Phys. *3* (1928) 105.

152. Harrand, M., Nouvelles recherches relatives à l'influence de la conjugaison sur l'intensité des raies Raman. — Compt. rend. *229* (1949) 1217.

153. Harrand, M., Influence de la conjugaison sur l'intensité des raies Raman. — Compt. rend. *229* (1949) 187.

154. Kohlrausch, K. W. F., and Pongratz, A., Studien zum Raman Effekt. Mitteilung XXXVII. Die Raman-Spektren des Molekültypus X.CO.Y. — Z. physik. Chem. *B 27* (1934) 176.
155. Herzberg, G., Infrared and Raman Spectra of Polyatomic Molecules, New York (1945).
156. Randall, H. M., Fowler, R. G., Fuson, N., and Dangl, J. R., Infrared Determination of Organic Structures, New York (1949).
157. Herzberg, G., Molecular Spectra and Molecular Structure. I. Spectra of Diatomic Molecules. Second Edition. New York (1950).
158. Pfann, H. F., Williams, V. Z., and Mark, H., Mechanism of Peroxide-Initiated Styrene Polymerization. Infrared Absorption of Some Polymer Samples. — J. Polymer Sci. *1* (1946) 14.
159. Price, C. C., Kell, R. W., and Krebs, E., Addition Polymerization Catalyzed by Substituted Acyl Peroxides. — J. Am. Chem. Soc. *64* (1942) 1103.
160. Price, C. C., and Durham, D. A., The Polymerization of Styrene Catalyzed by *p*-Bromobenzenediazonium Hydroxide. — J. Am. Chem. Soc. *64* (1942) 2508.
161. Price, C. C., and Tate, B. E., The Polymerization of Styrene in the Presence of 3,4,5-Tribromobenzoyl Peroxide. — J. Am. Chem. Soc. *65* (1943) 517.
162. Price, C. C., and Durham, D. A., The Polymerization of Styrene in the Presence of Nitrobenzene, 2,4-Dinitrochlorobenzene and Nitromethane. — J. Am. Chem. Soc. *65* (1943) 757.
163. Price, C. C., The Polymerization of Styrene in the Presence of Nitrothiophene and Chloranil. — J. Am. Chem. Soc. *65* (1943) 2380.
164. Kern, W., and Kämmerer, H., Die chemische Molekulargewichtsbestimmung von Polystyrolen I. und II. — J. prakt. Chem. *161* (1942) 81, 289.
165. Bartlett, P. D., and Cohen, S. G., The Ester Groups in Polystyrene Made with Chloro- and Bromobenzoyl Peroxide. — J. Am. Chem. Soc. *65* (1943) 543.
166. Bartlett, P. D., and Altschul, R., The Polymerization of Allyl Compounds. I. Factors Governing the Acyl Peroxide-Induced Polymerization of Allyl Acetate, and the Fate of the Peroxide. — J. Am. Chem. Soc. *67* (1945) 812.
167. Blomquist, A. T., Johnson, J. R., and Sykes, H. J., N-Nitrosoacylarylamines as Catalysts in Addition Polymerization. — J. Am. Chem. Soc. *65* (1943) 2446.
168. Pfann, H. F., Salley, D. J., and Mark, H., Mechanism of Peroxide Initiated Styrene Polymerization. — J. Am. Chem. Soc. *66* (1944) 983.
169. Dainton, F. S., and Sutherland, G. B. B. M., Application of Infrared Analysis to Elucidate the Mechanism of the Boron Trifluoride Catalyzed Vapor Phase Polymerization of Isobutene at Room Temperature. — J. Polymer Sci. *4* (1949) 37.
169a. Flett, M. St. C., and Plesch, P. H., The Low-temperature Polymerization of isoButene. Part III. The End-group Problem. — J. Chem. Soc. (1952) 3355.
170. Arnett, L. M., Kinetics of the Polymerization of Methyl Methacrylate with Aliphatic Azobisnitriles as Initiators. — J. Am. Chem. Soc. *74* (1952) 2027.
171. Arnett, L. M., and Peterson, J. H., Vinyl Polymerization with Radioactive Aliphatic Azobisnitrile Initiators. — J. Am. Chem. Soc. *74* (1952) 2031.
172. Katchalsky, A., and Wechsler, H., Determination of Catalyst Fragments in Polymers by Absorption in the Ultraviolet. — J. Polymer Sci. *1* (1946) 229.
173. *American Petroleum Institute Research Project 44.* Carnegie Institute of Technology. Catalog of Ultraviolet Spectral Data. Serial Nos. 354, 355 and 356, Benzoic acid in Isooctane, Methanol and Chloroform respectively, Serial Nos. 358 and 359, Ethyl benzoate in Isooctane and Chloroform respectively, Serial No. 360, Phenyl ben-

zoate in Isooctane, Serial No. 369, Benzoyl peroxide in Isooctane, Serial No. 376, Sodium benzoate in Water, contributed by the Shell Development Company, Emeryville, Calif., U.S.A.

174. Smakula, A., Zur Bestimmung der Molekulargewichte von Polystyrolen. — Angew. Chem. *47* (1934) 777.

175. Mark, H., Light Scattering in Polymer Solutions. — Burk, R. E., and Grummitt, O., editors, Chemical Architecture, Frontiers in Chemistry, Vol. V, New York (1948) 121.

176. Holiday, E. R., and Beaven, G. H., Some Practical Aspects of the Effects of Stray Radiation in Spectrophotometry. — P. S. G. Bulletin No. 3 (1950) Oct.

177. Saidel, L. J., Goldfarb, A. R., and Kalt, W. B., False Absorption Bands in the Region of 200–230 mμ Caused by Stray Radiation in the Beckman Spectrophotometer. — Science *113* (1951) 683.

178. Lothian, G. F., Absorption Spectrophotometry, London (1949).

179. Caster, W. O., Variability in the Beckman Spectrophotometer. — Anal. Chem. *23* (1951) 1229.

180. Goodeve, J. W., The Absorption Spectra of Methyl Methacrylate and its Polymer. — Trans. Faraday Soc. *34* (1938) 1239.

181. Scheibe, G., and Fauss, R., U.V.-Absorption bei Hochpolymeren. — Kolloid-Z. *125* (1952) 139.

182. *American Petroleum Institute Research Project 44.* Carnegie Institute of Technology. Catalog of Ultraviolet Spectral Data. Serial No. 2, Toluene, contributed by the Texas Company, Beacon, New York; Serial Nos. 3–6, *n*-Butylbenzene, Isobutylbenzene, *sec*-Butylbenzene, *tert*-Butylbenzene, and 1-Phenyleicosane, contributed by the Ethyl Corporation, Detroit, Michigan, U.S.A.

183. Meyerhoff, G., and Schulz, G. V., Molekulargewichtsbestimmungen an Polymethacrylsäureestern mittels Sedimentation in der Ultrazentrifuge und Diffusion. — Makromol. Chem. *7* (1951) 294.

184. Bischoff, J., and Desreux, V., Etude des solutions diluées de polyméthacrylate de méthyle I. — Bull. Soc. Chem. Belg. *61* (1952) 10.

185. Ewart, R. H., Significance of Viscosity Measurements on Dilute Solutions of High Polymers. — Mark, H., and Whitby, G. S., editors, Scientific Progress in the Field of Rubber and Synthetic Elastomers; Advances in Colloid Science, Vol. II, New York (1946) 197.

185a. Manson, J. A., and Cragg, L. H., Normal and cross-linked Polystyrene I. Huggins' k' as a measure of non linearity. — Can. J. Chem. *30* (1952) 482.

186. Thompson, H. W., Recent Advances in Infra-red Spectroscopy. — Ann. Repts. Chem. Soc. *42* (1945) 5.

187. Thompson, H. W., The Study of Macromolecules by Infra-Red Spectroscopy. — J. Chem. Soc. (1947) 289.

188. Sutherland, G. B. B. M., Some Problems in the Interpretation of the Infra-Red Spectra of Large Molecules. — Disc. Faraday Soc. *9* (1950) 274.

189. Gore, R. C., Infrared Spectroscopy. — Anal. Chem. *22* (1950) 7.

190. Gore, R. C., Infrared Spectroscopy. — Anal. Chem. *23* (1951) 7.

191. Gore, R. C., Infrared Spectroscopy. — Anal. Chem. *24* (1952) 8.

192. Barnes, R. B., and Gore, R. C., Infrared Spectroscopy. — Anal. Chem. *21* (1949) 7.

193. Barnes, R. B., Gore, R. C., Liddel, U., and Williams, V. Z., Infrared Spectroscopy. Industrial Applications and Bibliography, New York (1944).

194. Fox, J. J., and Martin, A. E., Investigations of Infrared Spectra. Determination of C–H frequencies (~ 3000 cm.$^{-1}$) in the Paraffins and Olefins with some Observations on "Polythenes". — Proc. Roy. Soc. (London) *A 175* (1940) 208.

195. Thompson, H. W., and Torkington, P., The Infra-Red Spectra of Compounds of High Molecular Weight. — Trans. Faraday Soc. *41* (1945) 246.

196. Thompson, H. W., and Torkington, P., The Infra-red spectra of polymers and related monomers I. — Proc. Roy. Soc. (London) *A 184* (1945) 3.

197. Cross, L. H., Richards, R. B., and Willis, H. A., The Infra-Red Spectrum of Ethylene Polymers. — Disc. Faraday Soc. *9* (1950) 235.

198. Thompson, H. W., and Torkington, P., The Infra-red spectra of polymers and related monomers II. — Proc. Roy. Soc. (London) *A 184* (1945) 21.

199. Williams, D., The Infrared Absorption of Rubber and Related Hydrocarbons. J. Chem. Phys. *4* (1946) 460.

200. Williams, D., and Dale, B., Further Studies of the Infra-Red Absorption of Rubber. — J. Applied Phys. *15* (1944) 585.

201. Barnes, R. B., Liddel, U., and Williams, V. Z., Synthetic Rubber. A Spectroscopic Method for Analysis and Control. — Ind. Eng. Chem. Anal. Ed. *15* (1943) 83.

202. Barnes, R. B., Williams, V. Z., Davis, A. R., and Giesecke, P., Physical Methods of Analysis of Synthetic and Natural Rubber. — Ind. Eng. Chem. Anal. Ed. *16* (1944) 9.

203. Dinsmore, H. L., and Smith, D. C., Analysis of Natural and Synthetic Rubber by Infrared Spectroscopy. — Anal. Chem. *20* (1948) 11.

204. Saunders, R. A., and Smith, D. C., Infra-Red Spectra and Structure of Hevea and Gutta Elastomers. — J. Applied Phys. *20* (1949) 953.

205. Salomon, G., van der Scheé, A. C., Ketelaar, J. A. A., and van Eyk, B. J., Infra-Red Analysis of Rubber Derivatives. — Disc. Faraday Soc. *9* (1950) 291.

206. Mochel, W. E., and Hall, M. B., The Structure of Neoprene. IV. Infrared Spectra and Spectral Changes with Crystallization. — J. Am. Chem. Soc. *71* (1949) 4082.

207. Thompson, H. W., and Torkington, P., The Vibrational Spectra of Acrylonitrile and Perbunan. — J. Chem. Soc. (1944) 597.

208. Hart, E. J., and Meyer, A. W., Infrared Studies of 1,2- and *trans*-1,4-Structure of Polybutadiene and Butadiene-Styrene Copolymers Polymerized at Various Temperatures. — J. Am. Chem. Soc. *71* (1949) 1980.

209. Hampton, R. R., Infrared Analysis of Low Temperature Polymers. — Anal. Chem. *21* (1949) 923.

210. Treumann, W. B., and Wall, F. T., Determination of 1,2 Addition in Polymers and Copolymers of Butadiene. — Anal. Chem. *21* (1949) 1161.

211*. Burgova, M. P., and Korotkov, A. A., Determination of rubber structure by the method of infrared spectroscopy (in Russian). — Izvest. Akad. Nauk. S.S.S.R., Ser. Fiz., *14* (1950) 452.

212. Sheppard, N., and Sutherland, G. B. B. M., Some Infra-Red Studies on the Vulcanisation of Rubber. — Trans. Faraday Soc. *41* (1945) 261.

213. Sears, W. C., Infra-Red Spectra of Rubber and High Polymers. — J. Applied Phys. *12* (1941) 35.

214*. Mann, J., Identification of accelerators and antioxidants in vulcanizates by infrared spectroscopy. — Trans. Inst. Rubber Ind. *27* (1951) 232.

215. Glatt, L., and Ellis, J. W., Infra-Red Dichroism Involving Hydrogen Bonds. — J. Chem. Phys. *15* (1947) 880.

216. Glatt, L., and Ellis, J. W., Infra-Red Dichroism in Aligned Polythene and "Paro-wax". — J. Chem. Phys. *15* (1947) 884.

217. Glatt, L., and Ellis, J. W., Near Infra-Red Absorption of Nylon Films: Dichroism and Rupture of N–H ··· O Bonds on Melting. — J. Chem. Phys. *16* (1948) 551.

218. Glatt, L., Webber, D. S., Seaman, C., and Ellis, J. W., Near Infra-Red Pleochroism. I. The Perturbed O–H and the C–H Modes in Polyvinyl Alcohol. — J. Chem. Phys. *18* (1950) 413.

219. Glatt, L., and Ellis, J. W., Near Infrared Pleochroism. II. The 0.8–2.5 μ Region of Some Linear Polymers. — J. Chem. Phys. *19* (1951) 449.

220. Elliot, A., Ambrose, E. J., and Temple, R. B., Polarized Infra-Red Radiation as an Aid to the Structural Analysis of Long-Chain Polymers. I. — J. Chem. Phys. *16* (1948) 877.

221. Sutherland, G. B. B. M., and Jones, A. V., The Application of Polarized Infra-Red Radiation to Problems in Molecular Structure. I. Polyisoprenes. — Disc. Faraday Soc. *9* (1950) 281.

222. King, G. W., Hainer, R. M., and McMahon, H. O., Infra-Red Absorption Spectra of Some Polymers at Liquid-Helium Temperatures. — J. Applied Phys. *20* (1949) 559.

223. Wells, A. J., The Infra-Red Transmission of Thin Films of Various Organic Materials. — J. Applied Phys. *11* (1940) 137.

224. Thompson, H. W., Nicholson, D. L., and Short, L. N., The Infra-Red Spectra of Complex Molecules. — Disc. Faraday Soc. *9* (1950) 222.

225. Magat, E. E., Chandler, L. B., Faris, B. F., Reith, J. E., and Salisbury, L. F., Acid-catalyzed Reactions of Nitriles. II. Polyamides from Formaldehyde and Dinitriles. — J. Am. Chem. Soc. *73* (1951) 1031.

226. Achhammer, B. G., Reiney, M. J., and Reinhart, F. W., Study of Degradation of Polystyrene, Using Infrared Spectrophotometry. — J. Research Natl. Bur. Standards *47* (1951) 116.

227. Bryant, K. C., Kennedy, G. T., and Tanner, E. M., Some Nuclear-methylated Styrenes and Related Compounds. Part III. Absorption Spectra. — J. Chem. Soc. (1949) 2389.

228*. Houtz, R. C., "Orlon" acrylic fiber: chemistry and properties. — Textile Research J. *20* (1950) 786.

229*. Haslam, J., Soppet, W., and Willis, H. A., Analytical examination of plasticisers obtained from polyvinyl chloride compositions. — J. Applied Chem. *1* (1951) 112.

230. Hausdorff, H. H., Short Cuts to the Analysis of Plastics by Infrared Spectroscopy. — Society for Applied Spectroscopy Bulletin Aug. 1951.

231*. Kronstein, M., Application of infrared spectroscopy to the study of drying oils and certain plastics. — Schweiz. Ver. Lack. u. Farben-Chem. u. Tech., Bull. No. *10* (1950) 4 and New York Univ. Coll. Eng., Symposium on Varnish and Paint Chemistry (1948) 13.

232*. Bezman, I. I. and Browning, D. D., Polymerization of styrene with drying oils in aqueous emulsion. — Paint, Oil a. Chem. Rev. *114* (1951) 10.

233. Kellner, L., Vibrations of an Infinitely Long Chain of CH_2-Groups and the Infra-Red Spectrum of Polythene. — Nature *163* (1949) 877.

234. Kellner, L., The Vibrations of an Infinitely Long Chain of CH_2-Groups and the Infra-Red Spectrum of Polythene. — Proc. Phys. Soc. (London) *A 64* (1951) 521.

235. Barrow, G. M., Remarks on the Interpretation of the CH_2 Vibrational Frequencies of *n*-Paraffins. — J. Chem. Phys. *19* (1951) 345.

236. *American Petroleum Institute Research Project 44.* Carnegie Institute of Technology. Catalog of Infrared Spectral Data. Serial No. 307, Benzene, contributed by the U.S. Naval Research Laboratory, Washington, D.C., and Serial No. 498, Benzene, contributed by The Texas Company, Beacon, New York, U.S.A.

237. Plyer, E. K., and Peters, C. W., Wavelengths for Calibration of Prism Spectrometers. — J. Research Natl. Bur. Standards *45* (1950) 462.

238. Martin, A. E., The Accuracy of Infra-Red Intensity Measurements. — Trans. Faraday Soc. *47* (1951) 1182.

239. Francis, S. A., Intensities of Some Characteristic Infra-red Bands of Ketones and Esters. — J. Chem. Phys. *19* (1951) 942.

240. Thompson, H. W., and Torkington, P., The Vibration Spectra of Esters and Ketones. — J. Chem. Soc. (1945) 640.

241. *American Petroleum Institute Research Project 44.* Carnegie Institute of Technology. Catalog of Infrared Spectral Data. Serial No. 761, Methyl methacrylate, contributed by the National Bureau of Standards, Radiometry Laboratory, Washington, D.C., U.S.A.

242. *American Petroleum Institute Research Project 44.* Carnegie Institute of Technology. Catalog of Infrared Spectral Data. Serial Nos. 308, Toluene, 313, *n*-Propylbenzene, 314, Isopropylbenzene, 468, *n*-Butylbenzene, 469, Isobutylbenzene, 470, *sec*-Butylbenzene, 471, *tert*-Butylbenzene, and 355, *n*-Hexylbenzene, contributed by the U.S. Naval Research Laboratory, Washington, D.C., and Serial No. 337, *n*-Octylbenzene, contributed by the Nation Aniline Division, Allied Chemical and Dye Corporation, Buffalo, N.Y., U.S.A.